

Peristaltic activity in frames of hydromagnetics and rotation



By

Maimona Rafiq

**Department of Mathematics
Quaid-i-Azam University
Islamabad, Pakistan
2017**

Peristaltic activity in frames of hydromagnetics and rotation



By

Maimona Rafiq

Supervised By

Prof. Dr. Tasawar Hayat

**Department of Mathematics
Quaid-i-Azam University
Islamabad, Pakistan
2017**

Peristaltic activity in frames of hydromagnetics and rotation



By

Maimona Rafiq

**A THESIS SUBMITTED IN THE PARTIAL FULFILLMENT OF THE REQUIREMENT FOR
THE DEGREE OF**

DOCTOR OF PHILOSOPHY

IN

MATHEMATICS

Supervised By

Prof. Dr. Tasawar Hayat

Department of Mathematics

Quaid-i-Azam University

Islamabad, Pakistan

2017



Acknowledgments

In the name of Allah, the most Merciful, the most Gracious. All praise is due to Allah; we praise Him, seek His help, and ask for His forgiveness. I am thankful to Allah, who supplied me with the courage, the guidance and the love to complete this research. Also, I cannot forget the ideal man of the world and most respectable personality for whom Allah created the whole universe, Prophet Mohammed (Peace Be Upon Him).

This thesis would not have been possible without the inspiration and support of a number of wonderful individuals — my thanks and appreciation to all of them for being part of this journey and making this thesis possible. Acknowledgement is due to Quad-I-Azam university for providing support to carry out this work.

Special appreciation goes to my supervisor, **Prof. Dr. Tasawar Hayat**, for his supervision and constant support. His invaluable help of constructive comments and suggestions throughout the research work have contributed to the success of this thesis. I am very grateful for him since he gave me the chance to work on an interesting and practical topic. In short, his tireless work, unique personality and dedication to profession cannot be expressed in words.

I would like to thank **Higher Education Commission (HEC)** of Pakistan for the scholarship granted through **5000 Indigenous Ph.D. Scholarship Program Phase II Batch II**.

I would like to express my special thanks of gratitude to my teachers **Prof. Dr. Muhammad Yousaf Malik (Chairman)**, **Prof. Dr. Muhammad Ayub**, **Prof. Dr. Sohail Nadeem** and **Dr. Masood Khan** for their valuable and constructive suggestions in all aspects.

I would also like to thank **Zahoorbhae**, **Sajidbhae**, **Safdarbhae**, **Sheraz sahib** and all other office staff of the department for their administrative support throughout the completion of Ph.D.

My highest and special thanks go to my seniors and friends **Dr. Humaira Yasmin**, **Dr. Sadia Asad** and **Dr. Maria Imtiaz** for their strong support during the work of the thesis and their great advice to me. I would also like to express my gratitude to **Dr. M. Farooq** for his guidance, enthusiastic encouragement and useful critiques of this research work. I would also like to thank my other research fellows **Anum Tanveer**, **Hina Zahir**, **Sadia Ayub**, **Shahid Farooq**, **M. Waqas**, **Sajid**, **Sumaira Qayyum**, **Sumaira Jabeen** for their valuable and polite discussions.

Sincere thanks to my friends **Mahwish Manzoor**, **Rehana Rahim** and **Sapna Makhdoom** for the wonderful times we shared at Quaid-I-Azam University. I would like to thank my hostel friends **Sidra-tul-Muntaha** and **Fehmi Aziz** who gave me the necessary distractions from my research.

Finally, my deep and sincere gratitude to my family for their continuous and unparalleled love, help and support. I am especially grateful to my parents, who supported me emotionally and financially. I always knew that you believed in me and wanted the best for me. Thank you for teaching me that my job in life was to learn, to be happy, and to know and understand myself; only then could I know and understand others. I am nothing without you my **Jannat(Amee Gee)** and **Abu Gee**. May Allah give you healthy long life (Ameen).I am grateful to my sister**Aamna** for always being there for me as a friend. Special thanks to my elder brothers **M. Bilal, M. Talal** and **bhabhi (Hiba)** for the love and affection they gave me. They selflessly encouraged me to explore new directions in life and seek my own destiny. How can I forget to thank little angels **Maheen, Abdul Hadi** and **Maleeha** for the love and care they gave me.This journey would not have been possible without my family and I dedicate this milestone to them.

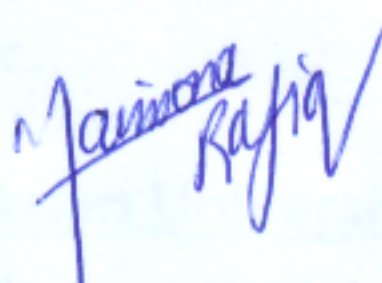
May Allah bless health and wealth to all those who pray for me (Ameen).

Maimona Rafiq

Author's Declaration

I Maimona Rafiq hereby state that my PhD thesis titled Peristaltic activity in frames of hydromagnetics and rotation is my own work and has not been submitted previously by me for taking any degree from the Quaid-i-Azam University Islamabad, Pakistan or anywhere else in the country/world.

At any time if my statement is found to be incorrect even after my graduate the university has the right to withdraw my PhD degree.



Name of Student: Maimona Rafiq

Date: 21-08-2017

DEDICATED TO

MY BELOVED PARENTS

Peristaltic activity in frames of hydromagnetics and rotation

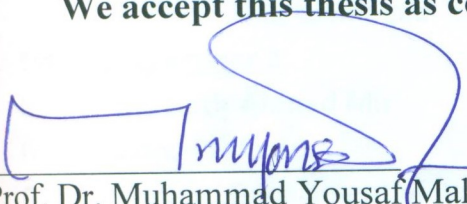
By

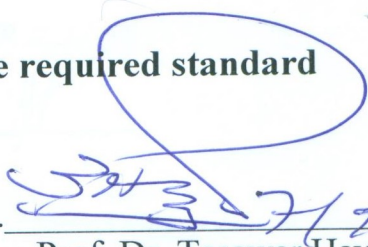
Maimona Rafiq

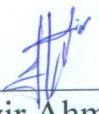
CERTIFICATE

A THESIS SUBMITTED IN THE PARTIAL FULFILLMENT OF THE
REQUIREMENTS FOR THE DEGREE OF THE DOCTOR OF
PHILOSOPHY

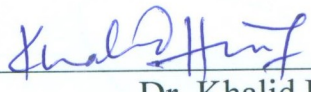
We accept this thesis as conforming to the required standard

1. 
Prof. Dr. Muhammad Yousaf Malik
(Chairman)

2. 
Prof. Dr. Tasawar Hayat
(Supervisor)

3. 
Prof. Dr. Nazir Ahmad Mir
Department of Basics Science
Riphah International University
I-14 Hajj Complex, Islamabad.

(External Examiner)

4. 
Dr. Khalid Hanif
Associate Professor
Islamabad Model Post-graduate
College, H-8, Islamabad

(External Examiner)

Certificate of Approval

This is to certify that the research work presented in this thesis entitled Peristaltic activity in frames of hydromagnetics and rotation was conducted by Ms Maimona Rafiq under the supervision of Prof. Dr. Tasawar Hayat. No part of this thesis has been submitted anywhere else for any other degree. This thesis is submitted to the Department of Mathematics, Quaid-i-Azam University, Islamabad in partial fulfillment of the requirements for the degree of Doctor of Philosophy in Field of Mathematics from Department of Mathematics, Quaid-i-Azam University Islamabad, Pakistan.

Student Name: Maimona Rafiq

Signature: 

External committee:

a) External Examiner 1:

Signature: 

Name: **Dr. Khalid Hanif**

Designation: Associate Professor

Office Address: Islamabad Model Postgraduate College

H-8, Islamabad.

b) External Examiner 2:

Signature: 

Name: **Dr. Nazir Ahmad Mir**

Designation: Professor

Office Address: Department of Basics Sciences

Riphah International University

I-14 Hajj Complex, Islamabad.

c) Internal Examiner :

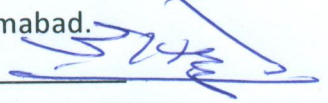
Signature: 

Name: **Dr. Tasawar Hayat**

Designation: Professor

Office Address: Department of Mathematics, QAU Islamabad.

Supervisor Name:

Signature: 

Prof. Dr. Tasawar Hayat

Name of Dean/ HOD

Signature: 

Prof. Dr. Muhammad Yousaf Malik

Preface

Peristalsis has pivotal role due to its applications in both industry and physiology under different conditions. Especially in mechanical discipline it has motivated engineers to construct pumps where fluid does not come in direct contact with any part of the machine. Applications include dialysis machines, open-heart bypass pump machines and infusion pumps. In addition, the study of hydro-magnetic peristaltic flow under the effect of magnetic field has played vital role in many engineering problems such as meteorology, biomedical engineering, solar physics, motion of earth's core and chemical engineering etc. Particularly the treatment of pathologies like gastroenric pathologies, rheumatisms, constipation, hypertension, targeted transport of drugs using magnetic particles as drug carriers are some applications. Blood is also known as the bio-magnetic fluid. It is because of complex interaction of the intercellular protein, cell membrane and the hemoglobin. The study of fluid flow in rotating frame of reference has promising applications in cosmic and geophysical flows. In such situation, Coriolis and Centrifugal forces are significant in relevant equations. The earth's liquid is strongly affected by the Coriolis force produced due to earth's rotation. Therefore, it is of great interest to study the flow of Newtonian/non-Newtonian fluids in rotating frame. Keeping this in mind the present thesis focus on the flow problems under different situation. Complex nonlinear differential systems for peristalsis of fluids under the aforementioned aspects are simplified through appropriate transformations. Suitable methods are employed to solve the nonlinear mathematical problems. Effects of rotation and heat/mass transfer are given due attention.

Keeping all such facts in mind we structure the present thesis as follows:

The review of some existing literature relevant to peristaltic transport and some fundamental equations is given in chapter one.

Chapter two addresses the peristaltic flow Jeffrey fluid in a symmetric rotating channel. Channel walls are considered compliant in nature. Fluid is electrically conducting. Thermal radiation and Joule heating effects are employed in energy equation. Long wavelength and low Reynolds number approximation is applied for problem simplification. Analysis has been carried out for axial and secondary velocity. Moreover, heat transfer analysis is also discussed. Several graphs of physical interest are displayed and discussed. The results of this chapter are **published in International Journal of Biomathematics 8(2015)1550061(21 pages) DOI: 10.1142/S1793524515500618.**

Chapter three deals with the peristaltic transport of Jeffrey fluid in a rotating channel. The channel walls satisfy the dynamic boundary conditions. This chapter is generalized work of previous chapter for Soret and Dufour and porous medium. The relevant flow analysis is first modeled and then computed for the exact solutions of velocities, temperature and concentration fields. Closed form expression of stream function is constructed. Plots are prepared for a parametric study reflecting the effects of Taylors, Soret, Dufour, Prandtl, Eckert and permeability parameters. The findings of this chapter have been **published in PLoS ONE 11 (2016) e0145525 DOI: 10.1371/journal.pone.0145525.**

Chapter four has been organized for the impacts of thermophoresis, chemical reaction and heat source/sink. Thermal radiation is also present. Computations of solutions are made for the velocity, temperature and concentration fields. Closed form expression of stream function is obtained. Results displayed and discussed for the effects of Taylors,

Hartman, Brinkman, Biot, Schmidt numbers, chemical reaction, radiation, thermophoretic and non-uniform heat source/sink parameters. The research presented in this chapter is **published in Journal of Magnetism and Magnetic Materials** **410 (2016) pp. 89-99.**

Heat transfer enhancement in industry and drug delivery in biomedical engineering increases the use of nanofluid. Therefore, chapter five is written to study heat transfer effects in peristaltic flow when the whole system is rotating ferrofluid. An incompressible fluid is considered in a channel with convective boundary conditions. This study is motivated towards investigating the physiological flows in rotating frame. Long wavelength and low Reynolds number approach is adopted. Effects of various physical parameters on the velocity profile, streamlines pattern, temperature profile and trapping are studied. Computational results are presented in graphical form. The contents of this chapter have been submitted for **publication in International Journal of Heat and Mass Transfer** **(2017).**

Chapter six is the extension of chapter five by considering the peristaltic transport of Cu-water nanofluid in a symmetric channel with slip boundary conditions. Mathematical modelling is based upon the conservation laws of mass, linear momentum and energy. Influence of Hall currents and porous medium on velocities and temperature is given consideration. Resulting equations have been solved after using long wavelength and low Reynolds number approximation. Results for the axial and secondary velocities and temperature profile are obtained. Expressions of the velocities, temperature and effective heat transfer are analyzed for various embedded parameters. The observations of conducted analysis are **published in International Journal of Thermal Sciences** **112 (2017) pp. 129-141.**

The current researches in thermal engineering have shown that the second law of thermodynamics is more efficient in optimizing the system when compared with first law since it does not determine the variations in energy and only manipulates the accounting of energy. Therefore, entropy generation analysis is helpful in studying the peristaltic flow of nanoparticles in a symmetric rotating channel that is discussed in chapter seven. The flow is generated because of peristaltic waves propagating along the channel walls. Heat transfer is examined in the presence of thermal radiations. Mathematical model is presented employing lubrication approach. The effects of Taylors, Hartman, Prandtl, Eckert, Brinkman numbers, radiation and wall parameters on the longitudinal and secondary velocities, temperature and entropy generation are studied in detail. Important conclusions have been pointed out. The contents of this chapter are **published in International Journal of Heat and Mass Transfer 108(2017) pp. 1775-1786.**

Chapter eight is the extension of chapter six with consideration of an incompressible Ree-Eyring fluid in a symmetric channel with Hall effects and slip boundary conditions. Mathematical formulation is completed by adopting Long wavelength and low Reynolds number approach. The solutions for velocities and temperature are obtained. Heat transfer rate for different embedding parameters is analyzed. Velocity and temperature distributions are analyzed for different parameters of interest. The findings of this chapter are **submitted for publication in Computers in Biology and Medicine (2017).**

Contents

1	Literature review and basic laws	5
1.1	Peristalsis	5
1.2	Literature survey	7
1.3	Basic equations	17
1.3.1	Mass conservation	17
1.3.2	Momentum conservation	17
1.3.3	Energy conservation	18
1.3.4	Concentration equation	18
1.3.5	Maxwells equations	19
1.3.6	Compliant wall	19
2	Peristaltic motion of Jeffrey fluid with simultaneous effects of rotation and radiation	21
2.1	Introduction	21
2.2	Physical model	21
2.3	Problem formulation	22
2.3.1	Non-dimensionalization	25
2.4	Exact solutions	28
2.5	Discussion	30
2.5.1	Analysis of axial velocity	31
2.5.2	Analysis of secondary velocity	31
2.5.3	Analysis of temperature profile	31

2.5.4	Heat transfer coefficient	32
2.5.5	Trapping phenomenon	32
2.6	Closing remarks	43
3	MHD peristaltic rotating flow of Jeffrey fluid in presence of porous medium and Soret and Dufour effects	44
3.1	Introduction	44
3.2	Problem development	44
3.3	Solution	49
3.4	Graphical results and discussion	52
3.5	Conclusions	64
4	Influence of rotation and thermophoresis on MHD peristaltic transport of Jeffrey fluid with convective conditions and wall properties	65
4.1	Introduction	65
4.2	Mathematical formulation	66
4.3	Solutions	70
4.4	Results and discussion	72
4.4.1	Axial and secondary velocities	72
4.4.2	Temperature profile	73
4.4.3	Concentration profile	73
4.4.4	Heat transfer coefficient	74
4.4.5	Trapping	74
4.5	Conclusions	85
5	Influence of convective conditions on peristalsis of ferrofluid in a rotating frame	86
5.1	Introduction	86
5.2	Mathematical formulation	86
5.3	Solutions	92
5.4	Graphical results and discussion	95

5.4.1	Axial velocity	95
5.4.2	Secondary velocity	96
5.4.3	Heat transfer analysis	96
5.4.4	Streamlines and Trapping	97
5.5	Conclusions	105
6	Investigation of Hall current and slip conditions on peristaltic transport of Cu-water nanofluid in a rotating frame	107
6.1	Introduction	107
6.2	Mathematical formulation	108
6.3	Solution	114
6.4	Discussion	115
6.4.1	Axial velocity	115
6.4.2	Secondary velocity	116
6.4.3	Heat transfer analysis	116
6.5	Conclusions	126
7	Entropy generation analysis for peristaltic flow of nanoparticles in a rotating frame	127
7.1	Introduction	127
7.2	Modeling	127
7.2.1	Entropy generation and viscous dissipation	133
7.2.2	Solutions	134
7.3	Discussion	135
7.3.1	Axial velocity	135
7.3.2	Secondary velocity	136
7.3.3	Heat transfer analysis	136
7.3.4	Entropy generation analysis	138
7.4	Conclusions	147

8	Heat transfer in peristaltic flow of Ree-Eyring fluid with Hall and slip effects in a rotating frame	148
8.1	Introduction	148
8.2	Flow description	148
8.3	Mathematical modeling	149
8.4	Exact solutions	154
8.5	Discussion	155
8.5.1	Axial velocity	155
8.5.2	Secondary Flow	156
8.5.3	Heat transfer analysis	156
8.6	Conclusions	164
9	Summary	165

Chapter 1

Literature review and basic laws

1.1 Peristalsis

Mathematical modeling is utilized as a part of biomechanics to study issues of the medical science. Biofluid mechanics is portion of biomechanics which portrays the kinematics and dynamics of body liquids in living creatures. Advanced biofluid mechanics measures and examines the liquid stream in the blood vessels, the respiratory tract, the lymphatic system, the gastrointestinal tract, the urinary tract and numerous other physiological systems. Recent findings are essential for clinical applications like artificial organs, vascular vessel advancement, designing medical instruments, creation of material membranes for orthopedics, among others. Similar mechanisms of bioliquids transport can be seen in wide range of situations within human body and the one that is prominent is peristalsis which provide basis for the present study. The main purpose of peristalsis is to drive the fluids through the tube without requiring an overall pressure difference. The term peristalsis originates from the Greek word peristaltikos, which means "compressing and claspings". A definition of peristalsis by Merriam-Webster's [1] is "Successive waves of involuntary contraction passing along the walls of a hollow muscular structure and forcing the contents onward".

The mechanism of peristalsis in human body initiated after food is chewed into a swallowed bolus and travelled through esophagus. Smooth muscles behind the bolus contract to prevent it moving back towards the mouth. After this, successive unidirectional waves work to push the food quickly into stomach. This process occurs in one direction only and its main purpose

is to move the food from mouth to stomach. It was first presented by Bayliss and Starling [2] as a type of motility in which there is contraction above and relaxation below a transported. Peristalsis is entirely unaffected by vagotomy or sympathetomy, describing its mediation by the intestine's local, intrinsic nervous system.

Peristalsis is a explanation of two particular reflexes within the enteric nervous system that are stimulated by a bolus of food stuff in the lumen. Mechanical distension and perhaps mucosal irritation induce afferent enteric neurons. These sensory neurons coincide with two sets of cholinergic interneurons, which exhibit two peculiar symptoms:

(i) One group of interneurons activates excitatory motor neurons above the bolus. These neurons, which contain acetylcholine and substance, stimulate contraction of smooth muscle above the bolus.

(ii) Another group of interneurons activates inhibitory motor neurons that stimulate relaxation of smooth muscle below the bolus. These inhibitor neurons appear to use nitric oxide, vasoactive intestinal peptide and ATP as neurotransmitters.

In industry, the peristaltic pumping is utilized in different applications as exchange of sterile fluids, blood pump in heart lung machines, transportation of interecine and dangerous liquids to prevent their involvement in surrounding environment etc. A noteworthy modern use of peristaltic pumping can be seen in designing the roller pumps which are used to avoid the contact of fluid with the pumping equipment. Pumps are designed in such a manner that they prevent the reverse flow and syphoning without the valves. Isolationistic design of pumps made them ideal for a variety of industries and applications like aseptic filling, biopharmaceutical, brewing, ceramics, chemical, food and beverage, industrial process, mining, print and packaging, pulp and paper, paint and pigments, science and research, water and waste applications. Peristaltic tube pumps provide accurate dosing of medication and chemical in printing and packaging industry. Incorporating exact dosage allows the tube pump to account the proficient addition to the manufacturing plant or laboratory. Only a little amount of panel mounted peristaltic hose and tube pumps are used in Original Equipment Manufacture (OEM). These are manufactured to suffice fairly inside the machinery and find variety of applications in print presses, dish washes and chemical dosing systems. Many biomedical devices are engineered on the principle of peristalsis like dialysis machine, heart-lung machine, infusion and blood pumps which are

used during heart surgery.

1.2 Literature survey

Investigations on peristalsis with respect to human physiological systems have received the attention of researchers earlier than the engineers. Main focus of engineers is to develop new devices for the technological advancements. Such requirements forced the investigators to dig the underlying phenomena of peristalsis. Peristaltic pumping was initially investigated in human ureter system by Engelmann [3] in his classical paper on the ureter. After his initial attempt, several other researchers put their efforts to elaborate the study particularly Lapiques [4], Kiil [5] and Boyarsky [6]. This kind of pumping is easy to understand when observed by keeping viewpoint fluid mechanics but difficult to observe from pathological viewpoint ([7, 8]). The problem arises due to some kind of hindrance in ureter which dilates the upstream ureter. In such condition, peristalsis occurs due to the wave travelling with small amplitude over a cylindrical tube which effects the pumping efficiency negatively. Shapiro [9] studied the peristaltic pumping by considering inertia free flow in a tube with flexible boundaries by considering small wave number (wavelength of peristaltic wave is large in comparison with width of the tube). Experimental work presented by Shapiro showed the same results as observed by Latham [10] in his initial experimental investigation. The theory of long wavelength and low Reynolds number was further confirmed through the studies of Eckstein [11] and Weinberg [12]. Afterwards, Weinberg et al. [13] and Lykoudis [14] further discussed the ureteral system as peristaltic pump by proposing more models for the ureteral waves. Relation between the biomechanical forces and ureteral muscles was presented by Fung [15, 16]. Peristaltic motion of Newtonian fluid in symmetric and asymmetric geometries is investigated by Burns and Parkes [17]. They made the small Reynolds number assumption to analyze Stokes flow situation. Barton and Reynor [18] analyzed the peristaltic flow for two different cases. The first analysis was presented for large wavelength when compared with average radius of the tube and same analysis was done by assuming small wavelength. Hanin [19] invoked the assumption of long wavelength with large Reynolds number while considering small amplitude ratio. Peristaltic flow of viscous fluid in a two-dimensional channel with reflux was investigated by Fung and Yih [20]. They found

that the reflux occurs in the centre of the channel. Shapiro et al. [21] presented the analysis by ignoring inertia effects (i.e. at low Reynolds number). They considered the flow both in planar and axisymmetric channels and investigated the problem by taking the range of amplitude ratio from zero to full occlusion. Reflux phenomena is found true for urinary and gastrointestinal systems. Peristaltic flow of viscous fluid through circular tube is studied by Yin and Fung [22]. They applied perturbation technique about small amplitude ratio and discussed the classical Poiseuille flow and Sommerfeld-Orr equation at zeroth and first order terms respectively. Zein and Ostrach [23] looked at the incompressible flow of viscous fluid in a two-dimensional geometry. Their analysis was aimed to find the possible application of peristalsis to human ureteral system. The work of Zein and Ostrach was extended by Li [24] for axisymmetric case. Chow [25] studied the flow of an incompressible Newtonian fluid through circular cylindrical tube for an axisymmetric case. The initial motion of flow was taken as Hagen-Poiseuille. Meginniss [26] addressed the inertial free lubrication theory to peristaltic flow in a tube of a roller pump. Lykoudis and Roos [27] developed a fluid-mechanical model for studying the functioning of human ureter. They presented the analysis by adopting the lubrication theory and found good agreement between theoretical and experimental pressure distribution. Jaffrin and Shapiro [28] worked on inertia-free peristaltic motion of viscous fluid and presented the physical picture of peristaltic pump. Lew et al. [29] discussed two different solutions for the peristaltic activity in small intestine, one for peristaltic carrying in which fluid flow is generated in the absence of net pressure gradient and the other one is a peristaltic compression in which net motion of the fluid is not considered. Axisymmetric motion of viscous fluid in a cylindrical tube with small Reynolds number is studied by Lew and Fung [30]. Their analysis provides physical significance of studying the fluid motion inside vessels (i.e. veins and lymphatic ducts) of living bodies. Weinberg et al. [31] conducted the experimental analysis of peristaltic pumping. The results of experiment confirmed the analysis of Shapiro et al. (ref. [21]) when Reynolds number was extended upto 1. Tong and Vawter [32] adopted finite-element method to discuss peristaltic pumping in a tube. They concluded that in the absence of net flow reflux occur on the axis when wavelength is short whereas for large wavelength reflux occurs off the axis. Jaffrin [33] considered the peristaltic motion of viscous fluid in a circular tube in the presence of inertial and streamline curvature effects. He presented the analysis by taking small wave number. Theoret-

ical investigation revealed that two-dimensional peristaltic motion with inertia and streamline effects physically presents the gastrointestinal tract and the roller pumps. Semleser et al. [34] presented a mathematical model for the swimming mechanism of spermatozoa in the cervix. The influence of Poiseuille flow on peristaltic flow in a two dimensional channel is studied by Mitra and Prasad [35]. Nergin et al. [36] extended the work of Tong and Vawter (ref. [32]) by discussing pressure rise per wavelength Δp_λ . Manton [37] discussed peristaltic flow in an axisymmetric tube for small Reynolds number when the wavelength of arbitrary shaped waves is large. Hung and Brown [38] discussed the mechanism of solid-particle transport through peristaltic motion in a two-dimensional geometry. He concluded that the bolus moves forward by a particle which results in oscillatory motion of the particle. Liron [39] discussed the peristaltic flow both in pipe and channel and developed the solution expression by double expansion for the square of wave number and Reynolds number. He analyzed the efficiency and performance of biological functions in terms of peristaltic flow. Brown and Hung [40] presented analytical solutions for peristaltic flow in a channel. Srivastava and Srivastava [41] addressed the peristaltic flow of a two-fluid, peripheral and core fluid, in a non-uniform channel and tube. The results of the study were in good agreement with the experimental results obtained by Weinberg et al. (ref. [31]). The influence of pulsatile flow in connection with peristalsis in circular cylindrical tube is studied by Srivastava and Srivastava [42]. A numerical solution of peristaltic pumping in a tube is found by using upwind finite-difference scheme by Takabatake et al. [43]. Li and Brasseur [44] presented the analysis for peristalsis in a finite length tubes with arbitrary wave shape and wavenumber whereas the flow is non-steady. Eytan and Elad [45] have discussed the peristaltic flow of Newtonian fluid in an asymmetric channel. Lubrication theory has been employed to obtain the solution in a fixed frame where as flow is taken to be time dependent. Investigation of an incompressible fluid in an asymmetric channel with inertia and streamline curvature effects has been done by Rao and Mishra [46]. Makheimer [47] gives detailed analysis of peristaltic flow of an incompressible viscous fluid through uniform and non-uniform annulus.

So far, we have focused our attention to discuss the behavior of Newtonian fluid in peristaltic flows. In reality, not all fluids exhibit the properties of Newtonian fluid. Therefore, we extend our discussion to non-Newtonian fluids. Most of the physiological fluids like blood, chyme, hydrocarbons, polymer melts, bubbly fluids and some industrial oils show the more complex

stress-strain relation than Newtonian fluid. There is no single constitutive relation which can determine the properties of all fluids. Due to this problem several constitutive models have been offered to determine characteristics of non-Newtonian fluids. Casson [48] extended the equations for flow of pigment oil suspensions used in printing ink type fluid. Eringen [49] discussed the theory of micropolar fluid and studied the properties like couple stresses, body couples, microrotation and microinertial effects in detail. Eringen [50] introduced the theory of microfluids of which micropolar is a special case. Raju and Devanathan [51] were the first to describe the peristaltic flow of power-law fluid in a tube with small wave amplitude. Devi and Devanathan [52] studied the peristaltic motion of micropolar fluid under the assumption of low Reynolds number. Johnson and Segalman [53] developed the theory for viscoelastic fluids exhibiting the property of non-affine deformation. Radhakrishnamacharya [54] observed the peristaltic motion of non-Newtonian fluid in two-dimensional channel with long wavelength consideration. Bohme and Friedrich [55] performed the analysis of an incompressible viscoelastic fluid in a planar channel with no inertia effects. Srivastava and Srivastava [56] modeled the peristaltic motion of blood as two layered fluid and give comparison of uniform and non-uniform tube. Peristaltic motion of blood through stenosed artery has been investigated by Chaturani and Samy [57]. The non-Newtonian fluids considered to satisfy Herschel-Bulkley equation. Moreover, they discussed some arterial diseases briefly. Siddiqui and Schwarz [58, 59] determined the flow characteristics of third and second order fluids in channel and duct. They employed perturbation technique for the solution of problem. Srivastava and Saxena [60] scrutinized the peristaltic flow of blood in a uniform diameter tube. They have used constitutive relation of Casson fluid for blood. Usha and Rao [61] modeled two-layered power law fluids within axisymmetric tubes. Elshehawey et al. [62] discussed the peristaltic motion of Carreau fluid adopting lubrication approach. They applied perturbation technique for small Weissenberg number. Eytan and Elad [63] looked intrauterine fluid motion due to myometric contractions as a peristaltic flow. Transport of food bolus through digestive tract is inspected by Misra and Pandey [64]. Theoretical investigation of peristaltic motion of Casson fluid in axisymmetric channel is done by Mernone and Mazumdar [65]. Hayat et al. [66] examined the influence of Oldroyd-B fluid on peristaltic transport in a two-dimensional channel assuming long wavelength approximation. Vajravelu et al. [67] studied the peristaltic flow of Herschel-Bulkley fluid in

contact with Newtonian fluid. They applied the study to blood flow in small vessels. Hariharan et al. [68] reported a study dealing with peristaltic flow of non-Newtonian fluids i.e. power law and Bingham, in a diverging tube and discussed different wave forms. Nadeem and Akram [69] have modeled the flow of hyperbolic tangent fluid in a two-dimensional channel undergoing peristaltic motion and adopted lubrication approach for problem simplification.

Significance of heat transfer cannot be ignored in industrial and medical applications. Particularly, heat transfer in human body is an important area of research. Bio-heat transfer in tissues has attracted the attention of biomedical engineers for thermotherapy [70] and the human thermoregulation system [71]. The heat transfer in humans takes place as conduction in tissues, perfusion of the arterial-venous blood through the pores of the tissue, metabolic heat generation etc. The other applications are destruction of undesirable cancer tissues, dilution technique in examining blood flow and vasodilation. In connection with peristalsis heat transfer become significant in oxygenation and hemodialysis. Several researchers investigated about heat transfer in peristaltically induced flows (c.f. Heat transfer- a review of 2003 literature by Goldstein et al. [72]).

Generally, viscous dissipation effect is ignored while performing theoretical analysis of fluid flow problems. However, considering this assumption may lead to some serious problems in certain flow situations. The need of considering viscous dissipation effects is felt while dealing with strong temperature-dependent viscosity, high viscosity fluids and high speed gas dynamics. Heat produced due to viscous dissipation may increase the temperature of tube wall consequently decreasing viscosity which results in increased velocity and temperature. Rheological behavior of silicate melts in polymer industry involves viscous dissipation effects [73]. Moreover, it play vital role in rarefied gasses flow by altering the value of Brinkman number [74].

Significance of bio-magnetic fluid dynamics attained a valuable place due to extensive applications which include materials processing, Magneto Hydro Dynamic (MHD) energy generators, cancer therapy [75] and biomedical flow control and separation devices [76]. Its application in biomedical engineering includes hyperthermia regulation in the cardiovascular system by magnetic induction [77], MHD drug targeting [78], magnetofluid rotary blood pumps, MHD bio-micro-fluidic device design and micro-circulation flows [79, 80] etc. Giant Magneto Resistive (GMR) technology is a device which applies magnetic field with very sensitive sensor and

detect small movements of an object in the domain of magnetic field. This technology has improved the research on peristaltic activity inside the tubular structures like bowel, fallopian tube and even in the vas deferens.

It is noticed that when we consider fluid as an ionized gas or conducting when strong magnetic field is applied, it experiences decreased conductivity in the direction transverse to magnetic field. Hence producing an induced current perpendicular to both electric and magnetic fields termed as Hall current. In addition, both electric and magnetic fields can influence the motion of ions and electrons to create drift between them and neutral particles. This drift is called ion slip. For weak magnetic field Hall and ion-slip effects are ignored but become prominent in the presence of strong magnetic field [81]. Therefore, several investigations regarding these effects in peristalsis are performed.

Magnetic field effect for blood flow is investigated by Sud et al. [82]. Agrawal and Anwaruddin [83] studies blood flow through equally branched channel undergoing peristaltic activity. They adopted lubrication approach for their analysis. They concluded that magnetic field may be used as a blood pump during cardiac surgeries. Radhakrishnamacharya and Murty [84] have analyzed heat transfer effects on the flow of Newtonian fluid through a non-uniform channel. Mekheimer [85] presented the study of MHD viscous fluid in a non-uniform channel. Tzirtzilakis [86] presented numerical analysis for flow of viscous fluid through duct under the influence of magnetic field. Elshahed and Haroun [87] discussed MHD peristalsis of Johnson-Segalman fluid in a planar channel. Magnetohydrodynamic peristaltic transport of fourth grade fluid in a wave frame is investigated by Hayat et al. [88]. They concluded that pressure rise and frictional force per wavelength is higher for non-Newtonian fluid than that of Newtonian. Wang et al. [89] explored the numerical solution for peristaltic transport of Sisko fluid under the influence of uniform magnetic field. Mekheimer and Elmagboud [90] canvassed the flow of viscous fluid in a vertical annulus with heat source/sink. Srinivas and Kothandapani [91] observed peristaltic flow of MHD Newtonian fluid in an asymmetric channel. Nadeem and Akbar [92] examined the peristalsis of viscous fluid in a planar channel. Required solution is obtained by employing Adomian Decomposition method. Nadeem and Akbar [93] also discussed the peristaltic flow of non-Newtonian fluid in a non-uniform geometry under long wavelength assumption. Sobh et al. [94] presented investigation for peristaltic activity of Oldroyd fluid in an asymmetric channel

with viscous dissipation effects. Heat transfer analysis of fourth grade fluid in a symmetric channel with induced magnetic field is observed by Hayat and Noreen [95]. Ali et al. [96] considered heat transfer effect on peristaltic motion of viscous fluid in curved channel. Solution for temperature field is calculated numerically. Influence of heat source/sink on electrically conducting hyperbolic tangent fluid in a vertical channel was deliberated by Nadeem and Akram [97]. Hayat et al. [98] considered effect of heat transfer on peristaltic mechanism with variable viscosity. Tripathi [99] modeled and analyzed the swallowing mechanism through esophagus and discussed the heat transfer effect reflux and trapping phenomena.

Investigations regarding fluid flow through porous medium gained considerable importance due to its applications engineering, geo-fluid dynamics and biomechanics. In human physiological systems such flows can be observed in kidneys, lungs, movement of small blood vessels, cartilage and bones etc. Inside human body the tissues can be regarded as deformable porous media. Their work depends on the transport of blood and different nutrients through them. The concept of porous medium in peristalsis was first introduced by Aarts and Ooms [100]. Afterwards, Affi and Gad [101] presented the study for peristaltic flow of pulsatile magneto-fluid saturating porous space. Mekheimer [102] considered the nonlinear peristaltic motion of Newtonian fluid filling an inclined channel with porous medium by making analysis about small wave number. Rao and Mishra [103] looked at peristalsis of power-law fluid through porous tube. They made the analysis in axisymmetric geometry and concluded that the results obtained can best describe the chyme motion in small intestine. Mishra and Rao [104] also examined the peristaltic flow through planar channel with porous medium in the peripheral region whereas viscous fluid fills the core region. A study regarding effect of porous medium on peristaltic flow in axisymmetric channel is presented by Elshehawey et al. [105]. Hall effects on peristaltic flow of Maxwell fluid in a planar channel with uniform porous medium are noticed by Hayat et al. [106]. Kothandapani and Srinivas [107] presented the study regarding peristaltic flow in an inclined channel with porous medium. Reasonable agreement between this and study [105] is noticed. Srinivas and Gayathri [108] have analyzed peristaltic activity in asymmetric vertical channel with heat transfer and porous space. Mekheimer et al. [109] addressed the influence of heat transfer on peristaltic motion of viscous fluid in a vertical channel with asymmetry in the presence of porous medium. Pandey and Chaube [110] presented out effect of external mag-

netic field on channel filled with micropolar fluid with porous medium by considering sinusoidal waves travelling down the walls of channel.

Mass transfer alludes to the movement of mass from one position to another. Regular occurrence of mass transfer can be observed in many engineering processes. Particularly, study of mass transfer has vital position in chemical engineering and more specifically in heat transfer, separation process and reaction engineering. Combined heat and mass transfer has many applications as drying, energy transfer in wet cooling tower, evaporation at the surface of a water body and the flow in dessert cooler. Simultaneous occurrence of heat and mass transfer develops complex relation between the fluxes and the driving potentials. Energy flux due to concentration gradient is termed as thermal diffusion or Dufour effect whereas mass flux generated by temperature gradient is known as Soret effect. Although the diffusion-thermo and thermal-diffusion are regarded small order of magnitude when compared with the influences due to Fouriers or Ficks law but there are conditions when such effects cannot be ignored. For example, the thermal diffusion effect is employed for isotope separation and in mixtures between gases with high molecular weight (H_2 , He) and of medium molecular weight (H_2 , air) [111], the diffusion-thermo effect cannot be omitted. Moreover, blood flow within human body involves heat and mass transfer simultaneously when nutrients diffuse out from blood vessels to the neighboring tissues. Ogulu [112] analyzed the effects of heat generation on the fluid flow with small Reynolds number and mass transport in a lymphatic vessel under the influence of uniform magnetic field. Eldabe et al. [113] considered unsteady peristaltic flow with mixed convection and temperature dependent viscosity. They discussed the situation where one wall is flat while other executing peristaltic activity. Nadeem and Akbar [114] studied the peristaltic motion in an annulus filled with Jeffrey-six constant in the presence of heat and mass transfer. Srinivas et al. [115] focused the attention on peristaltic flow of viscous fluid in vertical asymmetric channel with Soret and Dufour effects. Mixed convective flow of Jeffrey fluid in vertical channel undergoing peristaltic motion is addressed by Safia et al. [116]. Hayat et al. [117] documented influence of heat and mass transfer on peristaltic flow of pseudoplastic fluid where the walls are non-conductive and induced magnetic field is taken. Eldabe et al. [118] reported peristalsis of micropolar fluid by considering heat absorption and chemical reaction. They concluded that the micropolar parameter have deep effect on the convection in porous

medium. MHD peristaltic flow of Powell-Eyring fluid between two coaxial cylinders is examined by Shaaban and Abou-zeid [119].

Convection is a kind of heat transfer where it occurs due to mass transfer. Bulk motion of fluid causes enhancement in heat transfer that can be observed in various physical processes as between the fluid and a solid boundary. The process of conduction occurs due to heat transfer between a solid boundary and static fluid. Boundary conditions in such situation can be calculated through Fourier law of heat conduction. However, when the fluid is moving boundary conditions in such case involve both the conduction and convection. The boundary condition now are because of Fourier law of heat conduction and the Newton law of cooling. Such boundary conditions are termed as convective type [120,121]. Literature witness less attention towards the use of convective conditions in peristalsis (see refs. [122 – 126]).

Viscous theory of fluid satisfies the no-slip boundary condition for the flow analysis. However, when dealing with polymeric fluids, flows that occurs in capillary vessel [127] and rarefied fluid problems [128] no-slip boundary condition does not remain valid. There are devices where no-slip boundary condition is proved inappropriate for momentum and temperature such as flows in microdevices. Thus fluids showing boundary slip behavior can be used in many technological applications like polishing of artificial heart. Mandiwala and Archer [129] investigated the effect of slip conditions on inside wall of rectangular channel. Hayat et al. [130] explored the impact of partial slip on peristaltic motion of viscous liquid by adopting lubrication approach. Adomian Decomposition method is employed for the solution of stream function and velocity. Ali et al. [131] considered the flow of third grade fluid in a circular cylinder with peristaltic activity. They analyzed the problem for slip conditions and presented the comparison of series and numerical solutions. Nadeem and Akram [132] focused the attention on studying slip effects on peristaltic motion of Jeffrey liquid in a channel. A mathematical model for observing simultaneous influence of slip and heat source/sink parameter is studied by Hayat et al. [133]. Homotopy perturbation technique was employed by Yildirim and Sezer [134] to discuss partial slip effects on peristaltic motion of viscous fluid. Kumar et al. [135] discussed the peristalsis in an asymmetric channel with slip effect. Das [136] examined the peristaltic motion of Johnson-Segalman fluid with slip effects when asymmetric channel is inclined. Saravana et al. [137] talked about slip conditions on peristaltic motion of non-Newtonian fluid in an inclined

channel with heat and mass transfer effects. Jyothi and Rao [138] discussed the effect of slip in flow of electrically conducting Williamson fluid. Perturbation technique was adopted to solve nonlinear system of equations. Abbasi et al. [139] reported the influence of mixed convection on peristaltic flow of nanofluid under consideration of slip at the boundaries.

Existing literature indicates that peristaltic flows in different geometries are also discussed for the Newtonian and non-Newtonian fluids in compliant walls channel. The use of compliant coatings has fascinated scientists and engineers by its drag reduction ability. In human physiological systems compliance is defined as the ability of tubular organs to resist recoil to its original position. Some interesting studies may be mentioned to the peristaltic flows of Newtonian and non-Newtonian fluids in channel/tube with compliant boundaries. Mitra and Prasad [140] examined the influence of wall properties on peristaltic motion in a channel. They concluded that mean flow reversal exists both at the center and boundaries of channel. Camenschi [141] and Camenschi and Sandru [142] discussed the viscous fluid flow in thin pipes with elastic wall. Carew and Pedley [143] proposed a mathematical model to study wall deformation and fluid flow in human ureter. Davies and Carpenter [144] presented the stability analysis of channel flow between compliant boundaries. Muthu et al. [145] reported the viscoelastic behavior of circular cylindrical walls on peristaltic motion of flowing fluid. Mean flow reversal in a compliant wall asymmetric channel is addressed by Haroun [146]. Heat transfer characteristics of Newtonian fluid in a two dimensional channel with wall properties are investigated by Radhakrishnamacharya and Srinivasulu [147]. The characteristics of free pumping on peristaltic activity of micropolar fluid in circular cylinder with compliant boundaries are revealed by Muthu et al. [148]. Kothandapani and Srinivas [149] considered heat transfer and porous boundaries effects on magnetohydrodynamic peristaltic flow of viscous fluid in a flexible wall channel. Elnaby and Haroun [150] studied the flow of viscous fluid through a channel with flexible boundaries. Hayat et al. [151,152] explored the influence of compliant boundaries on peristaltic activity of Jhonson-Segalman and Maxwell fluids. MHD peristaltic motion of viscous fluid in a heated channel with flexible boundaries was examined by Srinivas et al. [153] (extension of ref. [149]). The theoretical investigation on the peristaltic flow in a compliant wall channel with heat and mass transfer effects were also looked by Srinivas and Kothandapani [154]. Mustafa et al. [155,156] discussed the analytical and numerical results by considering

nanofluid flow through a compliant wall channel with slip conditions and heat/mass transfer. Eldabe et al. [157] discussed peristalsis of power-law fluid in an asymmetric channel with wall properties. Carreau fluid in a symmetric channel with wall properties and porous space is analyzed by Salih and Abdulhadi [158]. Hayat et al. [159] noticed the effects of thermal radiation and Joule heating in flow of dusty fluid with simultaneous effects of heat and mass transfer.

1.3 Basic equations

It is appropriate to consider the physical laws of conservation while dealing with real flows. These are related with laws of conservation of mass, momentum and energy equations, respectively. Moreover, assumption of conservation of containment allows one to consider an equation additionally which is termed as concentration equation. These are explained as follows:

1.3.1 Mass conservation

The differential equation for law of conservation of mass is known as the continuity equation i.e.

$$\frac{\partial \rho}{\partial t} + \nabla \cdot (\rho \mathbf{V}) = 0, \quad (1.1)$$

in which ρ shows the density, ∇ is the gradient operator and \mathbf{V} stands for velocity. For incompressible fluid

$$\nabla \cdot \mathbf{V} = 0. \quad (1.2)$$

The analysis presented in this study will revolve around incompressible flows.

1.3.2 Momentum conservation

Basic equations of fluid flow describe the "flow field" in terms of velocity profile. These equations contain the velocity components derivative, pressure gradient of fluid and term describing the body force. In vectorial form, the equation can be written as

$$\rho \frac{d\mathbf{V}}{dt} = \nabla \cdot \boldsymbol{\tau} + \rho \mathbf{f}, \quad (1.3)$$

where \mathbf{V} defines the velocity field, $\boldsymbol{\tau}(= -p\mathbf{I} + \mathbf{S})$ presents Cauchy-stress tensor, p is the pressure, \mathbf{I} the identity tensor, \mathbf{S} the extra stress tensor and last term i.e. $\rho\mathbf{f}$ describes the body force. The momentum equation in the the presence of rotation can be modified as under:

$$\rho \frac{d\mathbf{V}}{dt} + \rho [\boldsymbol{\Omega} \times (\boldsymbol{\Omega} \times \mathbf{r}) + 2(\boldsymbol{\Omega} \times \mathbf{V})] = \nabla \cdot \boldsymbol{\tau} + \rho\mathbf{f}, \quad (1.4)$$

where second and third terms on the left hand side present the centrifugal and Coriolis force respectively.

1.3.3 Energy conservation

The equation representing conservation of energy is based on first law of thermodynamics applied on control volume. The transient form of energy equation obeying the ideal gas conditions along with subsonic velocity field can be written as:

$$\rho \frac{de}{dt} = -\nabla \cdot \mathbf{q} + S_t. \quad (1.5)$$

In above equation $e(= C_p T)$ shows internal energy where C_p is the specific heat, $\mathbf{q}(= -\kappa \text{ grad } T)$ stands for heat flux, κ is the thermal conductivity of fluid and S_t is the source term related to transport of energy. This term is also responsible for the modification of heat transport characteristics when velocity components, surface heating cooling, radiative heat flux and viscous dissipation are considered. Moreover, it also stands for Dufour and Joule heating effects.

1.3.4 Concentration equation

Movement of mass in fluid flows is involved in many engineering processes. Transport of mass can be referred to the movement of polluting chemical to particular matter. For driving concentration equation one has to assume conservation of mass within the fluid flow. Two mechanisms responsible for movement of mass are convection and molecular diffusion. Suppose C to be the mass concentration of fluid per unit volume, then the mass equation in vector form can be represented as:

$$\frac{dC}{dt} = D_m \nabla^2 C + \frac{D_m R T}{T_r} \nabla^2 T. \quad (1.6)$$

In above equation D_m stands for mass diffusion coefficient, R_T presents the thermal-diffusion ratio and T_r is the mean temperature.

1.3.5 Maxwells equations

Equations describing the behavior of electric and magnetic fields by discussing basic laws of electromagnetism are termed as Maxwells equations. These are:

Guass' law of electricity

$$\nabla \cdot \mathbf{E} = \frac{\rho_e}{\epsilon_0}. \quad (1.7)$$

Guass' law of magnetism

$$\nabla \cdot \mathbf{B} = 0. \quad (1.8)$$

Faradays law

$$\nabla \times \mathbf{E} = -\frac{\partial \mathbf{B}}{\partial t}. \quad (1.9)$$

Ampere-Maxwell law

$$\nabla \times \mathbf{B} = \mu_0 \mathbf{J} + \mu_0 \epsilon_0 \frac{\partial \mathbf{E}}{\partial t}. \quad (1.10)$$

In the above equations ρ_e shows the charge density, ϵ_0 the permittivity of free space, μ_0 the electric constant, $\mathbf{B}(= \mathbf{B}_0 + \mathbf{B}_1)$ the total magnetic field where \mathbf{B}_0 is the applied magnetic field and \mathbf{B}_1 is the induced magnetic field, \mathbf{E} the electric field and \mathbf{J} the current density.

1.3.6 Compliant wall

Compliance is a measure of tendency of an organ to turn back towards its original pattern upon removal of compressing source. Thus a wall with flexible, stretchable, damping and elastic nature is called compliant wall. It is also capable of keeping fluid in it. In most of the physical phenomena rigid wall assumption remains valid if the disturbance of pressure in the fluid is small so that the deformation of the wall is negligible. But if the channel/duct/tube wall is

assumed to be thin (i.e. ~ 0.05 of the radius or less), or the wall is made of deformable, then the compliant wall approach gives good results.

The governing equation of motion for flexible wall can be written as

$$L(\eta) = p - p_0,$$

$$L = \left[-\tau \frac{\partial^2}{\partial x^2} + m \frac{\partial^2}{\partial t^2} + d_1 \frac{\partial}{\partial t} + B \frac{\partial^4}{\partial x^4} + H \right], \quad (1.11)$$

where L is the operator that is used to represent the motions of stretched membrane, τ the elastic tension, m the mass per unit area, B the flexural rigidity of the plate, d_1 the coefficient of viscous damping and H the spring stiffness and P_0 is the pressure outside of the wall due to tension in the muscles. It is also assumed that $P_0 = 0$ and walls of the channel are inextensible.

Chapter 2

Peristaltic motion of Jeffrey fluid with simultaneous effects of rotation and radiation

2.1 Introduction

The objective of this chapter is to examine the influence of rotation on the peristaltic motion of non-Newtonian fluid. Constitutive relationship of Jeffrey fluid are employed in the mathematical formulation and related analysis. The thermal radiation and Joule heating are also considered. An electrically conducting fluid in a channel with compliant boundaries is taken. Solution expressions are established through assumptions of large wavelength and small Reynolds number. Impact of sundry variables on velocities (axial u and secondary v), temperature (θ) and heat transfer coefficient (Z) are analyzed. Streamline pattern is also discussed.

2.2 Physical model

We have considered an infinite channel of width $2d$ formed by two walls at $z = \pm\eta$. The channel is filled with an incompressible Jeffrey fluid. An infinite sinusoidal wave of wavelength λ and speed c travels along the flexible walls of channel. The fluid and channel are assumed in a state of rigid body rotation with a constant angular speed Ω about the z – *axis* (see Fig. 2.1).

Mathematically, the equation of wall surface is given by

$$z = \eta(x, t) = + \left[d + a \sin \frac{2\pi}{\lambda} (x - ct) \right] \quad \text{at} \quad \text{upper wall}, \quad (2.1)$$

$$z = \eta(x, t) = - \left[d + a \sin \frac{2\pi}{\lambda} (x - ct) \right] \quad \text{at} \quad \text{lower wall}. \quad (2.2)$$

where a and t are the wave amplitude and time respectively. A magnetic field of strength \mathbf{B}_0 is applied in positive z -direction i.e. normal to the channel walls. The magnetic Reynolds number is taken sufficiently small and thus the induced magnetic field is negligible. Velocity for corresponding flow problem is defined as

$$\mathbf{V} = (u(x, z, t), v(x, z, t), w(x, z, t)), \quad (2.3)$$

where the velocity components in the fixed frame of reference in corresponding directions are designated by $u(x, z, t)$, $v(x, z, t)$ and $w(x, z, t)$ respectively.

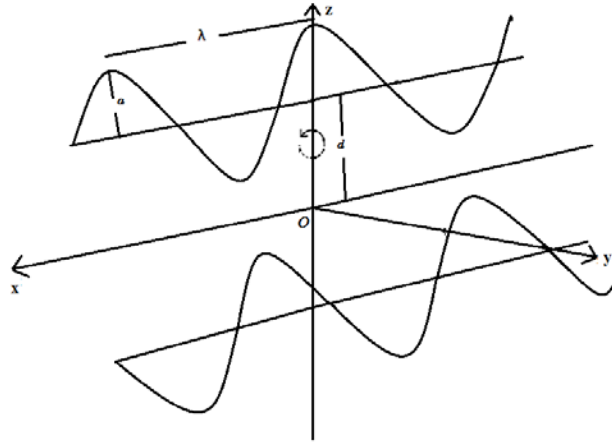


Fig. 2.1: Problem sketch

2.3 Problem formulation

The constitutive equations for the flow of an incompressible Jeffrey fluid are [132]

$$\boldsymbol{\tau} = -\bar{p}\mathbf{I} + \mathbf{S}, \quad (2.4)$$

$$\mathbf{S} = \frac{\mu}{1 + \lambda_1} \left(1 + \lambda_2 \frac{d}{dt} \right) \mathbf{A}_1, \quad (2.5)$$

where \bar{p} is the pressure, \mathbf{I} the identity tensor, μ the dynamic viscosity, λ_1 the ratio of relaxation to retardation times, λ_2 the retardation time and \mathbf{A}_1 the first Rivlin-Ericksen tensor defined as

$$\mathbf{A}_1 = (\text{grad } \mathbf{V}) + (\text{grad } \mathbf{V})^\circ,$$

where \circ indicates the matrix transpose.

The fundamental equations for an incompressible fluid in non-inertial frame are

$$\text{div } \mathbf{V} = 0, \quad (2.6)$$

$$\rho \frac{d\mathbf{V}}{dt} + \rho [\boldsymbol{\Omega} \times (\boldsymbol{\Omega} \times \mathbf{r}) + 2(\boldsymbol{\Omega} \times \mathbf{V})] = \boldsymbol{\nabla} \cdot \boldsymbol{\tau} + \mathbf{J} \times \mathbf{B}, \quad (2.7)$$

$$\rho C_p \frac{dT}{dt} = \kappa \nabla^2 T + \boldsymbol{\tau} \cdot \mathbf{L} + \frac{1}{\sigma} \mathbf{J} \cdot \mathbf{J} - \boldsymbol{\nabla} q_r, \quad (2.8)$$

$$\mathbf{J} = \sigma (\mathbf{V} \times \mathbf{B}),$$

in which \mathbf{V} is the velocity, ρ density of the fluid, $\boldsymbol{\Omega} = \Omega \hat{k}$, \hat{k} the unit vector parallel to z-axis, the angular velocity, $\boldsymbol{\tau}$ the Cauchy stress tensor, C_p the specific heat at constant volume, κ the thermal conductivity, T denotes the temperature, σ the electrical conductivity, q_r the radiative heat flux and $\frac{d}{dt}$ the material time derivative given by

$$\frac{d}{dt} = \frac{\partial}{\partial t} + u \frac{\partial}{\partial x} + v \frac{\partial}{\partial y}.$$

The radiative heat flux through Rosselands' approximation can be reduced in the form [160] :

$$q_r \cong \frac{-4\sigma^*}{3k^*} \frac{\partial T^4}{\partial y}, \quad (2.9)$$

where σ^* and k^* denote the Stefan-Boltzman and Rosseland mean absorption coefficients respectively. Using Taylor series one gets

$$T^4 \cong 4T_1'^3 T - 3T_1'^4, \quad (2.10)$$

where T_1' is the mean temperature of fluid.

Substituting Eq. (2.9) after using Eq. (2.10), the continuity, momentum and energy equa-

tions in the presence of body force become

$$\frac{\partial u}{\partial x} + \frac{\partial w}{\partial z} = 0, \quad (2.11)$$

$$\rho \left[\frac{du}{dt} \right] - 2\rho\Omega v = -\frac{\partial p}{\partial x} + \frac{\partial S_{xx}}{\partial x} + \frac{\partial S_{xy}}{\partial y} + \frac{\partial S_{xz}}{\partial z} - \sigma B_0^2 u, \quad (2.12)$$

$$\rho \left[\frac{dv}{dt} \right] + 2\rho\Omega u = -\frac{\partial p}{\partial y} + \frac{\partial S_{yx}}{\partial x} + \frac{\partial S_{yy}}{\partial y} + \frac{\partial S_{yz}}{\partial z} - \sigma B_0^2 v, \quad (2.13)$$

$$\rho \left[\frac{dw}{dt} \right] = -\frac{\partial p}{\partial z} + \frac{\partial S_{zx}}{\partial x} + \frac{\partial S_{zy}}{\partial y} + \frac{\partial S_{zz}}{\partial z}, \quad (2.14)$$

$$\begin{aligned} \rho C_p \frac{dT}{dt} = & \kappa \left[\frac{\partial^2 T}{\partial x^2} + \frac{\partial^2 T}{\partial y^2} + \frac{\partial^2 T}{\partial z^2} \right] + S_{xx} \frac{\partial u}{\partial x} + S_{xz} \left(\frac{\partial u}{\partial z} + \frac{\partial w}{\partial x} \right) \\ & + S_{zz} \frac{\partial w}{\partial z} + \sigma B_0^2 (u^2 + v^2) + \frac{16\sigma^* T_m^3}{3k^*} \frac{\partial^2 T}{\partial z^2}, \end{aligned} \quad (2.15)$$

where v is secondary velocity due to rotation and modified pressure p is defined as

$$p = \bar{p} - \frac{1}{2}\rho\Omega^2 (x^2 + y^2).$$

The boundary conditions are

$$u = 0, \quad v = 0, \quad T = \begin{Bmatrix} T_1 \\ T_0 \end{Bmatrix} \quad \text{at } z = \pm\eta, \quad (2.16)$$

where T_1 and T_0 are the temperatures of the upper and lower walls respectively. The related equation of motion for the compliant walls is

$$L(\eta) = p - p_0,$$

where L is an operator used to represent the motion of compliant walls with viscous damping forces as follows [140, 144]:

$$L = -\tau' \frac{\partial^2}{\partial x^2} + m_1 \frac{\partial^2}{\partial t^2} + d' \frac{\partial}{\partial t} + b \frac{\partial^4}{\partial x^4} + k_2. \quad (2.17)$$

In above equation τ' is the elastic tension in the membrane, m the mass per unit area, d' the coefficient of viscous damping forces, b the flexural rigidity, k_2 the constant spring stiffness and p_0 the pressure on the outer side of the wall due to the muscles tension. It is assumed that

$p_0 = 0$. The stress continuity condition implies that at the fluid and walls interfaces the pressure must be same as that which acts on the fluid at $z = \pm\eta$. Using x - momentum equation and continuity of stress at $z = \pm\eta$ the dynamic boundary condition can be expressed as follows:

$$\frac{\partial}{\partial x}L(\eta) = \frac{\partial p}{\partial x} = \frac{\partial S_{xx}}{\partial x} + \frac{\partial S_{xy}}{\partial y} + \frac{\partial S_{xz}}{\partial z} - \sigma B_0^2 u + 2\rho\Omega v - \rho \frac{du}{dt} \text{ at } (z = \pm\eta). \quad (2.18)$$

2.3.1 Non-dimensionalization

If $\psi(x, z, t)$ is the stream function then

$$u = \psi_z, \quad w = -\delta\psi_x,$$

Now continuity equation is identically satisfied. We introduce the following non-dimensional variables as follow:

$$\begin{aligned} x^* &= \frac{x}{\lambda}, \quad y^* = \frac{y}{\lambda}, \quad z^* = \frac{z}{d}, \quad p^* = \frac{d^2 p}{c\mu\lambda}, \quad t^* = \frac{ct}{\lambda}, \\ u^* &= \frac{u}{c}, \quad v^* = \frac{v}{c}, \quad w^* = \frac{w}{c}, \quad \mathbf{S}^* = \frac{d\mathbf{S}}{\mu c}, \quad \eta^* = \frac{\eta}{d}, \\ \lambda_2^* &= \frac{c}{d}\lambda_2, \quad \theta = \frac{T - T_0}{T_1 - T_0}. \end{aligned}$$

Using the above transformations and dropping asteriks we get non-dimensional form of Eqs. (2.12) – (2.18)

$$\text{Re } \delta \left[\frac{\partial^2 \psi}{\partial z \partial t} + \frac{\partial \psi}{\partial z} \frac{\partial^2 \psi}{\partial z \partial x} - \frac{\partial \psi}{\partial x} \frac{\partial^2 \psi}{\partial z^2} \right] - 2T' v = -\frac{\partial p}{\partial x} + \delta \frac{\partial}{\partial x} S_{xx} + \delta \frac{\partial}{\partial y} S_{xy} + \frac{\partial}{\partial z} S_{xz} - M^2 \psi_z, \quad (2.19)$$

$$\text{Re } \delta \left[\frac{\partial v}{\partial t} + \frac{\partial \psi}{\partial z} \frac{\partial v}{\partial x} - \frac{\partial \psi}{\partial x} \frac{\partial v}{\partial z} \right] + 2T' \frac{\partial \psi}{\partial z} = -\frac{\partial p}{\partial y} + \delta \frac{\partial}{\partial x} S_{yx} + \delta \frac{\partial}{\partial y} S_{yy} + \frac{\partial}{\partial z} S_{yz} - M^2 v, \quad (2.20)$$

$$\text{Re } \delta^2 \left[-\frac{\partial^2 \psi}{\partial x \partial t} - \frac{\partial \psi}{\partial z} \frac{\partial^2 \psi}{\partial x^2} + \frac{\partial \psi}{\partial x} \frac{\partial^2 \psi}{\partial x \partial z} \right] = -\frac{\partial p}{\partial z} + \delta \frac{\partial}{\partial x} S_{zx} + \delta \frac{\partial}{\partial y} S_{zy} + \frac{\partial}{\partial z} S_{zz}, \quad (2.21)$$

$$\begin{aligned} \delta \text{Pr Re } \left[\frac{\partial \theta}{\partial t} + \frac{\partial \psi}{\partial z} \frac{\partial \theta}{\partial x} + v \frac{\partial \theta}{\partial y} - \frac{\partial \psi}{\partial x} \frac{\partial \theta}{\partial z} \right] &= \left[\delta^2 \frac{\partial^2 \theta}{\partial x^2} + \delta^2 \frac{\partial^2 \theta}{\partial y^2} + \frac{\partial^2 \theta}{\partial z^2} \right] + R \frac{\partial^2 \theta}{\partial z^2} + Ec \text{Pr } M^2 \\ &\times \left(\frac{\partial \psi}{\partial z}^2 + v^2 \right) + \frac{Ec \text{Pr}}{(1 + \lambda_1)} \left(1 + \delta \lambda_2 \frac{d}{dt} \right) \\ &\times \left[4\delta^2 (\psi_{xz})^2 + (\psi_{zz} - \delta^2 \psi_{xx})^2 \right], \end{aligned} \quad (2.22)$$

$$\psi_z = 0, \quad v = 0, \quad \theta = \begin{cases} 1 \\ 0 \end{cases} \quad \text{at } z = \pm \eta, \quad (2.23)$$

$$\begin{aligned} \left[E_1 \frac{\partial^3}{\partial x^3} + E_2 \frac{\partial^3}{\partial x \partial t^2} + E_3 \frac{\partial^2}{\partial x \partial t} + E_4 \frac{\partial^5}{\partial x^5} + E_5 \frac{\partial}{\partial x} \right] \eta &= \delta \frac{\partial}{\partial x} S_{xx} + \delta \frac{\partial}{\partial y} S_{xy} + \frac{\partial}{\partial z} S_{xz} \\ &- M^2 \frac{\partial \psi}{\partial z} + 2T' v - \delta \text{Re } \frac{d\psi_z}{dt} \text{ at } z = \pm \eta, \end{aligned} \quad (2.24)$$

The dimensionless form of η is

$$\eta(x) = (1 + \epsilon \sin 2\pi (x - t)).$$

In above expressions $\text{Re} (= cd/\nu)$ is the Reynolds number, $\delta (= d/\lambda)$ the wave number, $T' (= \text{Re} \Omega d/c)$ the Taylors number, $M^2 (= B_0^2 d^2 \sigma_\mu)$ the Hartman number, $\text{Pr} (= \mu C_p / \kappa)$ the Prandtl number, $R \left(= \frac{16\sigma^* T_1^3}{3\kappa k^*} \right)$ the radiation parameter, $Ec (= c^2 / C_p (T_1 - T_0))$ the Eckert number, $\epsilon (= a/d)$ the amplitude ratio and $E_1 (= -\tau d^3 / \lambda^3 \mu c)$, $E_2 (= m_1 c d^3 / \lambda^3 \mu)$, $E_3 (= d' d^3 / \lambda^2 \mu)$, $E_4 (= b d^3 / c \lambda^5 \mu)$ and $E_5 (= k_2 d^3 / c \lambda \mu)$ are the non-dimensional elasticity parameters.

It should be pointed out that the theory of long wavelength and zero Reynolds number remains applicable for case of chyme transport in small intestine [161]. In this case $c = 2$

cm/min , $a = 1.25\text{ cm}$ and $\lambda = 8.01\text{ cm}$. Here half width of intestine is small in comparison to wavelength i.e. $a/\lambda = 0.156$. It is also declared by Lew et al. [29] that Reynolds number in small intestine was small. Further, the situation of intrauterine fluid flow due to myomaterial contractions is a peristaltic type fluid motion in a cavity. The sagittal cross section of the uterus reveals a narrow channel enclosed by two fairly parallel walls [45]. The $1 - 3\text{ mm}$ width of this channel is very small compared with its 50 mm length [162], defining an opening angle from cervix to fundus of about 0.04 rad . Analysis of dynamics parameters of the uterus revealed frequency, wavelength, amplitude and velocity of the fluid-wall interface during a typical contractile wave were found to be $0.01 - 0.057\text{ Hz}$, $10 - 30\text{ mm}$, $0.05 - 0.2\text{ mm}$ and $0.5 - 1.9\text{ mm/s}$ respectively. Therefore, applying long wavelength and low Reynolds number approximation [21], Eqs. (21 – 26) take the form

$$-2T'v = -\frac{\partial p}{\partial x} + \frac{1}{(1 + \lambda_1)}\psi_{zzz} - M^2\psi_z, \quad (2.25)$$

$$2T'\psi_z = -\frac{\partial p}{\partial y} + \frac{1}{(1 + \lambda_1)}v_{zz} - M^2v, \quad (2.26)$$

$$\frac{\partial p}{\partial z} = 0, \quad (2.27)$$

$$\theta_{zz} = -\frac{EcPr M^2}{(1 + R)}(\psi_z^2 + v^2) + \frac{EcPr}{(1 + R)(1 + \lambda_1)}\psi_{zz}^2, \quad (2.28)$$

$$\psi_z = 0, v = 0, \theta = \begin{cases} 1 \\ 0 \end{cases} \quad \text{at } z = \pm\eta, \quad (2.29)$$

$$\left[E_1 \frac{\partial^3}{\partial x^3} + E_2 \frac{\partial^3}{\partial x \partial t^2} + E_3 \frac{\partial^2}{\partial x \partial t} + E_4 \frac{\partial^5}{\partial x^5} + E_5 \frac{\partial}{\partial x} \right] \eta = \frac{1}{(1 + \lambda_1)}\psi_{zzz} - M^2\psi_z + 2T'v \quad \text{at } y = \pm\eta. \quad (2.30)$$

Equation (2.27) shows that pressure is not the function of z . By using this fact, the pressure can be eliminated from Eq. (2.25). Further, pressure term in Eq. (2.26) can be neglected, as the secondary flow is resulted by the rotation. In view of these facts, we can write Eqs. (2.25)

and (2.26) in the forms

$$-2T'v_z = \frac{1}{(1+\lambda_1)}\psi_{zzzz} - M^2\psi_{zz}, \quad (2.31)$$

$$2T'\psi_z = \frac{1}{(1+\lambda_1)}v_{zz} - M^2v. \quad (2.32)$$

2.4 Exact solutions

Exact solutions of Eqs. (2.28), (2.31) and (2.32) subject to boundary conditions are

$$\psi = B_{13}z + B_{14}\sinh\left[\sqrt{B_1}z\right] + B_{15}\sinh\left[\sqrt{B_2}z\right], \quad (2.33)$$

$$v = \left(B_{21} + B_{22}\cosh\left[\sqrt{B_1}z\right] + B_{23}\cosh\left[\sqrt{B_2}z\right]\right) \\ \times \left(\cosh^2\left[\left(\sqrt{B_1} + \sqrt{B_2}\right)z\right] - \sinh^2\left[\left(\sqrt{B_1} + \sqrt{B_2}\right)z\right]\right), \quad (2.34)$$

$$\theta = A_4z + A_5z^2 + A_6\cosh\left[\sqrt{B_1}z\right] + A_7\cosh^2\left[\sqrt{B_2}z\right] + A_8\cosh\left[2\sqrt{B_1}z\right] \\ + A_9\cosh\left[2\sqrt{B_2}z\right] + A_{10}\cosh\left[\sqrt{B_2}(z-\eta)\right] + A_{11}\cosh\left[\sqrt{B_2}(z+\eta)\right] \\ + A_{12}\cosh\left[\sqrt{B_1}z\right]\cosh\left[\sqrt{B_2}z\right] + A_{13}\sinh\left[\sqrt{B_1}z\right]\sinh\left[\sqrt{B_2}z\right] \\ + A_{14}\sinh^2\left[\sqrt{B_1}z\right] + A_{15}\sinh^2\left[\sqrt{B_2}z\right] + A_{16}. \quad (2.35)$$

The heat transfer coefficient at the wall is given below

$$Z = \eta_x\theta_z(\eta), \\ = A_4 + 2A_5z + A_6\sqrt{B_1}\sinh\left[\sqrt{B_1}z\right] + 2A_7\sqrt{B_2}\cosh\left[\sqrt{B_2}z\right]\sinh\left[\sqrt{B_2}z\right] \\ + 2A_8\sqrt{B_1}\sinh\left[2\sqrt{B_1}z\right] + 2A_9\sqrt{B_2}\sinh\left[2\sqrt{B_2}z\right] \\ + A_{10}\sqrt{B_2}\sinh\left[\sqrt{B_2}(z-\eta)\right] + A_{11}\sqrt{B_2}\sinh\left[\sqrt{B_2}(z+\eta)\right] \\ + A_{12}\left(\sqrt{B_1}\sinh\left[\sqrt{B_1}z\right]\cosh\left[\sqrt{B_2}z\right] + \sqrt{B_2}\cosh\left[\sqrt{B_1}z\right]\sinh\left[\sqrt{B_2}z\right]\right) \\ + A_{13}\left(\sqrt{B_1}\cosh\left[\sqrt{B_1}z\right]\sinh\left[\sqrt{B_2}z\right] + \sqrt{B_2}\sinh\left[\sqrt{B_1}z\right]\cosh\left[\sqrt{B_2}z\right]\right) \\ + 2A_{14}\sqrt{B_1}\sinh\left[\sqrt{B_1}z\right]\cosh\left[\sqrt{B_1}z\right] + 2A_{15}\sqrt{B_2}\sinh\left[\sqrt{B_2}z\right]\cosh\left[\sqrt{B_2}z\right] \quad (2.36)$$

where the values of constants α , β , L_0 , $A_{i's}$ ($i = 1 - 16$) and $B_{i's}$ ($i = 1 - 23$) are given as follows:

$$\begin{aligned}
\alpha &= M^2(1 + \lambda_1), \quad \beta = T'(1 + \lambda_1), \\
L_0 &= 8\epsilon\pi^3 \left(\frac{E_3}{2\pi} \sin[2\pi(x - t)] - (E_1 + E_2) \cos[2\pi(x - t)] + (4\pi^2 E_4 + \frac{E_5}{4\pi^2}) \cos[2\pi(x - t)] \right), \\
A_1 &= \frac{EcPrM^2}{(1 + R)}, \quad A_2 = \frac{EcPr}{(1 + R)(1 + \lambda_1)}, \quad A_3 = 2A_1(\alpha^3 + 20\alpha\beta^2 - 4\alpha^2\beta^2\eta^2 - 16\beta^4\eta^2), \\
A_4 &= \frac{1}{2\eta}, \\
A_5 &= \frac{1}{64B_3^2} L_0^2 \sec h^2[\sqrt{B_1}\eta] (-4A_2B_1B_2^2 - 4A_1(B_2B_1 + B_1(B_2 + 2\alpha + 4i\beta)) - 2B_1B_2(A_2B_1 \\
&\quad + (4A_1 + A_2\alpha - 2iA_2\beta) \cosh[2\sqrt{B_1}\eta] + 2A_1(\cosh[2(\sqrt{B_1} - \sqrt{B_2})\eta] \\
&\quad + \cosh[2(\sqrt{B_1} + \sqrt{B_2})\eta]) \sec h^2[\sqrt{B_2}\eta]), \\
A_6 &= \frac{A_1B_2L_0^2 \sec h[\sqrt{B_1}\eta]}{B_3^2}, \quad A_7 = \frac{A_2B_2^2L_0^2 \sec h^2[\sqrt{B_1}\eta]}{32B_3^2}, \quad A_8 = \frac{A_2B_2^2L_0^2 \sec h^2[\sqrt{B_1}\eta]}{128B_3^2}, \\
A_9 &= \frac{3A_2B_1^2L_0^2 \sec h^2[\sqrt{B_2}\eta]}{128B_3^2}, \quad A_{10} = \frac{A_1B_1L_0^2 \sec h^2[\sqrt{B_2}\eta]}{2B_3^2}, \quad A_{11} = \frac{A_1B_1L_0^2 \sec h^2[\sqrt{B_2}\eta]}{2B_3^2}, \\
A_{12} &= \frac{B_1B_2L_0^2 \sec h[\sqrt{B_1}\eta] \sec h[\sqrt{B_2}\eta]}{8B_3\beta^2} \left(\frac{A_1}{2\beta^2} + \frac{A_2\alpha}{B_3} \right), \\
A_{13} &= -\frac{\sqrt{B_1}\sqrt{B_2}L_0^2 \sec h[\sqrt{B_1}\eta] \sec h[\sqrt{B_2}\eta]}{8B_3\beta^2} \left(A_2 + \frac{A_1\alpha}{2} \right), \\
A_{14} &= \frac{A_2B_2^2L_0^2 \sec h^2[\sqrt{B_1}\eta]}{64B_3^2}, \quad A_{15} = \frac{A_2B_1^2L_0^2 \sec h^2[\sqrt{B_2}\eta]}{64B_3^2}, \\
A_{16} &= \frac{1}{256B_3^2\beta^2} (-4A_3L_0^2 + 32B_3^2\beta^2 - A_2L_0^2(\beta^2((-B_1 + B_2)\alpha + 2i(B_1 + B_2)\beta) + 4B_3(B_3 \\
&\quad - 4\alpha\beta^2\eta^2)) + (-4A_3L_0^2 + 32B_3^2\beta^2 + A_2L_0^2(B_1\beta^2 + 4B_2(-\alpha^3 + 2i\alpha^2\beta - 5\alpha\beta^2 + 6i\beta^3 \\
&\quad + 2B_1^2\beta^2\eta^2))) \times \cosh[2\sqrt{B_1}\eta] - 2(-8B_3^2\beta^2 + A_2L_0^2(\sqrt{B_1}\sqrt{B_2}B_3\alpha + \alpha^4 + 10\alpha^2\beta^2 + 8\beta^4) \\
&\quad + 2A_1L_0^2(\sqrt{B_1}\sqrt{B_2}B_3 + \alpha^3 + 20\alpha\beta^2 - 4\beta^2(\alpha^2 + 4\beta^2)\eta^2)) \cosh[2(\sqrt{B_1} - \sqrt{B_2})\eta] \\
&\quad + 2(8B_3^2\beta^2 + A_2L_0^2(\sqrt{B_1}\sqrt{B_2}B_3\alpha - \alpha^4 - 10\alpha^2\beta^2 - 8\beta^4) + 2A_1L_0^2 \\
&\quad \times (\sqrt{B_1}\sqrt{B_2}B_3 - \alpha(\alpha^2 + 20\beta^2) + 4\beta^2(\alpha^2 + 4\beta^2)\eta^2) \cosh[2(\sqrt{B_1} - \sqrt{B_2})\eta] \\
&\quad - (4A_3L_0^2 - 32B_3^2\beta^2 + A_2L_0^2(B_2^2\beta^2 + 4B_1(\alpha^3 + 2i\alpha^2\beta + 5\alpha\beta^2 + 6i\beta^3 \\
&\quad - 2B_2^2\beta^2\eta^2))) \cosh[2\sqrt{B_2}\eta]) \sec h^2[\sqrt{B_1}\eta] \sec h^2[\sqrt{B_2}\eta],
\end{aligned}$$

$$\begin{aligned}
B_1 &= (\alpha - 2\iota\beta), \quad B_2 = (\alpha + 2\iota\beta), \quad B_3 = (\alpha^2 + 4\beta^2), \quad B_4 = (-i\alpha - 2\beta), \\
B_5 &= (-i\alpha + 2\beta), \quad B_6 = (i\alpha + 2\beta), \quad B_7 = \frac{B_5 L_0 \alpha (4\beta + iB_2 \sec h[\sqrt{B_1}\eta] + B_4 \sec h[\sqrt{B_2}\eta])}{2B_3}, \\
B_8 &= \frac{B_6 L_0 \alpha (4\beta + iB_2 \sec h[\sqrt{B_1}\eta] + B_4 \sec h[\sqrt{B_2}\eta])}{2B_3}, \\
B_9 &= \frac{L_0 \alpha}{8\sqrt{B_1} B_2^{3/2} B_3 B_4} (4\beta + iB_2 \sec h[\sqrt{B_1}\eta] + B_4 \sec h[\sqrt{B_2}\eta]), \\
B_{10} &= (B_2 \alpha \cosh[\sqrt{B_2}\eta] + \cosh[\sqrt{B_1}\eta]) (B_1 \alpha + 8\beta^2 \cosh[\sqrt{B_2}\eta]), \\
B_{11} &= \frac{1}{4B_1^{3/2} B_{10} B_2^{3/2}} (2L_0 \alpha^2 + B_2 (B_8 - 2iL_0 \beta) \cosh[\sqrt{B_2}\eta] + B_1 (B_7 + 2iL_0 \beta) \cosh[\sqrt{B_2}\eta]), \\
B_{12} &= \frac{1}{2B_1^{3/2} B_{10} B_2^{3/2}} (2L_0 \alpha + (B_7 - B_1 L_0) \cosh[\sqrt{B_2}\eta] + \cosh[\sqrt{B_1}\eta] (B_8 - B_2 L_0 \\
&\quad - \frac{2L_0 \alpha \beta \cosh[\sqrt{B_2}\eta] (4\beta + iB_2 \sec h[\sqrt{B_1}\eta] + B_4 \cosh[\sqrt{B_2}\eta])}{B_3})), \\
B_{13} &= 2\sqrt{B_1 B_2} (-2B_{11} \alpha + B_{12} \alpha^2 + 4iB_9 \beta), \quad B_{14} = 2B_2^{3/2} (B_{11} - B_9 - iB_{12} \beta), \\
B_{15} &= 2B_1^{3/2} (B_{11} + B_9 + iB_{12} \beta), \quad B_{16} = (-B_3 B_8 + B_2 B_3 L_0 + 2B_4 L_0 \alpha \beta + 8L_0 \alpha \beta^2 \\
&\quad \times \cosh[\sqrt{B_2}\eta]), \\
B_{17} &= (B_2 (iB_8 + 2L_0 \beta) \cosh[\sqrt{B_1}\eta] + i(2L_0 \alpha^2 + B_1 (B_7 + 2iL_0 \beta) \cosh[\sqrt{B_2}\eta])),
\end{aligned}$$

$$\begin{aligned}
B_{18} &= (iB_2 \cosh[\sqrt{B_2}\eta] + \cosh[\sqrt{B_1}\eta] (B_4 + 4\beta \cosh[\sqrt{B_2}\eta])) \sec h[\sqrt{B_1}\eta] \sec h[\sqrt{B_2}\eta], \\
B_{19} &= (-2B_3 L_0 \alpha + B_{16} \cosh[\sqrt{B_1}\eta] + (-B_3 B_7 + B_1 B_3 L_0 + 2iB_2 L_0 \alpha \beta) \cosh[\sqrt{B_2}\eta]), \\
B_{20} &= (B_2 \alpha \cosh[\sqrt{B_2}\eta] + \cosh[\sqrt{B_1}\eta] (B_1 \alpha + 8\beta^2 \cosh[\sqrt{B_2}\eta])), \\
B_{21} &= \frac{1}{4B_2} \left(-\frac{8B_{17} \beta}{B_{20} B_4} + \frac{8B_{19} \alpha \beta}{B_1 B_{20} B_3} + \frac{8B_{18} L_0 \beta^2}{B_1 B_3} \right), \\
B_{22} &= \frac{1}{4B_2} \left(\frac{2B_{17} B_5}{B_{20} B_4} + \frac{B_{18} B_2 L_0 \alpha}{B_1 B_3} - \frac{4B_{19} B_2 \beta}{B_1 B_{20} B_3} \right), \\
B_{23} &= \frac{1}{4B_2} \left(\frac{2B_{17} B_6}{B_{20} B_4} + \frac{B_{18} L_0 \alpha}{B_3} - \frac{4B_{19} \beta}{B_{20} B_3} \right),
\end{aligned}$$

2.5 Discussion

This section is prepared to study the impact of embedded parameters on different flow quantities. Plots for axial and secondary velocities and temperature are displayed and analyzed through Figs. (2.2 – 2.27).

2.5.1 Analysis of axial velocity

Here Figs. (2.2 – 2.5) are prepared to analyze the influence of pertinent parameter on axial velocity. These Figs. show that velocity traces a parabolic path with maximum value at the center of the channel. Fig. (2.2) shows decrease in velocity when λ_1 is increased. As λ_1 represents the ratio of relaxation to retardation time and increase in its value enhances the relaxation time. It means fluid takes more time to regain its original position and hence velocity decreases. Velocity reduces when the value of M is increased. This is due to the fact that an applied magnetic field exerts a retarding force on the flow (see Fig. 2.3). From Fig. (2.4) it can be seen that increasing T' reduces the velocity of the fluid in axial direction. It is due to the fact that rotation produces flow in perpendicular direction. It shows decrease in the velocity in axial direction. It is also seen from the Fig. that in the absence of rotation velocity is greater. Fig. (2.5) shows that velocity enhances when elasticity parameters E_1 and E_2 are increased. There is decrease in velocity through larger E_3 , E_4 and E_5 . For larger E_1 and E_2 there is an increase in the flow whereas damping E_3 , E_4 and E_5 reduce the velocity when increased.

2.5.2 Analysis of secondary velocity

Figs. (2.6 – 2.9) are prepared for outcome of λ_1 , M , T' and wall properties on the secondary velocity v . The rotation of channel induces a velocity component in the y – direction which in turn produces a fluid flow called secondary flow. Fig. (2.6) shows that the secondary velocity v increases when λ_1 is enhanced. Similar effect is observed for M (see Fig. 2.7). In the absence of rotation there is no secondary velocity but velocity in y – direction increases in presence of rotation (see Fig. 2.8). We can observe the effect of wall properties on secondary flow v through Fig. (2.9). Decrease in v is observed by increasing E_1 and E_2 while it enhances with the increase of E_3 , E_4 and E_5 .

2.5.3 Analysis of temperature profile

To study the effect of pertinent parameter on temperature, Figs. (2.10 – 2.16) have been plotted. It can be noticed from Fig. (2.10) that temperature decreases when we increase the value of λ_1 . As fluid relaxation time increases due to the increment in the value of λ_1 causing decrease in fluid motion. As a result less energy is transferred and hence temperature decreases.

Fig. (2.11) displays that temperature is an increasing function of M . Effect of Ec on θ is shown in Fig. (2.12). It is clear from Fig. that temperature enhances by increasing Ec . Such rise in θ is resulted from the heat generation due to friction caused by shear in the flow. Similar behavior is noticed for Prandtl number (*see Fig. 2.13*). Since it is also related with the viscous effects produced in the flow. Effect of R on θ is depicted in Fig. (2.14). It is observed that temperature decreases by increasing R . Fig. (2.15) reveals that increase in T' causes decrease in θ . The rotation of channel forces the fluid to move fast which in turn makes particles collision strong. Due to this energy transfer enhances causing temperature to decrease. The effects of compliant wall parameters (E_1 , E_2 , E_3 , E_4 and E_5) on θ are sketched in the Fig. (2.16). It is shown that temperature increases via E_1 and E_2 but it decreases with the increase of E_3 , E_4 and E_5 .

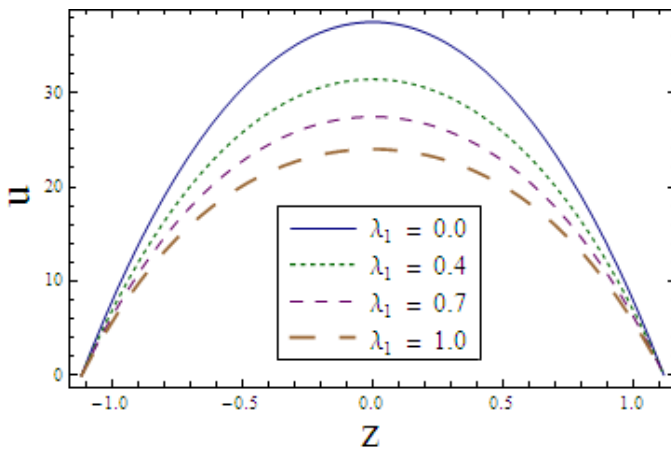
2.5.4 Heat transfer coefficient

Figs. (2.17 – 2.23) disclose the influence of various parameters on heat transfer coefficient Z . Effects of λ_1 and M on Z can be observed through Figs. (2.17) and (2.18) respectively. By increasing these parameters the absolute value of Z increases. The results show that larger Ec and Pr enhance the rate of heat transfer coefficient (*Figs. 2.19 and 2.20*). The effects of radiation (R) and rotation (T') parameters are shown in the Figs. (2.21) and (2.22). These Figs. depict that increase in R and T' results in the increase of Z . It is clear from Fig. (2.23) that larger E_1 and E_2 increase the rate of heat transfer whereas decrease in heat transfer rate is observed for E_3 , E_4 and E_5 .

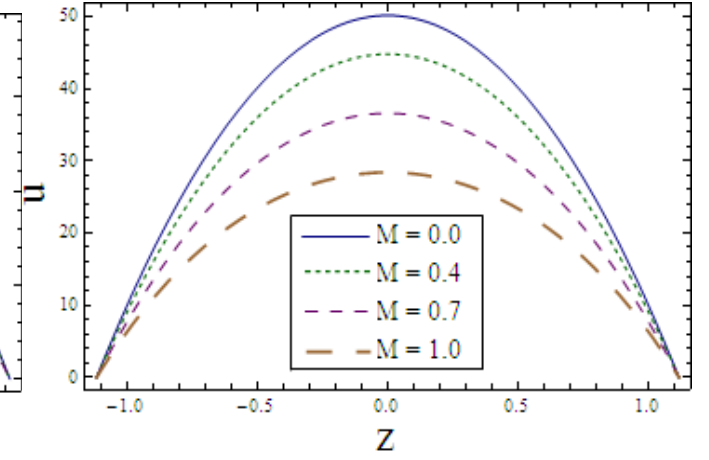
2.5.5 Trapping phenomenon

Figs. (2.24 – 2.27) illustrate the phenomenon of trapped bolus (internally circulating closed streamlines). Fig. (2.24) indicates that size of streamlines decreases with the increase of rotation parameter T' . The increase in the value of M causes decrease in size of streamlines which can be seen through Fig. (2.25). The effects for increasing value of λ_1 on the size and number of streamlines can be observed through Fig. (2.26). Here the size of streamlines decreases whereas number increases through λ_1 . Fig. (2.27) analyzes the effect of wall parameters on streamlines. Here size of streamlines decreases for increasing values of E_1 , E_2 and E_5 whereas it increases

for E_3 . The size and number of streamlines decrease for increasing values of E_4 .



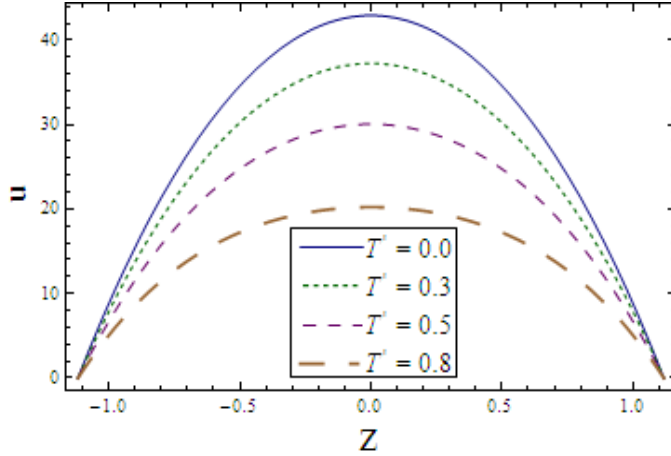
2.2



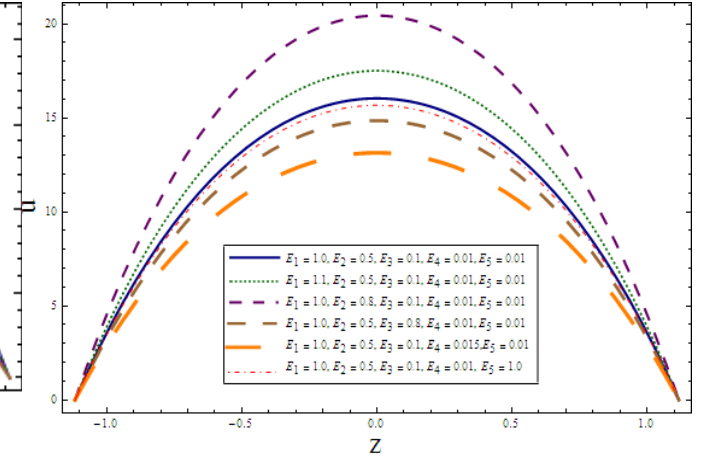
2.3

Fig. 2.2 : Variation of λ_1 on u when $E_1 = 3.0$, $E_2 = 3.0$, $E_3 = 0.01$, $E_4 = 0.1$, $E_5 = 0.1$,
 $T' = 0.5$, $M = 0.5$, $x = 0.2$, $t = 0.1$, $\epsilon = 0.2$.

Fig. 2.3 : Variation of M on u when $E_1 = 3.0$, $E_2 = 3.0$, $E_3 = 0.01$, $E_4 = 0.1$, $E_5 = 0.1$,
 $T' = 0.1$, $\lambda_1 = 0.5$, $x = 0.2$, $t = 0.1$, $\epsilon = 0.2$.



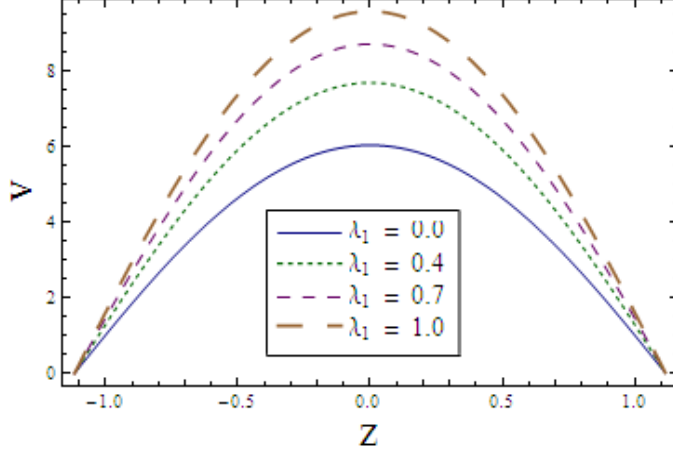
2.4



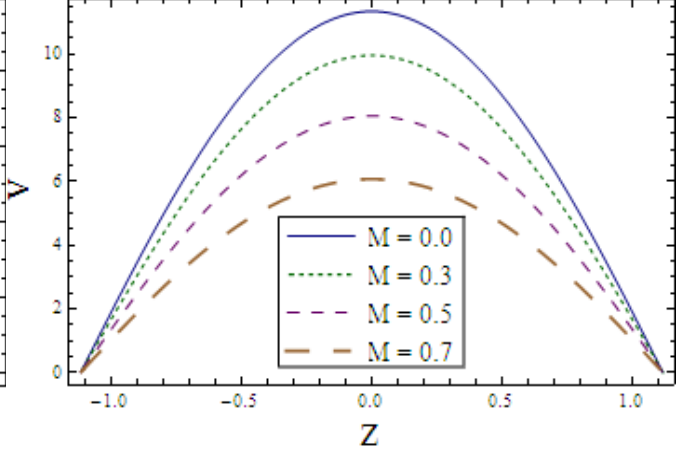
2.5

Fig. 2.4 : Variation of T' on u when $E_1 = 3.0$, $E_2 = 3.0$, $E_3 = 0.01$, $E_4 = 0.1$, $E_5 = 0.1$,
 $M = 0.5$, $\lambda_1 = 0.5$, $x = 0.2$, $t = 0.1$, $\epsilon = 0.2$.

Fig. 2.5 : Variation of wall properties on u when $T' = 0.1$, $\lambda_1 = 0.5$, $M = 0.5$, $x = 0.2$, $t = 0.1$,
 $\epsilon = 0.2$.



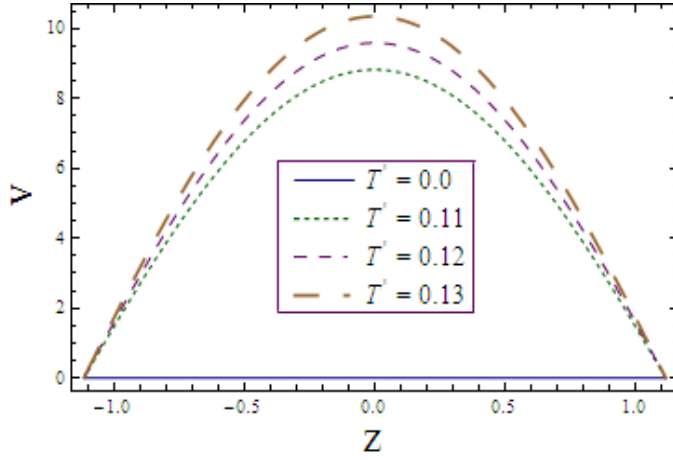
2.6



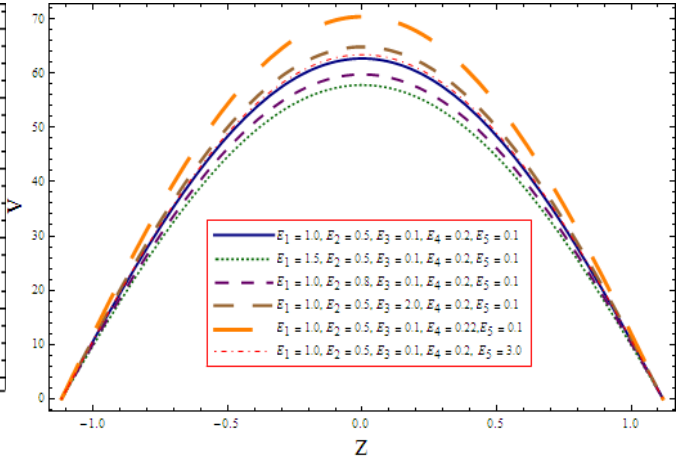
2.7

Fig. 2.6 : Variation of λ_1 on v when $E_1 = 0.5$, $E_2 = 0.5$, $E_3 = 0.01$, $E_4 = 0.1$, $E_5 = 0.6$,
 $M = 0.5$, $T' = 0.1$, $x = 0.2$, $t = 0.1$, $\epsilon = 0.2$.

Fig. 2.7 : Variation of M on v when $E_1 = 0.5$, $E_2 = 0.5$, $E_3 = 0.01$, $E_4 = 0.1$, $E_5 = 0.6$,
 $\lambda_1 = 0.5$, $T' = 0.1$, $x = 0.2$, $t = 0.1$, $\epsilon = 0.2$.



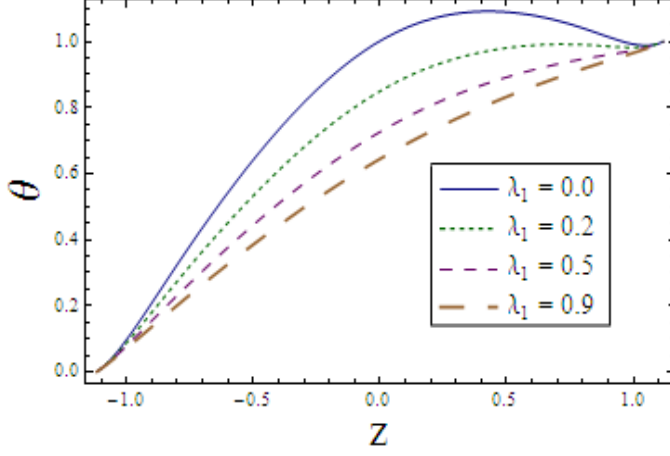
2.8



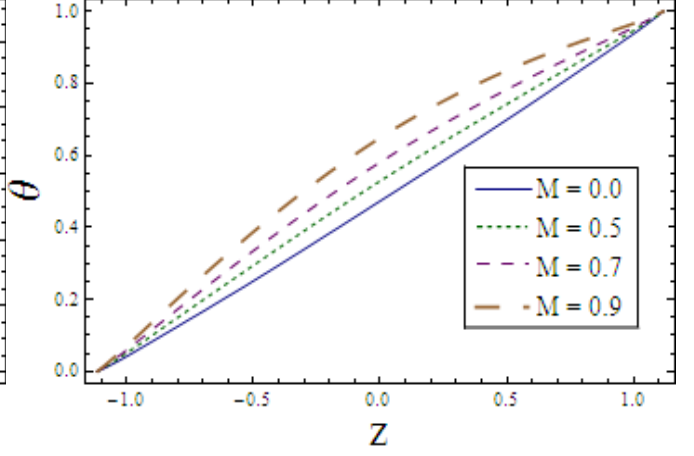
2.9

Fig. 2.8 : Variation of T' on v when $E_1 = 0.5$, $E_2 = 0.5$, $E_3 = 0.01$, $E_4 = 0.1$, $E_5 = 0.6$,
 $M = 0.5$, $\lambda_1 = 0.5$, $x = 0.2$, $t = 0.1$, $\epsilon = 0.2$.

Fig. 2.9 : Variation of wall properties on v when $M = 0.5$, $T' = 0.5$, $\lambda_1 = 0.5$, $x = 0.2$, $t = 0.1$,
 $\epsilon = 0.2$.



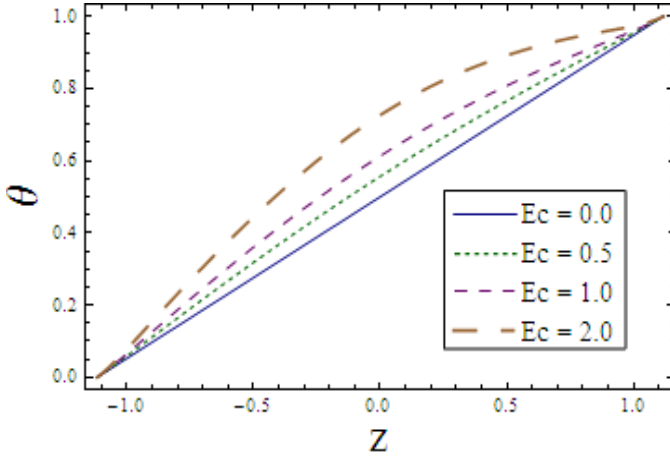
2.10



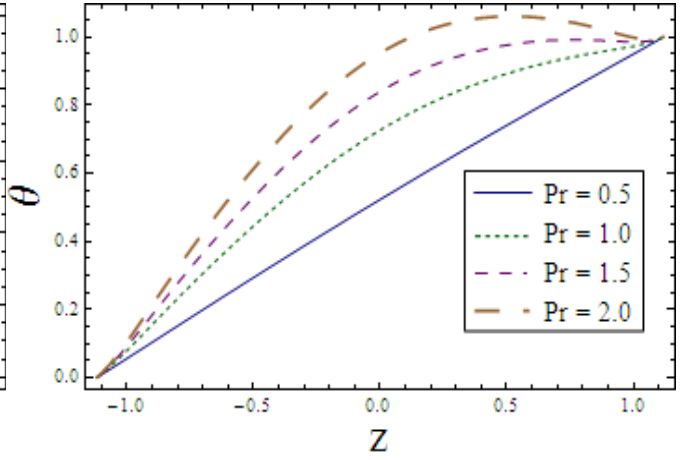
2.11

Fig. 2.10 : Variation of λ_1 on θ when $E_1 = 0.1$, $E_2 = 0.01$, $E_3 = 0.01$, $E_4 = 0.01$, $E_5 = 0.1$,
 $M = 0.8$, $T' = 5.0$, $Pr = 1.0$, $R = 0.8$, $Ec = 2.0$, $x = 0.2$, $t = 0.1$, $\epsilon = 0.2$.

Fig. 2.11 : Variation of M on θ when $E_1 = 0.1$, $E_2 = 0.01$, $E_3 = 0.01$, $E_4 = 0.01$, $E_5 = 0.1$,
 $\lambda_1 = 0.5$, $T' = 5.0$, $Pr = 1.0$, $R = 0.8$, $Ec = 2.0$, $x = 0.2$, $t = 0.1$, $\epsilon = 0.2$.



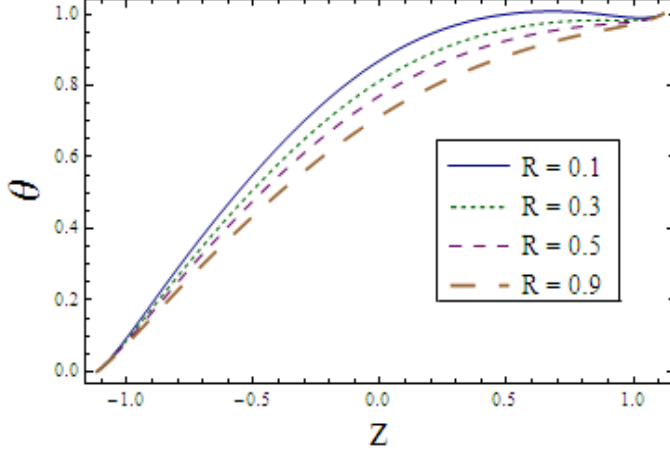
2.12



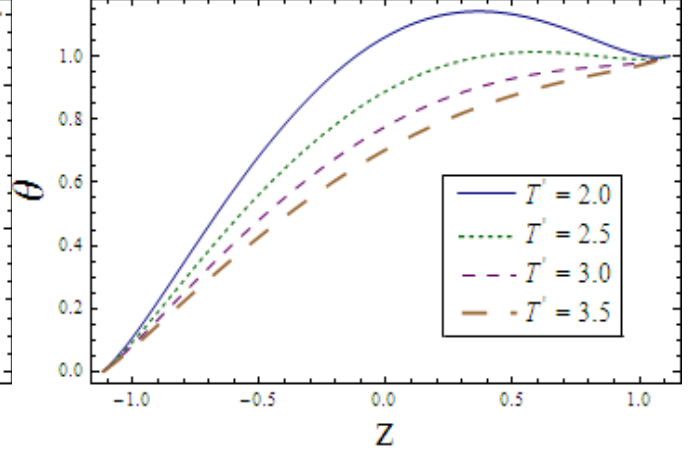
2.13

Fig. 2.12 : Variation of Ec on θ when $E_1 = 0.1$, $E_2 = 0.01$, $E_3 = 0.01$, $E_4 = 0.01$, $E_5 = 0.1$,
 $\lambda_1 = 0.5$, $T' = 5.0$, $Pr = 1.0$, $R = 0.8$, $M = 0.8$, $x = 0.2$, $t = 0.1$, $\epsilon = 0.2$.

Fig. 2.13 : Variation of Pr on θ when $E_1 = 0.1$, $E_2 = 0.01$, $E_3 = 0.01$, $E_4 = 0.01$, $E_5 = 0.1$,
 $\lambda_1 = 0.5$, $T' = 5.0$, $Ec = 2.0$, $R = 0.8$, $M = 0.8$, $x = 0.2$, $t = 0.1$, $\epsilon = 0.2$.



2.14



2.15

Fig. 2.14 : Variation of R on θ when $E_1 = 0.1$, $E_2 = 0.01$, $E_3 = 0.01$, $E_4 = 0.01$, $E_5 = 0.1$, $\lambda_1 = 0.5$, $T' = 5.0$, $Pr = 1.0$, $Ec = 2.0$, $M = 0.8$, $x = 0.2$, $t = 0.1$, $\epsilon = 0.2$.

Fig. 2.15 : Variation of T' on θ when $E_1 = 0.1$, $E_2 = 0.01$, $E_3 = 0.01$, $E_4 = 0.01$, $E_5 = 0.1$, $\lambda_1 = 0.5$, $R = 0.8$, $Pr = 1.0$, $Ec = 2.0$, $M = 0.8$, $x = 0.2$, $t = 0.1$, $\epsilon = 0.2$.

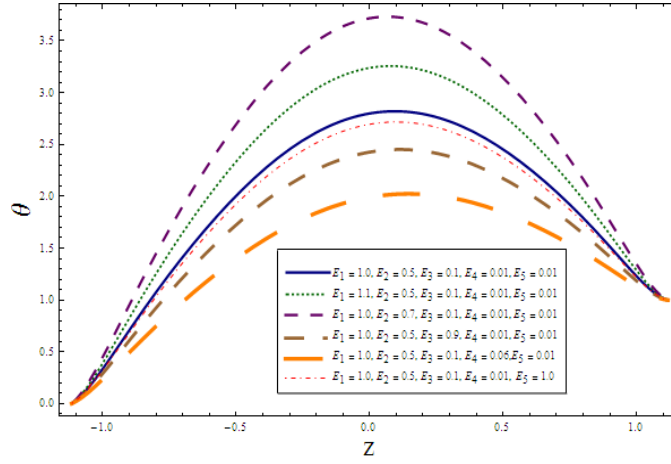
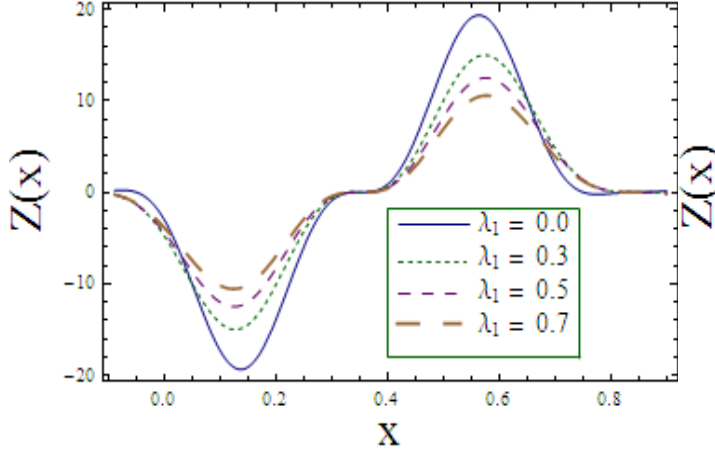
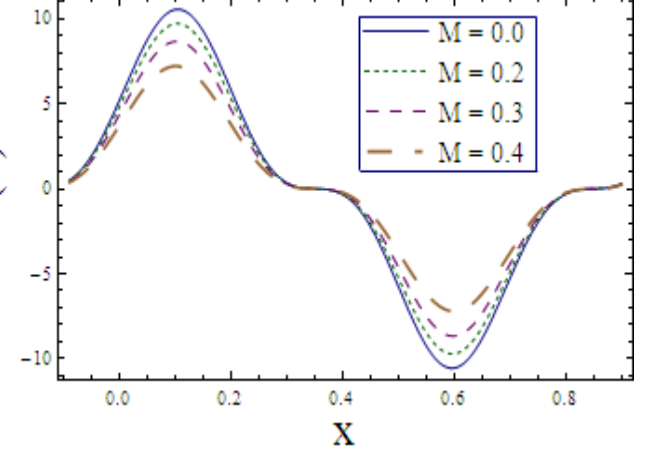


Fig. 2.16. Variation of wall properties on θ when $\lambda_1 = 0.5$, $R = 0.8$, $Pr = 1.0$, $Ec = 2.0$, $M = 0.8$, $T' = 5.0$, $x = 0.2$, $t = 0.1$, $\epsilon = 0.2$.



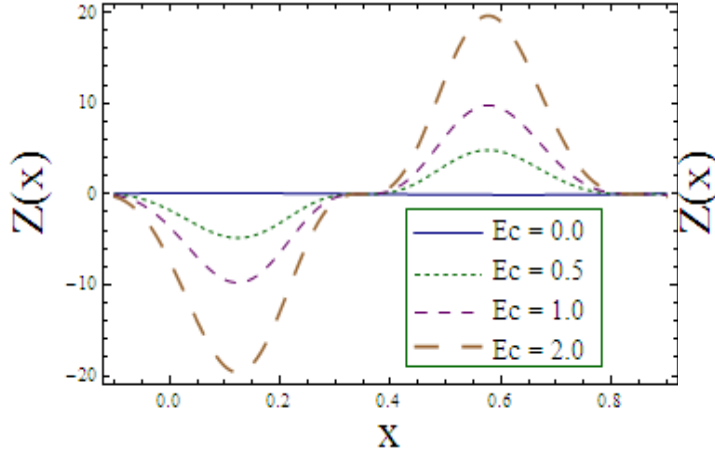
2.17



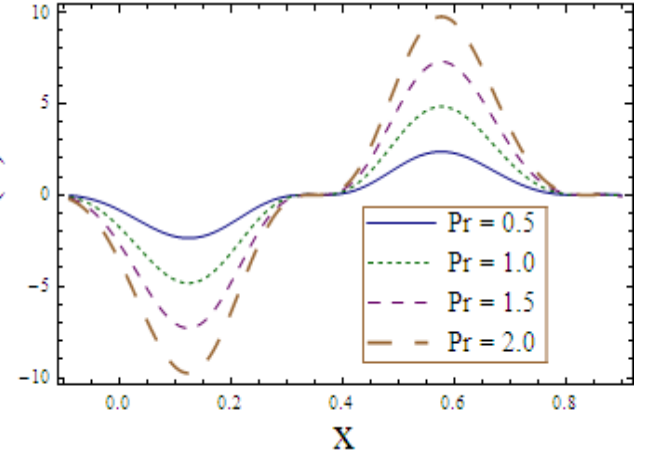
2.18

Fig. 2.17 : Variation of λ_1 on Z when $E_1 = 0.03$, $E_2 = 0.03$, $E_3 = 0.01$, $E_4 = 0.1$, $E_5 = 0.1$,
 $T' = 5.0$, $R = 0.8$, $Pr = 1.0$, $Ec = 2.0$, $M = 1.0$, $t = 0.1$, $\epsilon = 0.2$.

Fig. 2.18 : Variation of M on Z when $E_1 = 0.03$, $E_2 = 0.03$, $E_3 = 0.01$, $E_4 = 0.1$, $E_5 = 0.1$,
 $T' = 5.0$, $R = 0.8$, $Pr = 1.0$, $Ec = 2.0$, $\lambda_1 = 0.8$, $t = 0.1$, $\epsilon = 0.2$.



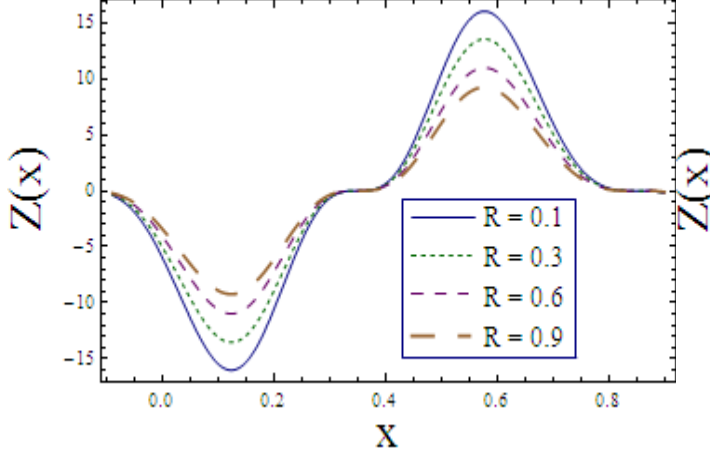
2.19



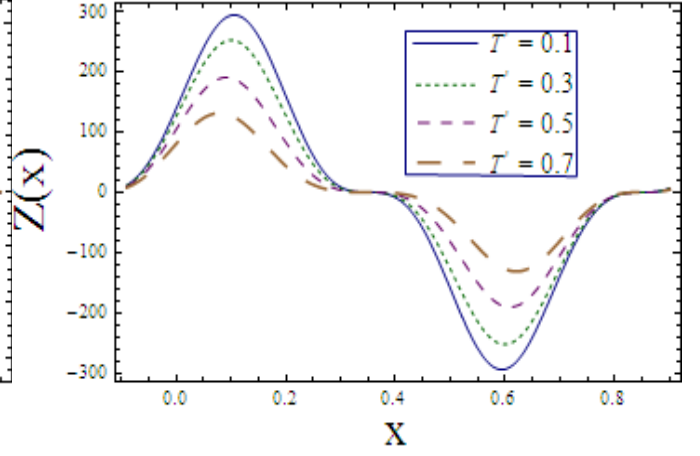
2.20

Fig. 2.19 : Variation of Ec on Z when $E_1 = 0.03$, $E_2 = 0.03$, $E_3 = 0.01$, $E_4 = 0.1$, $E_5 = 0.1$,
 $T' = 5.0$, $R = 0.8$, $Pr = 1.0$, $M = 1.0$, $\lambda_1 = 0.8$, $t = 0.1$, $\epsilon = 0.2$.

Fig. 2.20. Variation of Pr on Z when $E_1 = 0.03$, $E_2 = 0.03$, $E_3 = 0.01$, $E_4 = 0.1$, $E_5 = 0.1$,
 $T' = 5.0$, $R = 0.8$, $Ec = 2.0$, $M = 1.0$, $\lambda_1 = 0.8$, $t = 0.1$, $\epsilon = 0.2$.



2.21



2.22

Fig. 2.21 : Variation of R on Z when $E_1 = 0.03$, $E_2 = 0.03$, $E_3 = 0.01$, $E_4 = 0.1$, $E_5 = 0.1$, $T' = 5.0$, $Pr = 1.0$, $Ec = 2.0$, $M = 1.0$, $\lambda_1 = 0.8$, $t = 0.1$, $\epsilon = 0.2$.

Fig. 2.22 : Variation of T' on Z when $E_1 = 0.03$, $E_2 = 0.03$, $E_3 = 0.01$, $E_4 = 0.1$, $E_5 = 0.1$, $R = 0.8$, $Pr = 1.0$, $Ec = 2.0$, $M = 1.0$, $\lambda_1 = 0.8$, $t = 0.1$, $\epsilon = 0.2$.

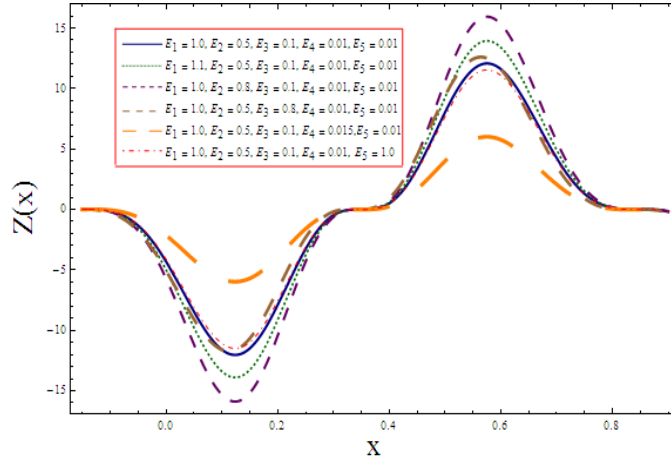


Fig. 2.23 : Variation of wall properties on Z when $T' = 5.0$, $R = 0.8$, $Pr = 1.0$, $Ec = 2.0$, $M = 1.0$, $\lambda_1 = 0.8$, $t = 0.1$, $\epsilon = 0.2$.

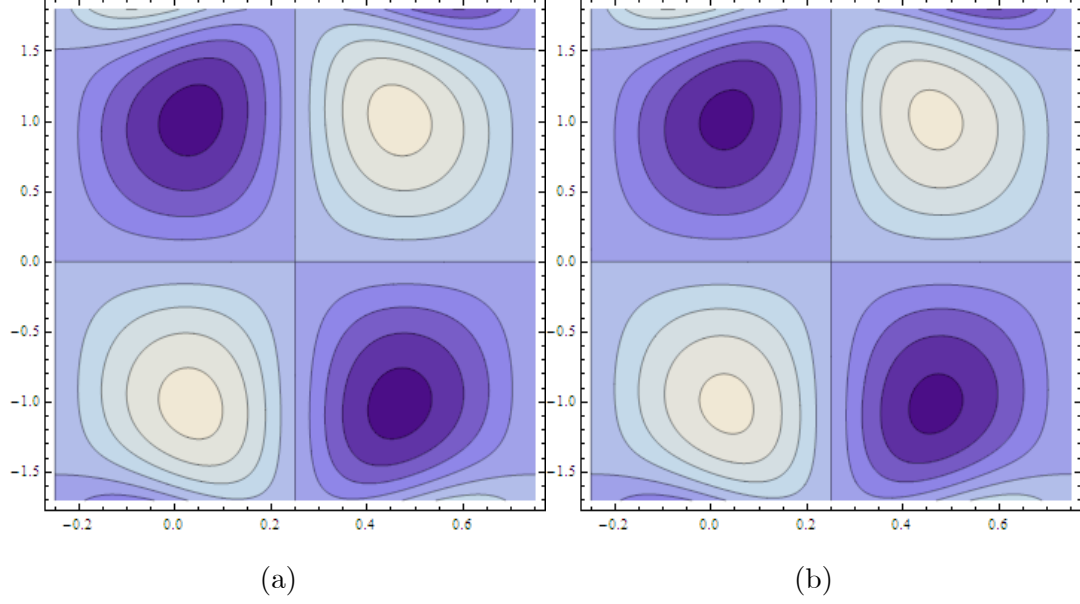


Fig. 2.24 : Streamlines for T' when $E_1 = 0.1$, $E_2 = 0.01$, $E_3 = 0.01$, $E_4 = 0.1$, $E_5 = 0.1$,
 $M = 0.8$, $\lambda_1 = 0.8$, $t = 0.1$, $\epsilon = 0.2$, (a) $T' = 0.1$, (b) $T' = 0.2$.

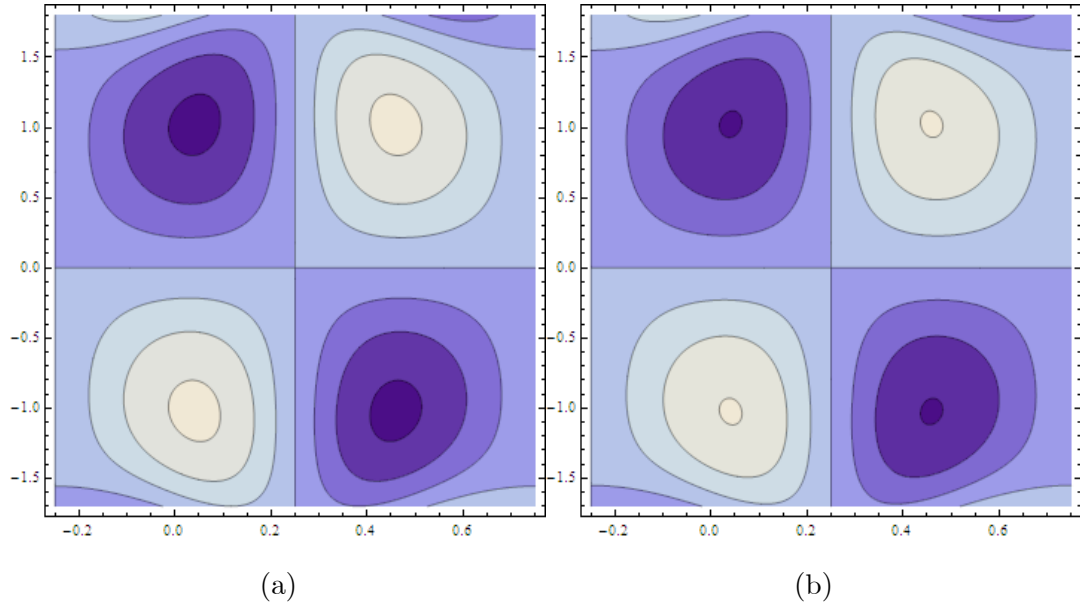


Fig. 2.25 : Streamlines for M when $E_1 = 0.1$, $E_2 = 0.01$, $E_3 = 0.01$, $E_4 = 0.1$, $E_5 = 0.1$,
 $T' = 0.1$, $\lambda_1 = 0.8$, $t = 0.1$, $\epsilon = 0.2$, (a) $M = 0.1$, (b) $M = 0.3$.

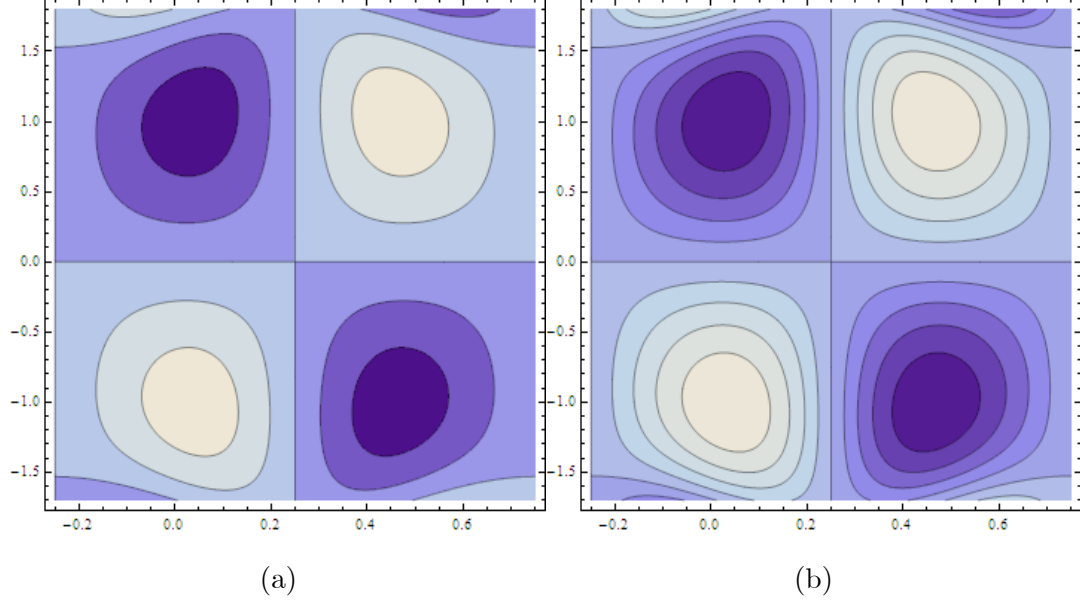
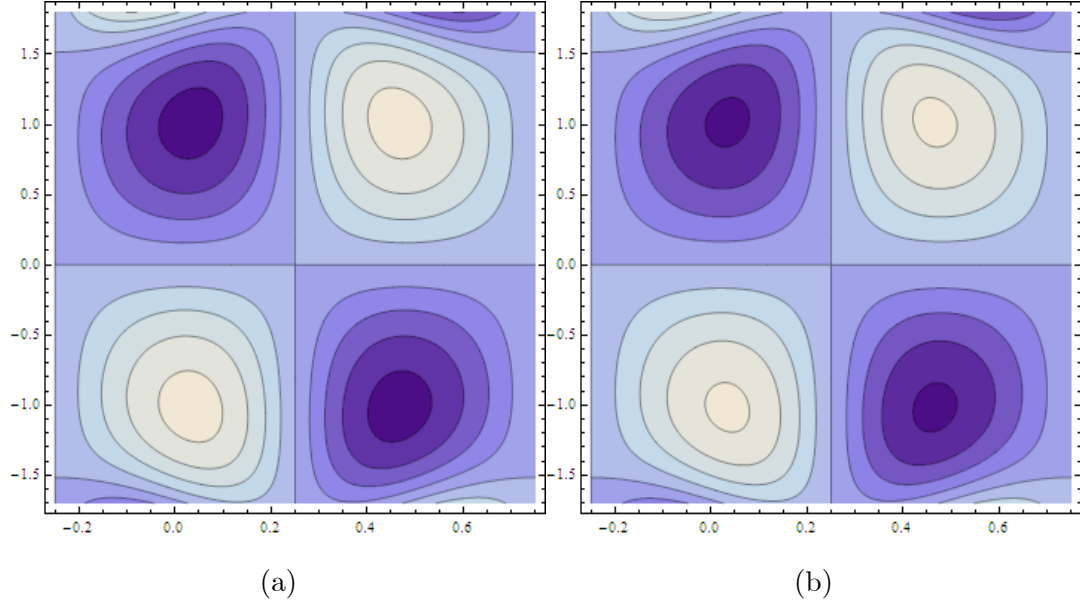
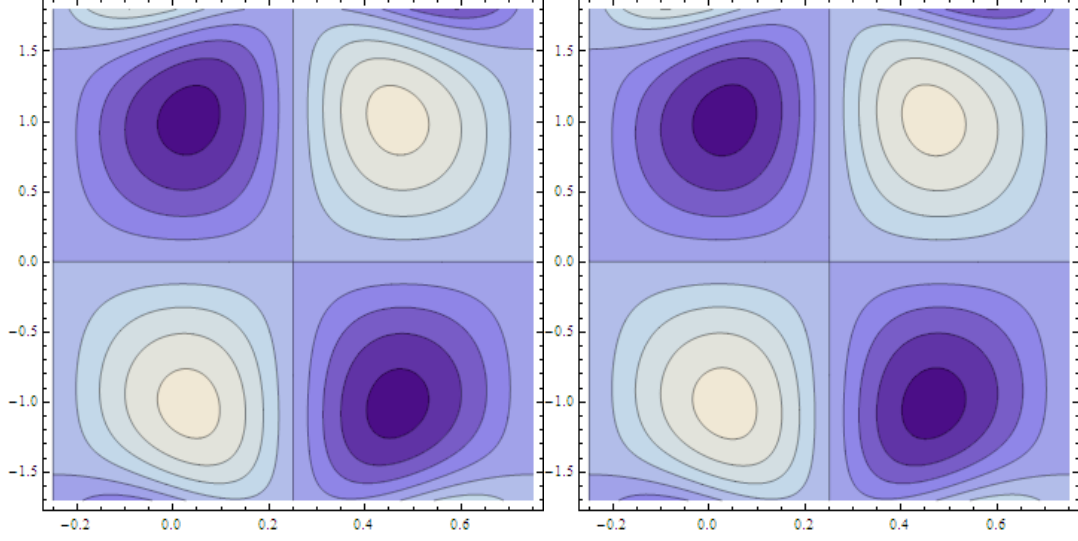


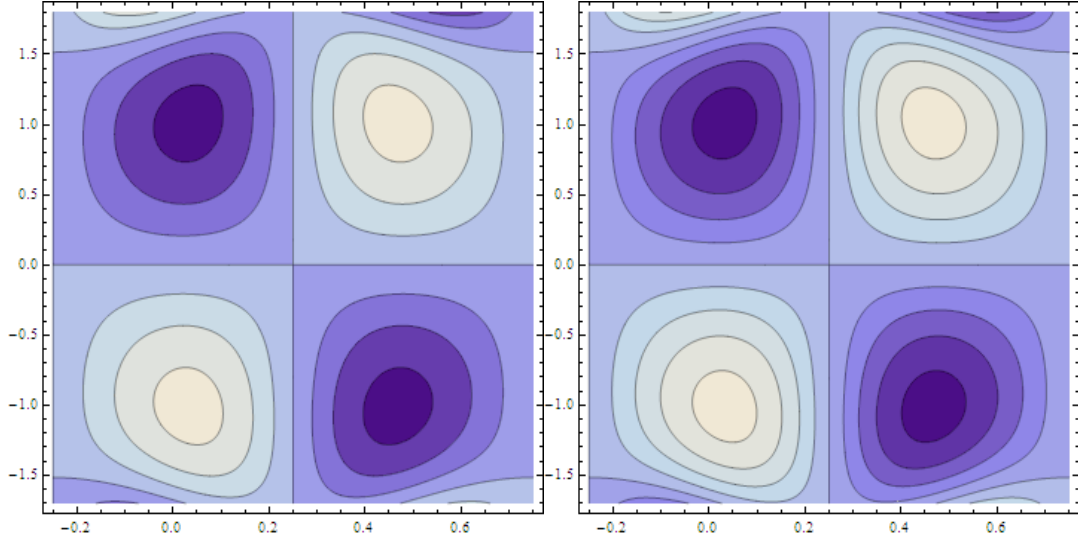
Fig. 2.26 : Streamlines for λ_1 when $E_1 = 0.1$, $E_2 = 0.01$, $E_3 = 0.01$, $E_4 = 0.1$, $E_5 = 0.1$,
 $T' = 0.1$, $M = 0.8$, $t = 0.1$, $\epsilon = 0.2$, (a) $\lambda_1 = 0.1$, (b) $\lambda_1 = 0.3$.





(c)

(d)



(e)

(f)

Fig. 2.27 : Streamlines for wall properties when $T' = 0.1$, $M = 0.8$, $t = 0.1$, $\epsilon = 0.2$, $\lambda_1 = 0.8$,
 (a) $E_1 = 0.1$, $E_2 = 0.01$, $E_3 = 0.01$, $E_4 = 0.1$, $E_5 = 0.1$, (b) $E_1 = 0.3$, (c) $E_2 = 0.03$, (d)
 $E_3 = 0.03$, (e) $E_4 = 0.3$, (f) $E_5 = 0.3$.

2.6 Closing remarks

The peristaltic flow of Jeffrey fluid in a channel with heat transfer is discussed. Both the fluid and channel are in rigid body rotation. Main findings of the study are:

- Axial velocity is decreasing function of λ_1 , M and T' .
- Similar behaviors on axial velocity are observed for E_1 and E_2 . However opposite behavior is seen for E_3 , E_4 and E_5 .
- Secondary velocity shows opposite effect to axial velocity for λ_1, T' and wall properties except for M .
- Temperature decreases for λ_1 , R and T' whereas it increases for Ec and Pr .
- Temperature and axial velocity show similar behavior for the wall parameters.
- Size of streamlines decreases for T' , M and λ_1 .
- Decrease in the size of trapped bolus is seen when we increase wall parameters except E_3 .

Chapter 3

MHD peristaltic rotating flow of Jeffrey fluid in presence of porous medium and Soret and Dufour effects

3.1 Introduction

This chapter addresses influence of rotation on peristaltic motion of an incompressible Jeffrey fluid in a channel with flexible walls. Analysis is presented by taking Soret and Dufour effects. Fluid saturates the porous medium. Modified Darcys law is employed. Modified Darcys law is employed. A uniform magnetic field is applied. Magnetic Reynolds number is taken small. Large wavelength and low Reynolds number is considered. Exact solutions for stream function, temperature and concentration profile are constructed. The impact of relevant parameters is graphically sketched.

3.2 Problem development

We examine peristaltic motion of Jeffrey liquid in a compliant wall channel. An incompressible liquid saturates the porous space between the flexible walls of channel. Fluid is electrically

conducting due to uniform applied magnetic field of strength B_0 . Induced magnetic field subject to low magnetic Reynolds number is neglected. Electric field contribution is not taken into account. Effects of Soret and Dufour and thermal radiation are retained. The whole system is in a rotating frame with constant angular velocity Ω . The channel walls are taken at $z = \pm\eta$. Shapes of the travelling waves are described by the following expression:

$$z = \pm\eta(x, t) = \pm \left[d + a \sin \frac{2\pi}{\lambda} (x - ct) \right], \quad (3.1)$$

where a depicts the wave amplitude, t the time, d the half width of channel, λ the wavelength and c the wave speed. The fundamental equations governing the present flow and heat/mass transfer are represented by

$$\nabla \cdot \mathbf{V} = 0, \quad (3.2)$$

$$\rho \frac{d\mathbf{V}}{dt} + \rho [\boldsymbol{\Omega} \times (\boldsymbol{\Omega} \times \mathbf{r}) + 2(\boldsymbol{\Omega} \times \mathbf{V})] = \nabla \cdot \boldsymbol{\tau} + \mathbf{J} \times \mathbf{B} + \mathbf{R}, \quad (3.3)$$

$$\rho C_p \frac{dT}{dt} = \kappa \nabla^2 T + \boldsymbol{\tau} \cdot \mathbf{L} + \frac{DK_T}{C_s} \nabla^2 C - \nabla q_r, \quad (3.4)$$

$$\frac{dC}{dt} = D \nabla^2 C + \frac{DK_T}{T_m} \nabla^2 T, \quad (3.5)$$

in which ρ shows the fluid density, $\boldsymbol{\tau}$ the Cauchy stress tensor, $\boldsymbol{\Omega} = \Omega \hat{k}$ the angular velocity, C_p the specific heat at constant volume, κ the thermal conductivity, T the temperature of fluid, D the coefficient of mass diffusivity, K_T the thermal diffusion ratio, C_s the concentration susceptibility, C the concentration of fluid, T_m the mean temperature of fluid and μ the dynamic viscosity.

On the basis of Jeffrey fluid model the expression of Darcys resistance is [174]:

$$\mathbf{R} = -\frac{\mu\Phi}{K(1+\lambda_1)} \left(1 + \lambda_2 \frac{d}{dt}\right) \mathbf{V}, \quad (3.6)$$

where Φ ($0 < \Phi < 1$) and K (> 0) are respectively the (constant) porosity and permeability of

the porous medium. Eqs. (3.2 – 3.5) after using Eq. (3.6) yield

$$\frac{\partial u}{\partial x} + \frac{\partial w}{\partial z} = 0, \quad (3.7)$$

$$\begin{aligned} \rho \left[\frac{du}{dt} \right] - 2\rho\Omega v &= -\frac{\partial p}{\partial x} + \frac{\partial S_{xx}}{\partial x} + \frac{\partial S_{xy}}{\partial y} + \frac{\partial S_{xz}}{\partial z} - \sigma B_0^2 u \\ &\quad - \frac{\mu\Phi}{K(1+\lambda_1)} \left(1 + \lambda_2 \frac{d}{dt}\right) u, \end{aligned} \quad (3.8)$$

$$\begin{aligned} \rho \left[\frac{dv}{dt} \right] + 2\rho\Omega u &= -\frac{\partial p}{\partial y} + \frac{\partial S_{yx}}{\partial x} + \frac{\partial S_{yy}}{\partial y} + \frac{\partial S_{yz}}{\partial z} - \sigma B_0^2 v \\ &\quad - \frac{\mu\Phi}{K(1+\lambda_1)} \left(1 + \lambda_2 \frac{d}{dt}\right) v, \end{aligned} \quad (3.9)$$

$$\begin{aligned} \rho \left[\frac{dw}{dt} \right] &= -\frac{\partial p}{\partial z} + \frac{\partial S_{zx}}{\partial x} + \frac{\partial S_{zy}}{\partial y} + \frac{\partial S_{zz}}{\partial z} - \frac{\mu\Phi}{K(1+\lambda_1)} \\ &\quad \times \left(1 + \lambda_2 \frac{d}{dt}\right) w. \end{aligned} \quad (3.10)$$

in which the modified pressure $\hat{p} = p - \frac{1}{2}\rho\Omega^2(x^2 + y^2)$. Employing Rosselands approximation for radiative heat flux [160] and considering Soret and Dufour [122] effects one can have energy and concentration Eqs. as follows:

$$\begin{aligned} \rho C_p \frac{dT}{dt} &= \kappa \left[\frac{\partial^2 T}{\partial x^2} + \frac{\partial^2 T}{\partial y^2} + \frac{\partial^2 T}{\partial z^2} \right] + S_{xx} \frac{\partial u}{\partial x} + S_{xz} \left(\frac{\partial u}{\partial z} + \frac{\partial w}{\partial x} \right) + S_{zz} \frac{\partial w}{\partial z} \\ &\quad + \frac{DK_T}{C_s} \left[\frac{\partial^2 C}{\partial x^2} + \frac{\partial^2 C}{\partial y^2} + \frac{\partial^2 C}{\partial z^2} \right] + \frac{16\sigma^* T_m^3}{3k^*} \frac{\partial^2 T}{\partial z^2}, \end{aligned} \quad (3.11)$$

$$\frac{dC}{dt} = D \left[\frac{\partial^2 C}{\partial x^2} + \frac{\partial^2 C}{\partial y^2} + \frac{\partial^2 C}{\partial z^2} \right] + \frac{DK_T}{T_m} \left[\frac{\partial^2 T}{\partial x^2} + \frac{\partial^2 T}{\partial y^2} + \frac{\partial^2 T}{\partial z^2} \right]. \quad (3.12)$$

Compliant wall condition is

$$\begin{aligned} \frac{\partial}{\partial x} L(\eta) &= \frac{\partial p}{\partial x} = \frac{\partial S_{xx}}{\partial x} + \frac{\partial S_{xy}}{\partial y} + \frac{\partial S_{xz}}{\partial z} - \sigma B_0^2 u + 2\rho\Omega v - \rho \frac{du}{dt} \\ &\quad - \frac{\mu\Phi}{K(1+\lambda_1)} \left(1 + \lambda_2 \frac{d}{dt}\right) u \quad \text{at} \quad (z = \pm\eta). \end{aligned} \quad (3.13)$$

Non-dimensional variables can be put into the following forms:

$$\begin{aligned} x^* &= \frac{x}{\lambda}, \quad y^* = \frac{y}{\lambda}, \quad z^* = \frac{z}{d}, \quad p^* = \frac{d^2 \hat{p}}{c\mu\lambda}, \quad t^* = \frac{ct}{\lambda}, \\ u^* &= \frac{u}{c}, \quad v^* = \frac{v}{c}, \quad w^* = \frac{w}{c}, \quad \mathbf{S}^* = \frac{d\mathbf{S}}{\mu c}, \quad \eta^* = \frac{\eta}{d}, \\ \lambda_2^* &= \frac{c}{d}\lambda_2, \quad \theta = \frac{T - T_0}{T_1 - T_0}, \quad \phi = \frac{C - C_0}{C_1 - C_0}. \end{aligned}$$

Using above mentioned variables and defining stream function by

$$u = \psi_z, \quad w = -\delta\psi_x,$$

Eqs. (3.8 – 3.12) give

$$\begin{aligned} \text{Re } \delta \left[\frac{\partial^2 \psi}{\partial z \partial t} + \frac{\partial \psi}{\partial z} \frac{\partial^2 \psi}{\partial z \partial x} - \frac{\partial \psi}{\partial x} \frac{\partial^2 \psi}{\partial z^2} \right] - 2T'v &= -\frac{\partial p}{\partial x} + \delta \frac{\partial}{\partial x} S_{xx} + \delta \frac{\partial}{\partial y} S_{xy} + \frac{\partial}{\partial z} S_{xz} - M^2 \psi_z \\ &\quad - \frac{1}{K_1(1 + \lambda_1)} \left[1 + \delta \lambda_2 \frac{d}{dt} \right] \psi_z, \end{aligned} \quad (3.14)$$

$$\begin{aligned} \text{Re } \delta \left[\frac{\partial v}{\partial t} + \frac{\partial \psi}{\partial z} \frac{\partial v}{\partial x} - \frac{\partial \psi}{\partial x} \frac{\partial v}{\partial z} \right] + 2T' \frac{\partial \psi}{\partial z} &= -\frac{\partial p}{\partial y} + \delta \frac{\partial}{\partial x} S_{yx} + \delta \frac{\partial}{\partial y} S_{yy} + \frac{\partial}{\partial z} S_{yz} - M^2 v \\ &\quad - \frac{1}{K_1(1 + \lambda_1)} \left[1 + \delta \lambda_2 \frac{d}{dt} \right] v, \end{aligned} \quad (3.15)$$

$$\begin{aligned} \text{Re } \delta^2 \left[-\frac{\partial^2 \psi}{\partial x \partial t} - \frac{\partial \psi}{\partial z} \frac{\partial^2 \psi}{\partial x^2} + \frac{\partial \psi}{\partial x} \frac{\partial^2 \psi}{\partial x \partial z} \right] &= -\frac{\partial p}{\partial z} + \delta \frac{\partial}{\partial x} S_{zx} + \delta \frac{\partial}{\partial y} S_{zy} + \frac{\partial}{\partial z} S_{zz} \\ &\quad + \frac{\delta}{K_1(1 + \lambda_1)} \left[1 + \delta \lambda_2 \frac{d}{dt} \right] \psi_x, \end{aligned} \quad (3.16)$$

$$\begin{aligned} \delta \text{Pr Re } \left[\frac{\partial \theta}{\partial t} + \frac{\partial \psi}{\partial z} \frac{\partial \theta}{\partial x} + v \frac{\partial \theta}{\partial y} - \frac{\partial \psi}{\partial x} \frac{\partial \theta}{\partial z} \right] &= \left[\delta^2 \frac{\partial^2 \theta}{\partial x^2} + \delta^2 \frac{\partial^2 \theta}{\partial y^2} + \frac{\partial^2 \theta}{\partial z^2} \right] + R \frac{\partial^2 \theta}{\partial z^2} \\ &\quad + Du \text{Pr} \left[\delta^2 \frac{\partial^2 \phi}{\partial x^2} + \delta^2 \frac{\partial^2 \phi}{\partial y^2} + \frac{\partial^2 \phi}{\partial z^2} \right] + \frac{Ec \text{Pr}}{(1 + \lambda_1)} \\ &\quad \times \left(1 + \delta \lambda_2 \frac{d}{dt} \right) \left[\begin{aligned} &4\delta^2 (\psi_{xz})^2 \\ &+ (\psi_{zz} - \delta^2 \psi_{xx})^2 \end{aligned} \right], \end{aligned} \quad (3.17)$$

$$\begin{aligned} \text{Re } \delta \left[\frac{\partial \phi}{\partial t} + \frac{\partial \psi}{\partial z} \frac{\partial \phi}{\partial x} + v \frac{\partial \phi}{\partial y} - \frac{\partial \psi}{\partial x} \frac{\partial \phi}{\partial z} \right] &= \frac{1}{Sc} \left[\delta^2 \frac{\partial^2 \phi}{\partial x^2} + \delta^2 \frac{\partial^2 \phi}{\partial y^2} + \frac{\partial^2 \phi}{\partial z^2} \right] \\ &\quad + Sr \left[\delta^2 \frac{\partial^2 \theta}{\partial x^2} + \delta^2 \frac{\partial^2 \theta}{\partial y^2} + \frac{\partial^2 \theta}{\partial z^2} \right]. \end{aligned} \quad (3.18)$$

where continuity equation (3.7) is identically satisfied. The boundary conditions are now re-

duced as follows:

$$\psi_z = 0, \quad v = 0, \quad \theta = \begin{Bmatrix} 1 \\ 0 \end{Bmatrix} \quad \text{at } z = \pm\eta, \quad (3.19)$$

$$\begin{aligned} \left[E_1 \frac{\partial^3}{\partial x^3} + E_2 \frac{\partial^3}{\partial x \partial t^2} + E_3 \frac{\partial^2}{\partial x \partial t} + E_4 \frac{\partial^5}{\partial x^5} + E_5 \frac{\partial}{\partial x} \right] \eta &= \delta \frac{\partial}{\partial x} S_{xx} + \delta \frac{\partial}{\partial y} S_{xy} + \frac{\partial}{\partial z} S_{xz} \\ &\quad - M^2 \frac{\partial \psi}{\partial z} + 2T' v - \delta \operatorname{Re} \frac{d\psi_z}{dt} \\ &\quad - \frac{1}{K_1(1+\lambda_1)} \left[1 + \delta \lambda_2 \frac{d}{dt} \right] \psi_z \quad \text{at } z = \pm\eta, \end{aligned} \quad (3.20)$$

where the dimensionless form of η is written as

$$\eta = (1 + \epsilon \sin 2\pi(x - t)),$$

where $\operatorname{Re} (= cd/\nu)$ is the Reynolds number, $\delta (= d/\lambda)$ the wave number, $T' (= \operatorname{Re} \Omega d/c)$ the Taylor number, $M^2 (= B_0^2 d^2 \varepsilon / \mu)$ the Hartman number, $K_1 (= \frac{K}{\Phi d^2})$ the permeability parameter, $\operatorname{Pr} (= \mu C_p / \kappa)$ the Prandtl number, $R (= \frac{16\sigma^* T_1^3}{3\kappa k^*})$ the radiation parameter, $Ec (= c^2 / C_p (T_1 - T_0))$ the Eckert number, $Du (= \frac{DK_T(C_1 - C_0)}{C_s \mu C_p (T_1 - T_0)})$ the Dufour number, $Sr (= \frac{\rho DK_T(T_1 - T_0)}{\mu T_m (C_1 - C_0)})$ the Soret number, $Sc (= \frac{\nu}{D})$ the Schmidt number, $\epsilon (= a/d)$ the amplitude ratio and $E_1 (= -\tau' d^3 / \lambda^3 \mu c)$, $E_2 (= m_1 c d^3 / \lambda^3 \mu)$, $E_3 (= d' d^3 / \lambda^2 \mu)$, $E_4 (= b d^3 / c \lambda^5 \mu)$ and $E_5 (= k_2 d^3 / c \lambda \mu)$ are the non-dimensional elasticity parameters. Invoking long wavelength and low Reynolds number approximations we obtain

$$-2T' v = -\frac{\partial p}{\partial x} + \frac{1}{(1+\lambda_1)} \psi_{zzz} - (M^2 + \frac{1}{K_1(1+\lambda_1)}) \psi_z, \quad (3.22)$$

$$2T' \psi_z = -\frac{\partial p}{\partial y} + \frac{1}{(1+\lambda_1)} v_{zz} - (M^2 + \frac{1}{K_1(1+\lambda_1)}) v, \quad (3.23)$$

$$\frac{\partial p}{\partial z} = 0, \quad (3.24)$$

$$\theta_{zz} = -\frac{Ec \operatorname{Pr}}{(1+R)(1+\lambda_1)} \psi_{zz}^2 - \frac{Du \operatorname{Pr}}{(1+R)} \phi_{zz}, \quad (3.25)$$

$$\phi_{zz} + Sc Sr \theta_{zz} = 0, \quad (3.26)$$

$$\psi_z = 0, \quad v = 0, \quad \theta = \begin{Bmatrix} 1 \\ 0 \end{Bmatrix}, \quad \phi = \begin{Bmatrix} 1 \\ 0 \end{Bmatrix} \quad \text{at } z = \pm\eta, \quad (3.27)$$

$$L_0 = \frac{1}{(1+\lambda_1)} \psi_{zzz} - \left(M^2 + \frac{1}{K_1(1+\lambda_1)} \right) \psi_z + 2T' v \quad \text{at } z = \pm\eta. \quad (3.28)$$

where

$$L_0 = 8\epsilon\pi^3 \left(\frac{E_3}{2\pi} \sin[2\pi(x-t)] - (E_1 + E_2) \cos[2\pi(x-t)] + (4\pi^2 E_4 + \frac{E_5}{4\pi^2}) \cos[2\pi(x-t)] \right).$$

Equation (3.24) shows that pressure is not a function of z . Hence, the pressure can be eliminated from Eq. (3.22). Further, pressure term in Eq. (3.23) can be neglected, the secondary flow is resulted by the rotation. In view of these facts, we can write Eqs. (3.22) and (3.23) in the forms

$$-2T'v_z = \frac{1}{(1+\lambda_1)}\psi_{zzzz} - \left(M^2 + \frac{1}{K_1(1+\lambda_1)} \right) \psi_{zz}, \quad (3.29)$$

$$2T'\psi_z = \frac{1}{(1+\lambda_1)}v_{zz} - \left(M^2 + \frac{1}{K_1(1+\lambda_1)} \right) v. \quad (3.30)$$

3.3 Solution

Solving Eqs. (3.29) and (3.30) we have the following relations of stream function and secondary velocity

$$\psi = B_{13}z + B_{14} \sinh \left[\sqrt{B_1}z \right] + B_{15} \sinh \left[\sqrt{B_2}z \right], \quad (3.31)$$

$$v = \left(B_{21} + B_{22} \cosh \left[\sqrt{B_1}z \right] + B_{23} \cosh \left[\sqrt{B_2}z \right] \right) \times \left(\cosh^2 \left[\left(\sqrt{B_1} + \sqrt{B_2} \right) z \right] - \sinh^2 \left[\left(\sqrt{B_1} + \sqrt{B_2} \right) z \right] \right). \quad (3.32)$$

Making use of Eqs. (3.31) and (3.32) into Eqs. (3.25) and (3.26) and solving the resulting expressions through lubrication approach we have

$$\begin{aligned} \theta = & A_3 + A_4z + A_5z^2 + A_6 \cosh \left[2\sqrt{B_1}z \right] + A_7 \cosh \left[2\sqrt{B_2}z \right] + A_8 \cosh[2\sqrt{B_2}z - 2\sqrt{B_1}\eta] \\ & + A_9 \cosh[2\sqrt{B_2}z + 2\sqrt{B_1}\eta] + A_{10} \cosh[2\sqrt{B_1}z - 2\sqrt{B_2}\eta] + A_{11} \cosh[2\sqrt{B_1}z + 2\sqrt{B_2}\eta] \\ & - A_{12} \cosh \left[\left(\sqrt{B_1} + \sqrt{B_2} \right) z - \left(\sqrt{B_1} + \sqrt{B_2} \right) \eta \right] + A_{13} \cosh \left[\left(\sqrt{B_1} - \sqrt{B_2} \right) z \right] \\ & + A_{14} \cosh \left[\left(\sqrt{B_1} + \sqrt{B_2} \right) z \right] - A_{15} \sinh \left[\left(\sqrt{B_1} + \sqrt{B_2} \right) \eta \right], \end{aligned} \quad (3.33)$$

$$\begin{aligned}
\phi = & F_1 z + F_2 z^2 + F_3 \cosh \left[2\sqrt{B_1} z \right] + F_4 \cosh \left[2\sqrt{B_2} z \right] + F_5 \cosh \left[2\sqrt{B_1} z \right]^2 \\
& + F_6 \cosh \left[\sqrt{B_1} z \right] \cosh \left[\sqrt{B_2} z \right] + F_7 \sinh \left[\sqrt{B_1} z \right]^2 + F_8 \sinh \left[\sqrt{B_2} z \right]^2 \\
& + F_9 \sinh \left[\sqrt{B_1} z \right] \sinh \left[\sqrt{B_2} z \right] + F_{10}.
\end{aligned} \tag{3.34}$$

The heat transfer coefficients at the walls are given by

$$\begin{aligned}
Z &= \eta_x \theta_z(\eta), \\
Z &= \eta_x \left[\begin{aligned} & A_4 + 2A_5\eta + 2\sqrt{B_1}A_6 \sinh \left[2\sqrt{B_1}\eta \right] + 2\sqrt{B_2}A_7 \sinh \left[2\sqrt{B_2}\eta \right] \\ & + 2\sqrt{B_2}A_8 \sinh[2(\sqrt{B_2} - \sqrt{B_1})\eta] + 2\sqrt{B_2}A_9 \sinh[2(\sqrt{B_2} + \sqrt{B_1})\eta] \\ & + 2\sqrt{B_1}A_{10} \sinh[2(\sqrt{B_1} - \sqrt{B_2})\eta] + 2\sqrt{B_1}A_{11} \sinh[2(\sqrt{B_1} + \sqrt{B_2})\eta] \\ & + (\sqrt{B_1} - \sqrt{B_2}) A_{13} \sinh[(\sqrt{B_1} - \sqrt{B_2})\eta] \\ & + (\sqrt{B_1} + \sqrt{B_2}) A_{14} \sinh[(\sqrt{B_1} + \sqrt{B_2})\eta] \end{aligned} \right] \tag{3.35}
\end{aligned}$$

in which $\alpha, \beta, A_1 \rightarrow A_{15}, B_1 \rightarrow B_{23}$ and $F_1 \rightarrow F_{10}$ are given below:

$$\begin{aligned}
\alpha^* &= \left(M^2 + \frac{1}{K_1(1 + \lambda_1)} \right) (1 + \lambda_1), \quad \beta^* = T'(1 + \lambda_1), \quad A_1 = \frac{Ec Pr}{(1 + R)(1 + \lambda_1)}, \\
A_2 &= 1 - \frac{Sr Du Pr Sc}{(1 + R)}, \quad A_3 = 2A_1(\alpha^{*3} + 20\alpha^*\beta^{*2} - 4\alpha^{*2}\beta^{*2}\eta^2 - 16\beta^{*4}\eta^2), \quad A_4 = \frac{1}{2\eta}, \\
A_5 &= \frac{1}{64B_3^2} L_0^2 \sec h^2[\sqrt{B_1}\eta] (-4A_2B_1B_2^2 - 4A_1(B_1B_2 + B_1(B_2 + 2\alpha^* + 4i\beta^*)) - 2B_1B_2 \\
& \times (A_2B_1 + (4A_1 + A_2\alpha^* - 2iA_2\beta^*) \cosh[2\sqrt{B_1}\eta] + 2A_1(\cosh[2(\sqrt{B_1} - \sqrt{B_2})\eta] \\
& + \cosh[2(\sqrt{B_1} + \sqrt{B_2})\eta])) \sec h^2[\sqrt{B_2}\eta]), \\
A_6 &= \frac{A_1B_2L_0^2 \sec h[\sqrt{B_1}\eta]}{B_3^2}, \quad A_7 = \frac{A_2B_2^2L_0^2 \sec h^2[\sqrt{B_1}\eta]}{32B_3^2}, \quad A_8 = \frac{A_2B_2^2L_0^2 \sec h^2[\sqrt{B_1}\eta]}{128B_3^2}, \\
A_9 &= \frac{3A_2B_1^2L_0^2 \sec h^2[\sqrt{B_2}\eta]}{128B_3^2}, \quad A_{10} = \frac{A_1B_1^2L_0^2 \sec h^2[\sqrt{B_2}\eta]}{2B_3^2}, \quad A_{11} = \frac{A_1B_1L_0^2 \sec h^2[\sqrt{B_2}\eta]}{2B_3^2}, \\
A_{12} &= \frac{A_2B_1B_2L_0^2 \sec h[\sqrt{B_1}\eta] \sec h[\sqrt{B_2}\eta]}{16B_3\beta^{*2}} + \frac{A_2B_1B_2L_0^2\alpha \sec h[\sqrt{B_1}\eta] \sec h[\sqrt{B_2}\eta]}{8B_3^2\beta^{*2}}, \\
A_{13} &= -\frac{A_2\sqrt{B_1}\sqrt{B_2}L_0^2 \sec h[\sqrt{B_1}\eta] \sec h[\sqrt{B_2}\eta]}{8B_3\beta^{*2}} - \frac{A_2\sqrt{B_1}\sqrt{B_2}L_0^2\alpha^* \sec h[\sqrt{B_1}\eta] \sec h[\sqrt{B_2}\eta]}{16B_3\beta^{*2}}, \\
A_{14} &= \frac{A_2B_2^2L_0^2 \sec h^2[\sqrt{B_1}\eta]}{64B_3^2}, \quad A_{15} = \frac{A_2B_1^2L_0^2 \sec h^2[\sqrt{B_2}\eta]}{64B_3^2},
\end{aligned}$$

$$\begin{aligned}
A_{16} &= \frac{1}{256B_3^2\beta^{*2}}(-4A_3L_0^2 + 32B_3^2\beta^{*2} - A_2L_0^2(\beta^{*2}((-B_1 + B_2)\alpha^* + 2i(B_1 + B_2)\beta^*) \\
&\quad + 4B_3(B_3 - 4\alpha^*\beta^{*2}\eta^2)) + (-4A_3L_0^2 + 32B_3^2\beta^{*2} + A_2L_0^2(B_1^2\beta^{*2} + 4B_2(-\alpha^{*3} \\
&\quad + 2i\alpha^{*2}\beta^* - 5\alpha^*\beta^{*2} + 6i\beta^{*3} + 2B_1^2\beta^{*2}\eta^2))) \cosh[\sqrt{B_1}\eta] - 2(-8B_3^2\beta^{*2} + A_2L_0^2 \\
&\quad \times (\sqrt{B_1}\sqrt{B_2}B_3\alpha^* + \alpha^{*4} + 10\alpha^{*2}\beta^{*2} + 8\beta^{*4}) + 2A_1L_0^2(\sqrt{B_1}\sqrt{B_2}B_3 + \alpha^{*3} + 20\alpha^*\beta^{*2} \\
&\quad - 4\beta^{*2}(\alpha^{*2} + 4\beta^{*2})\eta^2)) \cosh[(\sqrt{B_1} - \sqrt{B_2})\eta] + 2((8B_3^2\beta^{*2} + A_2L_0^2(\sqrt{B_1}\sqrt{B_2}B_3\alpha^* \\
&\quad - \alpha^{*4} - 10\alpha^{*2}\beta^{*2} - 8\beta^{*4}) + 2A_1L_0^2(\sqrt{B_1}\sqrt{B_2}B_3 - \alpha^{*3} - 20\alpha^*\beta^{*2} + 4\beta^{*2}(\alpha^{*2} + 4\beta^{*2}) \\
&\quad \times \eta^2)) \cosh[(\sqrt{B_1} + \sqrt{B_2})\eta] - (4A_3L_0^2 - 32B_3^2\beta^{*2} + A_2L_0^2(B_2^2\beta^{*2} + 4B_1 \\
&\quad \times (\alpha^{*3} + 2i\alpha^{*2}\beta^* + 5\alpha^*\beta^{*2} + 6i\beta^{*3} - 2B_2^2\beta^{*2}\eta^2))) \cosh[2\sqrt{B_2}\eta]) \\
&\quad \times \sec h^2[\sqrt{B_1}\eta] \sec h^2[\sqrt{B_2}\eta], \\
B_1 &= (\alpha^* - 2i\beta^*), \quad B_2 = (\alpha^* + 2i\beta^*), \quad B_3 = (\alpha^{*2} + 4\beta^{*2}), \quad B_4 = (-i\alpha^* - 2\beta^*), \\
B_5 &= (-i\alpha^* + 2\beta^*), \quad B_6 = (i\alpha^* + 2\beta^*), \\
B_7 &= \frac{B_5L_0\alpha^*(4\beta^* + iB_2 \sec h[\sqrt{B_1}\eta] + B_4 \sec h[\sqrt{B_2}\eta])}{2B_3}, \\
B_8 &= \frac{B_6L_0\alpha^*(4\beta^* + iB_2 \sec h[\sqrt{B_1}\eta] + B_4 \sec h[\sqrt{B_2}\eta])}{2B_3}, \\
B_9 &= \frac{L_0\alpha^*}{8\sqrt{B_1}B_2^{3/2}B_3B_4}(4\beta^* + iB_2 \sec h[\sqrt{B_1}\eta] + B_4 \sec h[\sqrt{B_2}\eta]), \\
B_{10} &= (B_2\alpha^* \cosh[\sqrt{B_2}\eta] + \cosh[\sqrt{B_1}\eta])(B_1\alpha^* + 8\beta^{*2} \cosh[\sqrt{B_2}\eta]), \\
B_{11} &= \frac{1}{4B_1^{3/2}B_{10}B_2^{3/2}}(2L_0\alpha^{*2} + B_2(B_8 - 2iL_0\beta^*) \cosh[\sqrt{B_2}\eta] + B_1(B_7 + 2iL_0\beta^*) \\
&\quad \times \cosh[\sqrt{B_2}\eta]), \\
B_{12} &= \frac{1}{2B_1^{3/2}B_{10}B_2^{3/2}}(2L_0\alpha^* + (B_7 - B_1L_0) \cosh[\sqrt{B_2}\eta] + \cosh[\sqrt{B_1}\eta](B_8 - B_2L_0 \\
&\quad - \frac{2L_0\alpha^*\beta^* \cosh[\sqrt{B_2}\eta](4\beta^* + iB_2 \sec h[\sqrt{B_1}\eta] + B_4 \cosh[\sqrt{B_2}\eta])}{B_3})), \\
B_{13} &= 2\sqrt{B_1B_2}(-2B_{11}\alpha^* + B_{12}\alpha^{*2} + 4iB_9\beta^*), \quad B_{14} = 2B_2^{3/2}(B_{11} - B_9 - iB_{12}\beta^*), \\
B_{15} &= 2B_1^{3/2}(B_{11} + B_9 + iB_{12}\beta^*), \quad B_{16} = (-B_3B_8 + B_2B_3L_0 + 2B_4L_0\alpha^*\beta^* + 8L_0\alpha^*\beta^{*2} \\
&\quad \times \cosh[\sqrt{B_2}\eta]), \\
B_{17} &= (B_2(iB_8 + 2L_0\beta^*) \cosh[\sqrt{B_1}\eta] + i(2L_0\alpha^{*2} + B_1(B_7 + 2iL_0\beta^*) \cosh[\sqrt{B_2}\eta])), \\
B_{18} &= (iB_2 \cosh[\sqrt{B_2}\eta] + \cosh[\sqrt{B_1}\eta](B_4 + 4\beta^* \cosh[\sqrt{B_2}\eta])) \sec h[\sqrt{B_1}\eta] \sec h[\sqrt{B_2}\eta], \\
B_{19} &= (-2B_3L_0\alpha^* + B_{16} \cosh[\sqrt{B_1}\eta] + (-B_3B_7 + B_1B_3L_0 + 2iB_2L_0\alpha^*\beta^*) \cosh[\sqrt{B_2}\eta]),
\end{aligned}$$

$$\begin{aligned}
B_{20} &= (B_2\alpha^* \cosh[\sqrt{B_2}\eta] + \cosh[\sqrt{B_1}\eta](B_1\alpha^* + 8\beta^{*2} \cosh[\sqrt{B_2}\eta])), \\
B_{21} &= \frac{8\beta^*}{4B_2} \left(-\frac{B_{17}}{B_{20}B_4} + \frac{B_{19}\alpha^*}{B_1B_{20}B_3} + \frac{B_{18}L_0\beta^*}{B_1B_3} \right), \\
B_{22} &= \frac{1}{4B_2} \left(\frac{2B_{17}B_5}{B_{20}B_4} + \frac{B_{18}B_2L_0\alpha^*}{B_1B_3} - \frac{4B_{19}B_2\beta^*}{B_1B_{20}B_3} \right), \\
B_{23} &= \frac{1}{4B_2} \left(\frac{2B_{17}B_6}{B_{20}B_4} + \frac{B_{18}L_0\alpha^*}{B_3} - \frac{4B_{19}\beta^*}{B_{20}B_3} \right), \quad F_1 = \frac{1}{2\eta}, \\
F_2 &= -\frac{A_1B_1B_2L_0^2ScSr}{64A_2B_3^2} (B_1 + B_2 + 2\alpha^* + 2B_1 \cosh[\sqrt{B_1}\eta] + 2B_2 \cosh[\sqrt{B_2}\eta]) \\
&\quad \times \sec h^2[\sqrt{B_1}\eta] \sec h^2[\sqrt{B_2}\eta], \\
F_3 &= \frac{A_1B_2^2L_0^2ScSr \sec h^2[\sqrt{B_1}\eta]}{128A_2B_3^2}, \quad F_4 = \frac{3A_1B_1^2L_0^2ScSr \sec h^2[\sqrt{B_2}\eta]}{128A_2B_3^2}, \\
F_5 &= \frac{A_1B_2^2L_0^2ScSr \sec h^2[\sqrt{B_1}\eta]}{32A_2B_3^2}, \quad F_6 = \frac{A_1L_0^2ScSr \sec h[\sqrt{B_1}\eta] \sec h[\sqrt{B_2}\eta]}{16A_2\beta^{*2}}, \\
F_7 &= \frac{A_1B_2^2L_0^2ScSr \sec h^2[\sqrt{B_1}\eta]}{64A_2B_3^2}, \quad F_8 = \frac{A_1B_1^2L_0^2ScSr \sec h^2[\sqrt{B_2}\eta]}{64A_2B_3^2}, \\
F_9 &= -\frac{A_1\sqrt{B_1}\sqrt{B_2}L_0^2ScSr\alpha^* \sec h[\sqrt{B_1}\eta] \sec h[\sqrt{B_2}\eta]}{16A_2\beta^{*2}B_3}, \\
F_{10} &= \frac{1}{128A_2B_3^2} (64A_2B_3^2 + \frac{1}{2\beta^{*2}} A_1L_0^2ScSr (B_1^2\beta^{*2} - B_2^2\beta^{*2} - 4B_1B_2(B_3 - 4\alpha^*\beta^{*2}\eta^2) \\
&\quad + (B_1^2\beta^{*2} + 4B_2(-\alpha^{*3} + 2i\alpha^{*2}\beta^* - 5\alpha^*\beta^{*2} + 6i\beta^{*3} + 2B_1^2\beta^{*2}\eta^2)) \cosh[2\sqrt{B_1}\eta] \\
&\quad - 2(\sqrt{B_1}\sqrt{B_2}B_3\alpha^* + \alpha^{*4} + 10\alpha^{*2}\beta^{*2} + 8\beta^{*4}) \cosh[2(\sqrt{B_1} - \sqrt{B_2})\eta] \\
&\quad + 2(\sqrt{B_1}\sqrt{B_2}B_3\alpha^* - \alpha^{*4} - 10\alpha^{*2}\beta^{*2} - 8\beta^{*4}) \cosh[2(\sqrt{B_1} + \sqrt{B_2})\eta] \\
&\quad - (B_2^2\beta^{*2} + 4B_1(\alpha^{*3} + 2i\alpha^{*2}\beta^* + 5\alpha^*\beta^{*2} + 6i\beta^{*3} - 2B_2^2\beta^{*2}\eta^2)) \cosh[2\sqrt{B_2}\eta]) \\
&\quad \times \sec h^2[\sqrt{B_1}\eta] \sec h^2[\sqrt{B_2}\eta]).
\end{aligned}$$

3.4 Graphical results and discussion

The main objective here is to predict the impact of sundry parameters on the velocity, temperature and concentration profiles. The theme of present study is to analyze the influence of rotation in the presence of Soret and Dufour effects. Here Figs. (3.1 – 3.18) are prepared for the velocity and temperature whereas the Figs. (3.19 – 3.34) show the variations of concentration and heat transfer rate respectively.

Here Figs. (3.1 – 3.4) are prepared to analyze the axial velocity. These Figures show that velocity traces a parabolic path with maximum value at the center of channel. Fig. (3.1)

shows that velocity enhances when elasticity parameters E_1 and E_2 are increased. There is decrease in velocity for larger E_3 , E_4 and E_5 . Since E_1 and E_2 represent the elastic parameters therefore increasing elasticity offers less resistance to the flow and hence velocity enhances. On the contrary the wall damping creates a resistive type force and so the velocity decreases when E_3 increases. Similar behavior is noticed for E_4 and E_5 in the presence of damping. Fig. (3.2) illustrates that increasing T' reduces the velocity of the fluid in axial direction. This Figure also provides a comparison for axial velocity for rotating and non-rotating channels. It is found that axial velocity is greater in non-rotating channel i.e. ($T' = 0$). Fig. (3.3) shows decrease in velocity when λ_1 is increased. Velocity enhances when the value of K_1 is increased (see Fig. 3.4). Porosity parameter depends on the permeability parameter K . Increase in K_1 leads to the higher permeability parameter. Ultimately the velocity thus increases through larger K_1 .

Figs. (3.5 – 3.8) highlight the effects of wall properties, T' , λ_1 and K_1 on the secondary velocity. The rotation of channel induces a velocity component in the y - direction which in turn produces a fluid flow in y - direction which is termed as secondary flow. We can observe the effect of wall properties on secondary flow v through Fig. (3.5). Decrease in v is observed by increasing E_1 and E_2 while it enhances through E_3 , E_4 and E_5 . In the absence of rotation there is no secondary velocity but velocity in y - direction increases in presence of rotation (see Fig. 3.6). Fig. (3.7) shows that the secondary velocity v increases for larger λ_1 . Similar effect is shown by K_1 which is observed in Fig. (3.8).

Impact of different parameters on temperature profile can be seen from Figs. (3.9 – 3.18). It is a known fact that temperature is the average kinetic energy of particles which in turn depends on the velocity. Therefore an increase in temperature θ is noticed for increasing values of E_1 and E_2 . On the contrary decrease in temperature is noticed for increasing values of E_3 , E_4 and E_5 (see Fig. 3.9). Fig. (3.10) reveals that an increase in T' causes decrease in θ . It is noticed that temperature enhances when we increase Sr and Du (see Figs. 3.11 and 3.12). In fact for increasing Sr and Du the thermal diffusion is increased and consequently the temperature enhances. Physically the diffusion-thermo or Dufour effect defines a heat flux produced when a chemical system undergoes a concentration gradient. These effects depend upon thermal diffusion which is though very small, but sometimes become substantial when the partaking

species differ by molecular weights. Mass diffusion follows by the uneven distribution of species creating a concentration gradient. A temperature gradient can also work as a driving force for mass diffusion called thermo-diffusion or Soret effect. Therefore the higher the temperature gradient, the larger the Soret effect. Fig. (3.13) reveals that temperature decreases when the value of λ_1 is increased. In fact higher λ_1 corresponds to larger relaxation time which provides more resistance to the fluid motion and thus the temperature profile enhances. As by increasing the value of porosity parameter K_1 the permeability of the medium increases which accelerates the fluid and thus temperature enhances (Fig. 3.14). Figs (3.15) and (3.16) display that temperature is decreasing function of Sc and R . Influence of Eckert number Ec on θ is displayed in Fig. (3.17). It is depicted from this Fig. that temperature enhances by increasing Ec . The heat generation due to internal friction caused by the shear in the flow is the reason behind such increase. Similar behavior is observed for Prandtl number Pr (Fig. 3.18).

Figs. (3.19 – 3.26) disclose the effect of various parameters on concentration ϕ . Fig. (3.19) displays the role of wall properties on ϕ . Decrease in concentration is noticed for increasing values of E_1 and E_2 but it increases for larger E_3 , E_4 and E_5 . Fig. (3.20) examines the behavior of ϕ for Taylor number T' . It is revealed that ϕ is increasing function of Taylor number. Concentration distribution for different Du and Sr is shown in Figs (3.21) and (3.22). Here concentration decreases with the increase of these parameters. Figs. (3.23) and (3.24) are displayed against values of λ_1 and K_1 . These Figures witness that ϕ decreases by increasing λ_1 and K_1 . Fig. (3.25) depicts that the concentration profile decreases when Sc increases. As Schmidt number is defined as the ratio of momentum diffusivity (viscosity) to mass diffusivity. Therefore increasing Sc decreases the mass diffusion which in turn reduces the concentration. For larger R concentration increases (see Fig. 3.26). It can be observed through the graphical results that concentration field has opposite effect when compared with temperature.

Behavior of heat transfer coefficient Z for various parameters is shown in the Figs. (3.27 – 3.34). The heat transfer coefficient is represented by $Z(x) = \eta_x \theta_z(\eta)$ which defines the rate of heat transfer or heat flux at the walls. As expected Z shows an oscillatory behavior which is because of the propagation of sinusoidal waves along the channel walls. Figs. (3.27) and (3.28) explore the effect of T' and wall properties on ϕ . It can be noticed that there is an increase in rate of heat transfer for E_1 , E_2 and T' whereas decrease in the heat transfer rate is observed for E_3 ,

E_4 and E_5 . Effects of Sr , Du , λ_1 and K_1 on Z can be observed through Figs. (3.29 – 3.32) respectively. By increasing these parameters the absolute value of Z increases. Effect of radiation parameter R can be seen in Fig. (3.33). Here increase in R enhances Z . It is clear from Fig. (3.34) that rate of heat transfer is increasing function of Schmidt number Sc .

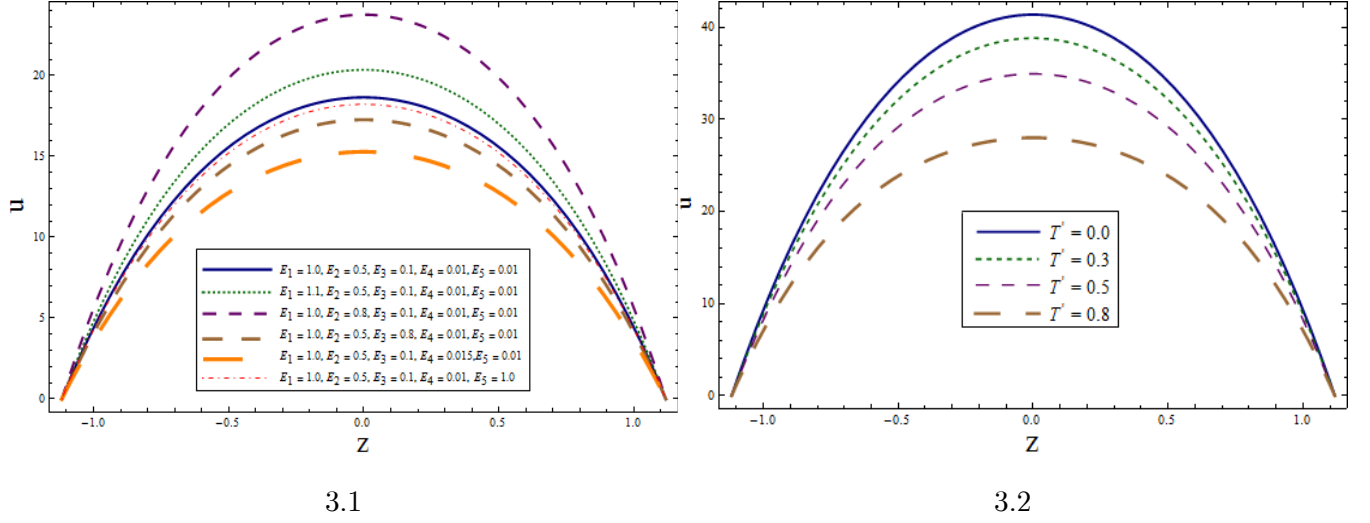
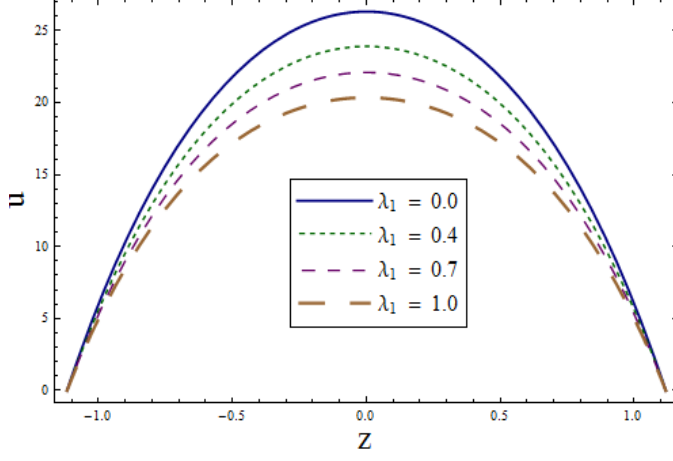
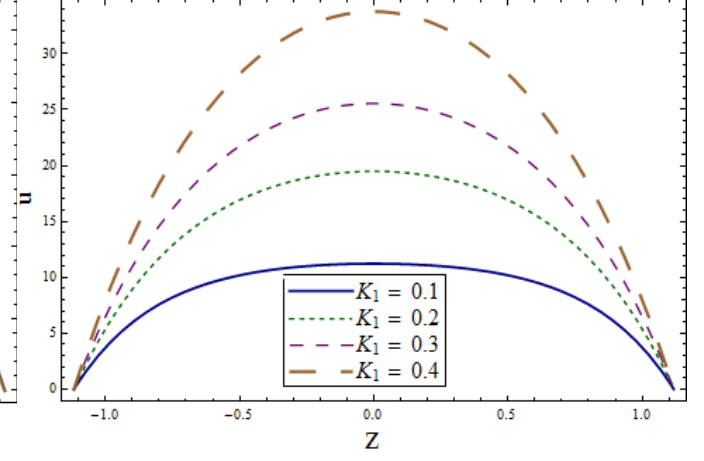


Fig. 3.1 : Impact of wall properties on u when $T' = \lambda_1 = M = K_1 = 0.5$, $x = \epsilon = 0.2$, $t = 0.1$.

Fig. 3.2 : Impact of T' on u when $E_1 = E_2 = 3.0$, $E_3 = 0.01$, $E_4 = E_5 = 0.1$,
 $M = \lambda_1 = K_1 = 0.5$, $x = \epsilon = 0.2$, $t = 0.1$.



3.3



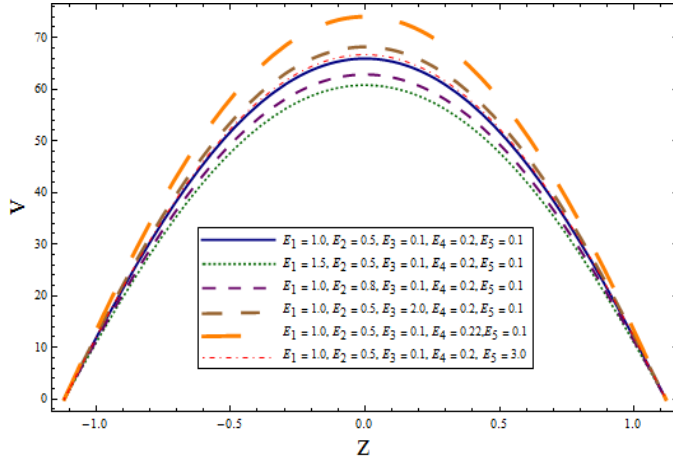
3.4

Fig. 3.3 : Impact of λ_1 on u when $E_1 = E_2 = 3.0$, $E_3 = 0.01$, $E_4 = E_5 = 0.1$,

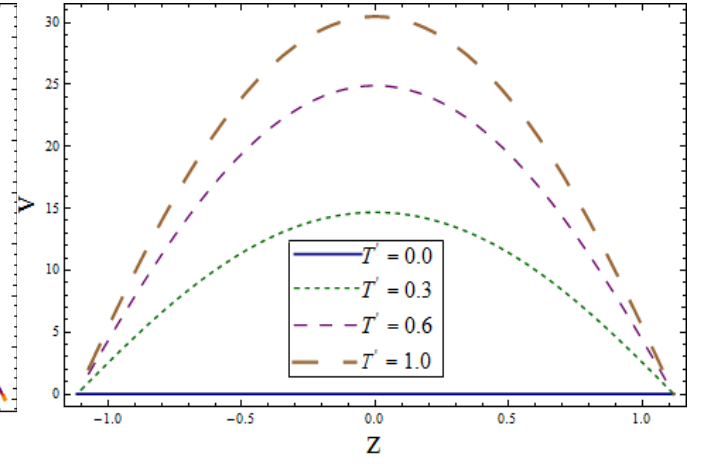
$$T' = K_1 = M = 0.5, x = \epsilon = 0.2, t = 0.1.$$

Fig. 3.4 : Impact of K_1 on u when $E_1 = E_2 = 3.0$, $E_3 = 0.01$, $E_4 = E_5 = 0.1$,

$$T' = \lambda_1 = M = 0.5, x = \epsilon = 0.2, t = 0.1.$$



3.5

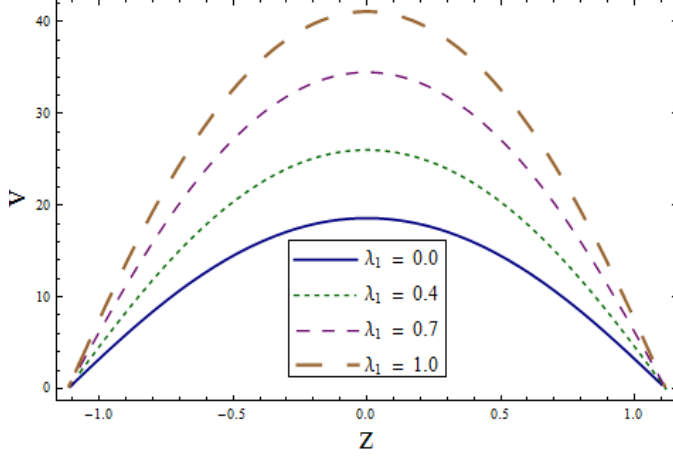


3.6

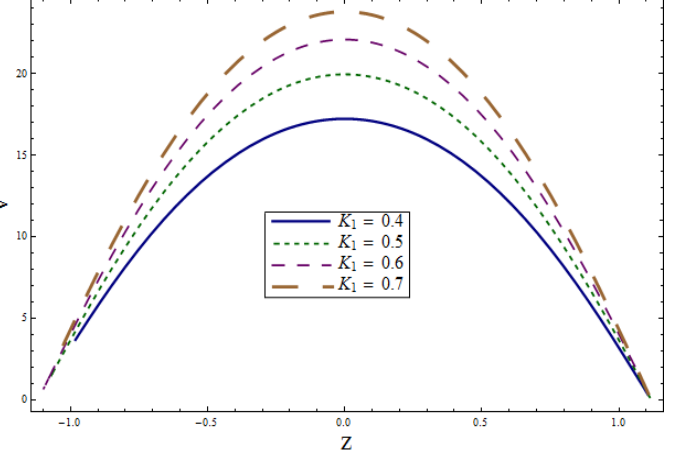
Fig. 3.5 : Impact of wall properties on v when $T' = \lambda_1 = M = K_1 = 0.5$, $x = \epsilon = 0.2$, $t = 0.1$.

Fig. 3.6 : Impact of T' on v when $E_1 = E_2 = 3.0$, $E_3 = 0.01$, $E_4 = E_5 = 0.1$,

$$M = \lambda_1 = K_1 = 0.5, x = \epsilon = 0.2, t = 0.1.$$



3.7



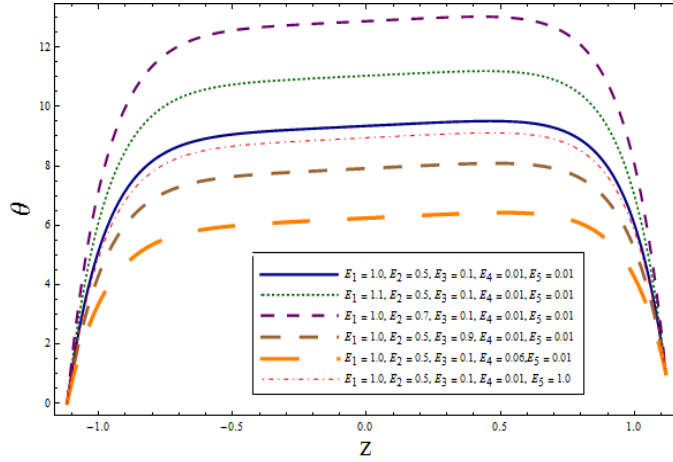
3.8

Fig. 3.7 : Impact of λ_1 on v when $E_1 = E_2 = 3.0$, $E_3 = 0.01$, $E_4 = E_5 = 0.1$,

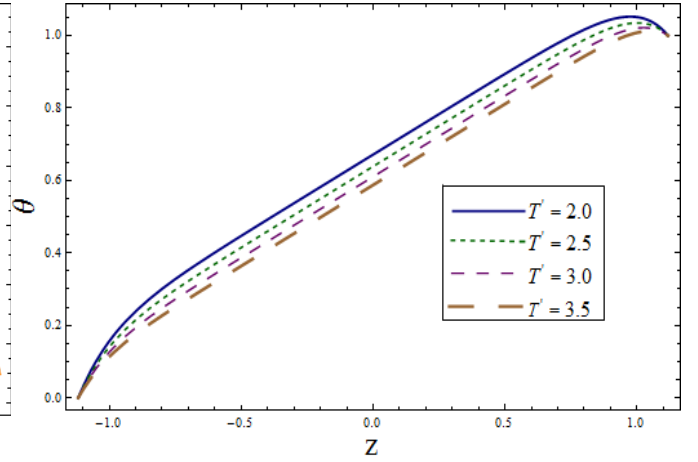
$$T' = K_1 = M = 0.5, x = \epsilon = 0.2, t = 0.1.$$

Fig. 3.8 : Impact of K_1 on v when $E_1 = E_2 = 3.0$, $E_3 = 0.01$, $E_4 = E_5 = 0.1$,

$$T' = \lambda_1 = M = 0.5, x = \epsilon = 0.2, t = 0.1.$$



3.9



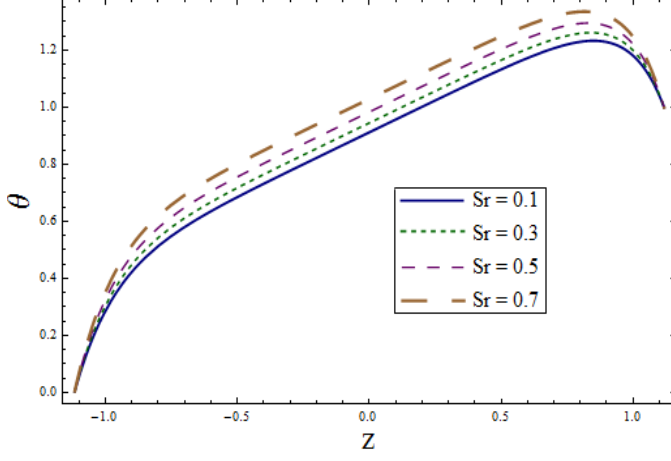
3.10

Fig. 3.9 : Variation of wall properties on θ when $Sr = Du = Sc = R = M = \lambda_1 = 0.8$,

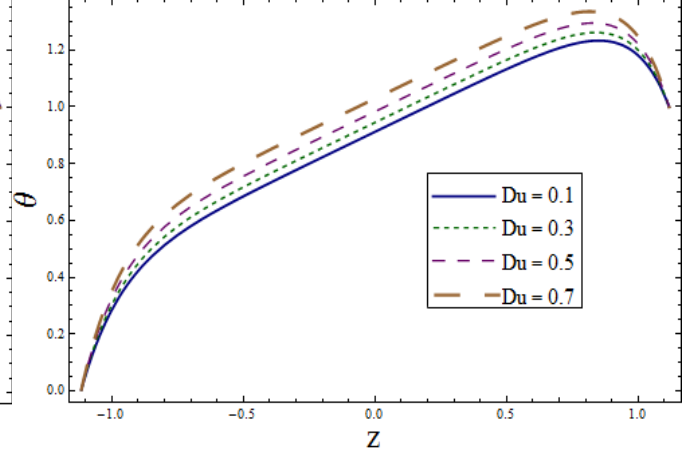
$$T' = Pr = 1.0, K_1 = 0.1, Ec = 2.0, x = \epsilon = 0.2, t = 0.1.$$

Fig. 3.10 : Variation of T' on θ when $E_1 = 0.2$, $E_2 = E_3 = E_4 = 0.01$, $E_5 = 0.1$,

$$Sr = Du = Sc = R = M = \lambda_1 = 0.8, K_1 = 0.1, Pr = 1.0, Ec = 2.0, x = \epsilon = 0.2, t = 0.1.$$



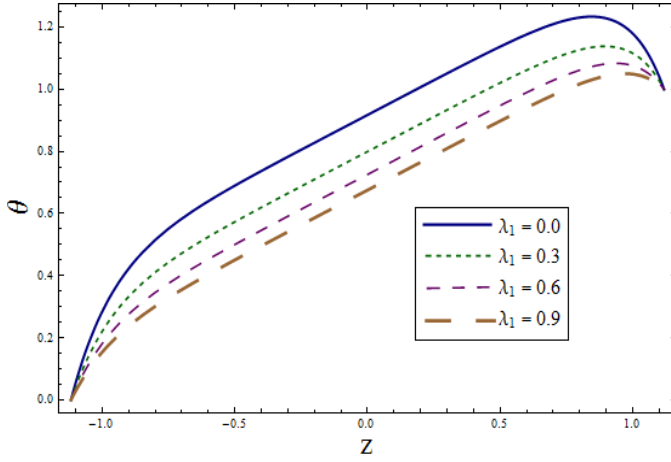
3.11



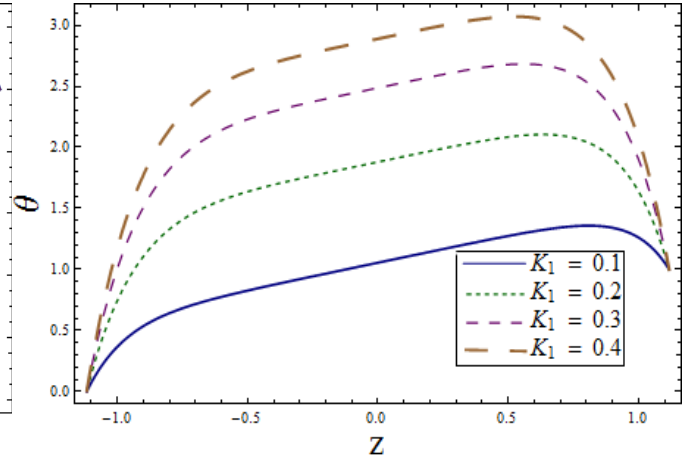
3.12

Fig. 3.11 : Variation of Sr on θ when $E_1 = 0.2$, $E_2 = E_3 = E_4 = 0.01$, $E_5 = 0.1$, $Du = Sc = R = M = \lambda_1 = 0.8$, $T' = 1.0$, $K_1 = 0.1$, $Pr = 1.0$, $Ec = 2.0$, $x = \epsilon = 0.2$, $t = 0.1$.

Fig. 3.12 : Variation of Du on θ when $E_1 = 0.2$, $E_2 = E_3 = E_4 = 0.01$, $E_5 = 0.1$, $Sr = Sc = R = M = \lambda_1 = 0.8$, $T' = 1.0$, $K_1 = 0.1$, $Pr = 1.0$, $Ec = 2.0$, $x = \epsilon = 0.2$, $t = 0.1$.



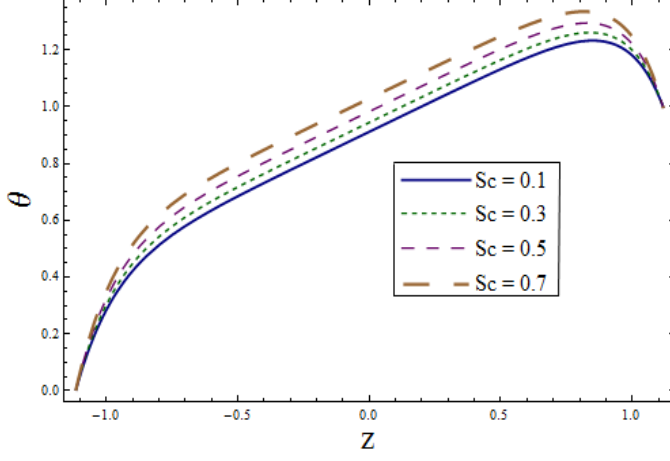
3.13



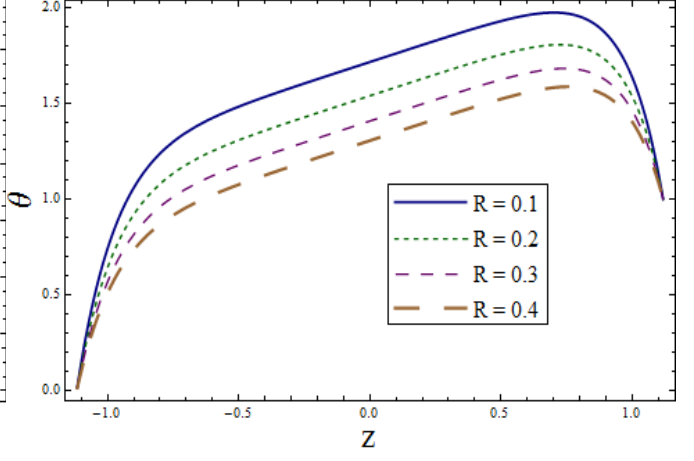
3.14

Fig. 3.13 : Variation of λ_1 on θ when $E_1 = 0.2$, $E_2 = E_3 = E_4 = 0.01$, $E_5 = 0.1$, $Sr = Du = Sc = R = M = 0.8$, $T' = 1.0$, $K_1 = 0.1$, $Pr = 1.0$, $Ec = 2.0$, $x = \epsilon = 0.2$, $t = 0.1$.

Fig. 3.14 : Variation of K_1 on θ when $E_1 = 0.2$, $E_2 = E_3 = E_4 = 0.01$, $E_5 = 0.1$, $Sr = Du = Sc = R = M = \lambda_1 = 0.8$, $T' = 1.0$, $Pr = 1.0$, $Ec = 2.0$, $x = \epsilon = 0.2$, $t = 0.1$.



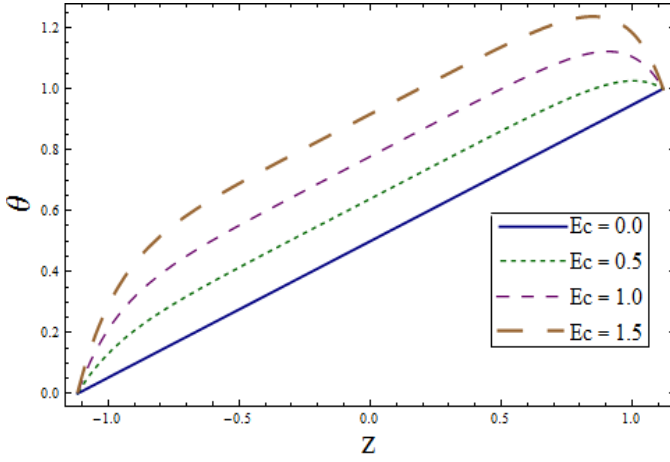
3.15



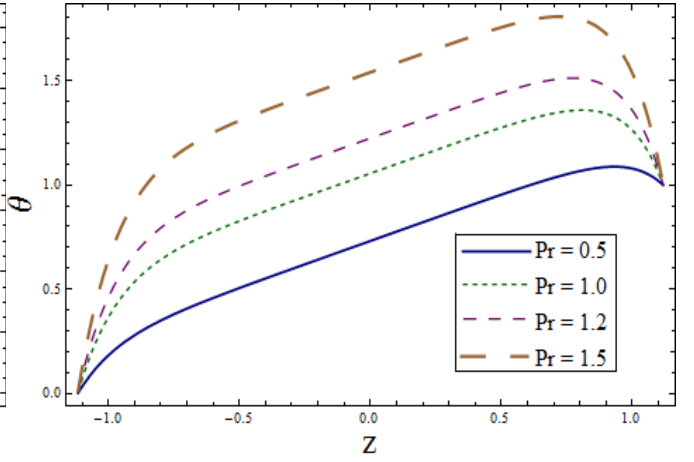
3.16

Fig. 3.15 : Variation of Sc on θ when $E_1 = 0.2$, $E_2 = E_3 = E_4 = 0.01$, $E_5 = 0.1$,
 $Sr = Du = R = M = \lambda_1 = 0.8$, $T' = 1.0$, $K_1 = 0.1$, $Pr = 1.0$, $Ec = 2.0$, $x = \epsilon = 0.2$, $t = 0.1$.

Fig. 3.16 : Variation of R on θ when $E_1 = 0.2$, $E_2 = E_3 = E_4 = 0.01$, $E_5 = 0.1$,
 $Sr = Du = Sc = M = \lambda_1 = 0.8$, $T' = 1.0$, $K_1 = 0.1$, $Pr = 1.0$, $Ec = 2.0$, $x = \epsilon = 0.2$, $t = 0.1$.



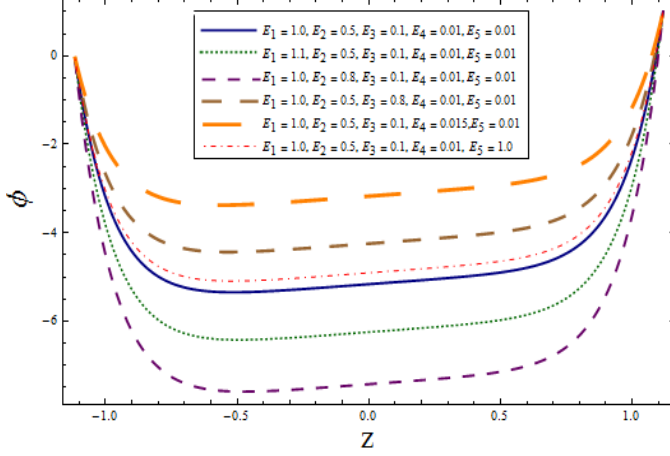
3.17



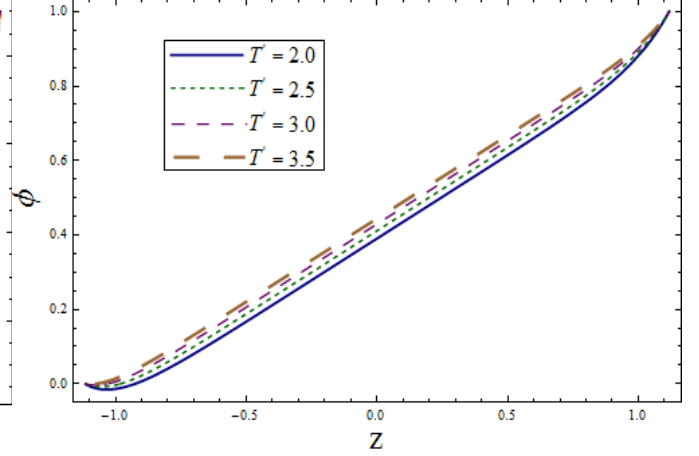
3.18

Fig. 3.17 : Variation of Ec on θ when $E_1 = 0.2$, $E_2 = E_3 = E_4 = 0.01$, $E_5 = 0.1$,
 $Sr = Du = R = M = \lambda_1 = 0.8$, $T' = 1.0$, $K_1 = 0.1$, $Pr = 1.0$, $Sc = 2.0$, $x = \epsilon = 0.2$, $t = 0.1$.

Fig. 3.18 : Variation of Pr on θ when $E_1 = 0.2$, $E_2 = E_3 = E_4 = 0.01$, $E_5 = 0.1$,
 $Sr = Du = Sc = M = R = \lambda_1 = 0.8$, $T' = 1.0$, $K_1 = 0.1$, $Ec = 2.0$, $x = \epsilon = 0.2$, $t = 0.1$.



3.19

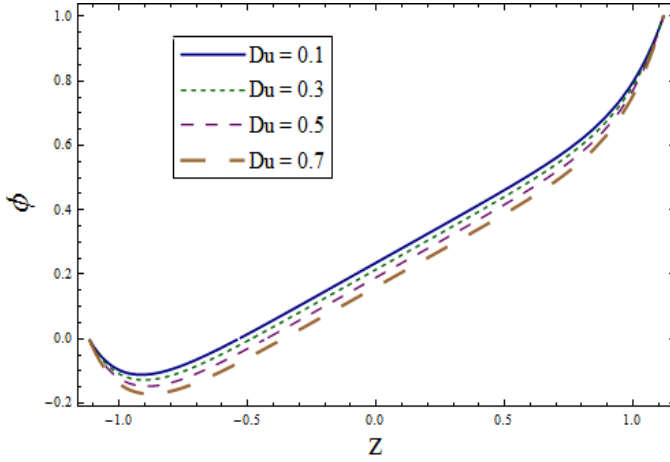


3.20

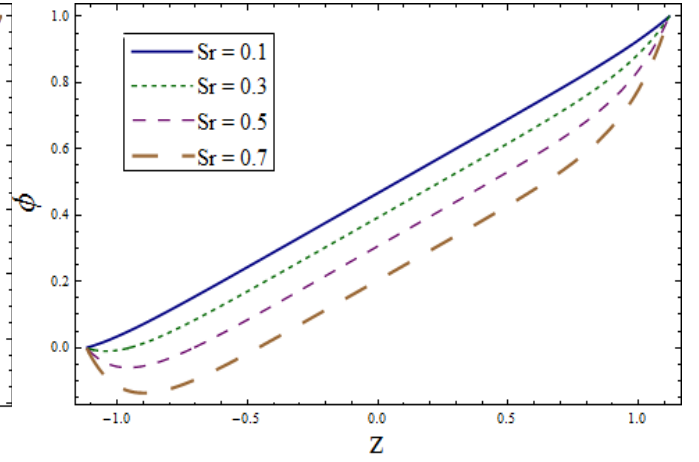
Fig. 3.19 : Influence of wall properties on ϕ when $Sr = Du = Sc = M = \lambda_1 = 0.8$,

$$Pr = T' = 1.0, K_1 = 0.1, Ec = 2.0, x = \epsilon = 0.2, t = 0.1.$$

Fig. 3.20 : Influence of T' on ϕ when $E_1 = 0.2, E_2 = E_3 = E_4 = 0.01, E_5 = 0.1$,
 $Sr = Du = Sc = R = M = \lambda_1 = 0.8, K_1 = 0.1, Pr = 1.0, Ec = 2.0, x = \epsilon = 0.2, t = 0.1$.



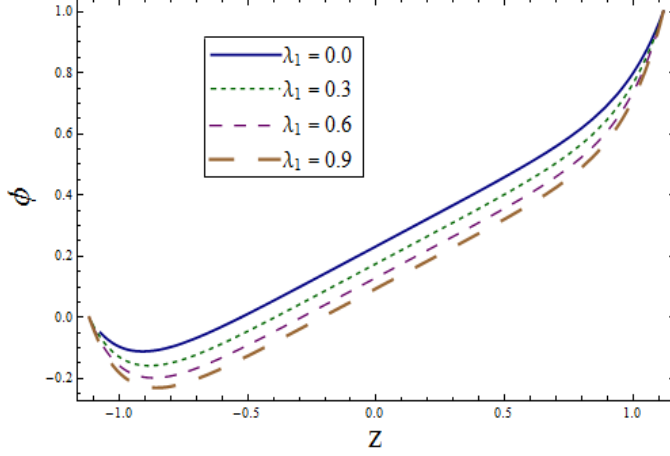
3.21



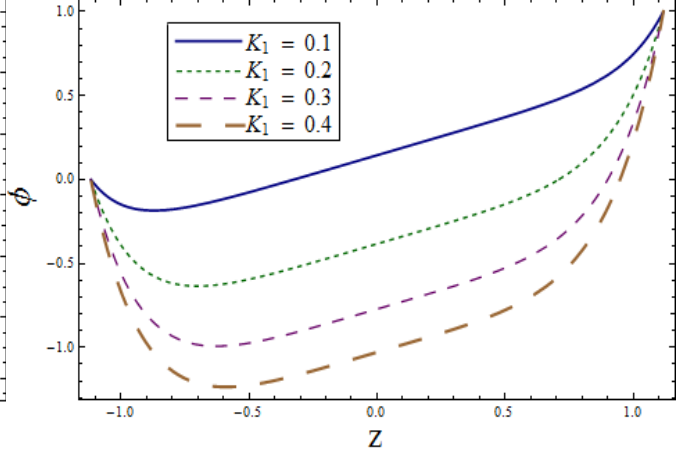
3.22

Fig. 3.21 : Influence of Du on ϕ when $E_1 = 0.2, E_2 = E_3 = E_4 = 0.01, E_5 = 0.1$,
 $Sr = Sc = M = R = \lambda_1 = 0.8, Pr = T' = 1.0, K_1 = 0.1, Ec = 2.0, x = \epsilon = 0.2, t = 0.1$.

Fig. 3.22 : Influence of Sr on ϕ when $E_1 = 0.2, E_2 = E_3 = E_4 = 0.01, E_5 = 0.1$,
 $Du = Sc = M = R = \lambda_1 = 0.8, Pr = T' = 1.0, K_1 = 0.1, Ec = 2.0, x = \epsilon = 0.2, t = 0.1$.



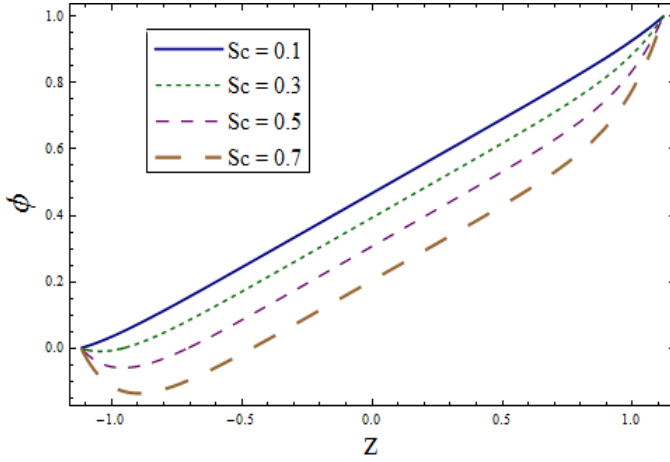
3.23



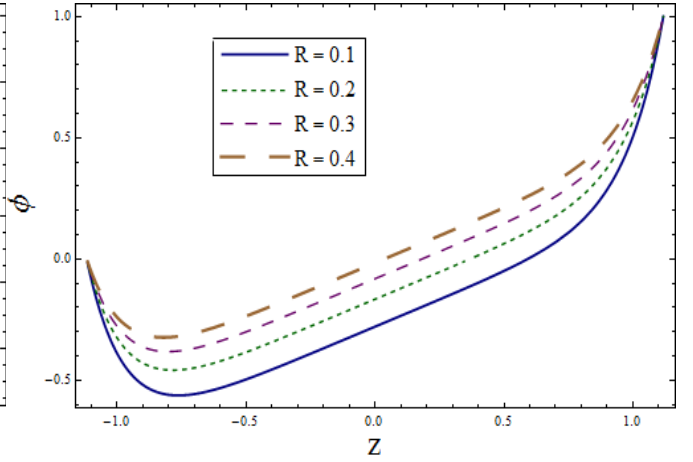
3.24

Fig. 3.23 : Influence of λ_1 on ϕ when $E_1 = 0.2$, $E_2 = E_3 = E_4 = 0.01$, $E_5 = 0.1$, $Sr = Du = Sc = M = R = 0.8$, $Pr = T' = 1.0$, $K_1 = 0.1$, $Ec = 2.0$, $x = \epsilon = 0.2$, $t = 0.1$.

Fig. 3.24 : Influence of K_1 on ϕ when $E_1 = 0.2$, $E_2 = E_3 = E_4 = 0.01$, $E_5 = 0.1$, $Sr = Du = Sc = M = R = \lambda_1 = 0.8$, $Pr = T' = 1.0$, $Ec = 2.0$, $x = \epsilon = 0.2$, $t = 0.1$.



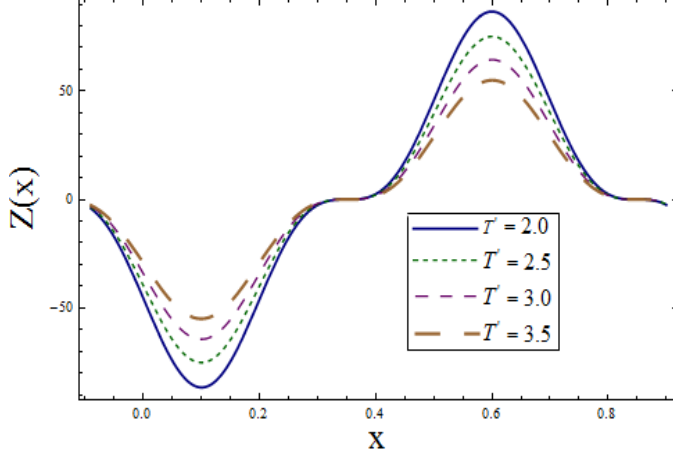
3.25



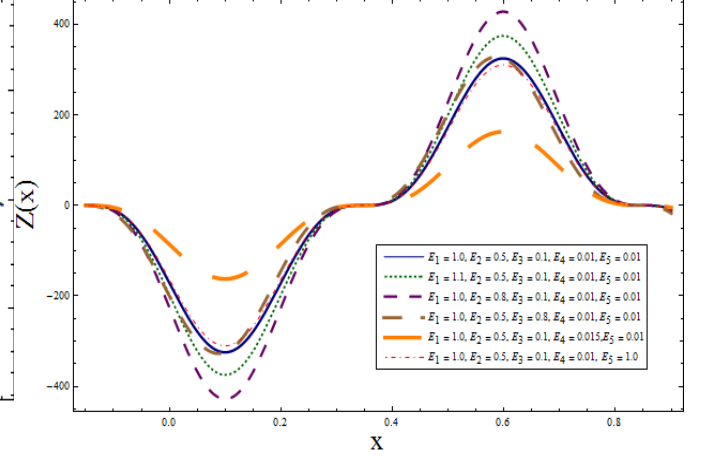
3.26

Fig. 3.25 : Influence of Sc on ϕ when $E_1 = 0.2$, $E_2 = E_3 = E_4 = 0.01$, $E_5 = 0.1$, $Sr = Du = M = R = \lambda_1 = 0.8$, $Pr = T' = 1.0$, $K_1 = 0.1$, $Ec = 2.0$, $x = \epsilon = 0.2$, $t = 0.1$.

Fig. 3.26 : Influence of R on ϕ when $E_1 = 0.2$, $E_2 = E_3 = E_4 = 0.01$, $E_5 = 0.1$, $Sr = Du = Sc = M = \lambda_1 = 0.8$, $Pr = T' = 1.0$, $K_1 = 0.1$, $Ec = 2.0$, $x = \epsilon = 0.2$, $t = 0.1$.



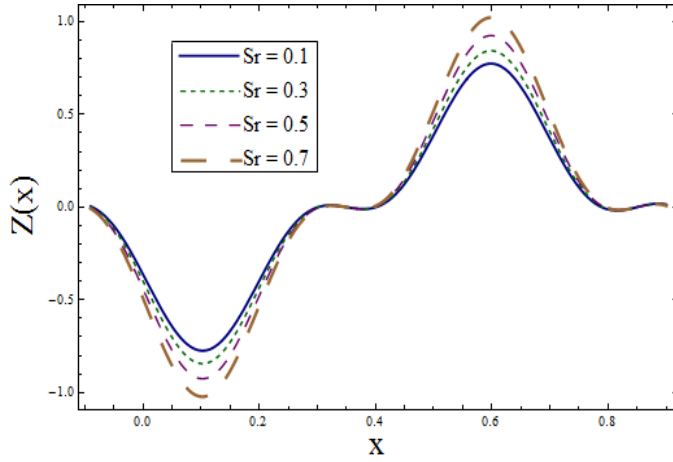
3.27



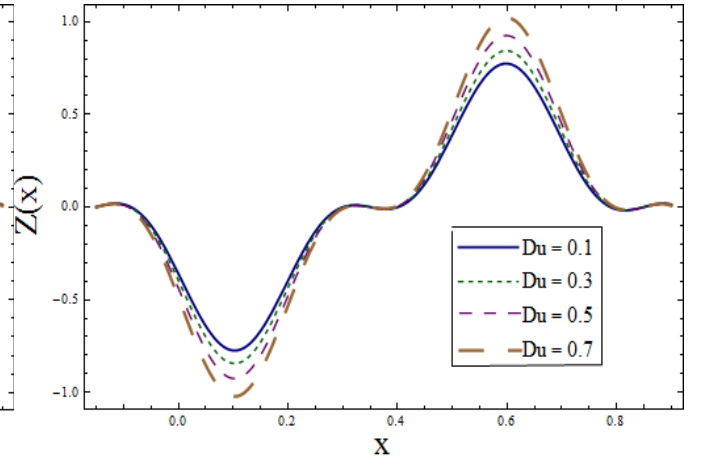
3.28

Fig. 3.27 : Effect of T' on Z when $E_1 = 0.2$, $E_2 = E_3 = E_4 = 0.01$, $E_5 = 0.1$,
 $Sr = Du = Sc = R = M = \lambda_1 = 0.8$, $K_1 = 0.1$, $Pr = 1.0$, $Ec = 2.0$, $t = 0.1$, $\epsilon = 0.2$.

Fig. 3.28 : Effect of wall properties on Z when $Sr = Du = Sc = R = M = \lambda_1 = 0.8$,
 $T' = Pr = 1.0$, $K_1 = 0.1$, $Ec = 2.0$, $t = 0.1$, $\epsilon = 0.2$.



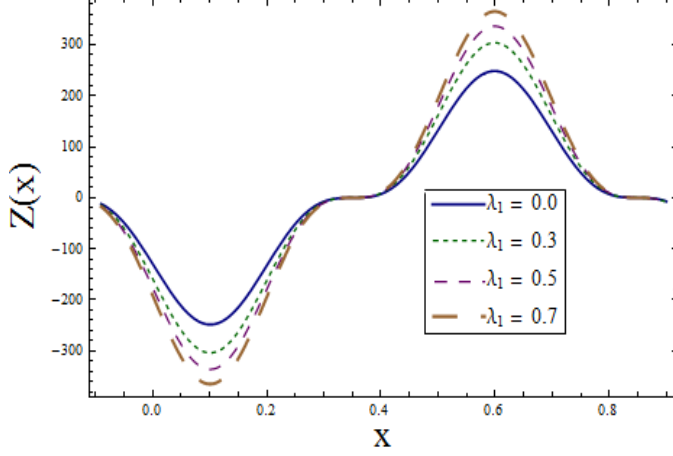
3.29



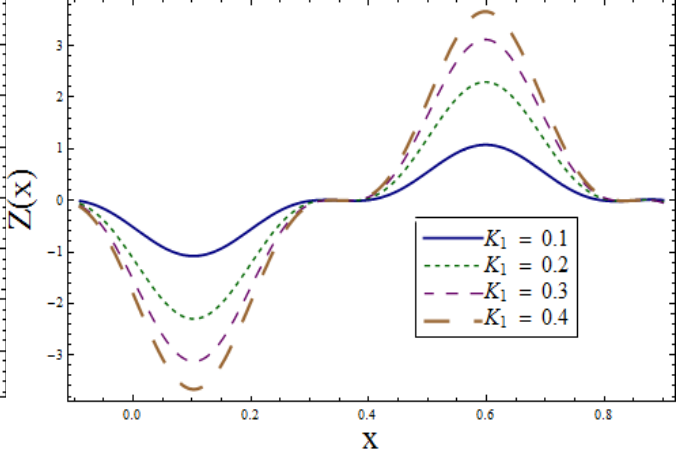
3.30

Fig. 3.29 : Effect of Sr on Z when $E_1 = 0.2$, $E_2 = E_3 = E_4 = 0.01$, $E_5 = 0.1$,
 $Du = Sc = R = M = \lambda_1 = 0.8$, $Pr = T' = 1.0$, $K_1 = 0.1$, $Ec = 2.0$, $t = 0.1$, $\epsilon = 0.2$.

Fig. 3.30 : Effect of Du on Z when $E_1 = 0.2$, $E_2 = E_3 = E_4 = 0.01$, $E_5 = 0.1$,
 $Sr = Sc = R = M = \lambda_1 = 0.8$, $Pr = T' = 1.0$, $K_1 = 0.1$, $Ec = 2.0$, $t = 0.1$, $\epsilon = 0.2$.



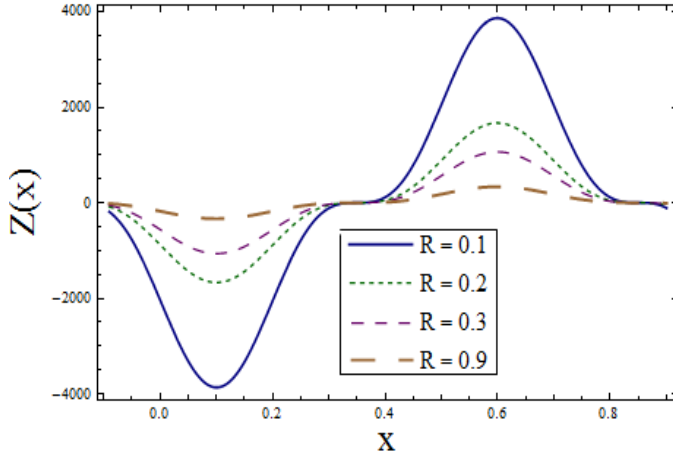
3.31



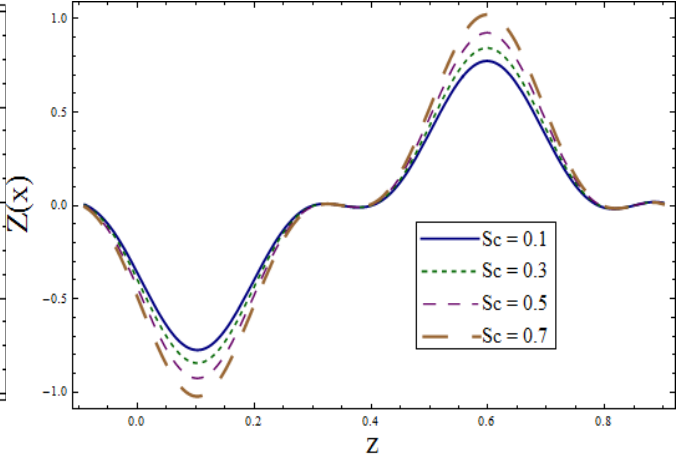
3.32

Fig. 3.31 : Effect of λ_1 on Z when $E_1 = 0.2$, $E_2 = E_3 = E_4 = 0.01$, $E_5 = 0.1$,
 $Sr = Du = Sc = R = M = 0.8$, $Pr = T' = 1.0$, $K_1 = 0.1$, $Ec = 2.0$, $t = 0.1$, $\epsilon = 0.2$.

Fig. 3.32 : Effect of K_1 on Z when $E_1 = 0.2$, $E_2 = E_3 = E_4 = 0.01$, $E_5 = 0.1$,
 $Sr = Du = Sc = R = M = \lambda_1 = 0.8$, $Pr = T' = 1.0$, $Ec = 2.0$, $t = 0.1$, $\epsilon = 0.2$.



3.33



3.34

Fig. 3.33 : Effect of R on Z when $E_1 = 0.2$, $E_2 = E_3 = E_4 = 0.01$, $E_5 = 0.1$,
 $Sr = Du = Sc = M = \lambda_1 = 0.8$, $Pr = T' = 1.0$, $K_1 = 0.1$, $Ec = 2.0$, $t = 0.1$, $\epsilon = 0.2$.

Fig. 3.34 : Effect of Sc on Z when $E_1 = 0.2$, $E_2 = E_3 = E_4 = 0.01$, $E_5 = 0.1$,
 $Sr = Du = R = M = \lambda_1 = 0.8$, $Pr = T' = 1.0$, $K_1 = 0.1$, $Ec = 2.0$, $t = 0.1$, $\epsilon = 0.2$.

3.5 Conclusions

Soret and Dufour effects on peristaltic transport of Jeffrey liquid in a channel with thermal radiation and porous medium are discussed in a rotating frame. It is observed in the present analysis that influence of wall parameters and Taylors number on both the velocities i.e. axial and secondary, are opposite. Moreover it is noticed that wall elastance parameters E_1 and E_2 show different behavior than E_i ($i = 3 - 5$) , due to viscous damping, on temperature. Soret, Dufour and Schmidt numbers behave in similar manner for temperature i.e. show increasing behavior for enhancing values of Sr , Du and Sc . Moreover, it is noted that concentration shows opposite behavior when compared with temperature profile. Heat transfer coefficient increases for Sr , Du and K_1 but it decrease for T' .

Chapter 4

Influence of rotation and thermophoresis on MHD peristaltic transport of Jeffrey fluid with convective conditions and wall properties

4.1 Introduction

This chapter aims to predict the effects of convective condition and particle deposition on peristaltic transport of Jeffrey fluid in a channel. The whole system is in a rotating frame of reference. The walls of channel are taken flexible. The fluid is electrically conducting in the presence of uniform magnetic field. Non-uniform heat source/sink is also considered. Mass transfer with chemical reaction is considered. Relevant equations for the problems under consideration are first modeled and then simplified using lubrication approach. Resulting equations for stream function and temperature are solved exactly whereas mass transfer equation is solved numerically. Impacts of various involved parameters appearing in the solutions are carefully analyzed.

4.2 Mathematical formulation

Here we investigate the problem for two-dimensional peristaltic flow of Jeffrey liquid in a symmetric channel of width $2d$. The channel walls are convectively heated. A uniform magnetic field of strength B_0 is applied. Electric field effects are taken zero and induced magnetic field is neglected due to small magnetic Reynolds number. Thermal radiation and non-uniform heat source/sink effects are present. The whole system is in a rotating frame of reference with constant angular velocity Ω . Flow inside the channel is induced due to propagation of sinusoidal waves of wavelength λ along the flexible walls of channel with constant speed c . The geometries of the wall surfaces are described by

$$z = \pm \eta(x, t) = \pm \left[d + a \sin \frac{2\pi}{\lambda} (x - ct) \right], \quad (4.1)$$

where t and a represent the time and wave amplitude respectively. Here $+$ and $-$ signs designate the upper and lower wall of channel. In rotating frame the set of pertinent field equations governing the flow are

$$\frac{\partial u}{\partial x} + \frac{\partial w}{\partial z} = 0, \quad (4.2)$$

$$\rho \left[\frac{du}{dt} \right] - 2\rho\Omega v = -\frac{\partial \hat{p}}{\partial x} + \frac{\partial S_{xx}}{\partial x} + \frac{\partial S_{xy}}{\partial y} + \frac{\partial S_{xz}}{\partial z} - \sigma B_0^2 u, \quad (4.3)$$

$$\rho \left[\frac{dv}{dt} \right] + 2\rho\Omega u = -\frac{\partial \hat{p}}{\partial y} + \frac{\partial S_{yx}}{\partial x} + \frac{\partial S_{yy}}{\partial y} + \frac{\partial S_{yz}}{\partial z} - \sigma B_0^2 v, \quad (4.4)$$

$$\rho \left[\frac{dw}{dt} \right] = -\frac{\partial \hat{p}}{\partial z} + \frac{\partial S_{zx}}{\partial x} + \frac{\partial S_{zy}}{\partial y} + \frac{\partial S_{zz}}{\partial z}, \quad (4.5)$$

$$\begin{aligned} \rho C_p \frac{dT}{dt} = & \kappa \left[\frac{\partial^2 T}{\partial x^2} + \frac{\partial^2 T}{\partial z^2} \right] + S_{xx} \frac{\partial u}{\partial x} + S_{xz} \left(\frac{\partial u}{\partial z} + \frac{\partial w}{\partial x} \right) + S_{zz} \frac{\partial w}{\partial z} \\ & - \frac{\partial q_r}{\partial z} + Q_0(T - T_a), \end{aligned} \quad (4.6)$$

$$\frac{dC}{dt} = D \left[\frac{\partial^2 C}{\partial x^2} + \frac{\partial^2 C}{\partial z^2} \right] - \frac{\partial (V_T(C - C_0))}{\partial z} - k_1(C - C_0), \quad (4.7)$$

in which $\hat{p} = p - \frac{1}{2}\rho\Omega^2(x^2 + y^2)$ represents the modified pressure. Here ρ is the fluid density, Ω the angular velocity, C_p the specific heat at constant volume, κ the thermal conductivity, T the temperature of fluid, T_a the ambient temperature, Q_0 the non-uniform heat source/sink parameter, D the coefficient of mass diffusivity, C the concentration of fluid, C_0 the concentration

at lower wall and d/dt the material time differentiation.

Thermophoretic velocity V_T can be defined in the form [163] :

$$V_T = k^{**}\nu \frac{\nabla T}{T_r} = -\frac{k^{**}\nu}{T_r} \frac{\partial T}{\partial z}, \quad (4.8)$$

in which T_r is the reference temperature, ν is the fluid kinematic viscosity and k^{**} is the thermophoretic coefficient. Invoking Eq. (4.8) into Eq. (4.7) we get

$$\frac{dC}{dt} = D \left[\frac{\partial^2 C}{\partial x^2} + \frac{\partial^2 C}{\partial y^2} + \frac{\partial^2 C}{\partial z^2} \right] + \frac{k^*\nu}{T_r} \left[\frac{\partial}{\partial z} \left(\frac{\partial T}{\partial z} (C - C_0) \right) \right] - k_1(C - C_0). \quad (4.9)$$

Governing equation for flexible wall satisfies

$$L(\eta) = p - p_0, \quad (4.10)$$

with

$$L = -\tau' \frac{\partial^2}{\partial x^2} + m_1 \frac{\partial^2}{\partial t^2} + d' \frac{\partial}{\partial t} + b \frac{\partial^4}{\partial x^4} + k_2.$$

In above equation τ' is the elastic tension in the membrane, m the mass per unit area, d' the coefficient of viscous damping forces, b the flexural rigidity, k_2 the constant spring stiffness and p_0 the pressure on the outer side of the wall due to the muscles tension. It is assumed that $p_0 = 0$. The stress continuity condition implies that at the fluid and walls interfaces the pressure must be same as that which acts on the fluid at $z = \pm\eta$. Using x - momentum equation and continuity of stress at $z = \pm\eta$ the dynamic boundary condition can be expressed as follows

$$\frac{\partial}{\partial x} L(\eta) = \frac{\partial p}{\partial x} = \frac{\partial S_{xx}}{\partial x} + \frac{\partial S_{xy}}{\partial y} + \frac{\partial S_{xz}}{\partial z} - \sigma B_0^2 u + 2\rho\Omega v - \rho \frac{du}{dt} \quad \text{at } (z = \pm\eta), \quad (4.11)$$

Boundary conditions for the flow under consideration are defined as follows:

$$u = 0, v = 0, \quad \text{at} \quad z = \pm\eta, \quad (4.12)$$

$$\begin{aligned} \kappa \frac{\partial T}{\partial z} &= -\eta_1 (T - T_a) \quad \text{at} \quad z = +\eta, \\ \kappa \frac{\partial T}{\partial z} &= -\eta_1 (T_a - T) \quad \text{at} \quad z = -\eta, \end{aligned} \quad (4.13)$$

$$\phi = \begin{Bmatrix} C_1 \\ C_0 \end{Bmatrix} \quad \text{at} \quad z = \pm\eta. \quad (4.14)$$

Here η_1 stands for heat transfer coefficient and C_1/C_0 are the concentration at the upper/lower walls respectively. We consider the non-dimensional variables as follows:

$$\begin{aligned} x^* &= \frac{x}{\lambda}, \quad y^* = \frac{y}{\lambda}, \quad z^* = \frac{z}{d}, \quad p^* = \frac{d^2 p}{c\mu\lambda}, \quad t^* = \frac{ct}{\lambda}, \\ u^* &= \frac{u}{c}, \quad v^* = \frac{v}{c}, \quad w^* = \frac{w}{c}, \quad \mathbf{S}^* = \frac{d\mathbf{S}}{\mu c}, \quad \eta^* = \frac{\eta}{d}, \\ \lambda_2^* &= \frac{c}{d}\lambda_2, \quad \theta = \frac{T - T_a}{T_a}, \quad \phi = \frac{C - C_0}{C_1 - C_0}, \quad \delta = \frac{d}{\lambda}, \\ \text{Re} &= \frac{cd}{\nu}, \quad u = \psi_z, \quad w = -\delta\psi_x. \end{aligned}$$

Utilizing the above mentioned variables and applying lubrication approach [21], Eqs. (4.3) – (4.6) and (4.9) – (4.14) give

$$-2T'v = -\frac{\partial p}{\partial x} + \frac{\partial}{\partial z}S_{xz} - M^2\psi_z, \quad (4.15)$$

$$2T'\frac{\partial\psi}{\partial z} = -\frac{\partial p}{\partial y} + \frac{\partial}{\partial z}S_{yz} - M^2v, \quad (4.16)$$

$$-\frac{\partial p}{\partial z} + \frac{\partial}{\partial z}S_{zz} = 0, \quad (4.17)$$

$$(1 + R)\frac{\partial^2\theta}{\partial z^2} + S\theta + Br\left(\frac{\partial^2\psi}{\partial z^2}\right)^2 = 0, \quad (4.18)$$

$$\frac{1}{Sc}\frac{\partial^2\phi}{\partial z^2} - \tau\left[\frac{\partial^2\theta}{\partial z^2}\phi + \frac{\partial\theta}{\partial z}\frac{\partial\phi}{\partial z}\right] - \gamma\phi = 0, \quad (4.19)$$

$$S_{xz} = \frac{1}{(1 + \lambda_1)}\frac{\partial^2\psi}{\partial z^2}, \quad (4.20)$$

$$S_{yz} = \frac{1}{(1 + \lambda_1)}\frac{\partial v}{\partial z}, \quad (4.21)$$

$$S_{zz} = 0, \quad (4.22)$$

where continuity equation (4.2) is identically satisfied. The boundary conditions in non-dimensionalized form are as follows:

$$\psi_z = 0, \quad v = 0, \quad \text{at} \quad z = \pm\eta, \quad (4.23)$$

$$\left[E_1 \frac{\partial^3}{\partial x^3} + E_2 \frac{\partial^3}{\partial x \partial t^2} + E_3 \frac{\partial^2}{\partial x \partial t} + E_4 \frac{\partial^5}{\partial x^5} + E_5 \frac{\partial}{\partial x} \right] \eta = \frac{\partial}{\partial z} S_{xz} - M^2 \frac{\partial \psi}{\partial z} + 2T' v \quad \text{at } z = \pm\eta, \quad (4.24)$$

$$\frac{\partial \theta}{\partial z} \pm Bi\theta = 0 \quad \text{at } z = \pm\eta, \quad (4.25)$$

$$\phi = \begin{cases} 1 \\ 0 \end{cases} \quad \text{at } z = \pm\eta, \quad (4.26)$$

where the dimensionless form of η is written as

$$\eta = (1 + \epsilon \sin 2\pi(x - t)).$$

In above expressions $T' (= \text{Re} \Omega d / c)$ is the Taylor number, $M^2 (= B_0^2 d^2 \sigma / \mu)$ the Hartman number, $Br (= \frac{c^2 \mu}{\kappa T_a})$ the Brinkman number, $R (= \frac{16 \sigma^* T_1^3}{3 \kappa k^*})$ the radiation parameter, $S (= \frac{Q_0 d^2}{\kappa})$ the non-uniform heat source/sink parameter, $Sc (= \frac{\nu}{D})$ the Schmidt number, $\tau (= \frac{-k^{**} T_a}{T_r})$ the thermophoretic parameter, $\gamma (= \frac{k_1 d^2}{\nu})$ the chemical reaction parameter (here $\gamma < 0$ shows the generative chemical reaction and $\gamma > 0$ for destructive chemical reaction), $Bi (= \frac{\eta_1 d}{\kappa})$ the Biot number, $\epsilon (= a/d)$ the amplitude ratio and $E_1 (= -\tau d^3 / \lambda^3 \mu c)$, $E_2 (= m_1 c d^3 / \lambda^3 \mu)$, $E_3 (= d' d^3 / \lambda^2 \mu)$, $E_4 (= b d^3 / c \lambda^5 \mu)$ and $E_5 (= k_2 d^3 / c \lambda \mu)$ the non-dimensional elasticity parameters.

Equations (4.17) and (4.22) show that pressure is not a function of z . Further we can neglect the pressure term in Eq. (4.16) as secondary flow is the result of rotation. In view of these facts, we can write Eqs. (4.15) and (4.16) in the forms

$$\frac{1}{(1 + \lambda_1)} \psi_{zzzz} - M^2 \psi_{zz} + 2T' v = 0, \quad (4.27)$$

$$\frac{1}{(1 + \lambda_1)} v_{zz} - M^2 v - 2T' \psi_z = 0. \quad (4.28)$$

4.3 Solutions

The Eqs. (4.18), (4.27) and (4.28) are solved exactly with corresponding boundary conditions (4.23 – 4.25). The exact solutions are given as

$$\psi = B_{13}z + B_{14} \sinh[\sqrt{B_1}z] + B_{15} \sinh[\sqrt{B_2}z], \quad (4.29)$$

$$\begin{aligned} v = & (B_{21} + B_{22} \cosh[\sqrt{B_1}z] + B_{23} \cosh[\sqrt{B_2}z]) \\ & \times \left(\cosh[(\sqrt{B_1} + \sqrt{B_2})z] - \sinh[(\sqrt{B_1} + \sqrt{B_2})z] \right) \\ & \times \left(\cosh[(\sqrt{B_1} + \sqrt{B_2})z] + \sinh[(\sqrt{B_1} + \sqrt{B_2})z] \right), \end{aligned} \quad (4.30)$$

$$\begin{aligned} \theta = & D_1 \cos[\sqrt{A_1}z] + D_2 \cos[2\sqrt{B_1}z] + D_3 \cosh[\sqrt{B_1}z] \cosh[\sqrt{B_2}z] \\ & + D_4 \cosh[\sqrt{B_2}z]^2 + D_5 \sinh[\sqrt{B_1}z] \sinh[\sqrt{B_2}z] + D_6 \sinh[\sqrt{B_2}z]^2 + D_7 \end{aligned} \quad (4.31)$$

The concentration equation (4.19) is solved numerically using NDSolve in MATHEMATICA where B_i ($i = 1 - 23$) and D_j ($j = 1 - 7$) are give below:

$$\begin{aligned} B_1 &= (\alpha - 2\iota\beta), \quad B_2 = (\alpha + 2\iota\beta), \quad B_3 = (\alpha^2 + 4\beta^2), \quad B_4 = (-i\alpha - 2\beta), \quad B_5 = (-i\alpha + 2\beta), \\ B_6 &= (i\alpha + 2\beta), \quad B_7 = \frac{B_5 L_0 \alpha (4\beta + iB_2 \sec h[\sqrt{B_1}\eta] + B_4 \sec h[\sqrt{B_2}\eta])}{2B_3}, \\ B_8 &= \frac{B_6 L_0 \alpha (4\beta + iB_2 \sec h[\sqrt{B_1}\eta] + B_4 \sec h[\sqrt{B_2}\eta])}{2B_3}, \\ B_9 &= \frac{L_0 \alpha}{8\sqrt{B_1} B_2^{3/2} B_3 B_4} (4\beta + iB_2 \sec h[\sqrt{B_1}\eta] + B_4 \sec h[\sqrt{B_2}\eta]), \\ B_{10} &= (B_2 \alpha \cosh[\sqrt{B_2}\eta] + \cosh[\sqrt{B_1}\eta]) (B_1 \alpha + 8\beta^2 \cosh[\sqrt{B_2}\eta]), \\ B_{11} &= \frac{1}{4B_1^{3/2} B_{10} B_2^{3/2}} (2L_0 \alpha^2 + B_2 (B_8 - 2iL_0 \beta) \cosh[\sqrt{B_2}\eta] + B_1 (B_7 + 2iL_0 \beta) \cosh[\sqrt{B_2}\eta]), \\ B_{12} &= \frac{1}{2B_1^{3/2} B_{10} B_2^{3/2}} (2L_0 \alpha + (B_7 - B_1 L_0) \cosh[\sqrt{B_2}\eta] + \cosh[\sqrt{B_1}\eta] (B_8 - B_2 L_0 \\ & \quad - \frac{2L_0 \alpha \beta \cosh[\sqrt{B_2}\eta] (4\beta + iB_2 \sec h[\sqrt{B_1}\eta] + B_4 \cosh[\sqrt{B_2}\eta])}{B_3})), \\ B_{13} &= 2\sqrt{B_1 B_2} (-2B_{11} \alpha + B_{12} \alpha^2 + 4iB_9 \beta), \quad B_{14} = 2B_2^{3/2} (B_{11} - B_9 - iB_{12} \beta), \end{aligned}$$

$$\begin{aligned}
B_{15} &= 2B_1^{3/2}(B_{11} + B_9 + iB_{12}\beta), \quad B_{16} = (-B_3B_8 + B_2B_3L_0 + 2B_4L_0\alpha\beta + 8L_0\alpha\beta^2 \cosh[\sqrt{B_2}\eta]), \\
B_{17} &= (B_2(iB_8 + 2L_0\beta) \cosh[\sqrt{B_1}\eta] + i(2L_0\alpha^2 + B_1(B_7 + 2iL_0\beta) \cosh[\sqrt{B_2}\eta])), \\
B_{18} &= (iB_2 \cosh[\sqrt{B_2}\eta] + \cosh[\sqrt{B_1}\eta](B_4 + 4\beta \cosh[\sqrt{B_2}\eta])) \sec h[\sqrt{B_1}\eta] \sec h[\sqrt{B_2}\eta], \\
B_{19} &= (-2B_3L_0\alpha + B_{16} \cosh[\sqrt{B_1}\eta] + (-B_3B_7 + B_1B_3L_0 + 2iB_2L_0\alpha\beta) \cosh[\sqrt{B_2}\eta]), \\
B_{20} &= (B_2\alpha \cosh[\sqrt{B_2}\eta] + \cosh[\sqrt{B_1}\eta](B_1\alpha + 8\beta^2 \cosh[\sqrt{B_2}\eta])), \\
B_{21} &= \frac{8\beta}{4B_2}(-\frac{B_{17}}{B_{20}B_4} + \frac{B_{19}\alpha}{B_1B_{20}B_3} + \frac{B_{18}L_0\beta}{B_1B_3}), \quad B_{22} = \frac{1}{4B_2}(\frac{2B_{17}B_5}{B_{20}B_4} + \frac{B_{18}B_2L_0\alpha}{B_1B_3} - \frac{4B_{19}B_2\beta}{B_1B_{20}B_3}), \\
B_{23} &= \frac{1}{4B_2}(\frac{2B_{17}B_6}{B_{20}B_4} + \frac{B_{18}L_0\alpha}{B_3} - \frac{4B_{19}\beta}{B_{20}B_3}), \\
D_1 &= C_1 = (A_2(-A_1(A_1 + 4B_1)B_{15}^2B_2^2(A_1^2 + (B_1 - B_2)^2 + 2A_1(B_1 + B_2))Bi_1 \cosh[\sqrt{B_2}\eta] \\
&\quad - 4A_1B_1(A_1 + 4B_1)B_{14}B_{15}B_2^{3/2}(A_1 + 4B_2) \cosh[\sqrt{B_2}\eta](-2\sqrt{B_1}Bi_1 \cosh[\sqrt{B_1}\eta] \\
&\quad + (A_1 - B_1 + B_2) \sinh[\sqrt{B_1}\eta] + (A_1 + 4B_2)(A_1^2 + (B_1 - B_2)^2 + 2A_1(B_1 + B_2)) \\
&\quad ((A_1 + 4B_1)(B_1^2B_{14}^2 + B_{15}^2B_2^2)Bi_1 - A_1B_1^2B_{14}^2(Bi_1 \cosh[2\sqrt{B_1}\eta] + 2\sqrt{B_1} \sinh[2\sqrt{B_1}\eta]) \\
&\quad - 4A_1B_1(A_1 + 4B_1)B_{14}B_{15}B_2(A_1 + 4B_2)(\sqrt{B_1}(A_1 + B_1 - B_2) \cosh[\sqrt{B_1}\eta] \\
&\quad + (A_1 + B_1 + B_2)Bi_1 \sinh[\sqrt{B_1}\eta]) \sinh[\sqrt{B_2}\eta] - 2A_1(A_1 + 4B_1)B_{15}^2B_2^{5/2}(A_1^2 \\
&\quad + (B_1 - B_2)^2 + 2A_1(B_1 + B_2)) \sinh[2\sqrt{B_2}\eta])), \\
D_2 &= -\frac{A_2B_1^2B_{14}^2}{2(A_1 + 4B_1)}, \quad D_3 = \frac{4A_2B_1^{3/2}B_{14}B_{15}B_2^{3/2}}{A_1^2 + (B_1 - B_2)^2 + 2A_1(B_1 + B_2)}, \quad D_4 = -\frac{A_2B_{15}^2B_2^2}{2(A_1 + 4B_1)}, \\
D_5 &= -\frac{2A_2B_1B_{14}B_{15}B_2(A_1 + B_1 + B_2)}{A_1^2 + (B_1 - B_2)^2 + 2A_1(B_1 + B_2)}, \quad D_6 = -\frac{A_2B_{15}^2B_2^2}{2(A_1 + 4B_1)}, \quad D_7 = \frac{A_2(B_1^2B_{14}^2 + B_{15}^2B_2^2)}{2A_1}.
\end{aligned}$$

The heat transfer coefficient at the walls is written as under:

$$\begin{aligned}
Z &= \eta_x \theta_z(\eta), \\
Z &= \eta_x(-\sqrt{A_1}D_1 \sin[\sqrt{A_1}\eta] + (\sqrt{B_1}D_3 + \sqrt{B_2}D_5) \cosh[\sqrt{B_2}\eta] \sinh[\sqrt{B_1}\eta] \\
&\quad + 2\sqrt{B_1}D_2 \sinh[\sqrt{B_1}\eta] + (\sqrt{B_2}D_3 + \sqrt{B_1}D_5) \cosh[\sqrt{B_1}\eta] \sinh[\sqrt{B_2}\eta] \\
&\quad + \sqrt{B_2}(D_4 + D_6) \sinh[2\sqrt{B_2}\eta]).
\end{aligned} \tag{4.32}$$

4.4 Results and discussion

Note that Figs. (4.1 – 4.8) depict the behavior of axial (u) and secondary (v) velocities whereas Figs. (4.9 – 4.24) show the results for temperature (θ) and concentration ϕ . The heat transfer coefficient Z and streamlines ψ are displayed in the Figs. (4.25 – 4.31).

4.4.1 Axial and secondary velocities

Fig. (4.1) studies the influence of wall parameters on axial velocity. The parameters E_1 and E_2 show elastic nature of the walls whereas E_3 represents dissipative property. Here E_4 and E_5 are rigidity and stiffness parameters respectively. It is noteworthy that for $E_3 = 0$, the wall moves up and down with no damping force on it. The velocity enhances for increasing the values of elastance parameters (i.e. E_1 and E_2) and it shows opposite behavior for E_3 , E_4 and E_5 . In fact wall damping is a kind of resistive force which decreases the velocity. This damping force has similar effect on velocity in the presence of rigidity and stiffness. We notice from Fig. (4.2) that by increasing rotation parameter T' the velocity decreases in axial direction. It can also be observed that axial velocity is greater in the absence of rotation. Decrease in velocity is seen for increasing values of λ_1 (see Fig. 4.3). Imposing magnetic field in normal direction to flow produces drag or resistive force that has tendency to suppress the movement of fluid which in turn reduces the axial velocity (Fig. 4.4).

The rotation of channel about z-axis induces a secondary flow v in y-direction. Figs. (4.5 – 4.8) are prepared to analyze the effects of involved parameters on v . Fig. (4.5) explains the influence of wall parameters on v . It is revealed that there is a decrease in E_2 . However secondary velocity enhances for larger values of E_3 , E_4 and E_5 . Effect of Taylor number T' on v is presented through Fig. (4.6). It is pertinent to mention here that secondary velocity enhances when rotation parameter increases. There is no secondary velocity for $T' = 0$. Increasing behavior is noticed for velocity for larger values of λ_1 (see Fig. 4.7). It is depicted from Fig. (4.8) that secondary velocity shows similar behavior for increasing Hartman number M as we observed for an axial velocity.

4.4.2 Temperature profile

Figs. (4.9 – 4.16) are displayed in order to study the behavior of temperature for the involved parameters. Fig. (4.9) is prepared to study wall properties. These results indicate that temperature starts increasing as we increase the values of E_1 and E_2 . On the other hand the temperature shows decreasing behavior for E_3 , E_4 and E_5 . Temperature is defined as an average kinetic energy of particles. Therefore as velocity increases for E_1 and E_2 then temperature rises. Similar behavior is noticed for E_3 , E_4 and E_5 corresponding to velocity. We noticed from Fig. (4.10) that θ decreases as we increase the rotation parameter T' . According to Fig. (4.11), θ decreases for larger radiation parameter R . The internal friction produced by shear in the flow generates the heat which in turn rises the temperature of fluid. Hence there is an enhancement of temperature for increasing values of Br (Fig.4.12). We have observed from Fig. (4.13) that temperature is greater for Jeffrey fluid when compared with the viscous case i.e. $\lambda_1 = 0$. Effect of Biot number is shown in Fig. (4.14). The Biot number is taken larger than one due to non-uniform temperature fields inside the fluid. However problems dealing with small Biot number are thermally simple due to uniform temperature distribution within the fluid. The obtained result shows decrease in temperature. Decreased thermal conductivity with an increase in Biot number justifies the temperature drop. Fig. (4.15) studies the influence of Hartman number M on temperature. Rise of temperature is noticed for increasing values of M . Effect of heat generation/absorption coefficient S is shown in Fig. (4.16). This Fig. indicates that for $S > 0$ (heat generation) the temperature increases whereas it decreases for $S < 0$ (heat absorption).

4.4.3 Concentration profile

Effect of several controlling parameters on dimensionless concentration ϕ is discussed in this subsection through Figs. (4.17 – 4.24). It is depicted from Fig. (4.17) that concentration field decreases for the increasing values of E_1 and E_2 whereas it increases for E_3 , E_4 and E_5 . Fig. (4.18) illustrates the influence of Taylor number T' on ϕ . It is noticed that concentration is decreased when we increase the value of T' . Here it can be seen that for increased Schmidt number Sc the concentration get decreased (Fig. 4.19). Since Sc is defined as the ratio of momentum diffusivity (viscosity) and mass diffusivity therefore it is used to characterize the

fluid flows in which there are simultaneous momentum and mass diffusion convection processes. Influence of chemical reaction parameter γ on concentration field cannot be ignored when discussing mass transfer. Chemical reaction increases the rate of interfacial mass transfer. Due to which local concentration is decreased thus increasing its concentration gradient and flux when we have constructive chemical reaction. That is why ϕ decreases for constructive chemical reaction ($\gamma > 0$) and it increases for destructive chemical reaction ($\gamma < 0$) (Fig. 4.20). Effects of λ_1 and M on concentration field are displayed through Figs. (4.21) and (4.22). Effect of heat generation/absorption coefficient on ϕ is demonstrated in Fig. (4.23). It is observed that concentration is increased when we consider heat generation. We have sketched Fig. 4.24 to analyze the effect of thermophoresis parameter τ on ϕ . It can be seen that concentration is decreased upon increasing the value of thermophoretic parameter.

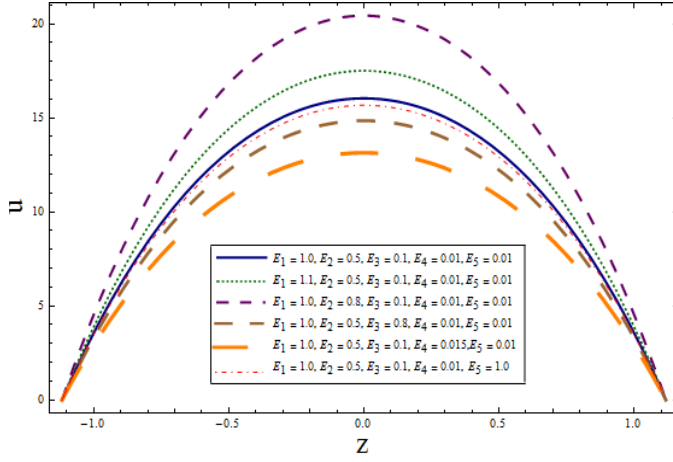
4.4.4 Heat transfer coefficient

The effects of wall properties, T' , Bi , S and R on the rate of heat transfer are plotted in Figs. (4.25 – 4.29). The heat transfer coefficient at the wall is denoted by $Z(x) = \eta_x \theta_z(\eta)$. It is noticed from Fig (4.25) that rate of heat transfer enhances for increasing values of E_1 and E_2 but it has opposite behavior for E_3 , E_4 and E_5 . Fig. (4.26) indicates a decrease in heat transfer between wall and fluid when rotation increases. Similar effect of heat transfer is observed for Biot number Bi (Fig. 4.27). Fig. (4.28) illustrates the influence of heat generation/absorption S on heat transfer coefficient. This Fig. shows that the rate of heat transfer is higher for heat generation ($S > 0$). The behavior of heat transfer coefficient for different values of R can be observed through Fig. (4.29). Decrease in the heat transfer rate is seen for increasing values of radiation parameter.

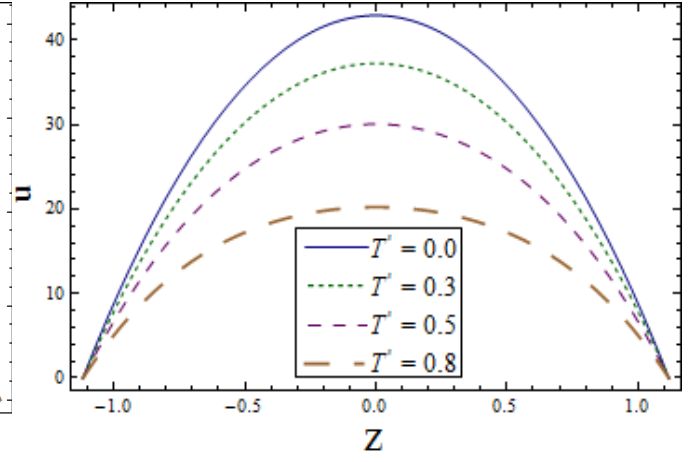
4.4.5 Trapping

In general the shape of streamlines is same as that of a boundary wall in the wave frame. Nevertheless some of streamlines split and enclose a bolus under certain conditions and this bolus moves as a whole with the waves. This phenomenon is known as trapping. Figs. (4.30(a) – 4.30(f)) are plotted to study the influence of wall parameters on streamlines. It is noticed that size of trapped bolus decreases for larger E_1 , E_2 and E_5 (see Figs. 4.30(b),

4.30(c) and 4.30(f)). From Fig. (4.30(d)) it is seen that by increasing the values of E_3 the size of bolus decreases. The size and number of streamlines decrease as we increase E_4 (see 4.30(e)). The streamlines for larger rotation parameter T' are shown in the Figs. (4.31(a)) and (4.31(b)). It is depicted from Fig. that size of streamlines are decreased for increasing values of T' .



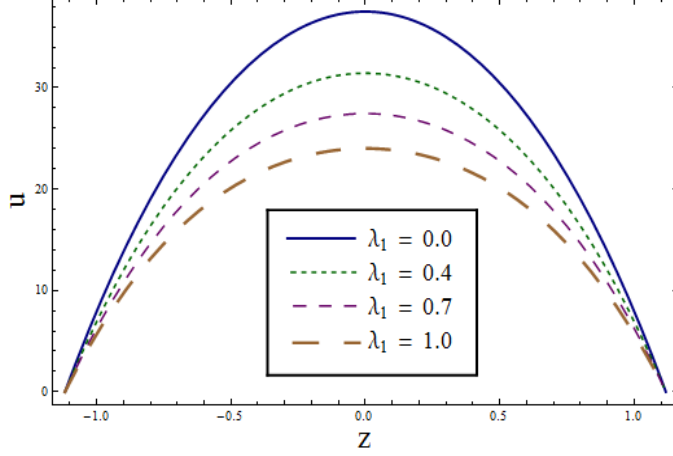
4.1



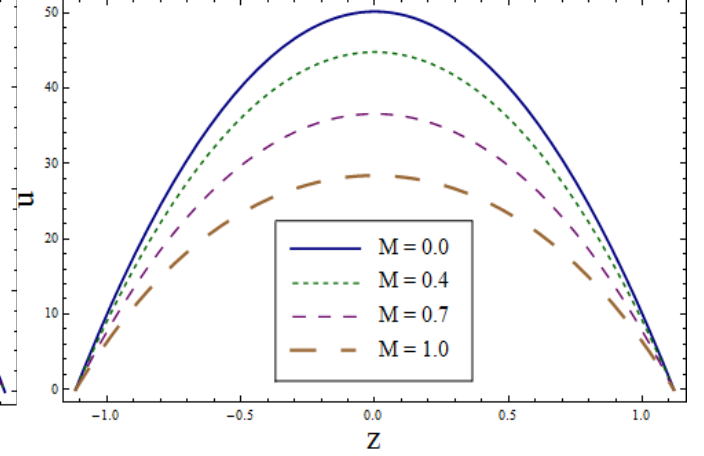
4.2

Fig. 4.1 : Variation of wall properties on u when $T' = 0.1$, $\lambda_1 = 0.5$, $M = 0.5$, $x = \epsilon = 0.2$, $t = 0.1$.

Fig. 4.2 : Variation of T' on u when $E_1 = E_2 = 3.0$, $E_3 = 0.01$, $E_4 = 0.1$, $E_5 = 0.1$, $M = 0.5$, $\lambda_1 = 0.5$, $x = \epsilon = 0.2$, $t = 0.1$.



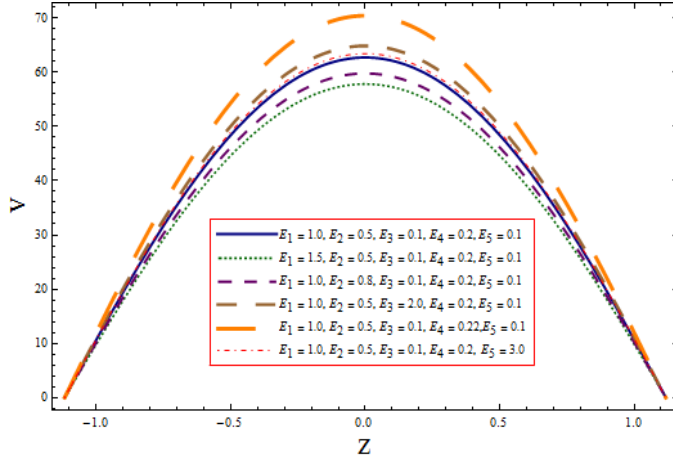
4.3



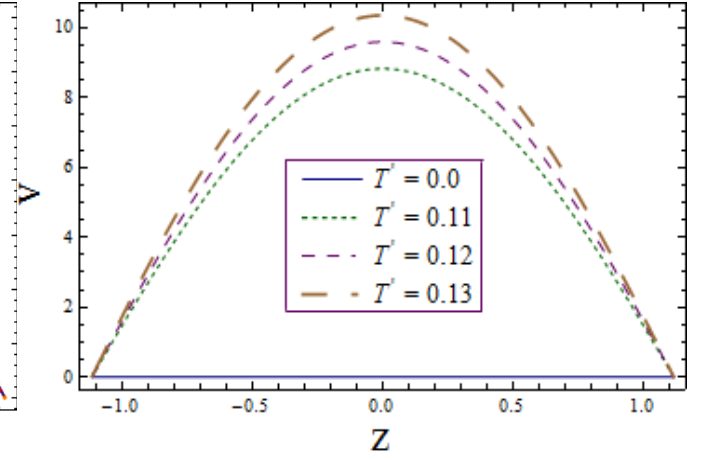
4.4

Fig. 4.3 : Variation of λ_1 on u when $E_1 = E_2 = 3.0$, $E_3 = 0.01$, $E_4 = 0.1$, $E_5 = 0.1$, $T' = 0.5$, $M = 0.5$, $x = \epsilon = 0.2$, $t = 0.1$.

Fig. 4.4 : Variation of M on u when $E_1 = E_2 = 3.0$, $E_3 = 0.01$, $E_4 = 0.1$, $E_5 = 0.1$, $T' = 0.5$, $\lambda_1 = 0.5$, $x = \epsilon = 0.2$, $t = 0.1$.



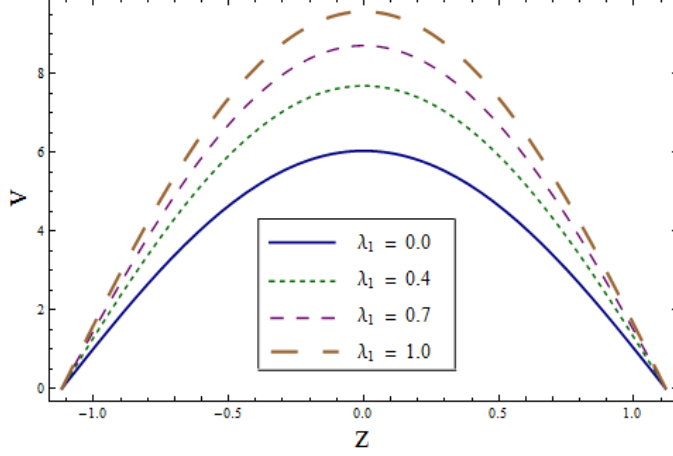
4.5



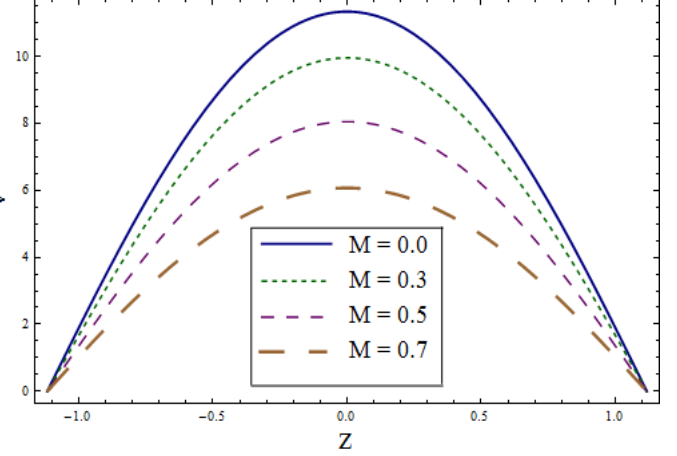
4.6

Fig. 4.5 : Variation of wall properties on v when $M = 0.5$, $\lambda_1 = 0.5$, $x = \epsilon = 0.2$, $t = 0.1$.

Fig. 4.6 : Variation T' on v when $E_1 = E_2 = 0.5$, $E_3 = 0.01$, $E_4 = E_5 = 0.1$, $M = \lambda_1 = 0.5$, $x = \epsilon = 0.2$, $t = 0.1$.



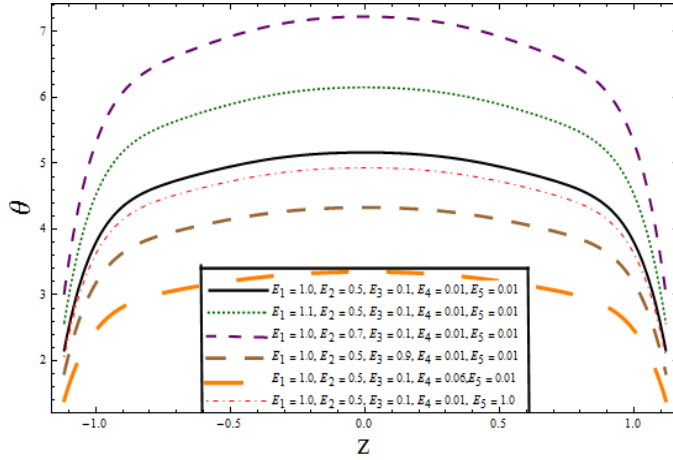
4.7



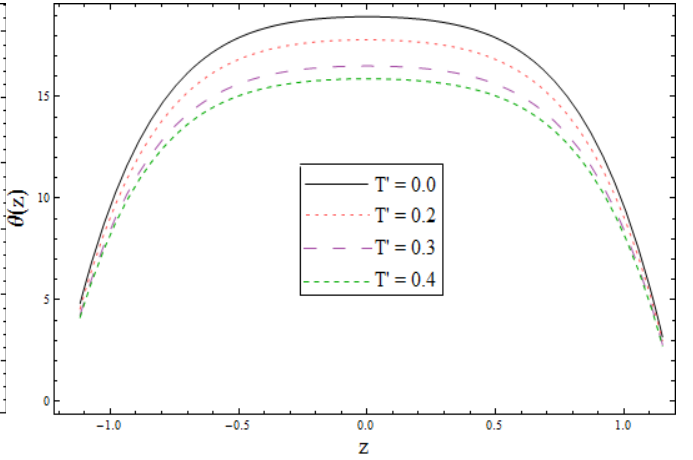
4.8

Fig. 4.7 : Variation of λ_1 on v when $E_1 = E_2 = 0.5$, $E_3 = 0.01$, $E_4 = 0.1$, $E_5 = 0.6$, $M = 0.5$, $T' = 0.1$, $x = \epsilon = 0.2$, $t = 0.1$.

Fig. 4.8 : Variation of M on v when $E_1 = E_2 = 0.5$, $E_3 = 0.01$, $E_4 = 0.1$, $E_5 = 0.6$, $\lambda_1 = 0.5$, $T' = 0.1$, $x = \epsilon = 0.2$, $t = 0.1$.



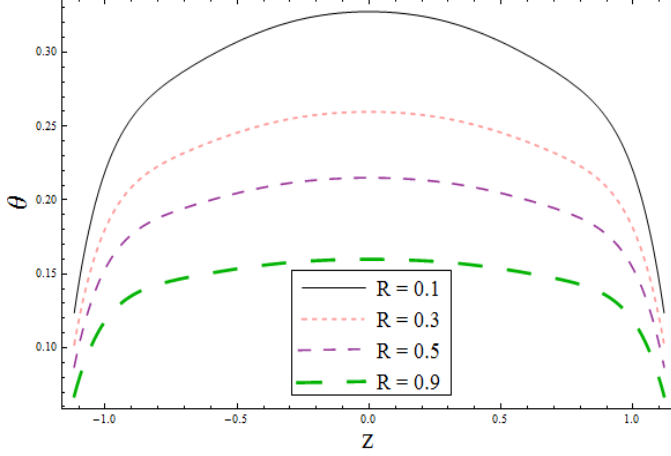
4.9



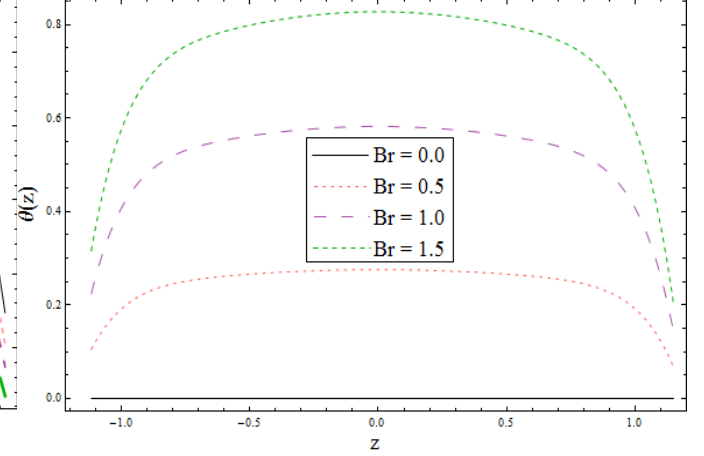
4.10

Fig. 4.9 : Variation of wall properties on θ when $R = M = \lambda_1 = 0.8$, $T' = Br = 2.0$, $Bi = 10.0$, $S = 0.5$, $x = \epsilon = 0.2$, $t = 0.1$.

Fig. 4.10 : Variation of T' on θ when $E_1 = E_2 = 0.1$, $E_3 = E_4 = 0.01$, $E_5 = 0.6$, $R = M = \lambda_1 = 0.8$, $Br = 2.0$, $Bi = 10.0$, $S = 0.5$, $x = \epsilon = 0.2$, $t = 0.1$.



4.11



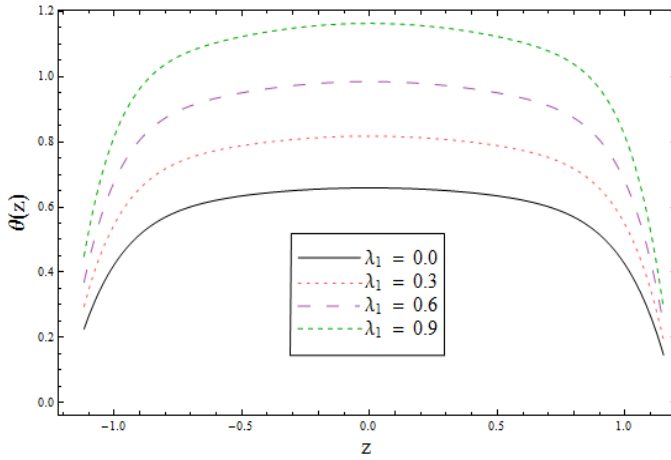
4.12

Fig. 4.11 : Variation of R on θ when $E_1 = E_2 = 0.1$, $E_3 = E_4 = 0.01$, $E_5 = 0.6$, $M = \lambda_1 = 0.8$,

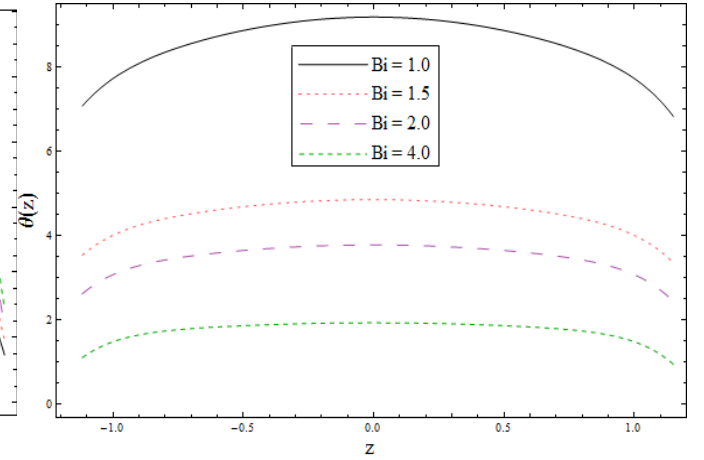
$$T' = Br = 2.0, Bi = 10.0, S = 0.5, x = \epsilon = 0.2, t = 0.1.$$

Fig. 4.12 : Variation of Br on θ when $E_1 = E_2 = 0.1$, $E_3 = E_4 = 0.01$, $E_5 = 0.6$,

$$R = M = \lambda_1 = 0.8, T' = 2.0, Bi = 10.0, S = 0.5, x = \epsilon = 0.2, t = 0.1.$$



4.13



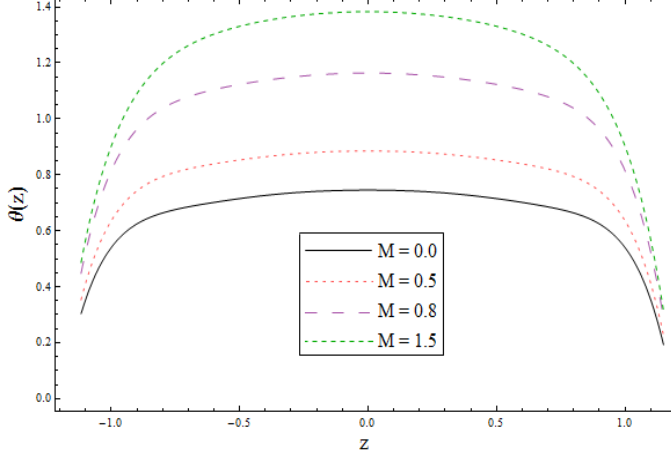
4.14

Fig. 4.13 : Variation of λ_1 on θ when $E_1 = E_2 = 0.1$, $E_3 = E_4 = 0.01$, $E_5 = 0.6$, $R = M = 0.8$,

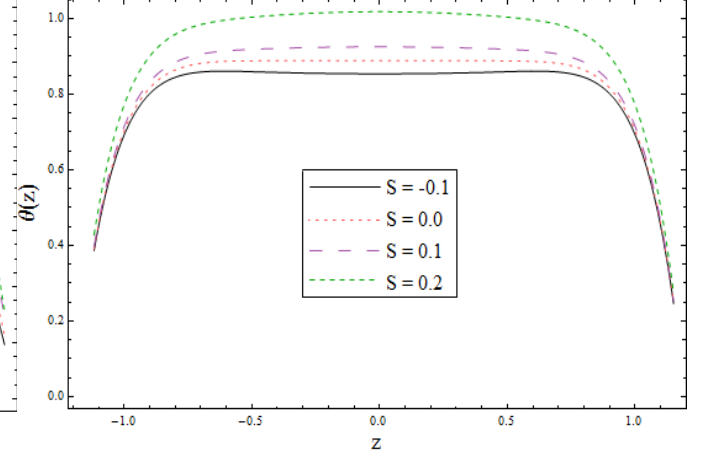
$$T' = Br = 2.0, Bi = 10.0, S = 0.5, x = \epsilon = 0.2, t = 0.1.$$

Fig. 4.14 : Variation of Bi on θ when $E_1 = E_2 = 0.1$, $E_3 = E_4 = 0.01$, $E_5 = 0.6$,

$$R = M = \lambda_1 = 0.8, T' = Br = 2.0, S = 0.5, x = \epsilon = 0.2, t = 0.1.$$



4.15



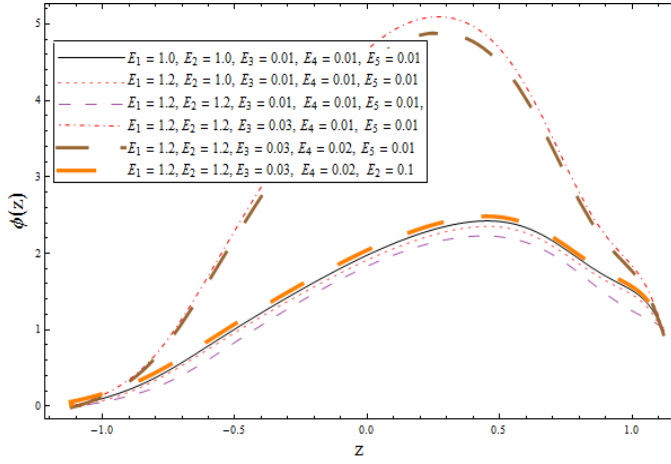
4.16

Fig. 4.15 : Variation of M on θ when $E_1 = E_2 = 0.1$, $E_3 = E_4 = 0.01$, $E_5 = 0.6$, $R = \lambda_1 = 0.8$,

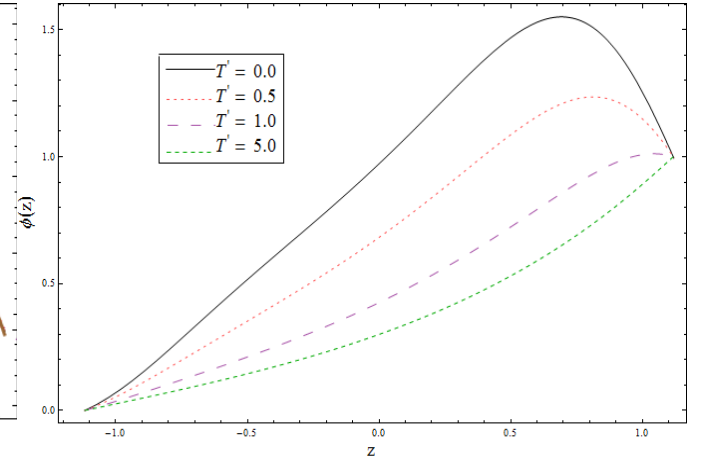
$$Tl = Br = 2.0, Bi = 10.0, S = 0.5, x = \epsilon = 0.2, t = 0.1.$$

Fig. 4.16 : Variation of S on θ when $E_1 = E_2 = 0.1$, $E_3 = E_4 = 0.01$, $E_5 = 0.6$,

$$R = M = \lambda_1 = 0.8, Tl = Br = 2.0, Bi = 10.0, x = \epsilon = 0.2, t = 0.1.$$



4.17



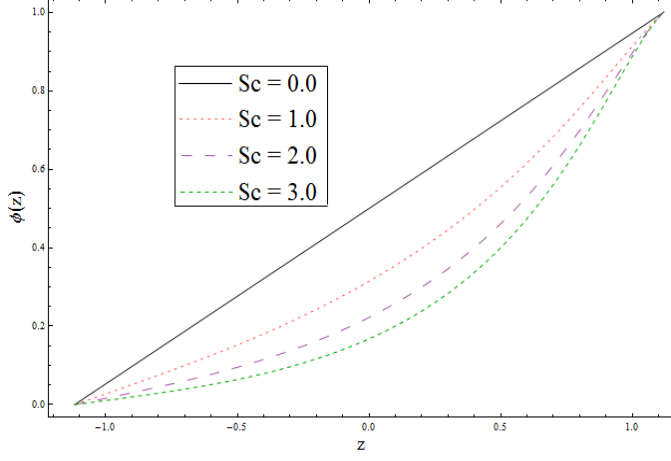
4.18

Fig. 4.17 : Variation of wall properties on ϕ when $\tau = 0.1$, $R = M = \lambda_1 = 0.8$, $Br = 2.0$,

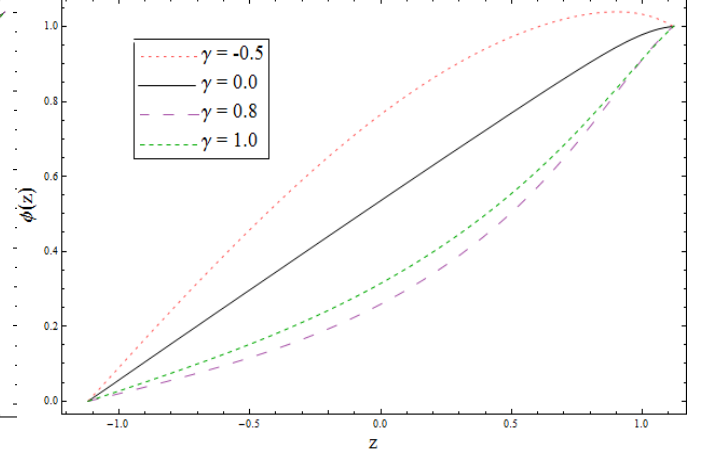
$$Bi = 10.0, S = 0.5, Sc = \gamma = 1.0, x = \epsilon = 0.2, t = 0.1.$$

Fig. 4.18 : Variation of T' on ϕ when $\tau = E_1 = E_2 = 0.1$, $E_3 = E_4 = 0.01$, $E_5 = 0.6$,

$$R = M = \lambda_1 = 0.8, Br = 2.0, Bi = 10.0, S = 0.5, Sc = \gamma = 1.0, x = \epsilon = 0.2, t = 0.1.$$



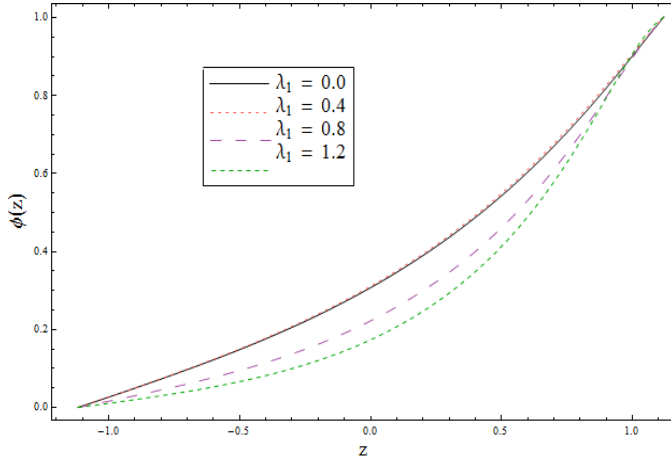
4.19



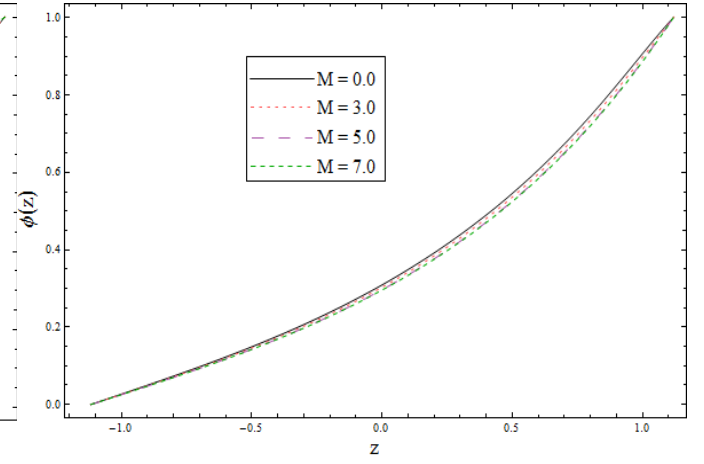
4.20

Fig. 4.19 : Variation of Sc on ϕ when $\tau = E_1 = E_2 = 0.1$, $E_3 = E_4 = 0.01$, $E_5 = 0.6$, $R = M = \lambda_1 = 0.8$, $T' = Br = 2.0$, $Bi = 10.0$, $S = 0.5$, $\gamma = 1.0$, $x = \epsilon = 0.2$, $t = 0.1$.

Fig. 4.20 : Variation of γ on ϕ when $\tau = E_1 = E_2 = 0.1$, $E_3 = E_4 = 0.01$, $E_5 = 0.6$, $R = M = \lambda_1 = 0.8$, $T' = Br = 2.0$, $Bi = 10.0$, $S = 0.5$, $Sc = 1.0$, $x = \epsilon = 0.2$, $t = 0.1$.



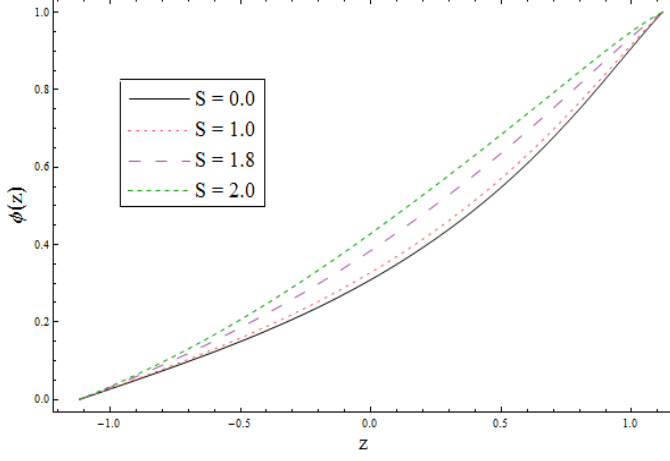
4.21



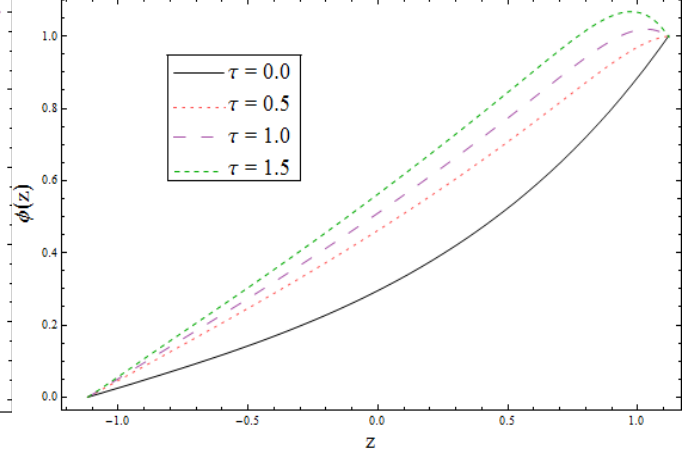
4.22

Fig. 4.21 : Variation of λ_1 on ϕ when $\tau = E_1 = E_2 = 0.1$, $E_3 = E_4 = 0.01$, $E_5 = 0.6$, $R = M = 0.8$, $T' = Br = 2.0$, $Bi = 10.0$, $S = 0.5$, $Sc = \gamma = 1.0$, $x = \epsilon = 0.2$, $t = 0.1$.

Fig. 4.22 : Variation of M on ϕ when $\tau = E_1 = E_2 = 0.1$, $E_3 = E_4 = 0.01$, $E_5 = 0.6$, $R = \lambda_1 = 0.8$, $T' = Br = 2.0$, $Bi = 10.0$, $S = 0.5$, $Sc = \gamma = 1.0$, $x = \epsilon = 0.2$, $t = 0.1$.



4.23



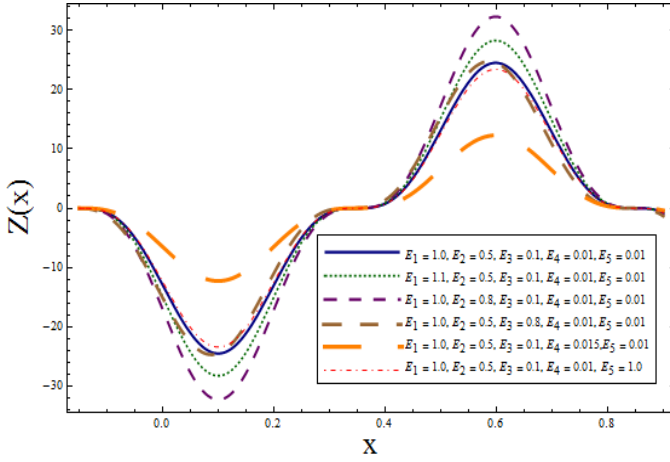
4.24

Fig. 4.23 : Variation of S on ϕ when $\tau = E_1 = E_2 = 0.1$, $E_3 = E_4 = 0.01$, $E_5 = 0.6$,

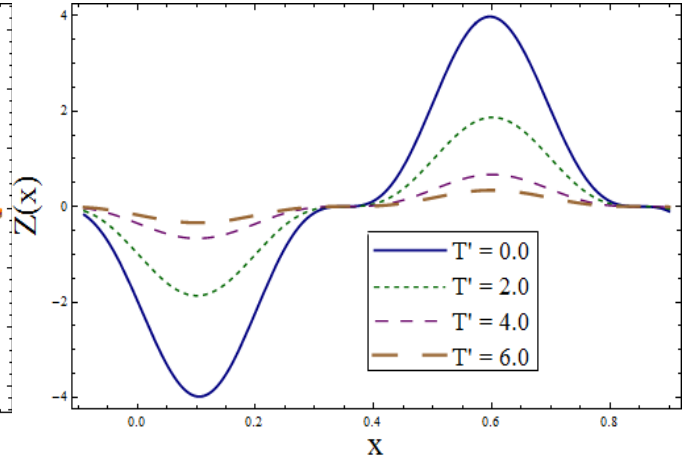
$R = M = \lambda_1 = 0.8$, $T' = Br = 2.0$, $Bi = 10.0$, $Sc = \gamma = 1.0$ $x = \epsilon = 0.2$, $t = 0.1$.

Fig. 4.24 : Variation of τ on ϕ when $E_1 = E_2 = 0.1$, $E_3 = E_4 = 0.01$, $E_5 = 0.6$,

$R = M = \lambda_1 = 0.8$, $T' = Br = 2.0$, $Bi = 10.0$, $S = 0.5$, $Sc = \gamma = 1.0$ $x = \epsilon = 0.2$, $t = 0.1$.



4.25



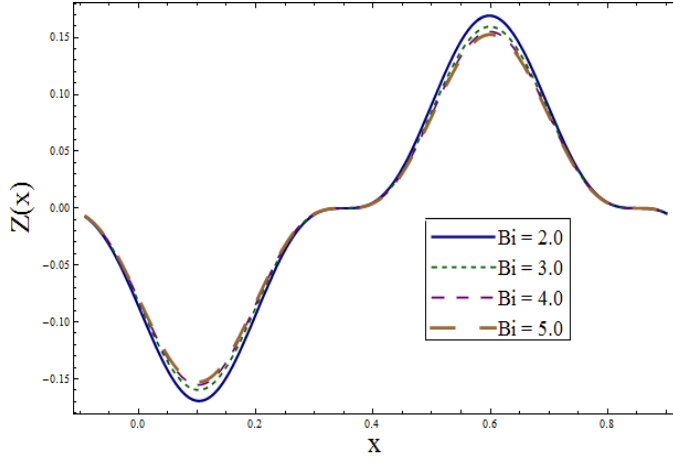
4.26

Fig. 4.25 : Effect of wall properties on Z when $R = M = \lambda_1 = 0.8$, $Br = 2.0$, $T' = Bi = 10.0$,

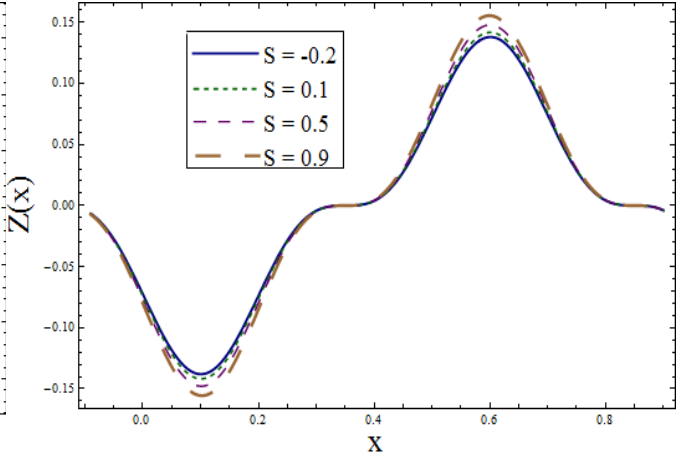
$S = 0.5$, $\epsilon = 0.2$, $t = 0.1$.

Fig. 4.26 : Effect of T' on Z when $E_1 = E_2 = 0.1$, $E_3 = E_4 = 0.01$, $E_5 = 0.6$,

$R = M = \lambda_1 = 0.8$, $Br = 2.0$, $Bi = 10.0$, $S = 0.5$, $\epsilon = 0.2$, $t = 0.1$.



4.27



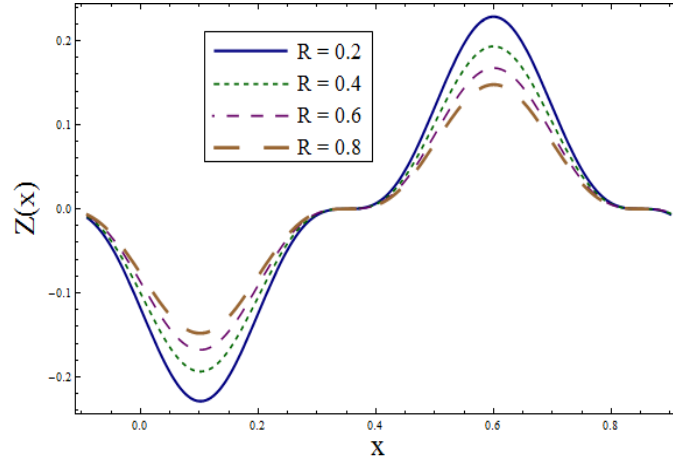
4.28

Fig. 4.27 : Effect of Bi on Z when $E_1 = E_2 = 0.1$, $E_3 = E_4 = 0.01$, $E_5 = 0.6$,

$R = M = \lambda_1 = 0.8$, $T' = 10.0$, $Br = 2.0$, $S = 0.5$, $\epsilon = 0.2$, $t = 0.1$.

Fig. 4.28 : Effect of S on Z when $E_1 = E_2 = 0.1$, $E_3 = E_4 = 0.01$, $E_5 = 0.6$,

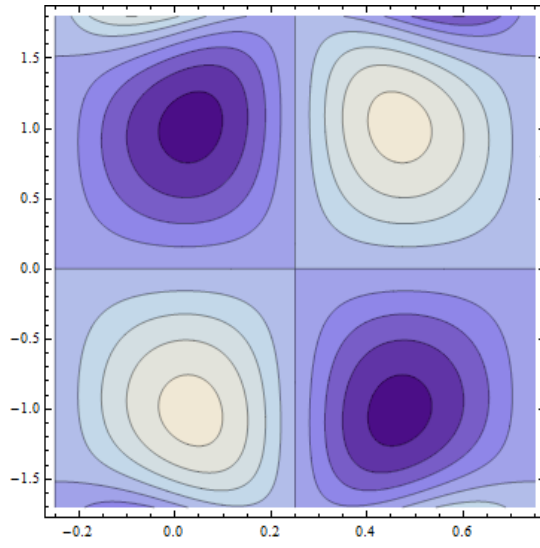
$R = M = \lambda_1 = 0.8$, $Br = 2.0$, $T' = Bi = 10.0$, $\epsilon = 0.2$, $t = 0.1$.



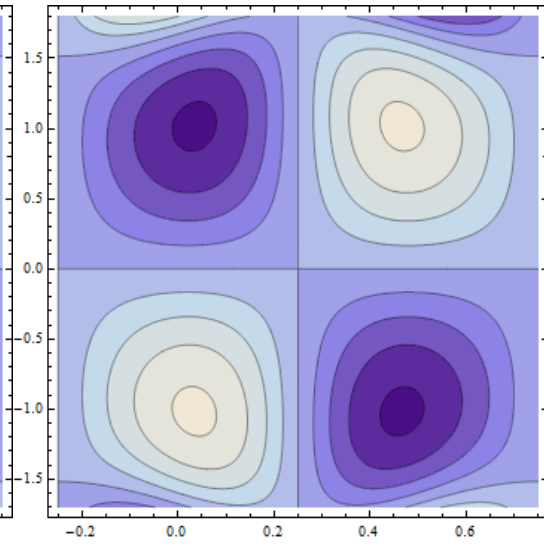
4.29

Fig. 4.29 : Effect of R on Z when $E_1 = E_2 = 0.1$, $E_3 = E_4 = 0.01$, $E_5 = 0.6$, $M = \lambda_1 = 0.8$,

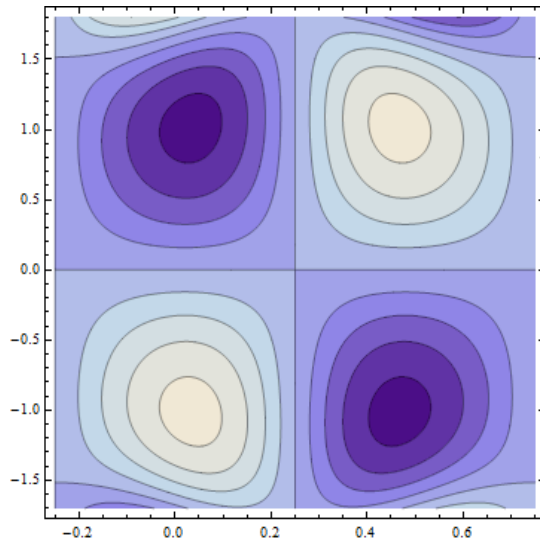
$Br = 2.0$, $T' = Bi = 10.0$, $S = 0.5$, $\epsilon = 0.2$, $t = 0.1$.



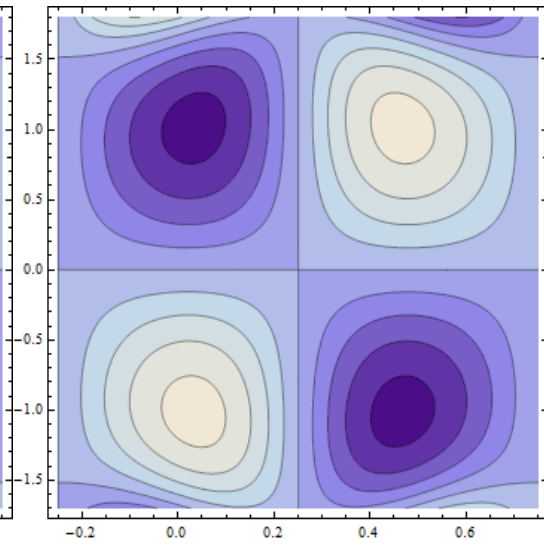
(a)



(b)



(c)



(d)

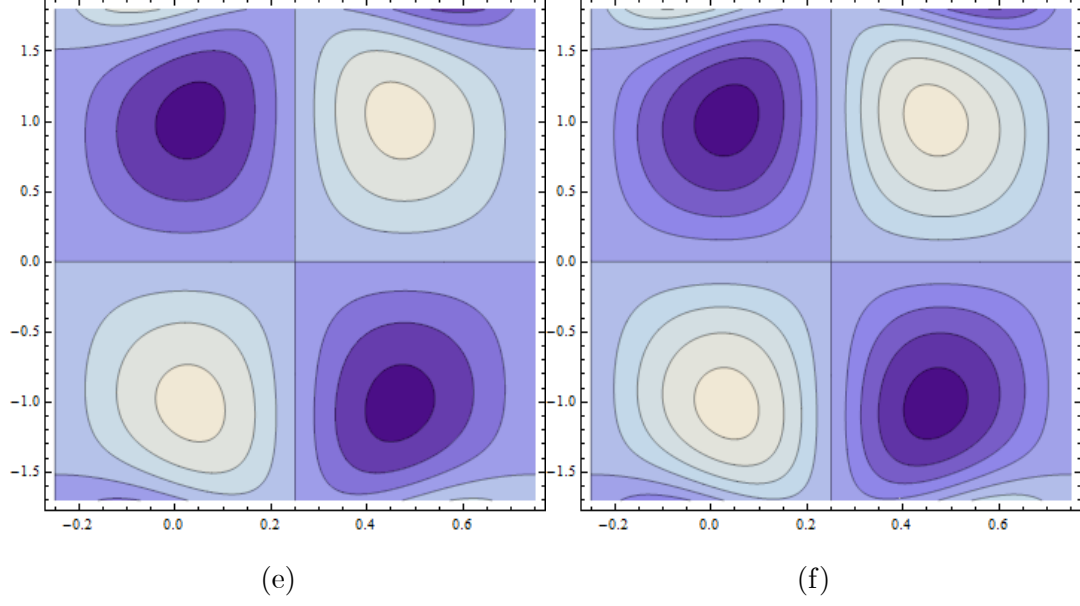


Fig. 4.30 : Streamlines for wall properties when $T' = 0.1$, $M = 0.8$, $t = 0.0$, $\epsilon = 0.2$, $\lambda_1 = 0.8$,
 (a) $E_1 = 0.1$, $E_2 = 0.01$, $E_3 = 0.01$, $E_4 = 0.1$, $E_5 = 0.1$, (b) $E_1 = 0.3$, (c) $E_2 = 0.03$, (d) $E_3 = 0.03$, (e) $E_4 = 0.3$, (f) $E_5 = 0.3$.

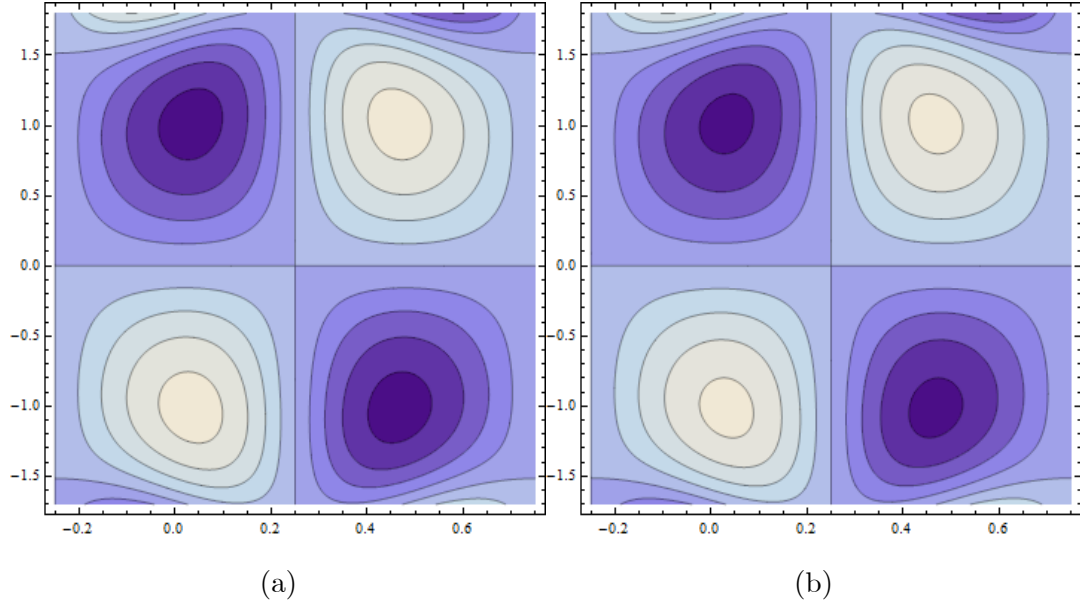


Fig. 4.31 : Streamlines for T' when $E_1 = 0.1$, $E_2 = 0.01$, $E_3 = 0.01$, $E_4 = 0.1$, $E_5 = 0.1$,
 $M = 0.8$, $\lambda_1 = 0.8$, $t = 0.0$, $\epsilon = 0.2$, (a) $T' = 0.1$, (b) $T' = 0.2$.

4.5 Conclusions

Here a mathematical model to study the peristaltic transport of an electrically conducting Jeffrey fluid in a convectively heated channel is developed in presence of thermal deposition of particles and chemical reaction. The key findings of the presented attempt are as follows:

- Axial velocity decreases when we increase the rotation whereas secondary velocity shows opposite behavior.
- Wall parameters (E_1, E_2, E_3, E_4 and E_5) show opposite behavior for the axial and secondary velocities.
- Temperature enhances by increasing the rotation parameter T' and Biot number Bi .
- Temperature is higher for heat generation coefficient ($S > 0$) when compared with case of absorption ($S < 0$).
- Concentration is decreasing function of rotation parameter T' and Schmidt number Sc .
- Generative chemical reaction ($\gamma > 0$) results in decreased concentration whereas for destructive chemical reaction ($\gamma < 0$) the concentration shows reverse behavior.
- Impact of particle deposition is decreasing on concentration.
- Rate of heat transfer is less in case of absorption ($S < 0$) than generation ($S > 0$).
- Decrease in rate of heat transfer is noticed for Bi , Rd and T' .
- Upon increasing rotation the size of streamlines is decreased.

Chapter 5

Influence of convective conditions on peristalsis of ferrofluid in a rotating frame

5.1 Introduction

This chapter addresses effect of convective heat transfer on peristaltic flow of ferrofluid in compliant wall channel. Magnetic field effect is also given consideration due to electrical conducting properties of the fluid. Energy equation is modelled by considering viscous dissipation and Joule heating effects. The whole system is taken in a rotating frame. The modeled problem is reduced by adopting lubrication approach. The computed results for velocity and temperature are shown graphically for various embedded physical parameters. Effective heat transfer at the walls and trapping phenomenon are also discussed in detail.

5.2 Mathematical formulation

Here our intention is to investigate peristalsis of ferrofluid (Magnetite, Fe_3O_4) in a flexible walls channel of width $2d$. A magnetic field of constant strength acts in a transverse direction to flow. Induced magnetic field under low magnetic Reynolds number is neglected. Coordinate system is chosen in such a way that x-axis lies along the center of channel and z-axis perpendicular to it.

The whole system rotates about z-axis with constant angular speed Ω . Wave train propagating along the walls with speed c generates the flow in channel.

Mathematical form of walls is

$$z = \pm \eta(x, t) = \pm \left[d + a \sin \frac{2\pi}{\lambda} (x - ct) \right], \quad (5.1)$$

where a defines wave amplitude, λ wavelength and t for time. The velocity is

$$\mathbf{V} = [u(x, z, t), v(x, z, t), w(x, z, t)]. \quad (5.2)$$

Lorentz force is considered in the form

$$\mathbf{F} = \mathbf{J} \times \mathbf{B}, \quad (5.3)$$

where $\mathbf{B} = [0, 0, B_0]$ defines the applied magnetic field and \mathbf{J} shows current density given by

$$\mathbf{J} = \sigma_{eff} [\mathbf{E} + (\mathbf{V} \times \mathbf{B})]. \quad (5.4)$$

In above expression σ_{eff} stands for effective electric conductivity of nanofluid. We get from Eqs. (5.3) and (5.4) the following expression:

$$\mathbf{F} = [-\sigma_{eff} B_0^2 u, -\sigma_{eff} B_0^2 v, 0]. \quad (5.5)$$

For the two phase flow model the effective electric conductivity of considered magnetite particles is [164] :

$$\frac{\sigma_{eff}}{\sigma_f} = 1 + \frac{3 \left(\frac{\sigma_p}{\sigma_f} - 1 \right) \phi}{\left(\frac{\sigma_p}{\sigma_f} + 2 \right) - \left(\frac{\sigma_p}{\sigma_f} - 1 \right) \phi}, \quad (5.6)$$

where σ_p shows the electric conductivity of magneto-nanoparticles and σ_f corresponds to that of base fluid (*i.e.* water) whereas ϕ is the volume fraction of nanoparticles. Effective electric conductivity of nanoparticles equals to the base fluid in their absence ($\phi = 0$). Taking $\phi = 1$ we get the electric conductivity of magnetite. Using (5.4) in (5.3) we get the Lorentz force in

the form:

$$\mathbf{F} = [-A\sigma_f B_0^2 u, -A\sigma_f B_0^2 v, 0], \quad (5.7)$$

where

$$A = 1 + \frac{3 \left(\frac{\sigma_p}{\sigma_f} - 1 \right) \phi}{\left(\frac{\sigma_p}{\sigma_f} + 2 \right) - \left(\frac{\sigma_p}{\sigma_f} - 1 \right) \phi}.$$

The Ohmic heating term is represented by [165] :

$$\frac{1}{\sigma_{eff}} \mathbf{J} \cdot \mathbf{J} = A\sigma_f B_0^2 (u^2 + v^2). \quad (5.8)$$

Now the relevant equations for the flow analysis take the form:

Conservation of mass:

$$\frac{\partial u}{\partial x} + \frac{\partial w}{\partial z} = 0. \quad (5.9)$$

Conservation of momentum equation:

$$\rho_{eff} \left[\frac{du}{dt} - 2\Omega v \right] = -\frac{\partial \hat{p}}{\partial x} + \mu_{eff} \left(\frac{\partial^2 u}{\partial x^2} + \frac{\partial^2 u}{\partial z^2} \right) - A\sigma_f B_0^2 u, \quad (5.10)$$

$$\rho_{eff} \left[\frac{dv}{dt} + 2\Omega v \right] = -\frac{\partial \hat{p}}{\partial y} + \mu_{eff} \left(\frac{\partial^2 v}{\partial x^2} + \frac{\partial^2 v}{\partial z^2} \right) - A\sigma_f B_0^2 v, \quad (5.11)$$

$$\rho_{eff} \frac{dw}{dt} = -\frac{\partial \hat{p}}{\partial z} + \mu_{eff} \left(\frac{\partial^2 w}{\partial x^2} + \frac{\partial^2 w}{\partial z^2} \right), \quad (5.12)$$

where modified pressure is defined as:

$$\hat{p} = p - \frac{1}{2} \rho \Omega^2 (x^2 + y^2).$$

Conservation of energy equation:

$$\begin{aligned} (\rho C)_{eff} \frac{dT}{dt} = & K_{eff} \left(\frac{\partial^2 T}{\partial x^2} + \frac{\partial^2 T}{\partial z^2} \right) + \mu_{eff} \left[2 \left\{ \left(\frac{\partial u}{\partial x} \right)^2 + \left(\frac{\partial w}{\partial z} \right)^2 \right\} + \left(\frac{\partial u}{\partial z} + \frac{\partial w}{\partial x} \right)^2 \right] \\ & + A\sigma_f B_0^2 (u^2 + v^2). \end{aligned} \quad (5.13)$$

where ρ_{eff} , μ_{eff} , C_{eff} and K_{eff} are the effective density, viscosity, specific heat and thermal conductivity of nanofluid. Here T is the temperature.

Boundary conditions are

$$u = 0, \quad v = 0 \quad \text{at} \quad z = \pm\eta, \quad (5.14)$$

$$\frac{\partial L(\eta)}{\partial x} = \frac{\partial p}{\partial x} = \mu_{eff} \left(\frac{\partial^2 u}{\partial x^2} + \frac{\partial^2 u}{\partial z^2} \right) - A\sigma_f B_0^2 u \quad (5.15)$$

$$-\rho_{eff} \left[\frac{du}{dt} - 2\Omega v \right] \quad \text{at} \quad z = \pm\eta,$$

$$K_{eff} \frac{\partial T}{\partial z} = -h_1 (T - T_1) \quad \text{at} \quad z = +\eta,$$

$$K_{eff} \frac{\partial T}{\partial z} = -h_2 (T_0 - T) \quad \text{at} \quad z = -\eta, \quad (5.16)$$

where

$$L = -\tau' \frac{\partial^2}{\partial x^2} + m_1 \frac{\partial^2}{\partial t^2} + d' \frac{\partial}{\partial t}.$$

In above Eqs. h_1 and h_2 are the heat transfer coefficients at the walls. Here T_1 and T_0 define the temperature at upper and lower walls respectively, τ' is the tension, m_1 the mass and d' defines the viscous damping coefficient.

The effective density, effective specific heat and effective viscosity of nanofluid are

$$\begin{aligned} \rho_{eff} &= (1 - \phi) \rho_f + \phi \rho_p, \\ (\rho C)_{eff} &= (1 - \phi) (\rho C)_f + \phi (\rho C)_p, \\ \mu_{eff} &= \frac{\mu_f}{(1 - \phi)^{2.5}}. \end{aligned} \quad (5.17)$$

The effective thermal conductivity of nanofluid according to Maxwell-Garnet model is [166]:

$$\frac{K_{eff}}{K_f} = \frac{K_p + 2K_f - 2\phi(K_f - K_p)}{K_p + 2K_f + \phi(K_f - K_p)}. \quad (5.18)$$

In above Eqs. ρ_f , μ_f , C_f and K_f describe the density, viscosity, specific heat capacity and thermal conductivity of base fluid i.e. water respectively whereas ρ_p is the density, μ_p the viscosity, C_p the specific heat capacity and K_p show the thermal conductivity of magnetite-nanofluid. Numerical values of thermophysical properties of magnetite and water can be seen through Table 1.

Table 1

Numerical values of thermophysical properties of magnetite and water [179, 180].

Phase	$\rho(kg/m^3)$	$K(W/mK)$	$C(J/kgK)$	$\sigma(S/m)$
Water	997.1	0.613	4179	0.05
Magnetite	5180	9.7	671	25000

Now Eqs. (5.9) – (5.16) after using Eqs. (5.7), (5.8), (5.17) and (5.18) take the form:

$$\frac{\partial u}{\partial x} + \frac{\partial w}{\partial z} = 0, \quad (5.19)$$

$$[(1 - \phi) \rho_f + \phi \rho_p] \left[\frac{du}{dt} - 2\Omega v \right] = -\frac{\partial p}{\partial x} + \frac{\mu_f}{(1 - \phi)^{2.5}} \left(\frac{\partial^2 u}{\partial x^2} + \frac{\partial^2 u}{\partial z^2} \right) - A\sigma_f B_0^2 u, \quad (5.20)$$

$$[(1 - \phi) \rho_f + \phi \rho_p] \left[\frac{dv}{dt} + 2\Omega u \right] = -\frac{\partial p}{\partial y} + \frac{\mu_f}{(1 - \phi)^{2.5}} \left(\frac{\partial^2 v}{\partial x^2} + \frac{\partial^2 v}{\partial z^2} \right) - A\sigma_f B_0^2 v, \quad (5.21)$$

$$[(1 - \phi) \rho_f + \phi \rho_p] \frac{dw}{dt} = -\frac{\partial p}{\partial z} + \frac{\mu_f}{(1 - \phi)^{2.5}} \left(\frac{\partial^2 w}{\partial x^2} + \frac{\partial^2 w}{\partial z^2} \right), \quad (5.22)$$

$$\begin{aligned} [(1 - \phi) \rho_f + \phi \rho_p] \frac{dT}{dt} &= K_f \left(\frac{K_p + 2K_f - 2\phi(K_f - K_p)}{K_p + 2K_f + \phi(K_f - K_p)} \right) \left(\frac{\partial^2 T}{\partial x^2} + \frac{\partial^2 T}{\partial z^2} \right) \\ &\quad + A\sigma_f B_0^2 (u^2 + v^2) + \frac{\mu_f}{(1 - \phi)^{2.5}} \\ &\quad \times \left[2 \left\{ \left(\frac{\partial u}{\partial x} \right)^2 + \left(\frac{\partial w}{\partial z} \right)^2 \right\} + \left(\frac{\partial u}{\partial z} + \frac{\partial w}{\partial x} \right)^2 \right], \end{aligned} \quad (5.23)$$

$$u = 0, \quad v = 0 \quad \text{at} \quad z = \pm\eta, \quad (5.24)$$

$$\begin{aligned} \frac{\partial L(\eta)}{\partial x} = \frac{\partial p}{\partial x} &= \frac{\mu_f}{(1 - \phi)^{2.5}} \left(\frac{\partial^2 u}{\partial x^2} + \frac{\partial^2 u}{\partial z^2} \right) - A\sigma_f B_0^2 u - ((1 - \phi) \rho_f + \phi \rho_p) \\ &\quad \left[\frac{du}{dt} - 2\Omega v \right] \quad \text{at} \quad z = \pm\eta, \end{aligned} \quad (5.25)$$

$$\begin{aligned} K_f \left(\frac{K_p + 2K_f - 2\phi(K_f - K_p)}{K_p + 2K_f + \phi(K_f - K_p)} \right) \frac{\partial T}{\partial z} &= -h_1 (T - T_1) \quad \text{at} \quad z = +\eta, \\ K_f \left(\frac{K_p + 2K_f - 2\phi(K_f - K_p)}{K_p + 2K_f + \phi(K_f - K_p)} \right) \frac{\partial T}{\partial z} &= -h_2 (T_0 - T) \quad \text{at} \quad z = -\eta. \end{aligned} \quad (5.26)$$

Writing the following non-dimensional parameters:

$$\begin{aligned}
x^* &= \frac{x}{\lambda}, \quad y^* = \frac{y}{\lambda}, \quad z^* = \frac{z}{d}, \quad p^* = \frac{d^2 p}{c \mu_f \lambda}, \quad t^* = \frac{ct}{\lambda}, \quad u^* = \frac{u}{c}, \\
v^* &= \frac{v}{c}, \quad w^* = \frac{w}{c}, \quad \eta^* = \frac{\eta}{d}, \quad \theta = \frac{T - T_0}{T_1 - T_0}, \quad \text{Re} = \frac{\rho_f c d}{\mu_f}, \\
\delta &= \frac{d}{\lambda}, \quad T' = \frac{\text{Re} \Omega d}{c}, \quad M^2 = B_0^2 d^2 \frac{\sigma_f}{\mu_f}, \quad \text{Pr} = \frac{\mu_f C_f}{\kappa_f}, \quad \epsilon = \frac{a}{d}, \\
Ec &= \frac{c^2}{C_f (T_1 - T_0)}, \quad Br = \text{Pr} Ec, \quad E_1 = \frac{-\tau d^3}{\lambda^3 \mu c}, \quad E_2 = \frac{m_1 c d^3}{\lambda^3 \mu}, \\
E_3 &= \frac{d' d^3}{\lambda^2 \mu}, \quad Bi_1 = \frac{h_1 d}{K_f}, \quad Bi_2 = \frac{h_2 d}{K_f}, \quad u = \frac{\partial \psi}{\partial z}, \quad w = -\delta \frac{\partial \psi}{\partial x},
\end{aligned} \tag{5.27}$$

and applying long wavelength and low Reynolds number approximation [21] one can write

$$-\frac{\partial p}{\partial x} + A_1 \frac{\partial^3 \psi}{\partial z^3} - AM^2 \frac{\partial \psi}{\partial z} + 2T' A_3 v = 0, \tag{5.28}$$

$$-\frac{\partial p}{\partial y} + A_1 \frac{\partial^2 \psi}{\partial z^2} - AM^2 v - 2T' A_3 \frac{\partial \psi}{\partial z} = 0, \tag{5.29}$$

$$\frac{\partial p}{\partial z} = 0, \tag{5.30}$$

$$A_2 \frac{\partial^2 \theta}{\partial z^2} + AA_1 M^2 Br \left[\left(\frac{\partial \psi}{\partial z} \right)^2 + v^2 \right] + \frac{2Br}{(1 - \phi)^{2.5}} \left(\frac{\partial^2 \psi}{\partial z^2} \right)^2 = 0, \tag{5.31}$$

where

$$\begin{aligned}
A_1 &= \frac{1}{(1 - \phi)^{2.5}}, \\
A_2 &= \frac{K_p + 2K_f - 2\phi(K_f - K_p)}{K_p + 2K_f + \phi(K_f - K_p)}, \\
A_3 &= \left[(1 - \phi) + \phi \frac{\rho_p}{\rho_f} \right].
\end{aligned} \tag{5.32}$$

It is noticed from Eq. (5.30) that pressure is not a function of z . Also the pressure term in Eq. (5.29) is ignored. It is due to the fact that secondary flow is not caused by the pressure

gradient but due to rotation. Solving Eqs. (5.28) and (5.30) we get

$$A_1 \frac{\partial^4 \psi}{\partial z^4} - AM^2 \frac{\partial^2 \psi}{\partial z^2} + 2T' A_3 \frac{\partial v}{\partial z} = 0, \quad (5.33)$$

$$A_1 \frac{\partial^2 \psi}{\partial z^2} - AM^2 v - 2T' A_3 \frac{\partial \psi}{\partial z} = 0. \quad (5.34)$$

Boundary conditions for the flow analysis now become

$$\frac{\partial \psi}{\partial z} = 0, \quad v = 0 \quad \text{at} \quad z = \pm \eta, \quad (5.35)$$

$$\left[E_1 \frac{\partial^3}{\partial x^3} + E_2 \frac{\partial^3}{\partial x \partial t^2} + E_3 \frac{\partial^2}{\partial x \partial t} \right] \eta = A_1 \frac{\partial^3 \psi}{\partial z^3} - AM^2 \frac{\partial \psi}{\partial z} + A_3 v \quad \text{at} \quad z = \pm \eta, \quad (5.36)$$

$$\begin{aligned} \frac{\partial \theta}{\partial z} + \frac{Bi_1}{A_2} \theta &= 0 \quad \text{at} \quad z = +\eta, \\ \frac{\partial \theta}{\partial z} - \frac{Bi_2}{A_2} \theta &= 0 \quad \text{at} \quad z = -\eta. \end{aligned} \quad (5.37)$$

The non-dimensional form of η is written as

$$\eta = (1 + \epsilon \sin 2\pi(x - t)),$$

where T' is the Taylor's number, M^2 the Hartman number, Br the Brinkman number, E_1 , E_2 and E_3 define the wall elastance parameters, ϵ the amplitude ratio whereas Bi_1 and Bi_2 the Biot numbers at upper and lower walls respectively.

5.3 Solutions

Solving Eqs. (5.31), (5.33) and (5.34) we have the following relations of stream function, secondary velocity and temperature

$$\psi = \frac{1}{2} L_0 \left[-\frac{2AM^2 z}{\alpha' \beta'} + \sqrt{A_1} \left(\frac{\sec h[\frac{\sqrt{\alpha'} \eta}{\sqrt{A_1}}] \sin h[\frac{\sqrt{\alpha'} z}{\sqrt{A_1}}]}{\alpha'^{\frac{3}{2}}} + \frac{\sec h[\frac{\sqrt{\beta'} \eta}{\sqrt{A_1}}] \sin h[\frac{\sqrt{\beta'} z}{\sqrt{A_1}}]}{\beta'^{\frac{3}{2}}} \right) \right] \quad (5.38)$$

$$v = -\frac{L_0}{2\alpha' \beta'} \left[-4A_3 T' + \zeta \cos h[\frac{\sqrt{\alpha'} z}{\sqrt{A_1}}] \sec h[\frac{\sqrt{\alpha'} \eta}{\sqrt{A_1}}] + \gamma \cos h[\frac{\sqrt{\alpha'} z}{\sqrt{A_1}}] \sec h[\frac{\sqrt{\alpha'} \eta}{\sqrt{A_1}}] \right], \quad (5.39)$$

whereas

$$L_0 = 8\epsilon\pi^3 \left(\frac{E_3}{2\pi} \sin[2\pi(x-t)] - (E_1 + E_2) \cos[2\pi(x-t)] \right),$$

$$\begin{aligned}
\theta = & B_0 + B_1(\cosh[(z-\eta)\sqrt{\frac{\alpha'}{A_1}}] + \cosh[(z+\eta)\sqrt{\frac{\alpha'}{A_1}}]) + B_2(\cosh[(z-\eta)\sqrt{\frac{\alpha'}{A_1}} - 2\eta\sqrt{\frac{\beta'}{A_1}}] \\
& + \cosh[(z+\eta)\sqrt{\frac{\alpha'}{A_1}} - 2\eta\sqrt{\frac{\beta'}{A_1}}] + \cosh[(z-\eta)\sqrt{\frac{\alpha'}{A_1}} + 2\eta\sqrt{\frac{\beta'}{A_1}}] + \cosh[(z+\eta)\sqrt{\frac{\alpha'}{A_1}} \\
& + 2\eta\sqrt{\frac{\beta'}{A_1}}]) + B_3(\cosh[(z-\eta)\sqrt{\frac{\beta'}{A_1}}] + \cosh[(z+\eta)\sqrt{\frac{\beta'}{A_1}}]) + B_4(\cosh[(z-\eta)\sqrt{\frac{\beta'}{A_1}} \\
& - 2\eta\sqrt{\frac{\alpha'}{A_1}}] + \cosh[(z-\eta)\sqrt{\frac{\beta'}{A_1}} + 2\eta\sqrt{\frac{\alpha'}{A_1}}] + \cosh[(z+\eta)\sqrt{\frac{\beta'}{A_1}} - 2\eta\sqrt{\frac{\alpha'}{A_1}}] \\
& + \cosh[(z+\eta)\sqrt{\frac{\beta'}{A_1}} + 2\eta\sqrt{\frac{\alpha'}{A_1}}]) - (B_5 - B_6) \cosh[\frac{z}{\sqrt{A_1}}(\sqrt{\alpha'} - \sqrt{\beta'}) \\
& + \frac{\eta}{\sqrt{A_1}}(\sqrt{\alpha'} - \sqrt{\beta'})] + B_7(\cosh[\frac{2}{\sqrt{A_1}}(z\sqrt{\alpha'} - \sqrt{\beta'}\eta)] + \cosh[\frac{2}{\sqrt{A_1}}(z\sqrt{\alpha'} + \sqrt{\beta'}\eta)]) \\
& + B_8 \cosh[2z\sqrt{\frac{\alpha'}{A_1}}] + B_9(\cosh[\frac{2}{\sqrt{A_1}}(z\sqrt{\beta'} - \sqrt{\alpha'}\eta)] + \cosh[\frac{2}{\sqrt{A_1}}(z\sqrt{\beta'} + \sqrt{\alpha'}\eta)]) \\
& + B_{10} \cosh[2z\sqrt{\frac{\beta'}{A_1}}] + B_{11}(\cosh[\frac{z}{\sqrt{A_1}}(\sqrt{\alpha'} - \sqrt{\beta'}) - \frac{\eta}{\sqrt{A_1}}(\sqrt{\alpha'} + \sqrt{\beta'})] \\
& + \cosh[\frac{z}{\sqrt{A_1}}(\sqrt{\alpha'} - \sqrt{\beta'}) - \frac{\eta}{\sqrt{A_1}}(\sqrt{\alpha'} - \sqrt{\beta'})] + \cosh[\frac{z}{\sqrt{A_1}}(\sqrt{\alpha'} - \sqrt{\beta'}) \\
& + \frac{\eta}{\sqrt{A_1}}(\sqrt{\alpha'} + \sqrt{\beta'})]) + B_{12} \cosh[\frac{z}{\sqrt{A_1}}(\sqrt{\alpha'} + \sqrt{\beta'}) - \frac{\eta}{\sqrt{A_1}}(\sqrt{\alpha'} + \sqrt{\beta'})] \\
& + B_{13}(\cosh[\frac{z}{\sqrt{A_1}}(\sqrt{\alpha'} + \sqrt{\beta'}) + \frac{\eta}{\sqrt{A_1}}(\sqrt{\alpha'} - \sqrt{\beta'})] + \cosh[\frac{z}{\sqrt{A_1}}(\sqrt{\alpha'} + \sqrt{\beta'}) \\
& - \frac{\eta}{\sqrt{A_1}}(\sqrt{\alpha'} - \sqrt{\beta'})] + \cosh[\frac{z}{\sqrt{A_1}}(\sqrt{\alpha'} + \sqrt{\beta'}) + \frac{\eta}{\sqrt{A_1}}(\sqrt{\alpha'} + \sqrt{\beta'})] \\
& + B_{14}z^2 + B_{15}z - B_{16},
\end{aligned} \tag{5.40}$$

in which

$$\alpha' = AM^2 - 2iA_3T',$$

$$\beta' = AM^2 + 2iA_3T',$$

$$\zeta = -iAM^2 + 2A_3T',$$

$$\gamma' = iAM^2 + 2A_3T',$$

where $B_0 \rightarrow B_{16}$ are given below:

$$\begin{aligned} B_0 &= \frac{A_2(A^2M^4 + 4A_3^2T^2)^2(A_2 + Bi_2\eta)}{\alpha'^2\beta'^2(A_2(Bi_1 + Bi_2) + 2Bi_1Bi_2\eta)}, \\ B_1 &= \frac{AA_1BrL_0^2M^2 \sec h^2[\sqrt{\alpha'/A_1}\eta] \sec h^2[\sqrt{\beta'/A_1}\eta]}{4A^2A_2M^4\alpha' + 16A_2A_3^2T^2\alpha'}, \\ B_2 &= \frac{1}{2}B_1, \quad B_3 = \frac{AA_1BrL_0^2M^2 \sec h^2[\sqrt{\alpha'/A_1}\eta] \sec h^2[\sqrt{\beta'/A_1}\eta]}{4A^2A_2M^4\beta' + 16A_2A_3^2T^2\beta'}, \quad B_4 = \frac{1}{2}B_3, \\ B_5 &= \frac{AA_1BrL_0^2M^2 \sec h^2[\sqrt{\alpha'/A_1}\eta] \sec h^2[\sqrt{\beta'/A_1}\eta]}{8A_2(A^2M^4 + 4A_3^2T^2)(\sqrt{\alpha} - \sqrt{\beta})^2}, \\ B_6 &= \frac{A_1BrL_0^2\sqrt{\alpha}\sqrt{\beta} \sec h^2[\sqrt{\alpha'/A_1}\eta] \sec h^2[\sqrt{\beta'/A_1}\eta]}{8A_2(A^2M^4 + 4A_3^2T^2)(\sqrt{\alpha} - \sqrt{\beta})^2}, \\ B_7 &= -\frac{A_1BrL_0^2M^2 \sec h^2[\sqrt{\alpha'/A_1}\eta] \sec h^2[\sqrt{\beta'/A_1}\eta]}{64A_2\alpha'(AM^2 - 2iA_2A_3T)}, \quad B_8 = 2B_7, \\ B_9 &= -\frac{A_1BrL_0^2M^2 \sec h^2[\sqrt{\alpha'/A_1}\eta] \sec h^2[\sqrt{\beta'/A_1}\eta]}{64A_2\alpha'(AM^2 + 2iA_2A_3T)}, \quad B_{10} = 2B_9, \end{aligned}$$

$$\begin{aligned} B_{11} &= \frac{A_1BrL_0^2(\sqrt{\alpha}\sqrt{\beta} - AM^2) \sec h^2[\sqrt{\alpha'/A_1}\eta] \sec h^2[\sqrt{\beta'/A_1}\eta]}{8A_2(A^2M^4 + 4A_3^2T^2)(\sqrt{\alpha} - \sqrt{\beta})^2}, \quad B_{12} = -B_{11}, \\ B_{13} &= -\frac{A_1BrL_0^2(\sqrt{\alpha}\sqrt{\beta} + AM^2) \sec h^2[\sqrt{\alpha'/A_1}\eta] \sec h^2[\sqrt{\beta'/A_1}\eta]}{8A_2(A^2M^4 + 4A_3^2T^2)(\sqrt{\alpha} + \sqrt{\beta})^2}, \\ B_{14} &= -\frac{1}{(16A_2(A^2M^4 + 4A_3^2T^2))} (BrL_0^2((AM^2 + 2iA_3T) \cosh[2\sqrt{\alpha'/A_1}\eta] \\ &\quad + AM^2(\cosh[\frac{2}{\sqrt{A_1}}(\sqrt{\alpha'} - \sqrt{\beta'})\eta] + \cosh[\frac{2}{\sqrt{A_1}}(\sqrt{\alpha'} + \sqrt{\beta'})\eta]) \\ &\quad + (AM^2 - 2iA_3T) \cosh[2\sqrt{\beta'/A_1}\eta]) \sec h^2[\sqrt{\alpha'/A_1}\eta] \sec h^2[\sqrt{\beta'/A_1}\eta]), \\ B_{15} &= \sec h^2[\sqrt{\alpha'/A_1}\eta] \sec h^2[\sqrt{\beta'/A_1}\eta] (c_1 + c_2 \cosh[2\sqrt{\alpha'/A_1}\eta] + c_3(\cosh[\frac{2}{\sqrt{A_1}}(\sqrt{\alpha'} \\ &\quad - \sqrt{\beta'})\eta] + \cosh[\frac{2}{\sqrt{A_1}}(\sqrt{\alpha'} + \sqrt{\beta'})\eta]) + c_4 \cosh[2\sqrt{\beta'/A_1}\eta] + c_5 \sec h^2[\sqrt{\alpha'/A_1}\eta] \\ &\quad + c_7 \sinh[\frac{2}{\sqrt{A_1}}(\sqrt{\alpha'} - \sqrt{\beta'})\eta] + c_8 \sinh[\frac{2}{\sqrt{A_1}}(\sqrt{\alpha'} + \sqrt{\beta'})\eta] + c_9 \sinh[2\sqrt{\beta'/A_1}\eta]), \end{aligned}$$

$$\begin{aligned}
c_0 &= \alpha\beta(A_2(Bi_1 + Bi_2) + 2Bi_1Bi_2\eta), \quad c_1 = \frac{A_2Bi_2(A^2M^4 + 4A_3^2T^2)}{4c_0}, \\
c_2 &= \frac{(2A^2A_2Bi_2M^4 + 8A_2A_3^2Bi_2T^2 + (-Bi_1 + Bi_2)BrL_0^2\beta\eta)}{8c_0}, \\
c_3 &= \frac{(A_2Bi_2(A^2M^4 + 4A_3^2T^2) + A(-Bi_1 + Bi_2)BrL_0^2M^2\eta)}{8c_0}, \\
c_4 &= \frac{(2A^2A_2Bi_2M^4 + 8A_2A_3^2Bi_2T^2 + (-Bi_1 + Bi_2)BrL_0^2\alpha\eta)}{8c_0}, \\
c_5 &= \frac{\sqrt{A_1}(Bi_1 - Bi_2)BrL_0^2(AM^2 + 2iA_3T)}{16\sqrt{\alpha}c_0}, \\
c_6 &= -\frac{\sqrt{A_1}(Bi_1 - Bi_2)BrL_0^2(AM^2(\sqrt{\alpha} - \sqrt{\beta}) - 2iA_3T(\sqrt{\alpha} + \sqrt{\beta}))}{32\sqrt{\alpha}\sqrt{\beta}c_0}, \\
c_7 &= \frac{\sqrt{A_1}(Bi_1 - Bi_2)BrL_0^2(AM^2(\sqrt{\alpha} + \sqrt{\beta}) - 2iA_3T(\sqrt{\alpha} - \sqrt{\beta}))}{32\sqrt{\alpha}\sqrt{\beta}c_0}, \\
c_8 &= \frac{\sqrt{A_1}(Bi_1 - Bi_2)BrL_0^2(AM^2 - 2iA_3T)}{16\sqrt{\beta}c_0},
\end{aligned}$$

where B_{16} can be evaluated using MATHEMATICA.

5.4 Graphical results and discussion

Effect of various parameters on streamlines (ψ), velocities (u (axial) and v (secondary)) and temperature (θ) are conferred in this section through Figs. (5.1 – 5.21). Effective heat transfer at the walls are also the part of discussion.

5.4.1 Axial velocity

Figs. (5.1 – 5.4) display the influence of wall parameters (E_1 , E_2 and E_3), nanoparticle volume fraction (ϕ), rotation parameter (T') and Hartman number (M^2) on axial velocity. It is inferred from the Fig. 5.1 that large values of elastance parameters (E_1 and E_2) enhance the velocity while velocity has decreasing behavior for damping parameter (E_3). Reason behind this result lies in the fact that wall elasticity creates less hindrance for the fluid flow and hence velocity enhances. On the contrary damping is resistive force that cause velocity to reduce. Enhancing nanoparticle volume fraction shows decreasing effect for velocity. As the addition of nanoparticles creates more resistance for fluid to flow (see Fig. 5.2). It is also depicted from Fig. (5.3) that velocity in axial direction decreases as the rotation increases. Moreover

axial velocity is greater for non-rotating frame ($T' = 0$). The Fig. (5.4) exhibits the effect of Hartman number M^2 . Resistive nature of Lorentz force decreases the velocity.

5.4.2 Secondary velocity

Secondary velocity v in y-direction is generated when the channel is rotated with constant angular velocity Ω . The present subsection addresses the influence of pertinent parameters on v . From Fig. (5.5) we noticed that secondary velocity decreases as we increase E_1 and E_2 whereas it is increased for higher values of damping parameter E_3 . It is shown by the Fig. (5.6) that increasing nanoparticle volume fraction ϕ velocity in y-direction also decreases due to the increased resistance offered by nanoparticles. Fig. (5.7) illustrates the effect of Taylor's number on v . Noticeable increase in velocity is seen as the value of rotation parameter T' is increased. It is also noteworthy that there is no secondary velocity in the absence of rotation. Notably secondary velocity decays with the consideration of large values of Hartman number M^2 (see Fig. 5.8).

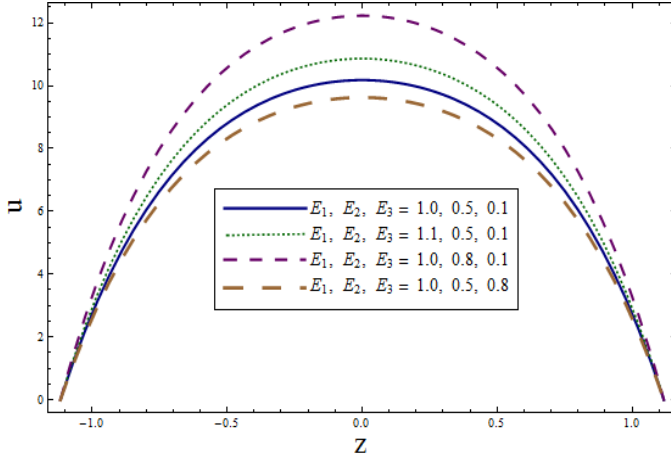
5.4.3 Heat transfer analysis

Basic reason behind the use of nanofluids is their fast heat transfer ability. To study this aspect Figs. (5.9 – 5.15) are plotted. It is clearly visible from Fig (5.9) that θ enhances for increasing values of E_1 and E_2 while showing decrease for E_3 . Since temperature defines the average kinetic energy of particles which greatly effect the velocity. Therefore we get same behavior for temperature as observed for velocity. Thermal conductivity of nanofluid is improved when the volume fraction ϕ of nanoparticles is increased. This causes increase in rate of heat transfer hence resulting in temperature decrease (see Fig. 5.10). As we increase the rotation more particles collide with eachother and transfer energy which results in decreased temperature (see Fig. 5.11). It is evident from from Fig. (5.12) that temperature θ rises due to heat generation with magnetic field. This behavior results due to consideration of Joule heating effect. This observation is in good agreement with Reddy and Reddy [168]. Fig. (5.13) also discloses the influence of Biot number on temperature profile θ . It is noticed from the Fig that temperature decays near the upper wall while there is no significant effect near the lower wall for Bi_1 . On the other hand there is noticeable decrease in temperature near the lower wall but no significant

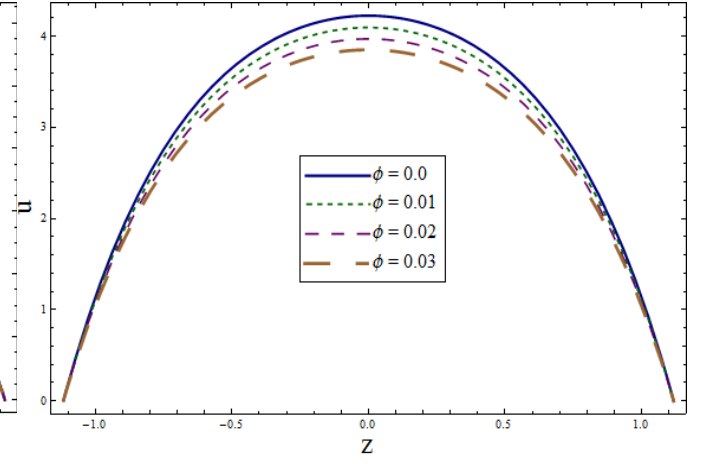
effect on θ near upper wall for Bi_2 (see Fig. 5.14). Consideration of Biot number greater than one is justified because of the non-uniformity of temperature fields inside the fluid. Whereas uniform temperature field inside the fluid are thermally simple. Therefore Biot number Bi is taken less than one in this case. Energy production inside the fluid due to friction between fluid layers is represented through Brinkman number Br . Larger Br increase the temperature (Fig. 5.15). To study the effective thermal conductivity of nanofluid defined as $(-\frac{K_{eff}}{K_f})\theta'(\eta)$, the Figs. (5.16 – 5.18) are plotted. It is noticed from Fig. 5.16 that heat transfer enhances as we increase the nanoparticles volume fraction ϕ . The fact behind this behavior is the increased thermal conductivity of nanoparticles. For increasing Hartman number M^2 the rate of heat transfer get enhanced at the walls (see Fig. 5.17). Fig. (5.18) is just sketched to study the influence of Brinkman number Br on effective heat transfer. Increasing Br leads to an enhancement of temperature. Figs. (5.19) and (5.20) are sketched to analyze the influence of Biot numbers on the rate of effective heat transfer. It can be seen through the Figs. that increase in the values of $Bi_{i's}$ enhance the convective heat transfer.

5.4.4 Streamlines and Trapping

Streamline patterns for various values of wall parameters (E_1, E_2, E_3) , Taylor and Hartman numbers $(T' \text{ and } M^2)$ are shown in the Figs. (5.19 – 5.21). Effect of wall parameters on the size of streamlines is found increasing (see Fig. 5.19). To study the influence of rotation parameter T' on trapping bolus Fig. (5.20) is sketched. Noticeable decrease in size of trapped bolus is seen when the value of T' is increased. Effect of Hartman number M^2 on trapped bolus can be seen through Fig. (5.21). Size of streamlines decreases when we make increment in the value of M^2 .



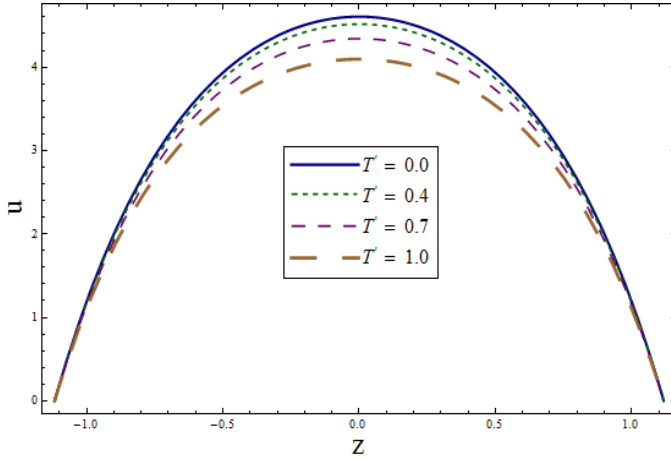
5.1



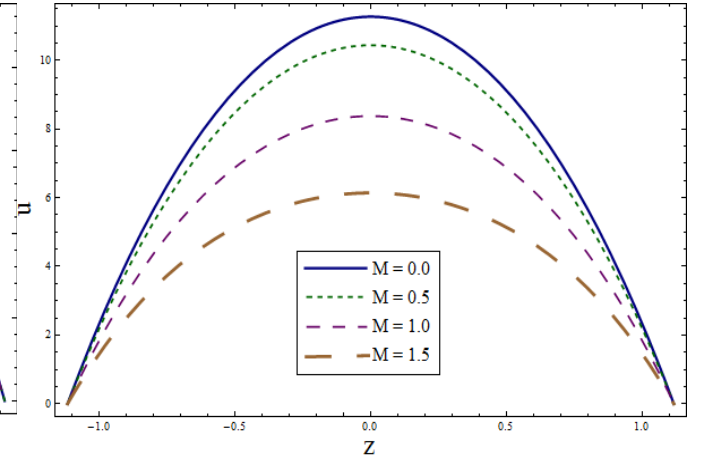
5.2

Fig. 5.1 : u via change in wall properties when $T' = 1.0$, $M = 2.0$, $\phi = 0.01$, $x = \epsilon = 0.2$, $t = 0.1$.

Fig. 5.2 : u change in ϕ when $E_1 = E_2 = 0.3$, $E_3 = 0.01$, $T' = 1.0$, $M = 2.0$, $x = \epsilon = 0.2$, $t = 0.1$.



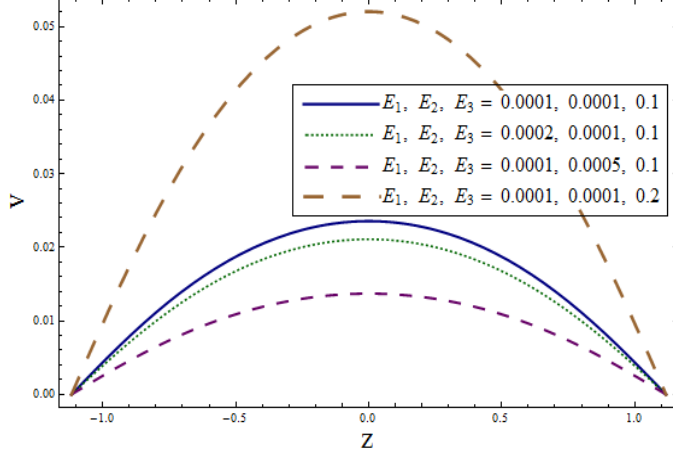
5.3



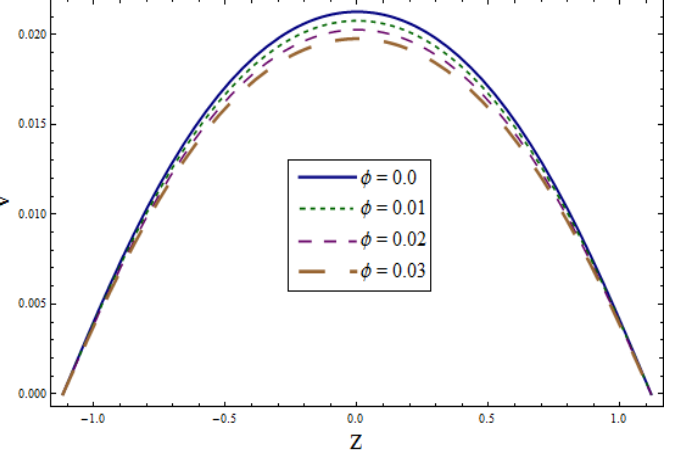
5.4

Fig. 5.3 : u via change in T' when $E_1 = E_2 = 0.3$, $E_3 = 0.01$, $M = 2.0$, $\phi = 0.01$, $x = \epsilon = 0.2$, $t = 0.1$.

Fig. 5.4 : u via change in M when $E_1 = E_2 = 0.3$, $E_3 = 0.01$, $T' = 1.0$, $M = 2.0$, $\phi = 0.01$, $x = \epsilon = 0.2$, $t = 0.1$.



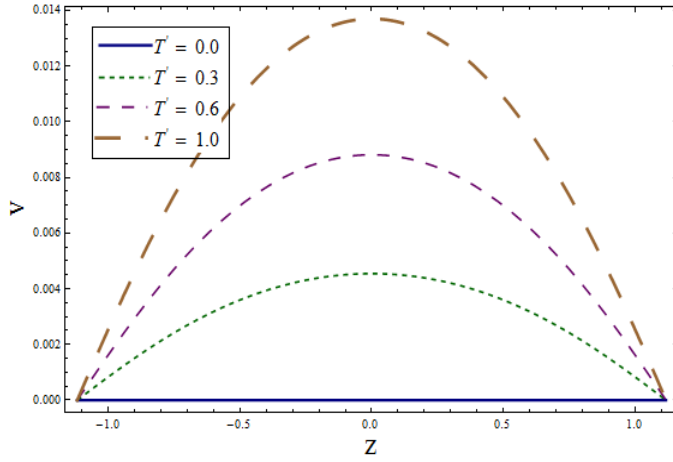
5.5



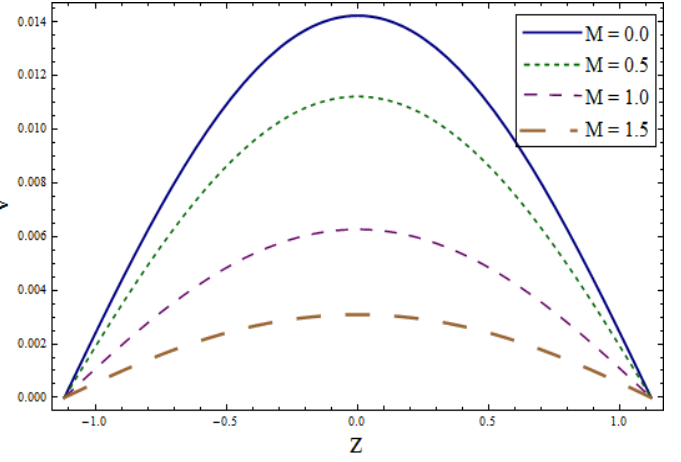
5.6

Fig. 5.5 : v via change in wall properties when $T' = 1.0$, $M = 2.0$, $\phi = 0.01$, $x = \epsilon = 0.2$,
 $t = 0.1$.

Fig. 5.6 : v via change in ϕ when $E_1 = E_2 = 0.0003$, $E_3 = 0.1$, $T' = 1.0$, $M = 2.0$, $x = \epsilon = 0.2$,
 $t = 0.1$.



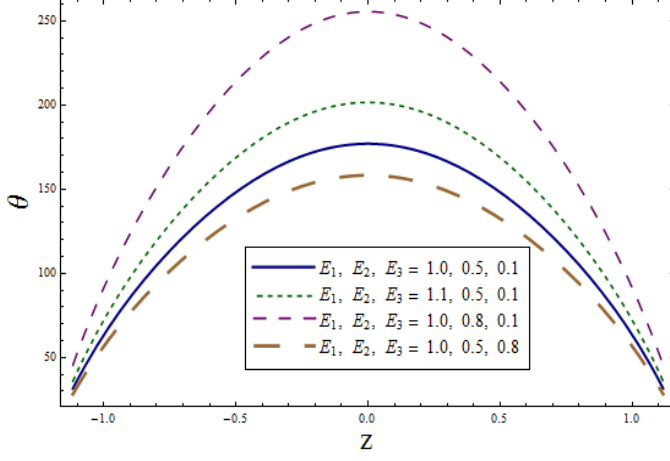
5.7



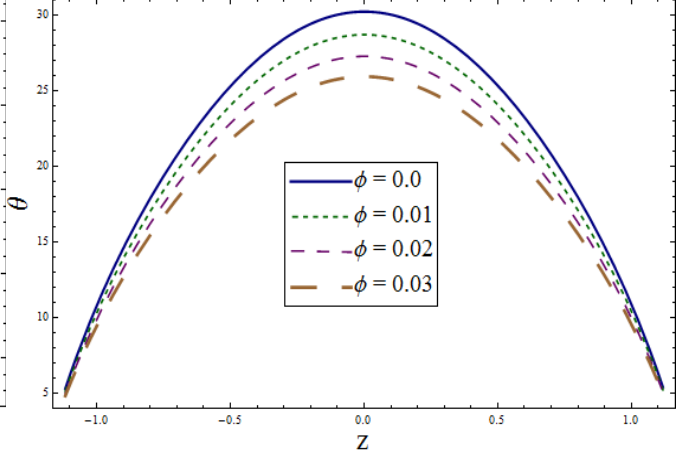
5.8

Fig. 5.7 : v via change in T' when $E_1 = E_2 = 0.0003$, $E_3 = 0.1$, $M = 2.0$, $\phi = 0.01$,
 $x = \epsilon = 0.2$, $t = 0.1$.

Fig. 5.8 : v via change in M when $E_1 = E_2 = 0.0003$, $E_3 = 0.1$, $T' = 1.0$, $M = 2.0$, $\phi = 0.01$,
 $x = \epsilon = 0.2$, $t = 0.1$.



5.9



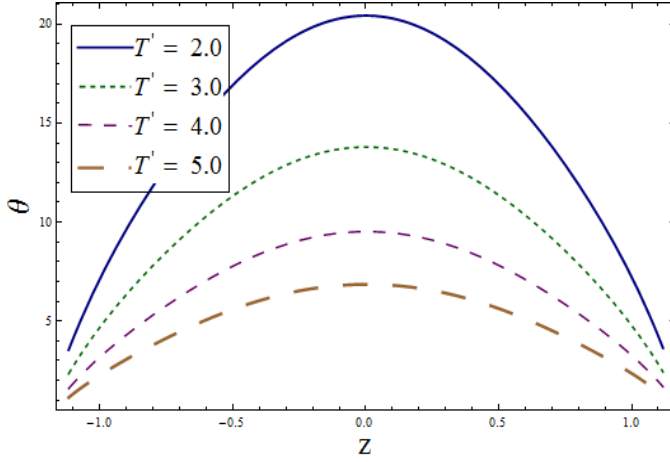
5.10

Fig. 5.9 : θ via change in wall properties when $Br = 0.5$, $T' = 1.0$, $M = 2.0$,

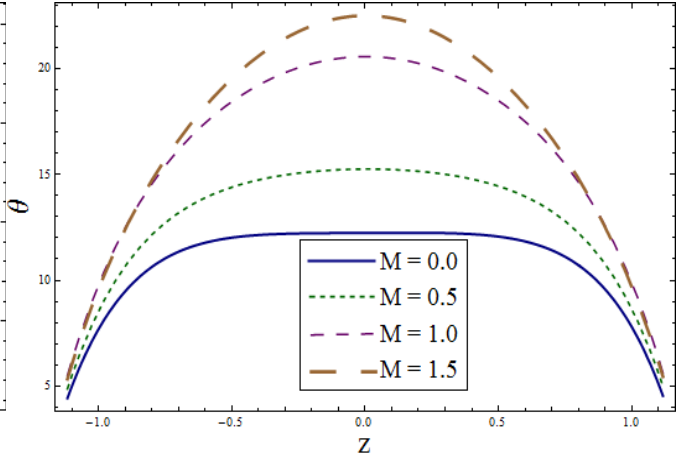
$$Bi_1 = Bi_2 = 10.0, \phi = 0.01, x = \epsilon = 0.2, t = 0.1.$$

Fig. 5.10 : θ via change in ϕ when $E_1 = E_2 = 0.3$, $E_3 = 0.01$, $M = 2.0$, $Br = 0.5$, $T' = 1.0$,

$$Bi_1 = Bi_2 = 10.0, x = \epsilon = 0.2, t = 0.1.$$



5.11



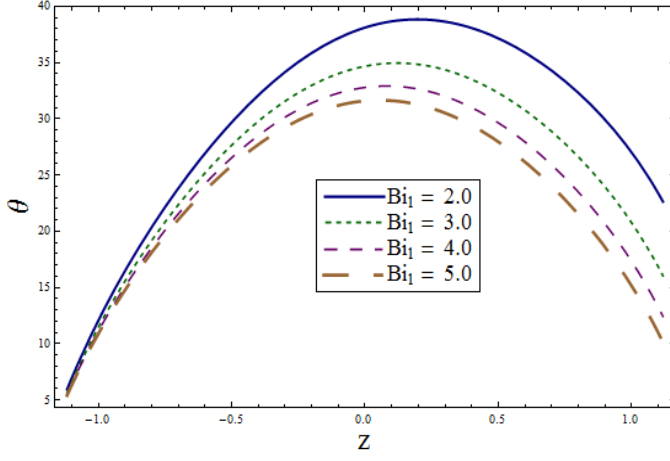
5.12

Fig. 5.11 : θ via change in T' when $E_1 = E_2 = 0.3$, $E_3 = 0.01$, $M = 2.0$, $Br = 0.5$,

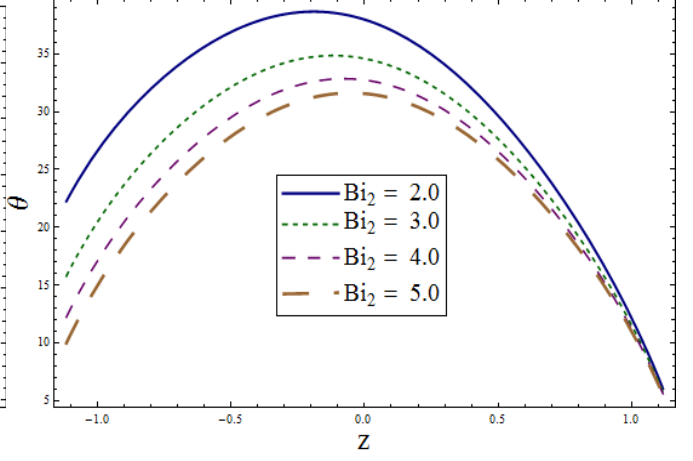
$$Bi_1 = Bi_2 = 10.0, \phi = 0.01, x = \epsilon = 0.2, t = 0.1.$$

Fig. 5.12 : θ via change in M when $E_1 = E_2 = 0.3$, $E_3 = 0.01$, $Br = 0.5$, $T' = 1.0$, $\phi = 0.01$,

$$Bi_1 = Bi_2 = 10.0, x = \epsilon = 0.2, t = 0.1.$$



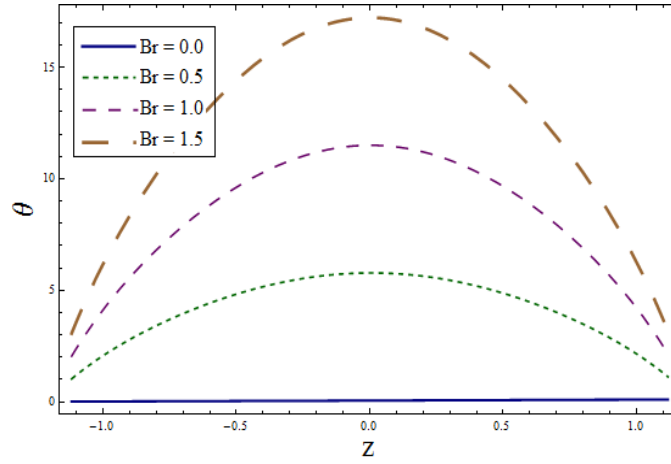
5.13



5.14

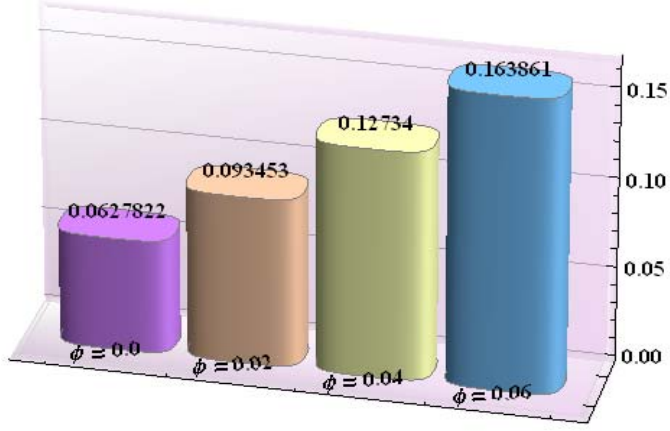
Fig. 5.13 : θ via change in Bi_1 when $E_1 = E_2 = 0.3$, $E_3 = 0.01$, $M = 2.0$, $Br = 0.5$, $T' = 1.0$, $\phi = 0.01$, $Bi_2 = 10.0$, $x = \epsilon = 0.2$, $t = 0.1$.

Fig. 5.14 : θ via change in Bi_2 when $E_1 = E_2 = 0.3$, $E_3 = 0.01$, $M = 2.0$, $T' = 1.0$, $Br = 0.5$, $Bi_1 = 10.0$, $\phi = 0.01$, $x = \epsilon = 0.2$, $t = 0.1$.

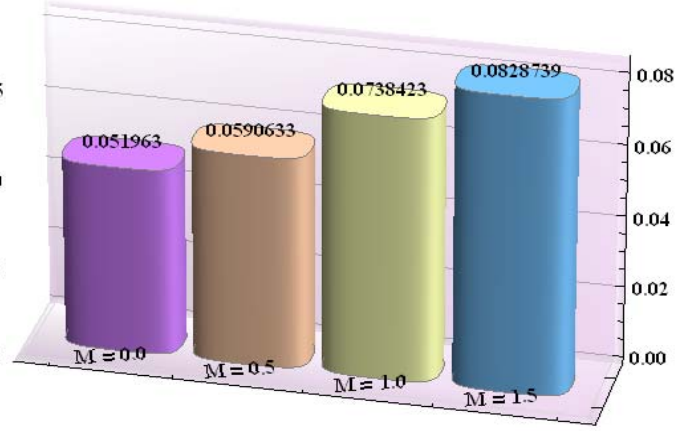


5.15

Fig. 5.15 : θ via change in Br when $E_1 = E_2 = 0.3$, $E_3 = 0.01$, $M = 2.0$, $T' = 1.0$, $\phi = 0.01$, $Bi_1 = Bi_2 = 10.0$, $x = \epsilon = 0.2$, $t = 0.1$.



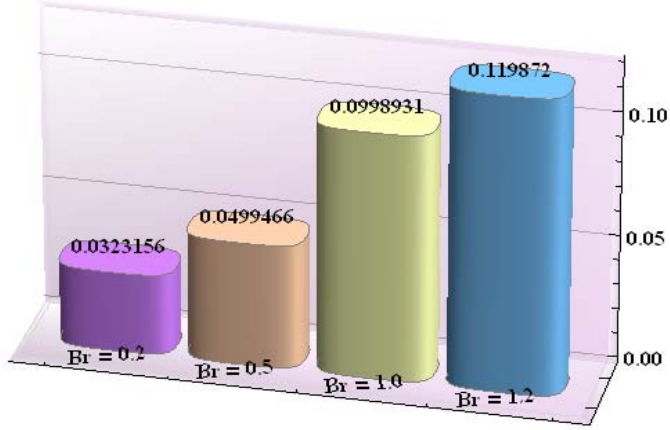
5.16



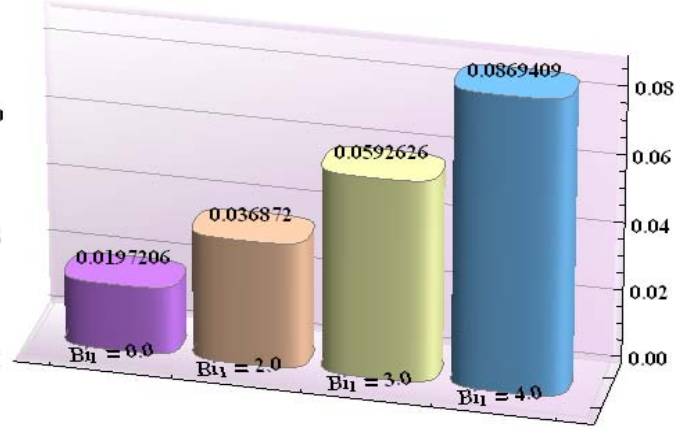
5.17

Fig. 5.16 : Impact of ϕ on heat transfer rate at the wall $(-(\frac{K_{eff}}{K_f})\theta'(\eta))$ when $E_1 = E_2 = 0.03$, $E_3 = 0.1$, $M = 2.0$, $Br = 0.8$, $Bi_1 = Bi_2 = 10.0$, $T' = 10.0$, $\epsilon = 0.2$, $t = 0.1$.

Fig. 5.17 : Impact of M^2 on heat transfer rate at the wall $(-(\frac{K_{eff}}{K_f})\theta'(\eta))$ when $E_1 = E_2 = 0.01$, $E_3 = 0.1$, $Br = 0.8$, $T' = 10.0$, $\phi = 0.01$, $Bi_1 = Bi_2 = 10.0$, $\epsilon = 0.2$, $t = 0.1$.



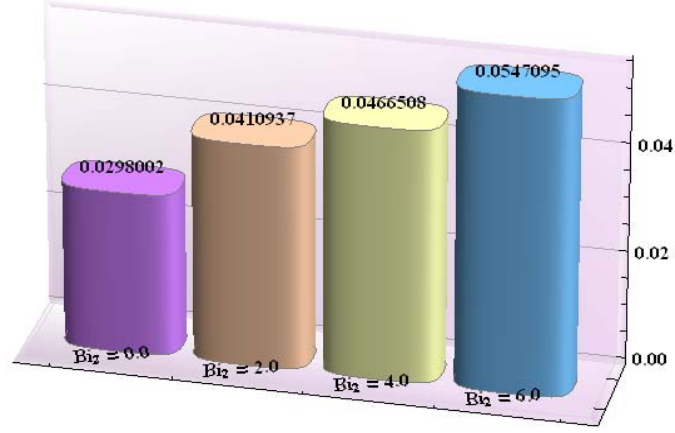
5.18



5.19

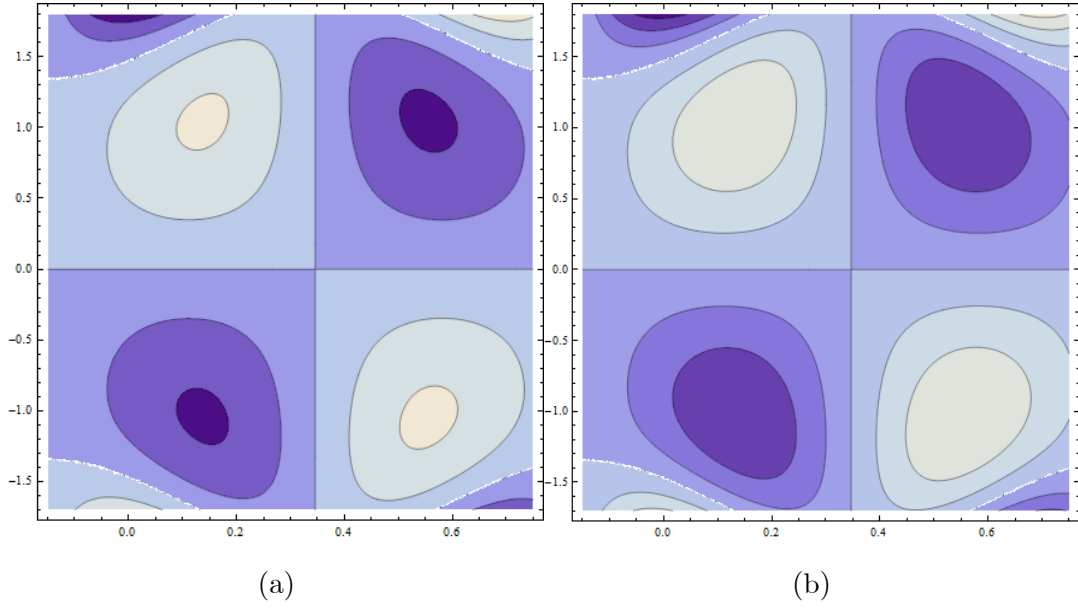
Fig. 5.18 : Impact of Br on heat transfer rate at the wall $(-(\frac{K_{eff}}{K_f})\theta'(\eta))$ when $E_1 = E_2 = 0.01$, $E_3 = 0.1$, $M = 2.0$, $T' = 10.0$, $Bi_1 = Bi_2 = 10.0$, $\phi = 0.01$, $\epsilon = 0.2$, $t = 0.1$.

Fig. 5.19 : Impact of Bi_1 on heat transfer rate at the wall $(-(\frac{K_{eff}}{K_f})\theta'(\eta))$ when $E_1 = E_2 = 0.01$, $E_3 = 0.1$, $M = 2.0$, $Br = 0.8$, $T' = 10.0$, $Bi_2 = 10.0$, $\phi = 0.01$, $\epsilon = 0.2$, $t = 0.1$.



5.20

Fig. 5.20 : Impact of Bi_2 on heat transfer rate at the wall $(-(\frac{K_{eff}}{K_f})\theta'(\eta))$ when $E_1 = E_2 = 0.01$, $E_3 = 0.1$, $M = 2.0$, $Br = 0.8$, $T' = 10.0$, $Bi_1 = 10.0$, $\phi = 0.01$, $\epsilon = 0.2$, $t = 0.1$.



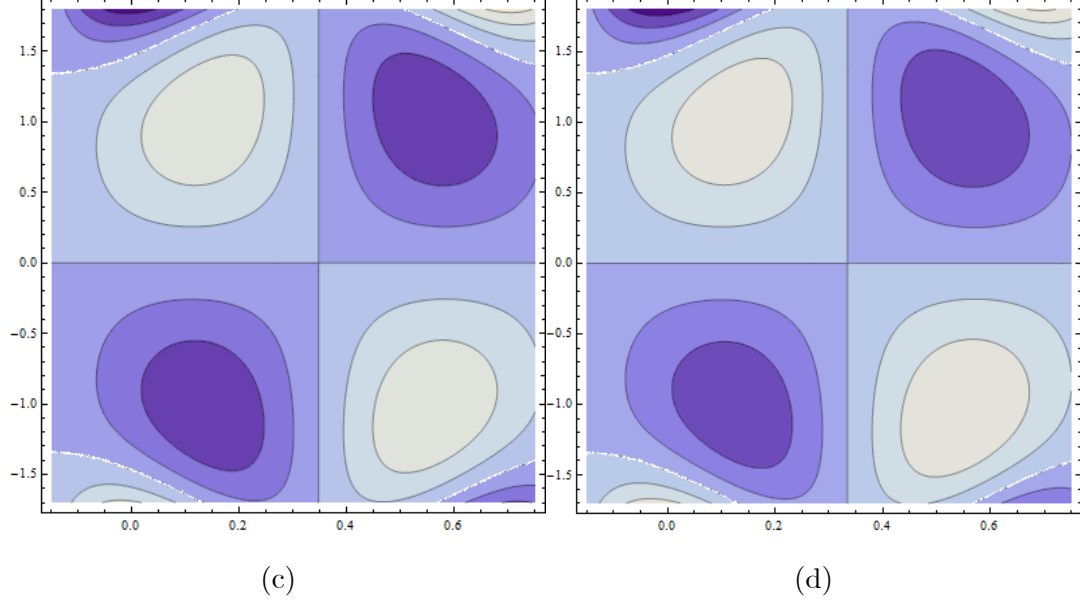


Fig. 5.21 : Streamlines for wall properties when $T' = 1.0$, $M = 0.8$, $t = 0.1$, $\epsilon = 0.2$, $\phi = 0.01$,
 (a) $E_1 = 0.03$, $E_2 = 0.03$, $E_3 = 0.01$, (b) $E_1 = 0.05$, (c) $E_2 = 0.05$, (d) $E_3 = 0.05$.

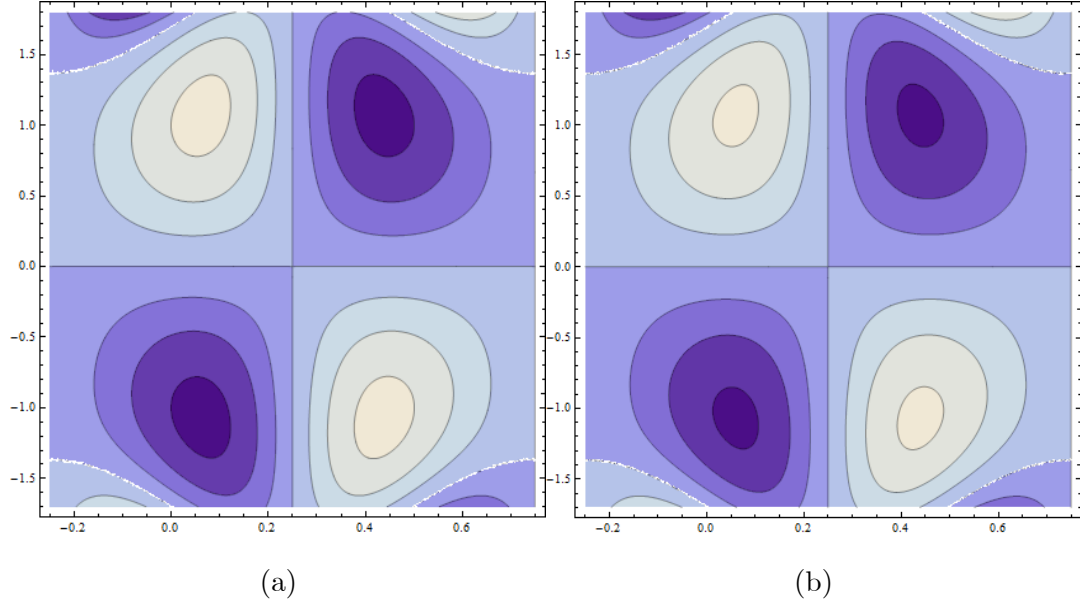


Fig. 5.22 : Streamlines for T' when $E_1 = E_2 = 0.3$, $E_3 = 0.01$, $M = 0.8$, $t = 0.1$, $\epsilon = 0.2$,
 $\phi = 0.01$, (a) $T' = 0.1$, (b) $T' = 0.3$.

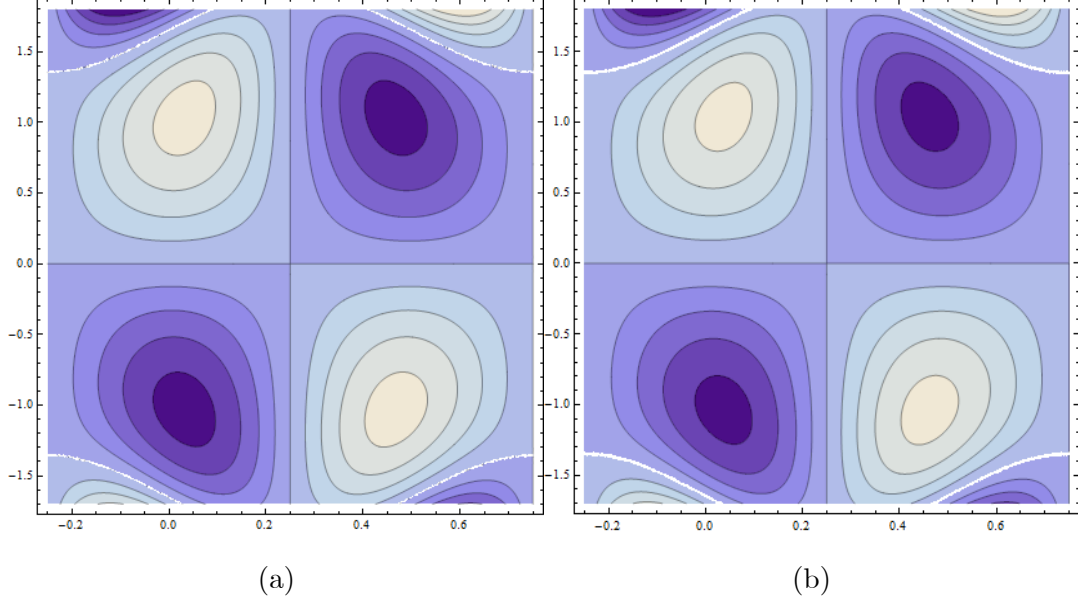


Fig. 5.23 : Streamlines for M when $E_1 = E_2 = 0.3$, $E_3 = 0.01$, $T' = 1.0$, $t = 0.1$, $\epsilon = 0.2$, $\phi = 0.01$, (a) $M = 0.1$, (b) $M = 0.6$.

5.5 Conclusions

Peristalsis of magnetite in a channel with rigid body rotation is addressed in this chapter. Analysis is done in the presence of magnetic field and Joule heating. Temperature distribution at walls is studied through convective heat transfer. Main observation of the analysis is presented through following points:

- Axial velocity is increasing for wall elastance parameters (E_1, E_2) whereas it decreases for damping parameter E_3 .
- No secondary velocity is noticed in the case of non-rotating channel.
- Both velocity components (axial and secondary) and temperature show decreasing behavior as nanoparticle volume fraction ϕ is increased.
- Temperature shows decreasing behavior for Biot numbers (Bi_1, Bi_2).
- Effective thermal conductivity of nanofluid increases through enhancing nanoparticle volume fraction ϕ .

- Size of trapped bolus decreases for both Taylor T' and Hartman M^2 numbers.

Chapter 6

Investigation of Hall current and slip conditions on peristaltic transport of Cu-water nanofluid in a rotating frame

6.1 Introduction

Main objective of this chapter is to analyze the effect of rotation on peristaltic transport of copper-water nanofluid. Two phase nanofluid is employed. The fluid fills the porous space. The channel walls are taken flexible. Hall current and viscous dissipation effects are also given consideration in the modeling. Analysis also studies the slip conditions in presence of heat generation/absorption. Resulting coupled system of equations is simplified by employing lubrication approach. Exact solutions are presented for the stream function whereas energy equation is solved numerically. Impact of sundry parameters on flow quantities are discussed and displayed via graphs.

6.2 Mathematical formulation

We consider the flow of an incompressible copper-water nanofluid through channel of width $2d$. The channel walls are taken compliant in nature. The channel is filled with homogeneous porous medium having permeability k_1 . Both the base fluid and copper nanoparticles are taken to be thermally consistent with respect to each other. The fluid and channel are in state of rigid body rotation with constant angular speed Ω about z-axis (see Fig. 2.1). The flow in a channel is generated due to propagation of the waves with amplitude a and wavelength λ along the walls located at $z = \pm\eta$. The shapes of travelling waves are expressed by the following relations:

$$z = \pm\eta(x, t) = \pm \left[d + a \sin \frac{2\pi}{\lambda} (x - ct) \right], \quad (6.1)$$

in which t shows the time, d the half width of channel and c stands for wave speed.

A strong uniform magnetic field of strength B_0 is applied along z-axis. The effects of induced magnetic field are neglected by taking small magnetic Reynolds number. Generalized Ohms law with Hall current is represented by [165] :

$$\mathbf{J} = \sigma_{eff} \left[\mathbf{E} + \mathbf{V} \times \mathbf{B} - \frac{1}{en_e} [\mathbf{J} \times \mathbf{B}] \right]. \quad (6.2)$$

In above equation \mathbf{J} is the current density, σ_{eff} shows the effective electric conductivity of copper water nanofluid, \mathbf{E} stands for electric field, $\mathbf{V} = [u(x, z, t), v(x, z, t), w(x, z, t)]$ defines the velocity field, e the electron charge and n_e the number density of free electrons. In the absence of electric field \mathbf{E} , Lorentz force takes the form

$$\begin{aligned} \mathbf{J} \times \mathbf{B} = & \left[\frac{\sigma_{eff} B_0^2}{1 + (\sigma_{eff} B_0 / en_e)^2} (-u + (\sigma_{eff} B_0 / en_e) v), \right. \\ & \left. \frac{-\sigma_{eff} B_0^2}{1 + (\sigma_{eff} B_0 / en_e)^2} (v + (\sigma_{eff} B_0 / en_e) u), 0 \right]. \end{aligned} \quad (6.3)$$

The effective electric conductivity of Cu-water nanofluid considering two phase flow model is defined as follows [169]:

$$\frac{\sigma_{eff}}{\sigma_f} = 1 + \frac{3 \left(\frac{\sigma_p}{\sigma_f} - 1 \right) \phi}{\left(\frac{\sigma_p}{\sigma_f} + 2 \right) - \left(\frac{\sigma_p}{\sigma_f} - 1 \right) \phi}, \quad (6.4)$$

in which σ_p and σ_f are the electric conductivities of copper nanoparticles and water respectively. Here ϕ shows the nanoparticles volume fraction. We noticed that for $\phi = 0$ (in the absence of nanoparticles) the effective electric conductivity becomes equal to that of water. For $\phi = 1$ the effective electric conductivity corresponds to the case of copper. Using (6.4) in (6.3) we get

$$\mathbf{J} \times \mathbf{B} = \left[\frac{A_1 \sigma_f B_0^2}{1 + (A_1 m)^2} (-u + A_1 m v), \frac{-A_1 \sigma_f B_0^2}{1 + (A_1 m)^2} (v + A_1 m u), 0 \right], \quad (6.5)$$

where A_1 and m (Hall parameter) are defined below in the forms

$$A_1 = 1 + \frac{3 \left(\frac{\sigma_p}{\sigma_f} - 1 \right) \phi}{\left(\frac{\sigma_p}{\sigma_f} + 2 \right) - \left(\frac{\sigma_p}{\sigma_f} - 1 \right) \phi}, \quad m = \frac{\sigma_f B_0}{en_e}.$$

For the flow under consideration the continuity equation is

$$\frac{\partial u}{\partial x} + \frac{\partial w}{\partial z} = 0. \quad (6.6)$$

Components of momentum equation for the flow of nanofluid in a channel undergoing rigid body rotation are:

$$\rho_{eff} \left[\frac{du}{dt} - 2\Omega v \right] = -\frac{\partial \hat{p}}{\partial x} + \mu_{eff} \left(\frac{\partial^2 u}{\partial x^2} + \frac{\partial^2 u}{\partial z^2} \right) + \frac{A_1 \sigma_f B_0^2}{1 + (A_1 m)^2} (-u + A_1 m v) - \frac{\mu_{eff} u}{k_1}, \quad (6.7)$$

$$\rho_{eff} \left[\frac{dv}{dt} + 2\Omega u \right] = -\frac{\partial \hat{p}}{\partial y} + \mu_{eff} \left(\frac{\partial^2 v}{\partial x^2} + \frac{\partial^2 v}{\partial z^2} \right) - \frac{A_1 \sigma_f B_0^2}{1 + (A_1 m)^2} (v + A_1 m u) - \frac{\mu_{eff} v}{k_1}, \quad (6.8)$$

$$\rho_{eff} \frac{dw}{dt} = -\frac{\partial \hat{p}}{\partial z} + \mu_{eff} \left(\frac{\partial^2 w}{\partial x^2} + \frac{\partial^2 w}{\partial z^2} \right), \quad (6.9)$$

where modified pressure \hat{p} is

$$\hat{p} = p - \frac{1}{2} \rho \Omega^2 (x^2 + y^2).$$

The energy equation under the effects of viscous dissipation and heat generation/absorption (Φ) takes the form

$$(\rho C)_{eff} \frac{dT}{dt} = K_{eff} \left(\frac{\partial^2 T}{\partial x^2} + \frac{\partial^2 T}{\partial y^2} + \frac{\partial^2 T}{\partial z^2} \right) + \frac{\mu_{eff} u^2}{k_1} + \Phi + \mu_{eff} \left[\begin{array}{c} 2 \left\{ \left(\frac{\partial u}{\partial x} \right)^2 + \left(\frac{\partial w}{\partial z} \right)^2 \right\} \\ + \left(\frac{\partial u}{\partial z} + \frac{\partial w}{\partial x} \right)^2 \end{array} \right]. \quad (6.10)$$

The effective density ρ_{eff} , specific heat C_{eff} , thermal conductivity K_{eff} and effective viscosity for the two-phase flow model of nanofluid are [170]:

$$\begin{aligned}\rho_{eff} &= (1 - \phi) \rho_f + \phi \rho_p, \\ (\rho C)_{eff} &= (1 - \phi) (\rho C)_f + \phi (\rho C)_p, \\ \frac{K_{eff}}{K_f} &= \frac{K_p + 2K_f - 2\phi(K_f - K_p)}{K_p + 2K_f + \phi(K_f - K_p)}, \\ \mu_{eff} &= \frac{\mu_f}{(1 - \phi)^{2.5}},\end{aligned}$$

where subscripts p and f denote the nanoparticle and fluid phase respectively. Numerical values of thermophysical properties of water and copper are given in *Table 1*.

Table 1

Numerical values of thermophysical properties of copper and water [171].					
Phase	$\rho(kg/m^3)$	$K(W/mK)$	$C(J/kgK)$	$\beta(1/k) \times 10^{-6}$	$\sigma(S/m)$
Water	997.1	0.613	4179	210	0.05
Copper	8933	401	385	16.65	5.96×10^7

After using above mentioned quantities in Eqs. (6.7 – 6.10) one can write

$$\begin{aligned}[(1 - \phi) \rho_f + \phi \rho_p] \left[\frac{du}{dt} - 2\Omega v \right] &= -\frac{\partial p}{\partial x} + \frac{\mu_f}{(1 - \phi)^{2.5}} \left(\frac{\partial^2 u}{\partial x^2} + \frac{\partial^2 u}{\partial z^2} \right) + \frac{A_1 \sigma_f B_0^2}{1 + (A_1 m)^2} \\ &\quad \times (-u + A_1 m v) - \frac{\mu_f u}{(1 - \phi)^{2.5} k_1},\end{aligned}\tag{6.11}$$

$$\begin{aligned}[(1 - \phi) \rho_f + \phi \rho_p] \left[\frac{dv}{dt} + 2\Omega u \right] &= -\frac{\partial p}{\partial y} + \frac{\mu_f}{(1 - \phi)^{2.5}} \left(\frac{\partial^2 v}{\partial x^2} + \frac{\partial^2 v}{\partial z^2} \right) - \frac{A_1 \sigma_f B_0^2}{1 + (A_1 m)^2} \\ &\quad \times (v + A_1 m u) - \frac{\mu_f v}{(1 - \phi)^{2.5} k_1},\end{aligned}\tag{6.12}$$

$$[(1 - \phi) \rho_f + \phi \rho_p] \frac{dw}{dt} = -\frac{\partial p}{\partial z} + \frac{\mu_f}{(1 - \phi)^{2.5}} \left(\frac{\partial^2 w}{\partial x^2} + \frac{\partial^2 w}{\partial z^2} \right),\tag{6.13}$$

$$\begin{aligned}[(1 - \phi) \rho_f + \phi \rho_p] \frac{dT}{dt} &= K_{eff} \left(\frac{\partial^2 T}{\partial x^2} + \frac{\partial^2 T}{\partial y^2} + \frac{\partial^2 T}{\partial z^2} \right) + \frac{\mu_f u^2}{(1 - \phi)^{2.5} k_1} + \Phi + \frac{\mu_f}{(1 - \phi)^{2.5}} \\ &\quad \times \left[2 \left\{ \left(\frac{\partial u}{\partial x} \right)^2 + \left(\frac{\partial w}{\partial z} \right)^2 \right\} + \left(\frac{\partial u}{\partial z} + \frac{\partial w}{\partial x} \right)^2 \right].\end{aligned}\tag{6.14}$$

Equation of motion for the compliant walls can be expressed as

$$L(\eta) = p - p_0, \quad (6.15)$$

with

$$L = -\tau' \frac{\partial^2}{\partial x^2} + m_1 \frac{\partial^2}{\partial t^2} + d' \frac{\partial}{\partial t}, \quad (6.16)$$

$$\begin{aligned} \frac{\partial}{\partial x} L(\eta) &= \frac{\partial p}{\partial x} = \frac{\mu_f}{(1-\phi)^{2.5}} \left(\frac{\partial^2 u}{\partial x^2} + \frac{\partial^2 u}{\partial z^2} \right) + \frac{A_1 \sigma_f B_0^2}{1 + (A_1 m)^2} (-u + A_1 m v) - \frac{\mu_f u}{(1-\phi)^{2.5} k_1} \\ &\quad - [(1-\phi) \rho_f + \phi \rho_p] \left[\frac{du}{dt} - 2\Omega v \right]. \end{aligned} \quad (6.17)$$

Non-dimensional quantities used in the above Eqs. are

$$\begin{aligned} x^* &= \frac{x}{\lambda}, \quad y^* = \frac{y}{\lambda}, \quad z^* = \frac{z}{d}, \quad p^* = \frac{d^2 p}{c \mu_f \lambda}, \quad t^* = \frac{ct}{\lambda}, \quad u^* = \frac{u}{c}, \\ v^* &= \frac{v}{c}, \quad w^* = \frac{w}{c}, \quad \eta^* = \frac{\eta}{d}, \quad \theta = \frac{T - T_m}{T_1 - T_0}, \quad T_m = \frac{T_0 + T_1}{2}, \\ \text{Re} &= \frac{\rho_f c d}{\mu_f}, \quad \delta = \frac{d}{\lambda}, \quad \beta_1^* = \frac{\mu_f \beta_1}{d}, \quad \beta_2^* = \frac{\mu_f \beta_2}{d}, \quad \beta_3^* = \frac{\beta_3}{d}, \\ T' &= \frac{\text{Re} \Omega d}{c}, \quad M = B_0 d \sqrt{\frac{\sigma_f}{\mu_f}}, \quad K_1 = \frac{k_1}{d^2}, \quad \text{Pr} = \frac{\mu_f C_f}{\kappa_f}, \\ Ec &= \frac{c^2}{C_f (T_1 - T_0)}, \quad Br = \text{Pr} Ec, \quad \epsilon_1 = \frac{d^2 \Phi}{\kappa_f (T_1 - T_0)}, \\ E_1 &= \frac{-\tau d^3}{\lambda^3 \mu c}, \quad E_2 = \frac{m_1 c d^3}{\lambda^3 \mu}, \quad E_3 = \frac{d' d^3}{\lambda^2 \mu}, \end{aligned}$$

where T_m is the mean temperature of nanofluid and T_1/T_0 are the temperatures at upper/lower wall. Using above mentioned variables and defining stream function by

$$u = \psi_z, \quad w = -\delta \psi_x,$$

equations (6.11 – 6.17) give

$$\begin{aligned} \text{Re } \delta \left[(1 - \phi) + \phi \frac{\rho_p}{\rho_f} \right] \frac{d}{dt} \left(\frac{\partial \psi}{\partial z} \right) - 2T' \left[(1 - \phi) + \phi \frac{\rho_p}{\rho_f} \right] v &= -\frac{\partial p}{\partial x} + \frac{1}{(1 - \phi)^{2.5}} \left(\delta^2 \frac{\partial^3 \psi}{\partial x^2 \partial z} \right. \\ &\quad \left. + \frac{\partial^3 \psi}{\partial z^3} \right) - \frac{A_1 M^2}{1 + (A_1 m)^2} \left(\frac{\partial \psi}{\partial z} \right. \\ &\quad \left. - A_1 m v \right) - \frac{u}{(1 - \phi)^{2.5} K_1} \quad (6.18) \end{aligned}$$

$$\begin{aligned} \text{Re } \delta \left[(1 - \phi) + \phi \frac{\rho_p}{\rho_f} \right] \frac{dv}{dt} + 2T' \left[(1 - \phi) + \phi \frac{\rho_p}{\rho_f} \right] u &= -\frac{\partial p}{\partial y} + \frac{1}{(1 - \phi)^{2.5}} \left(\delta^2 \frac{\partial^2 v}{\partial x^2} \right. \\ &\quad \left. + \frac{\partial^2 \psi}{\partial z^2} \right) - \frac{A_1 M^2}{1 + (A_1 m)^2} \left(v \right. \\ &\quad \left. + A_1 m \frac{\partial \psi}{\partial z} \right) - \frac{v}{(1 - \phi)^{2.5} K_1} \quad (6.19) \end{aligned}$$

$$\begin{aligned} -\text{Re } \delta^2 \left[(1 - \phi) + \phi \frac{\rho_p}{\rho_f} \right] \frac{d}{dt} \left(\frac{\partial \psi}{\partial z} \right) &= -\frac{\partial p}{\partial z} + \frac{1}{(1 - \phi)^{2.5}} \\ &\quad \left(\delta^3 \frac{\partial^3 \psi}{\partial x^3} - \delta \frac{\partial^3 \psi}{\partial x \partial z^2} \right), \quad (6.20) \end{aligned}$$

$$\begin{aligned} \delta \text{Pr Re} \left[(1 - \phi) + \phi \frac{\rho_p}{\rho_f} \right] \left[\frac{\partial \theta}{\partial t} + \frac{\partial \psi}{\partial z} \frac{\partial \theta}{\partial x} + v \frac{\partial \theta}{\partial y} - \frac{\partial \psi}{\partial x} \frac{\partial \theta}{\partial z} \right] &= A_2 \left[\delta^2 \frac{\partial^2 \theta}{\partial x^2} + \delta^2 \frac{\partial^2 \theta}{\partial y^2} + \frac{\partial^2 \theta}{\partial z^2} \right] \\ &\quad + \frac{Br}{K_1 (1 - \phi)^{2.5}} \left(\frac{\partial \psi}{\partial z} \right)^2 + \epsilon_1 \\ &\quad + \frac{Br}{(1 - \phi)^{2.5}} \left[4\delta^2 \left(\frac{\partial^2 \psi}{\partial x \partial z} \right)^2 \right. \\ &\quad \left. + 2 \left(\frac{\partial^2 \psi}{\partial z^2} - \delta^2 \frac{\partial^2 \psi}{\partial x^2} \right)^2 \right]. \quad (6.21) \end{aligned}$$

where continuity equation (6.6) is identically satisfied.

In above expressions Re is the Reynolds number, δ the wave number, T' the Taylor number, M the Hartman number, K_1 the permeability parameter, Pr the Prandtl number, Ec the Eckert number, ϵ_1 the heat generation/absorption parameter, Br the Brinkman number and E_1 , E_2 and E_3 the non-dimensional elasticity parameters. The term A_2 in Eq.(6.21) is

$$A_2 = \frac{K_p + 2K_f - 2\phi(K_f - K_p)}{K_p + 2K_f + \phi(K_f - K_p)}. \quad (6.22)$$

After employing long wavelength and low Reynold assumptions, Eqs. (6.18 – 6.21) are reduced

to

$$-\frac{\partial p}{\partial x} + \frac{1}{(1-\phi)^{2.5}} \frac{\partial^3 \psi}{\partial z^3} - \frac{A_1 M^2}{1+(A_1 m)^2} \left(\frac{\partial \psi}{\partial z} - A_1 m v \right) - \frac{u}{(1-\phi)^{2.5} K_1} + 2T' \left[(1-\phi) + \phi \frac{\rho_p}{\rho_f} \right] v = 0, \quad (6.23)$$

$$-\frac{\partial p}{\partial y} + \frac{1}{(1-\phi)^{2.5}} \frac{\partial^2 \psi}{\partial z^2} - \frac{A_1 M^2}{1+(A_1 m)^2} \left(v + A_1 m \frac{\partial \psi}{\partial z} \right) - \frac{v}{(1-\phi)^{2.5} K_1} - 2T' \left[(1-\phi) + \phi \frac{\rho_p}{\rho_f} \right] \frac{\partial \psi}{\partial z} = 0, \quad (6.24)$$

$$\frac{\partial p}{\partial z} = 0, \quad (6.25)$$

$$A_2 \frac{\partial^2 \theta}{\partial z^2} + \frac{Br}{K_1(1-\phi)^{2.5}} \left(\frac{\partial \psi}{\partial z} \right)^2 + \epsilon_1 + \frac{2Br}{(1-\phi)^{2.5}} \left(\frac{\partial^2 \psi}{\partial z^2} \right)^2 = 0, \quad (6.26)$$

The non-dimensionalized boundary conditions are [172]:

$$\frac{\partial \psi}{\partial z} \pm \beta_1 \frac{\partial^2 \psi}{\partial z^2} = 0, \quad \text{at } z = \pm \eta, \quad (6.27)$$

$$\left[E_1 \frac{\partial^3}{\partial x^3} + E_2 \frac{\partial^3}{\partial x \partial t^2} + E_3 \frac{\partial^2}{\partial x \partial t} \right] \eta = \frac{1}{(1-\phi)^{2.5}} \frac{\partial^3 \psi}{\partial z^3} - \left(\frac{A_1 M^2}{1+(A_1 m)^2} + \frac{1}{K(1-\phi)^{2.5}} \right) \frac{\partial \psi}{\partial z} + \left\{ 2T' \left[(1-\phi) + \phi \frac{\rho_p}{\rho_f} \right] + \frac{A_1 m M^2}{1+(A_1 m)^2} \right\} v \quad \text{at } z = \pm \eta, \quad (6.28)$$

$$v \pm \frac{\beta_2}{(1-\phi)^{2.5}} \frac{\partial v}{\partial z} = 0, \quad \text{at } z = \pm \eta, \quad (6.29)$$

$$\begin{aligned} \theta + \beta_3 \frac{\partial \theta}{\partial z} &= \frac{1}{2}, \quad \text{at } z = +\eta, \\ \theta - \beta_3 \frac{\partial \theta}{\partial z} &= -\frac{1}{2}, \quad \text{at } z = -\eta. \end{aligned} \quad (6.30)$$

Here β_1 and β_2 are velocity slip parameters and β_3 symbolizes the thermal slip parameter. It is clear from Eq. (6.25) that pressure is not a function of z . Hence pressure can be eliminated from Eq. (6.23). Further pressure term in Eq. (6.24) can be neglected since the secondary flow is resulted by the rotation. In view of these facts, we can write Eq. (6.23) in the form

$$\frac{1}{(1-\phi)^{2.5}} \frac{\partial^4 \psi}{\partial z^4} - \frac{A_1 M^2}{1+(A_1 m)^2} \left(\frac{\partial^2 \psi}{\partial z^2} - A_1 m \frac{\partial v}{\partial z} \right) - \frac{1}{(1-\phi)^{2.5} K} \frac{\partial^2 \psi}{\partial z^2} + 2T' \left[(1-\phi) + \phi \frac{\rho_p}{\rho_f} \right] \frac{\partial v}{\partial z}. \quad (6.31)$$

6.3 Solution

Solving Eqs. (6.24) and (6.31) with boundary conditions (6.27 – 6.29) we have the following exact relations of stream function and secondary velocity:

$$\begin{aligned}
\psi = & B_2 z - e^{-\frac{z(\sqrt{\gamma_1} + \sqrt{\zeta_1})}{\sqrt{\alpha_1}}} (B_3 (\cosh[\sqrt{\frac{\gamma_1}{\alpha_1}} z] + \sinh[\sqrt{\frac{\gamma_1}{\alpha_1}} z]) \\
& + (B_4 \cosh[\frac{z(2\sqrt{\gamma_1} + \sqrt{\zeta_1})}{\sqrt{\alpha_1}}] + \sinh[\frac{z(2\sqrt{\gamma_1} + \sqrt{\zeta_1})}{\sqrt{\alpha_1}}]) \\
& + B_5 (\cosh[\frac{z(\sqrt{\gamma_1} + 2\sqrt{\zeta_1})}{\sqrt{\alpha_1}}] + \sinh[\frac{z(\sqrt{\gamma_1} + 2\sqrt{\zeta_1})}{\sqrt{\alpha_1}}]) \\
& + B_6 (\cosh[\sqrt{\frac{\zeta_1}{\alpha_1}}] + \sinh[\sqrt{\frac{\zeta_1}{\alpha_1}}])), \tag{6.32}
\end{aligned}$$

$$\begin{aligned}
v = & -B_7 + e^{-\frac{z(\sqrt{\gamma_1} + \sqrt{\zeta_1})}{\sqrt{\alpha_1}}} (B_8 (\cosh[\sqrt{\frac{\gamma_1}{\alpha_1}} z] + \sinh[\sqrt{\frac{\gamma_1}{\alpha_1}} z] \cosh[\frac{z(\sqrt{\gamma_1} + 2\sqrt{\zeta_1})}{\sqrt{\alpha_1}}] \\
& + \sinh[\frac{z(\sqrt{\gamma_1} + 2\sqrt{\zeta_1})}{\sqrt{\alpha_1}}]) + B_9 (\cosh[\frac{z(2\sqrt{\gamma_1} + \sqrt{\zeta_1})}{\sqrt{\alpha_1}}] + \sinh[\frac{z(2\sqrt{\gamma_1} + \sqrt{\zeta_1})}{\sqrt{\alpha_1}}] \\
& + \cosh[\sqrt{\frac{\zeta_1}{\alpha_1}} z] + \sinh[\sqrt{\frac{\zeta_1}{\alpha_1}} z])), \tag{6.33}
\end{aligned}$$

where

$$\begin{aligned}
A_3 &= \left(\frac{A_1 M^2}{1 + A_1^2 m^2} + \frac{\alpha_1}{K_1} \right), \quad A_4 = \left(2T'(1 - \phi + \phi \frac{\rho_p}{\rho_f}) + \frac{A_1^2 m^2 M^2}{1 + A_1^2 m^2} \right), \\
\alpha_1 &= \frac{1}{(1 - \phi)^{2.5}}, \quad \zeta_1 = A_3 - iA_4, \quad \gamma_1 = A_3 + iA_4,
\end{aligned}$$

and B_i ($i = 1 - 19$) are given as

$$\begin{aligned}
B_1 &= \sqrt{\alpha_1 \gamma_1}, \quad B_2 = \left(\frac{iA_3 A_4 C_1}{(-iA_3 - A_4)\gamma_1} + \frac{A_3^2 C_4}{\zeta_1 \gamma_1} - \frac{A_3 C_6 \alpha_1}{\zeta_1 \gamma_1} \right), \\
B_3 &= \frac{(A_3^2 + A_4^2) B_1 (-iA_4 C_4 + C_6 \alpha) + A_3 (-iA_3 + A_4) B_1 C_1 \zeta_1}{4(A_3 - iA_4) \gamma_1^{3/2} \zeta_1^{3/2}}, \\
B_4 &= -\frac{\sqrt{\alpha_1} ((iA_3 + A_4)(A_4 C_4 - iC_6 \alpha_1) + iA_3 C_1 \zeta_1)}{4\gamma_1^{3/2} \zeta_1}, \\
B_5 &= \frac{iB_1 ((A_3^2 + A_4^2)(A_4 C_4 + iC_6 \alpha_1) + A_3 (A_3 + iA_4) C_1 \zeta_1)}{4(A_3 - iA_4) \gamma_1^{3/2} \zeta_1^{3/2}}, \quad B_6 = -B_4, \\
B_7 &= \frac{A_4}{\gamma_1} \left(-\frac{C_6 \alpha}{A_3 - iA_4} + \left(\frac{-A_4 C_1 + A_3 C_4}{\zeta_1} \right) \right),
\end{aligned}$$

$$\begin{aligned}
B_8 &= \frac{(A_3^2 + A_4^2)(A_3C_1 + A_4C_4) + i(A_3 + iA_4)C_6\alpha_1\zeta_1}{4(A_3 - iA_4)\gamma_1\zeta_1}, \\
B_9 &= \frac{(A_3 - iA_4)(A_3C_1 + A_4C_4) - C_6\alpha_1\zeta_1}{4\gamma_1\zeta_1}.
\end{aligned}$$

The Eq. (6.26) is solved numerically using NDSolve in MATHEMATICA by employing boundary condition defined in Eq. (6.30). This technique is based on the standard shooting method with fourth order Runge-Kutta integration procedure. Graphical interpretation is presented in the next section.

6.4 Discussion

Results obtained are discussed via graphs in this section. Impact of involved parameters on axial u and secondary v velocities, temperature θ and rate of heat transfer at the boundary are examined by plotting graphs.

6.4.1 Axial velocity

Figures (6.1 – 6.8) show the behavior of axial velocity under the variation of wall elastance parameters (E_1, E_2, E_3) , nanoparticles volume fraction ϕ , rotation parameter T' , Hartman number M , Hall parameter m , permeability parameter K_1 and velocities slip parameters β_1/β_2 . It is noticed from Fig. (6.1) that velocity increases for elasticity parameters (E_1, E_2) but it decreases for wall damping parameter E_3 . The fact behind this behavior is that the elasticity of walls offer less resistance to the flow and as a result the velocity increases. On the contrary, damping force is resistive in nature and it causes reduction in velocity. Velocity profile is found to decrease with the increase of nanoparticle volume fraction ϕ (see Fig. 6.2). In fact addition of copper nanoparticles offer more resistance to the flow and hence velocity decreases. Fig. (6.3) illustrates the behavior of rotation parameter T' on velocity. It can be seen from the Fig. that velocity in axial direction decreases as the rotation parameter is increased. It is noteworthy to mention that velocity is greater in non-rotating frame when compared with rotating case. Impact of Hartman number on velocity is shown through Fig. (6.4). Decrease in velocity is noticed for M due to resistive nature of Lorentz force. Fig. (6.5) studies the influence of Hall parameter m on velocity. It is observed that increasing value of m reduces effective conductivity

of copper nanoparticles which results in decreased magnetic damping force and thus velocity increases. High permeability of porous medium decreases the resistive force and thus causes increase in velocity (see Fig. 6.6). Figs. (6.7) and (6.8) show that increase in slip parameters (in both directions) results in the increase of axial velocity. Velocity is directly related to slip parameter. Enhancing slip effects causes reduction in the resistance offered by walls of the channel which in turn accelerates the velocity of the flow.

6.4.2 Secondary velocity

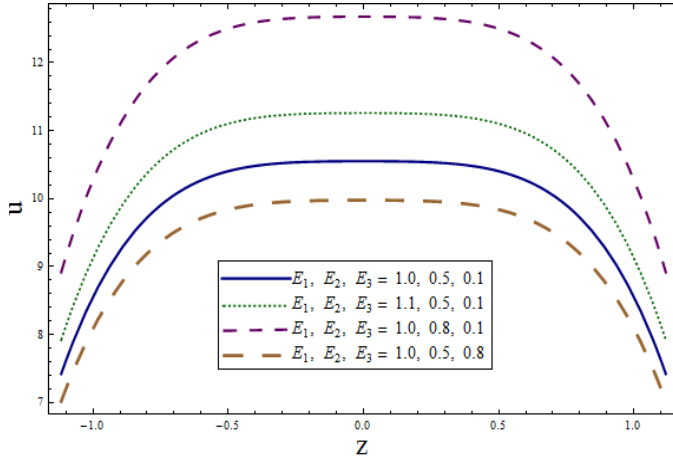
Effect of angular velocity induces a velocity component in y-direction which give rise to velocity which is termed as secondary velocity v . In this section the Figs. (6.9 – 6.16) are prepared to study the effects of pertinent parameters on secondary velocity. In Fig. (6.9) decrease in velocity profile is noticed for E_1 and E_2 but opposite behavior is seen for E_3 i.e. velocity is increasing. For increasing copper nanoparticles volume fraction the secondary velocity also decreases due to resistance offered by the particles (see Fig. 6.10). Fig. (6.11) elucidates the influence of rotation parameter T' and Hartman number M on v . The results indicate that there is no secondary velocity in absence of rotation i.e., ($T' = 0$). However higher values of secondary velocity are obtained in case of $T' \neq 0$ (see Fig. 7a). It is clearly indicated by Fig. (6.12) that velocity v decreases in view of Lorentz force for larger values of Hartman number M . Since magnetic field creates resistance for fluid to flow resulting in decreased velocity. Fig. (6.13) depicts the effect of Hall parameter m on v . This Fig. indicates that secondary velocity v is greater in the presence of Hall effects. Velocity is increasing function of permeability parameter as shown through Fig. (6.14). To study the influence of slip parameters (β_1 and β_2) in secondary velocity the Figs. (6.15) and (6.16) are plotted. Increase in slip parameters enhances velocity in y-direction. The results show that both axial and secondary velocities have similar behavior for most of the parameters involved.

6.4.3 Heat transfer analysis

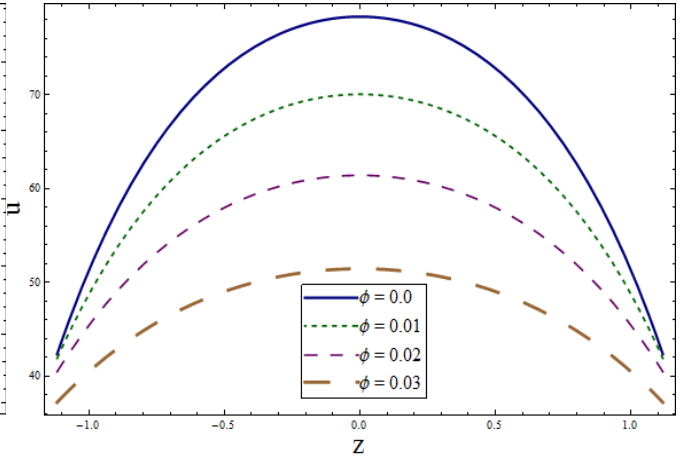
Main objective of using nanofluid is the enhancement of heat transfer process. Therefore we have plotted Figs. (6.17 – 6.29) to analyze the heat transfer process in present flow situation. Behavior of involved parameters on temperature θ is discussed through Figs. (6.17 – 6.25).

Influences of wall parameters (E_1, E_2, E_3) on temperature θ have been illustrated in Fig. (6.17). We know that temperature is defined as the average kinetic energy of particles which effects the fluid velocity. Thus increase in values of E_1 and E_2 results in rise of temperature and opposite behavior is noticed for increasing values of E_3 . It is observed from Fig. (6.18) that copper free fluid have higher temperature. It is noteworthy to mention here that addition of nanoparticles and increasing their volume fraction has considerable effects on temperature of fluid. It is found that temperature decreases when volume fraction of nanoparticles is increased. In fact thermal conductivity of nanofluid is enhanced with the increase of nanoparticle volume fraction which facilitates the heat transfer thus, reducing the temperature. By increasing the value of rotation parameter the temperature θ decreases (see Fig. 6.19). Large rotation of the channel causes fluid to move faster which in turn accelerates the heat transfer rate. Therefore the temperature decreases. Increasing the impact of magnetic field reduces the fluid temperature θ . As Lorentz force resist the motion of fluid and hence effecting the temperature. Fig. (6.20) is sketched to describe this fact. Figs. (6.21) and (6.22) are prepared to study the impact of Hall parameter m and permeability of porous medium K_1 on temperature. It is noticed from the Figs. that temperature enhances when the values of these parameters are increased. Increase in the value of Hall parameter enhances electrical conductivity of fluid i.e. more free electrons are available to conduct electric current. Increase in conduction rate enhances the temperature. Moreover increasing permeability enhances the velocity of fluid. This in turn increases the average kinetic energy of molecules and thus temperature enhancement is ensured. Fig. (6.23) elucidates the effect of heat generation/absorption coefficient ϵ_1 on θ . For $\epsilon_1 > 0$ (heat generation) temperature increases whereas it decreases for $\epsilon_1 < 0$ (heat absorption). Presence of heat source ($\epsilon_1 > 0$) generates more heat in the fluid which results in the enhancement of temperature. On the other hand heat sink ($\epsilon_1 < 0$) absorbs excess heat generated in the fluid which results in decline of temperature. Fig. (6.24) studies the effect of heat generation due to internal friction caused by shear in the flow. This effect is characterized by Br . Fig. (6.25) is prepared to analyze the effect of thermal slip on θ . Increase in temperature is noticed for higher values of β_3 . As temperature difference between walls and fluid increases more heat transfer takes place from one point to another. This results in rise of temperature. In absence of slip the temperature is less when compared with slip condition. Fig. (6.26) is plotted

to study rate of heat transfer when volume fraction ϕ of copper nanoparticles is increased. As expected the heat transfer rate enhances because of the increased thermal conductivity. Fig. (6.27) shows that by increasing permeability K_1 of porous medium the heat transfer rate at the boundary is increased. Heat transfer rate decays by increasing Hartman number. Ultimate the temperature decreases when M is increased. (see Fig. 6.28). Influence of Hall parameter m on the rate of heat transfer is also similar to M (see Fig. 6.29). To analyze the effect of thermal slip parameter β_3 on heat transfer rate Fig. 6.30 is drawn. It is observed from the Fig. that rate of heat transfer enhances as the temperature difference between wall and fluid is increased.



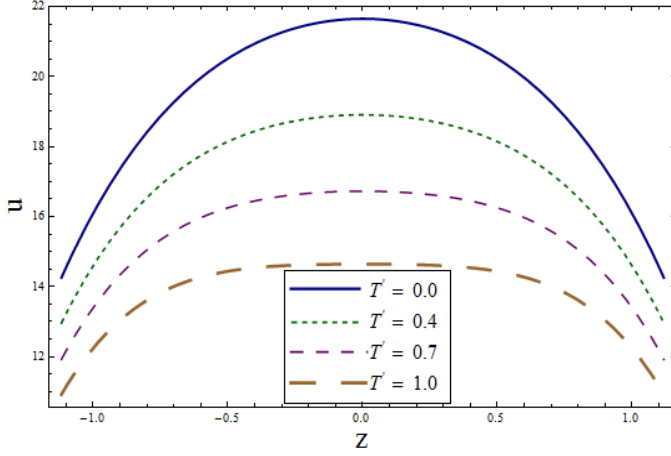
6.1



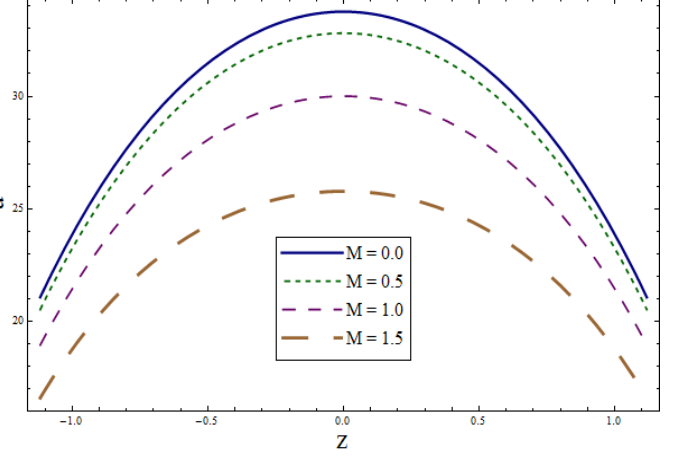
6.2

Fig. 6.1 : Variation of wall properties on u when $\beta_1 = \beta_2 = K_1 = 0.8$, $T' = 1.0$, $M = m = 2.0$, $\phi = 0.01$, $x = \epsilon = 0.2$, $t = 0.1$.

Fig. 6.2 : Variation of ϕ on u when $E_1 = E_2 = \beta_1 = \beta_2 = K_1 = 0.8$, $E_3 = 0.5$, $T' = 1.0$, $M = m = 2.0$, $x = \epsilon = 0.2$, $t = 0.1$.



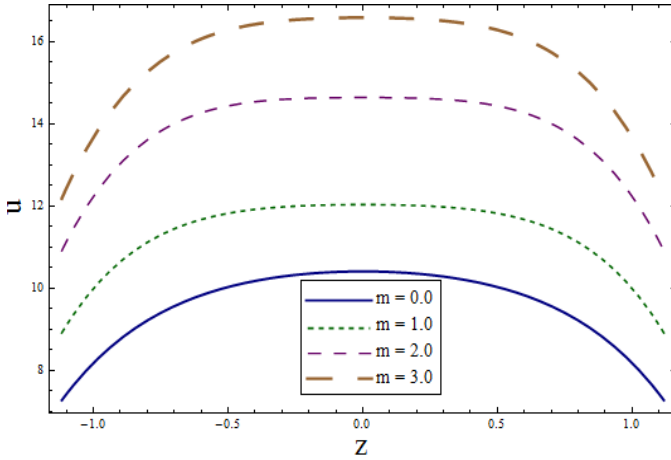
6.3



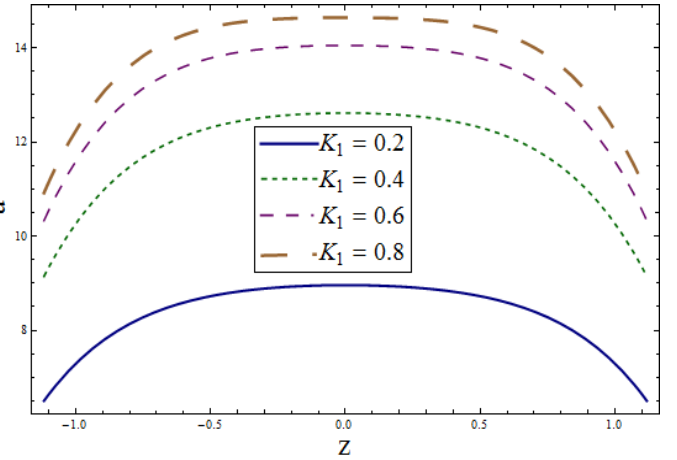
6.4

Fig. 6.3 : Variation of T' on u when $E_1 = E_2 = \beta_1 = \beta_2 = K_1 = 0.8$, $E_3 = 0.5$, $M = m = 2.0$, $\phi = 0.01$, $x = \epsilon = 0.2$, $t = 0.1$.

Fig.6.4 : Variation of M on u when $E_1 = E_2 = \beta_1 = \beta_2 = K_1 = 0.8$, $E_3 = 0.5$, $T' = 1.0$, $M = m = 2.0$, $\phi = 0.01$, $x = \epsilon = 0.2$, $t = 0.1$.



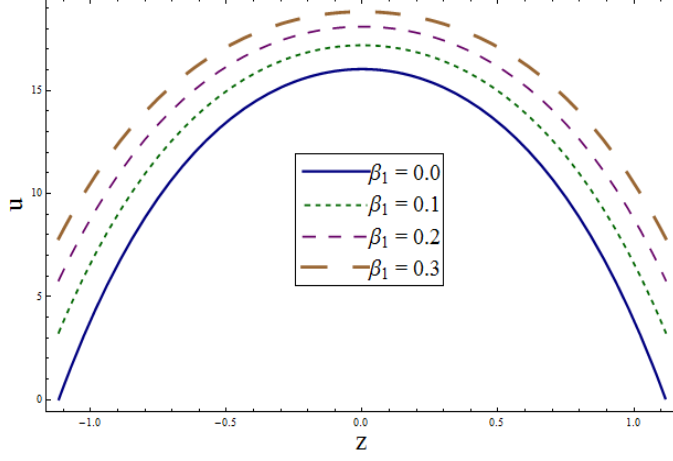
6.5



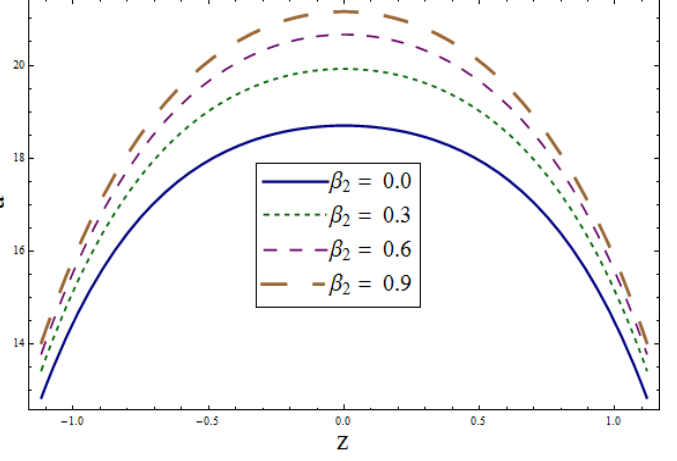
6.6

Fig. 6.5 : Variation of m on u when $E_1 = E_2 = \beta_1 = \beta_2 = K_1 = 0.8$, $E_3 = 0.5$, $T' = 1.0$, $\phi = 0.01$, $M = 2.0$, $x = \epsilon = 0.2$, $t = 0.1$.

Fig. 6.6 : Variation of K_1 on u when $E_1 = E_2 = \beta_1 = \beta_2 = 0.8$, $E_3 = 0.5$, $T' = 1.0$, $M = m = 2.0$, $\phi = 0.01$, $x = \epsilon = 0.2$, $t = 0.1$.



6.7



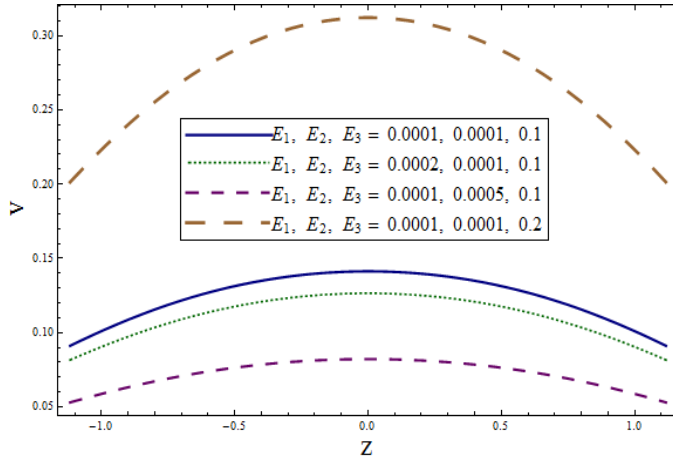
6.8

Fig. 6.7 : Variation of β_1 on u when $E_1 = E_2 = \beta_2 = K_1 = 0.8$, $E_3 = 0.5$, $T' = 1.0$,

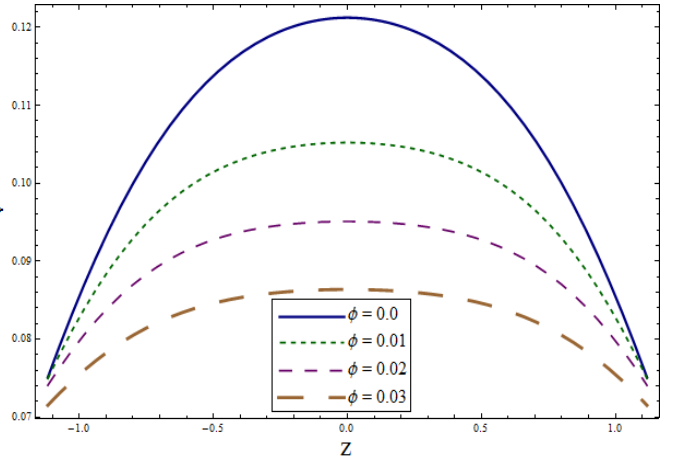
$M = m = 2.0$, $\phi = 0.01$, $x = \epsilon = 0.2$, $t = 0.1$.

Fig. 6.8 : Variation of β_2 on u when $E_1 = E_2 = K_1 = \beta_1 = 0.8$, $E_3 = 0.5$, $T' = 1.0$,

$M = m = 2.0$, $\phi = 0.01$, $x = \epsilon = 0.2$, $t = 0.1$.



6.9



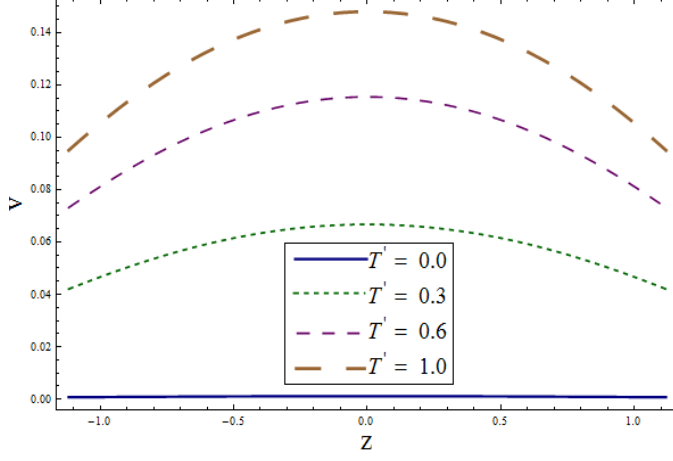
6.10

Fig. 6.9 : Variation of wall properties on v when $\beta_1 = \beta_2 = K_1 = 0.8$, $T' = 1.0$, $M = m = 2.0$,

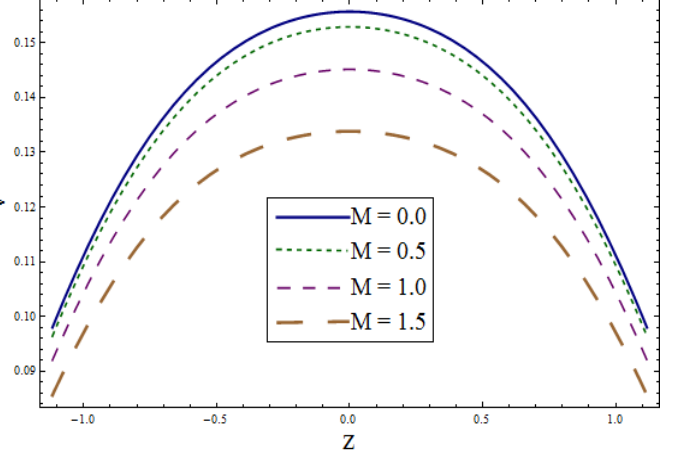
$\phi = 0.01$, $x = \epsilon = 0.2$, $t = 0.1$.

Fig. 6.10 : Variation of ϕ on v when $E_1 = E_2 = 0.001$, $\beta_1 = \beta_2 = K_1 = 0.8$, $E_3 = 0.1$,

$T' = 1.0$, $M = m = 2.0$, $x = \epsilon = 0.2$, $t = 0.1$.



6.11



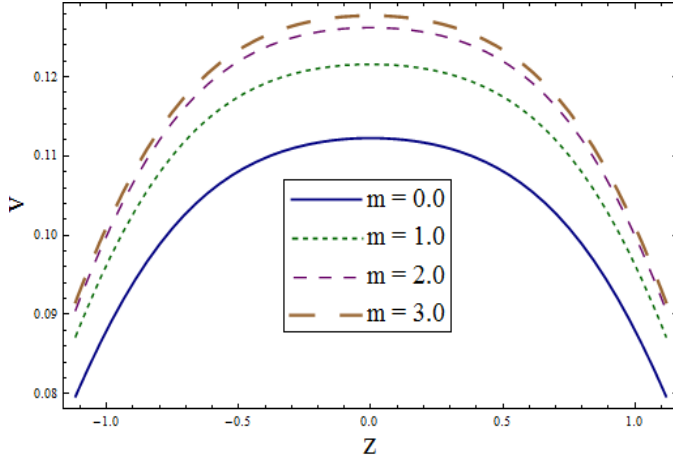
6.12

Fig. 6.11 : Variation of T' on v when $E_1 = E_2 = 0.0001$, $\beta_1 = \beta_2 = K_1 = 0.8$, $E_3 = 0.1$,

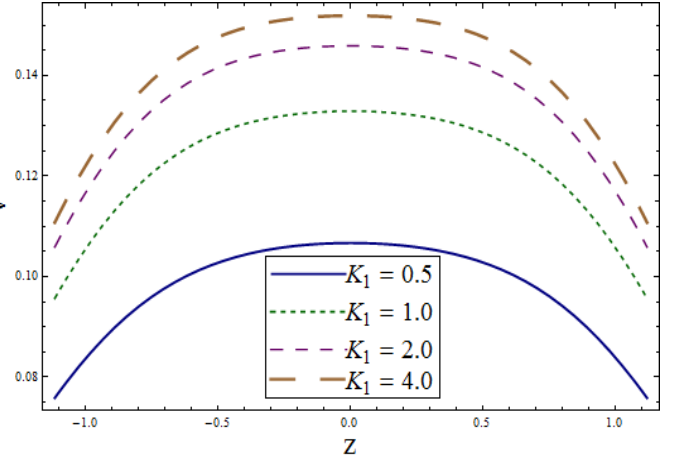
$M = m = 2.0$, $\phi = 0.01$, $x = \epsilon = 0.2$, $t = 0.1$.

Fig. 6.12 : Variation of M on v when $E_1 = E_2 = 0.0001$, $\beta_1 = \beta_2 = K_1 = 0.8$, $E_3 = 0.1$,

$T' = 1.0$, $M = m = 2.0$, $\phi = 0.01$, $x = \epsilon = 0.2$, $t = 0.1$.



6.13



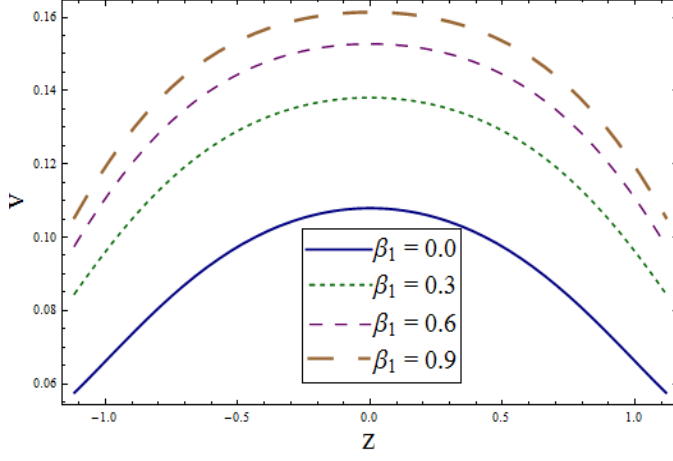
6.14

Fig. 6.13 : Variation of m on v when $E_1 = E_2 = 0.0001$, $\beta_1 = \beta_2 = K_1 = 0.8$, $E_3 = 0.1$,

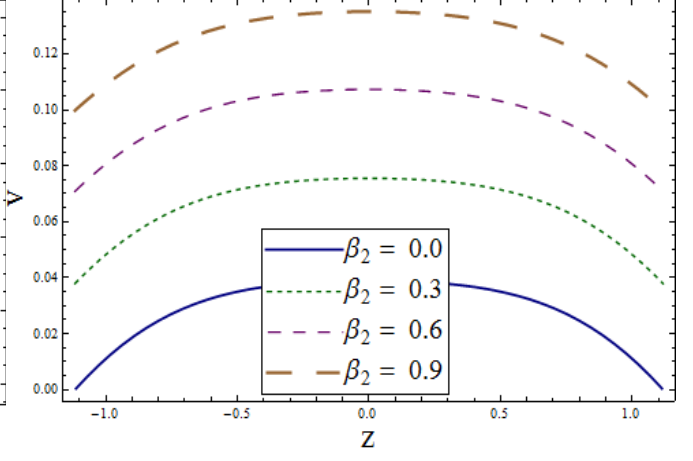
$T' = 1.0$, $M = 2.0$, $\phi = 0.01$, $x = \epsilon = 0.2$, $t = 0.1$.

Fig. 6.14 : Variation of K_1 on v when $E_1 = E_2 = 0.0001$, $\beta_1 = \beta_2 = 0.8$, $E_3 = 0.1$, $T' = 1.0$,

$M = m = 2.0$, $\phi = 0.01$, $x = \epsilon = 0.2$, $t = 0.1$.



6.15



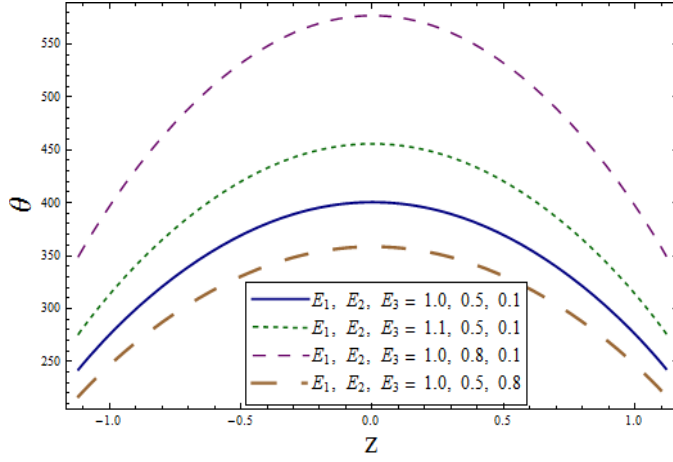
6.16

Fig. 6.15 : Variation of β_1 on v when $E_1 = E_2 = 0.0001$, $\beta_2 = K_1 = 0.8$, $E_3 = 0.1$, $T' = 1.0$,

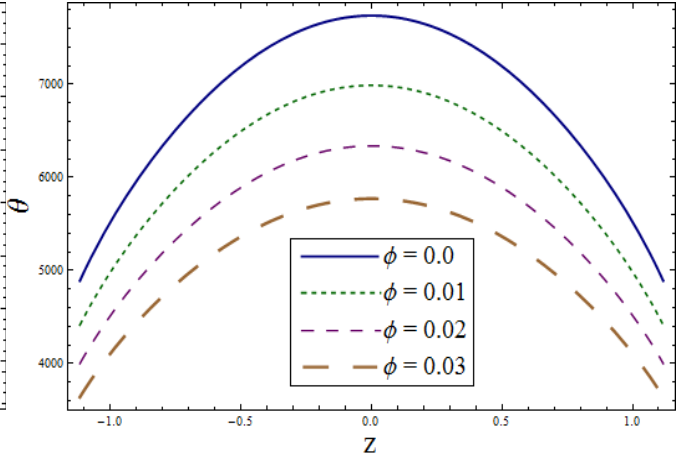
$M = m = 2.0$, $\phi = 0.01$, $x = \epsilon = 0.2$, $t = 0.1$.

Fig. 6.16 : Variation of β_2 on v when $E_1 = E_2 = 0.0001$, $\beta_1 = K_1 = 0.8$, $E_3 = 0.1$, $T' = 1.0$,

$M = m = 2.0$, $\phi = 0.01$, $x = \epsilon = 0.2$, $t = 0.1$.



6.17



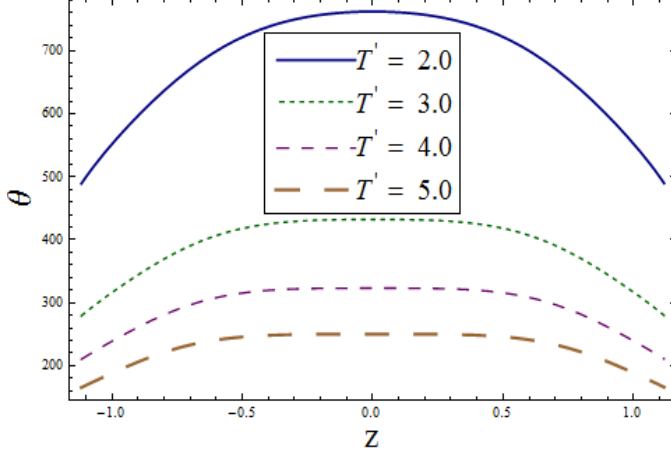
6.18

Fig. 6.17 : Variation of wall properties on θ when $\beta_1 = \beta_2 = \beta_3 = K_1 = 0.8$, $\epsilon_1 = 2.0$,

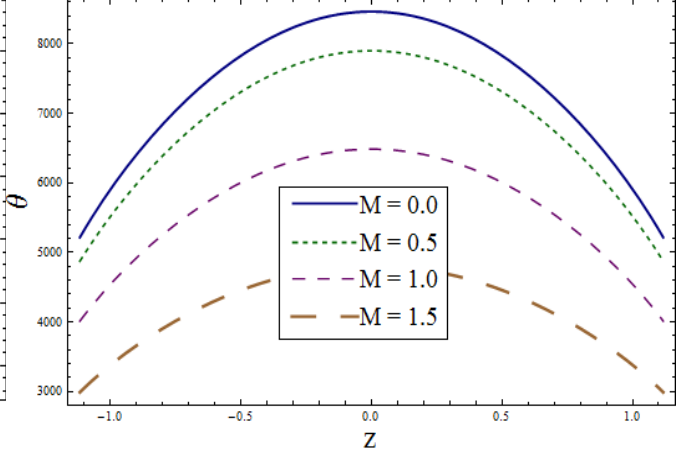
$Br = T' = 1.0$, $M = m = 2.0$, $\phi = 0.01$, $x = \epsilon = 0.2$, $t = 0.1$.

Fig. 6.18 : Variation of ϕ on θ when $E_1 = E_2 = \beta_1 = \beta_2 = \beta_3 = K_1 = 0.8$, $E_3 = 0.5$,

$\epsilon_1 = M = m = 2.0$, $Br = T' = 1.0$, $x = \epsilon = 0.2$, $t = 0.1$.



6.19



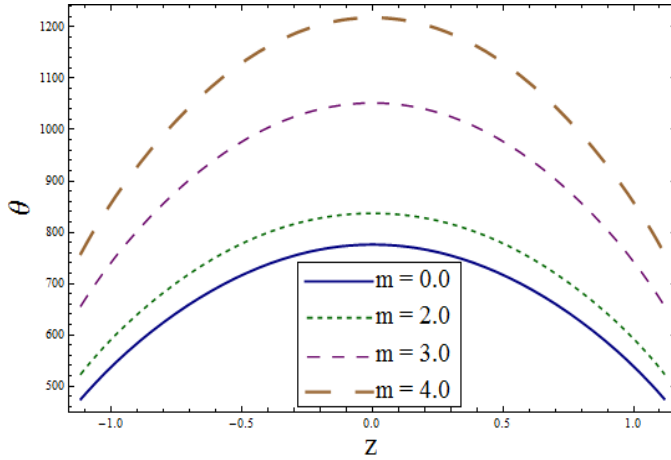
6.20

Fig. 6.19 : Variation of T' on θ when $E_1 = E_2 = \beta_1 = \beta_2 = \beta_3 = K_1 = 0.8$, $E_3 = 0.5$,

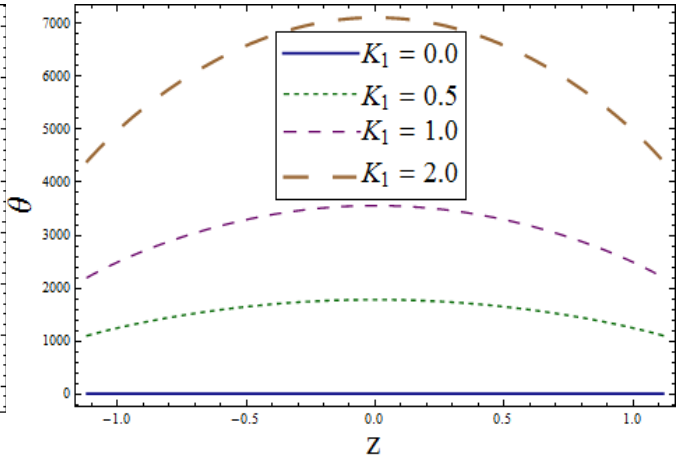
$M = m = \epsilon_1 = 2.0$, $Br = 1.0$, $\phi = 0.01$, $x = \epsilon = 0.2$, $t = 0.1$.

Fig. 6.20 : Variation of M on θ when $E_1 = E_2 = \beta_1 = \beta_2 = \beta_3 = K_1 = 0.8$, $E_3 = 0.5$,

$m = \epsilon_1 = 2.0$, $Br = T' = 1.0$, $\phi = 0.01$, $x = \epsilon = 0.2$, $t = 0.1$.



6.21



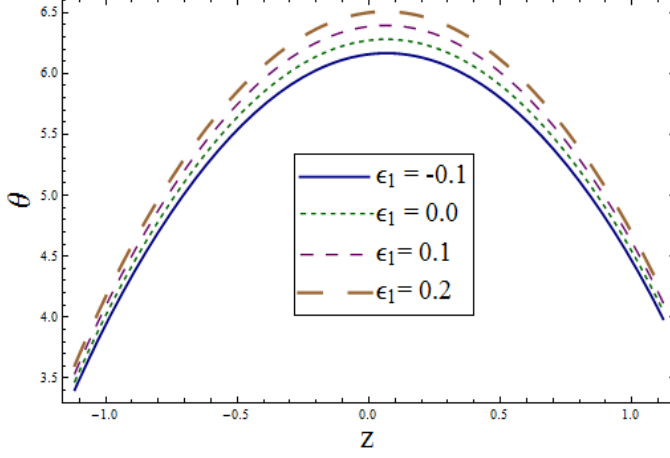
6.22

Fig. 6.21 : Variation of m on θ when $E_1 = E_2 = \beta_1 = \beta_2 = \beta_3 = K_1 = 0.8$, $E_3 = 0.5$,

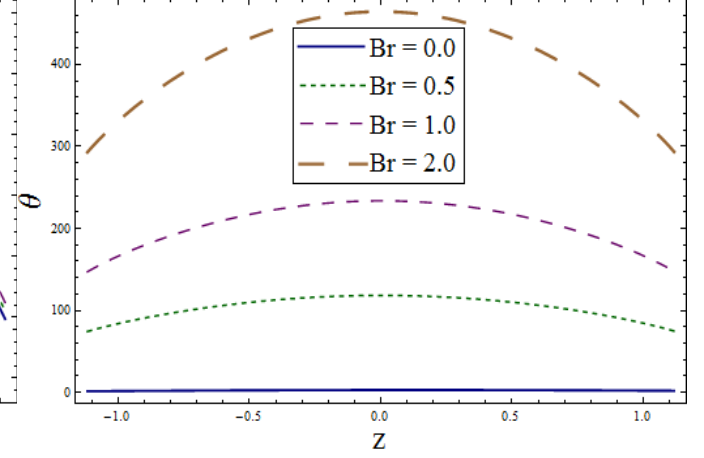
$M = \epsilon_1 = 2.0$, $Br = T' = 1.0$, $\phi = 0.01$, $x = \epsilon = 0.2$, $t = 0.1$.

Fig. 6.22 : Variation of K_1 on θ when $E_1 = E_2 = \beta_1 = \beta_2 = \beta_3 = 0.8$, $E_3 = 0.5$,

$M = m = \epsilon_1 = 2.0$, $Br = T' = 1.0$, $\phi = 0.01$, $x = \epsilon = 0.2$, $t = 0.1$.



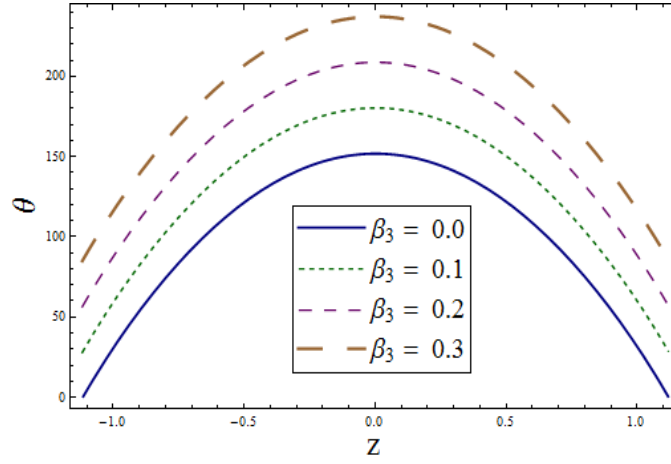
6.23



6.24

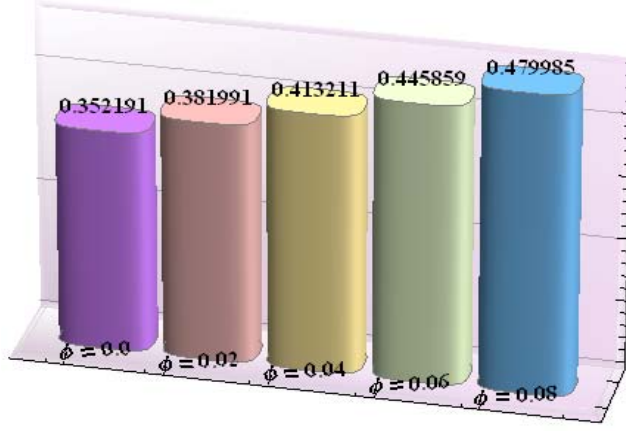
Fig. 6.23 : Variation of ϵ_1 on θ when $E_1 = E_2 = \beta_1 = \beta_2 = \beta_3 = K_1 = 0.8$, $E_3 = 0.5$,
 $M = m = 2.0$, $Br = T' = 1.0$, $\phi = 0.01$, $x = \epsilon = 0.2$, $t = 0.1$.

Fig. 6.24 : Variation of Br on θ when $E_1 = E_2 = \beta_1 = \beta_2 = \beta_3 = K_1 = 0.8$, $E_3 = 0.5$,
 $M = m = \epsilon_1 = 2.0$, $T' = 1.0$, $\phi = 0.01$, $x = \epsilon = 0.2$, $t = 0.1$.

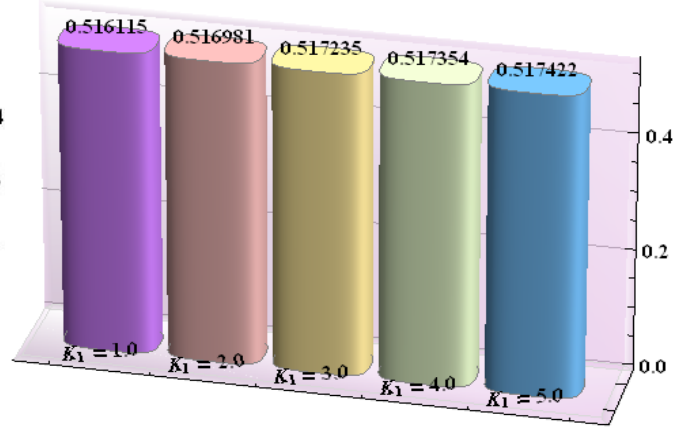


6.25

Fig. 6.25 : Variation of β_3 on θ when $E_1 = E_2 = \beta_1 = \beta_2 = K_1 = 0.8$, $E_3 = 0.5$,
 $M = m = \epsilon_1 = 2.0$, $Br = T' = 1.0$, $\phi = 0.01$, $x = \epsilon = 0.2$, $t = 0.1$.



6.26



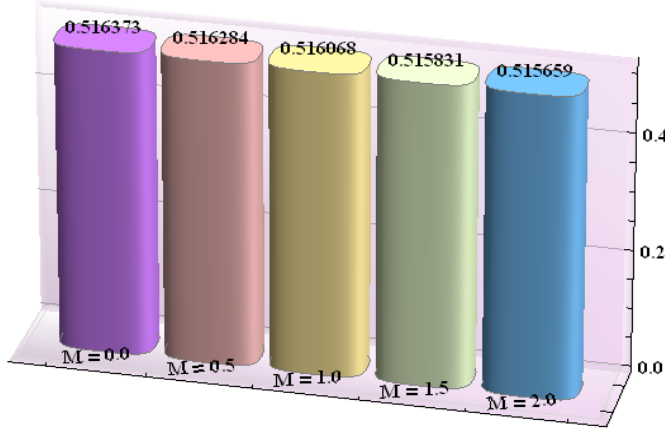
6.27

Fig. 6.26 : Effect of ϕ on heat transfer rate at the wall $(-(\frac{K_{eff}}{K_f})\theta'(\eta))$ when $E_1 = E_2 = 0.01$,

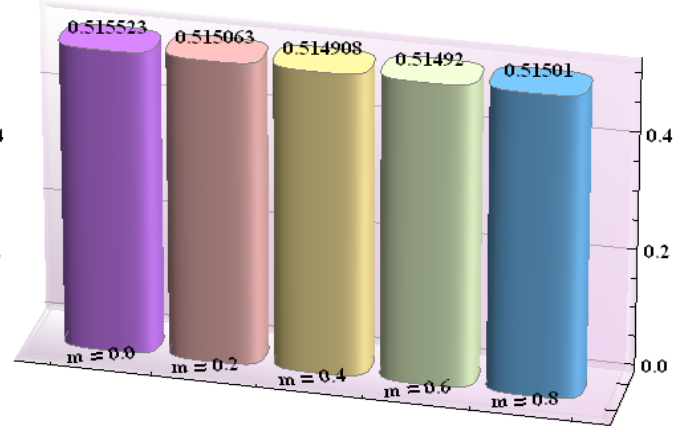
$E_3 = 0.03$, $\beta_1 = \beta_2 = \beta_3 = K_1 = 0.8$, $M = m = \epsilon_1 = Br = T' = 2.0$, $\epsilon = 0.2$, $t = 0.1$.

Fig. 6.27 : Effect of K_1 on heat transfer rate at the wall $(-(\frac{K_{eff}}{K_f})\theta'(\eta))$ when $E_1 = E_2 = 0.01$,

$E_3 = 0.03$, $\beta_1 = \beta_2 = \beta_3 = 0.8$, $M = m = \epsilon_1 = Br = T' = 2.0$, $\phi = 0.01$, $\epsilon = 0.2$, $t = 0.1$.



6.28



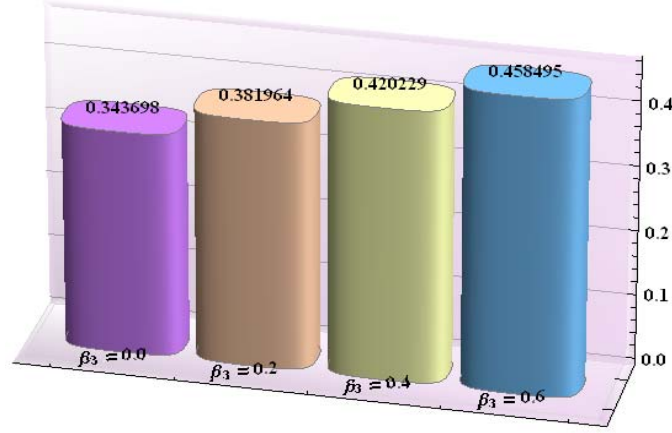
6.29

Fig. 6.28 : Effect of M on heat transfer rate at the wall $(-(\frac{K_{eff}}{K_f})\theta'(\eta))$ when $E_1 = E_2 = 0.01$,

$E_3 = 0.03$, $\beta_1 = \beta_2 = \beta_3 = K_1 = 0.8$, $m = \epsilon_1 = Br = T' = 2.0$, $\phi = 0.01$, $\epsilon = 0.2$, $t = 0.1$.

Fig. 6.29 : Effect of m on heat transfer rate at the wall $(-(\frac{K_{eff}}{K_f})\theta'(\eta))$ when $E_1 = E_2 = 0.01$,

$E_3 = 0.03$, $\beta_1 = \beta_2 = \beta_3 = 0.8$, $M = \epsilon_1 = Br = T' = 2.0$, $\phi = 0.01$, $\epsilon = 0.2$, $t = 0.1$.



6.30

Fig. 6.30 : Effect of β_3 on heat transfer rate at the wall $(-\frac{K_{eff}}{K_f})\theta'(\eta)$ when $E_1 = E_2 = 0.01$, $E_3 = 0.03$, $\beta_1 = \beta_2 = 0.8$, $M = m = \epsilon_1 = Br = T' = 2.0$, $\phi = 0.01$, $\epsilon = 0.2$, $t = 0.1$.

6.5 Conclusions

Peristaltic flow of copper-water nanofluid with Hall effect and heat generation/absorption is analyzed in a rotating frame. Velocity slips and temperature jump are also applied to model the problem. The key findings of present study are listed below.

- Increasing nanoparticles volume fraction ϕ reduces both axial u and secondary v velocities.
- Both axial u and secondary v velocities increase for larger velocity slip parameters.
- No secondary velocity is induced in the absence of rotation.
- Hartman number M and Hall parameter m show similar behavior for velocities (u, v) and temperature θ .
- Temperature is greater in case of heat generation $\epsilon_1 > 0$ than absorption $\epsilon_1 < 0$.
- Higher rate of heat transfer occurs at boundary for larger values of nanoparticle volume fraction ϕ and permeability K_1 .

Chapter 7

Entropy generation analysis for peristaltic flow of nanoparticles in a rotating frame

7.1 Introduction

The present chapter is intended to examine entropy generation on peristaltic flow of nanoparticles in a rotating frame. The flow is subject to an external magnetic field. Viscous dissipation and thermal radiation effects are considered for modeling energy equation. The nonlinearity of resulting problem is simplified by adopting lubrication approach. Exact solutions for streamlines, velocity and temperature are calculated. Effective heat transfer is also studied via graphs. Moreover, the effect of pertinent parameters on entropy generation is also a part of discussion.

7.2 Modeling

The peristaltic flow of nanofluid comprising of nanoparticles (Al_2O_3 and CuO) in a symmetric channel of width $2d$ is studied. Water is used as a base fluid. Both the fluid and nanoparticles are in thermodynamical equilibrium. Thermophysical properties of nanofluid are mentioned in *Table 1*. A magnetic field of strength B_0 acts in transverse direction to flow. Coordinates are selected in such a manner that x-axis is along the flow direction and z-axis is at right angle

to it. The channel is rotating about z-axis with angular velocity Ω . Wall properties make the channel walls flexible. The fluid motion is caused by sinusoidal waves along the channel walls (see sketch in Fig. 1). Therefore, wall geometry can be expressed mathematically as

$$z = \pm\eta(x, t) = \pm \left[d + a \sin \frac{2\pi}{\lambda} (x - ct) \right], \quad (7.1)$$

where a stands for amplitude, λ the wavelength, c wave speed and t the time. Here $+\eta$ and $-\eta$ are the upper and lower position of channel boundaries respectively. Velocity field for the considered flow analysis is taken in the form

$$\mathbf{V} = [u(x, z, t), v(x, z, t), w(x, z, t)].$$

The heat transfer analysis of nanofluid with considered nanoparticles is carried out by taking temperature T_1 and T_0 at the upper and lower walls respectively. Viscous dissipation and radiation effects are also employed in energy equation. The radiative heat flux q_r is defined as:

$$q_r = -\frac{4\sigma^*}{3k^*} \frac{\partial T^4}{\partial z}, \quad (7.2)$$

where σ^* denotes the Stefan-Boltzman constant and k^* the Rosseland mean absorption coefficient. Temperature difference within the flow field is considered small which allows the expansion of T^4 as linear function of T . Hence expanding Taylors series of T^4 about T_m and ignoring higher-order terms we can write q_r as

$$T^4 \cong 4T_m^3 T - 3T_m^4. \quad (7.3)$$

The Maxwell-Garnet model for effective thermal conductivity (K_{eff}) used in the present flow problem is defined as:

$$\frac{K_{eff}}{K_f} = \frac{K_p + 2K_f - 2\phi(K_f - K_p)}{K_p + 2K_f + \phi(K_f - K_p)}. \quad (7.4)$$

The effective density (ρ_{eff}) , effective heat capacity $(\rho C)_{eff}$ and effective electric conductivity (σ_{eff}) of considered nanoparticles for two phase flow model are:

$$\begin{aligned}\rho_{eff} &= (1 - \phi) \rho_f + \phi \rho_p, \quad (\rho C)_{eff} = (1 - \phi) (\rho C)_f + \phi (\rho C)_p, \\ \frac{\sigma_{eff}}{\sigma_f} &= 1 + \frac{3 \left(\frac{\sigma_p}{\sigma_f} - 1 \right) \phi}{\left(\frac{\sigma_p}{\sigma_f} + 2 \right) - \left(\frac{\sigma_p}{\sigma_f} - 1 \right) \phi}.\end{aligned}\tag{7.5}$$

The effective viscosity due Brinkman is mathematically written as

$$\mu_{eff} = \frac{\mu_f}{(1 - \phi)^{2.5}}.\tag{7.6}$$

In the above expressions ρ , C , σ and ϕ define the density, specific heat, electric conductivity and nanoparticle volume fraction, respectively. The subscripts p and f denote the nanoparticle and fluid phases, respectively.

The relevant flow equations are

$$\frac{\partial u}{\partial x} + \frac{\partial w}{\partial z} = 0,\tag{7.7}$$

$$\rho_{eff} \left[\frac{du}{dt} - 2\Omega v \right] = -\frac{\partial \hat{p}}{\partial x} + \mu_{eff} \left(\frac{\partial^2 u}{\partial x^2} + \frac{\partial^2 u}{\partial z^2} \right) - \sigma_{eff} B_0^2 u,\tag{7.8}$$

$$\rho_{eff} \left[\frac{dv}{dt} + 2\Omega v \right] = -\frac{\partial \hat{p}}{\partial y} + \mu_{eff} \left(\frac{\partial^2 v}{\partial x^2} + \frac{\partial^2 v}{\partial z^2} \right) - \sigma_{eff} B_0^2 v,\tag{7.9}$$

$$\rho_{eff} \frac{dw}{dt} = -\frac{\partial \hat{p}}{\partial z} + \mu_{eff} \left(\frac{\partial^2 w}{\partial x^2} + \frac{\partial^2 w}{\partial z^2} \right),\tag{7.10}$$

$$\begin{aligned}(\rho C)_{eff} \frac{dT}{dt} &= K_{eff} \left(\frac{\partial^2 T}{\partial x^2} + \frac{\partial^2 T}{\partial z^2} \right) + \mu_{eff} \left[2 \left\{ \left(\frac{\partial u}{\partial x} \right)^2 + \left(\frac{\partial w}{\partial z} \right)^2 \right\} + \left(\frac{\partial u}{\partial z} + \frac{\partial w}{\partial x} \right)^2 \right] \\ &\quad - \frac{\partial q_r}{\partial z},\end{aligned}\tag{7.11}$$

where modified pressure is defined as:

$$\hat{p} = p - \frac{1}{2} \rho \Omega^2 (x^2 + y^2).$$

The equation of motion for compliant walls can be expressed as

$$L = -\tau' \frac{\partial^2}{\partial x^2} + m' \frac{\partial^2}{\partial t^2} + d' \frac{\partial}{\partial t}. \quad (7.12)$$

Here τ' is the tension, m' the mass and d' defines the viscous damping coefficient. The associated boundary conditions for the problem are

$$u = 0, \quad v = 0 \quad \text{at} \quad z = \pm\eta, \quad (7.13)$$

$$T = \begin{Bmatrix} T_1 \\ T_0 \end{Bmatrix} \quad \text{at} \quad z = \pm\eta. \quad (7.14)$$

The dynamic boundary conditions at the walls is given by

$$\begin{aligned} \frac{\partial L(\eta)}{\partial x} = \frac{\partial p}{\partial x} = \mu_{eff} \left(\frac{\partial^2 u}{\partial x^2} + \frac{\partial^2 u}{\partial z^2} \right) - \sigma_{eff} B_0^2 u \\ - \rho_{eff} \left[\frac{du}{dt} - 2\Omega v \right] \quad \text{at} \quad z = \pm\eta. \end{aligned} \quad (7.15)$$

Table 1:

Numerical values of thermophysical properties of nanoparticles and water.

Phase	$\rho(kg/m^3)$	$K(W/mK)$	$C(J/kgK)$	$\sigma(S/m)$
Water (H ₂ O)	997.1	0.613	4179	0.05
Aluminium oxide (Al ₂ O ₃)	3970	40	765	1×10^{-10}
Copper oxide (CuO)	6320	76.5	531.8	2.7×10^{-8}

Incorporating Eqs. (7.2 – 7.6) into Eqs. (7.7 – 7.11) and (7.13 – 7.15) we get:

$$\frac{\partial u}{\partial x} + \frac{\partial w}{\partial z} = 0, \quad (7.16)$$

$$\begin{aligned} [(1 - \phi) \rho_f + \phi \rho_p] \left[\frac{du}{dt} - 2\Omega v \right] = -\frac{\partial p}{\partial x} + \frac{\mu_f}{(1 - \phi)^{2.5}} \left(\frac{\partial^2 u}{\partial x^2} + \frac{\partial^2 u}{\partial z^2} \right) \\ - \left(1 + \frac{3 \left(\frac{\sigma_p}{\sigma_f} - 1 \right) \phi}{\left(\frac{\sigma_p}{\sigma_f} + 2 \right) - \left(\frac{\sigma_p}{\sigma_f} - 1 \right) \phi} \right) \sigma_f B_0^2 u, \end{aligned} \quad (7.17)$$

$$\begin{aligned}
[(1-\phi)\rho_f + \phi\rho_p] \left[\frac{dv}{dt} + 2\Omega u \right] &= -\frac{\partial p}{\partial y} + \frac{\mu_f}{(1-\phi)^{2.5}} \left(\frac{\partial^2 v}{\partial x^2} + \frac{\partial^2 v}{\partial z^2} \right) \\
&\quad - \left(1 + \frac{3 \left(\frac{\sigma_p}{\sigma_f} - 1 \right) \phi}{\left(\frac{\sigma_p}{\sigma_f} + 2 \right) - \left(\frac{\sigma_p}{\sigma_f} - 1 \right) \phi} \right) \sigma_f B_0^2 v, \tag{7.18}
\end{aligned}$$

$$[(1-\phi)\rho_f + \phi\rho_p] \frac{dw}{dt} = -\frac{\partial p}{\partial z} + \frac{\mu_f}{(1-\phi)^{2.5}} \left(\frac{\partial^2 w}{\partial x^2} + \frac{\partial^2 w}{\partial z^2} \right), \tag{7.19}$$

$$\begin{aligned}
[(1-\phi)\rho_f + \phi\rho_p] \frac{dT}{dt} &= K_f \left(\frac{K_p + 2K_f - 2\phi(K_f - K_p)}{K_p + 2K_f + \phi(K_f - K_p)} \right) \left(\frac{\partial^2 T}{\partial x^2} + \frac{\partial^2 T}{\partial z^2} \right) \\
&\quad + \frac{16\sigma^* T_m^3}{3k^*} \frac{\partial^2 T}{\partial z^2} + \frac{\mu_f}{(1-\phi)^{2.5}} \left[2 \left\{ \left(\frac{\partial u}{\partial x} \right)^2 + \left(\frac{\partial w}{\partial z} \right)^2 \right\} \right. \\
&\quad \left. + \left(\frac{\partial u}{\partial z} + \frac{\partial w}{\partial x} \right)^2 \right] \tag{7.20}
\end{aligned}$$

The boundary conditions become

$$u = 0, \quad v = 0 \quad \text{at} \quad z = \pm\eta, \tag{7.21}$$

$$\begin{aligned}
\frac{\partial L(\eta)}{\partial x} = \frac{\partial p}{\partial x} &= \frac{\mu_f}{(1-\phi)^{2.5}} \left(\frac{\partial^2 u}{\partial x^2} + \frac{\partial^2 u}{\partial z^2} \right) - \left(1 + \frac{3 \left(\frac{\sigma_p}{\sigma_f} - 1 \right) \phi}{\left(\frac{\sigma_p}{\sigma_f} + 2 \right) - \left(\frac{\sigma_p}{\sigma_f} - 1 \right) \phi} \right) \sigma_f B_0^2 u \\
&\quad - ((1-\phi)\rho_f + \phi\rho_p) \left[\frac{du}{dt} - 2\Omega v \right] \quad \text{at} \quad z = \pm\eta, \tag{7.22}
\end{aligned}$$

$$T = \left\{ \begin{matrix} T_1 \\ T_0 \end{matrix} \right\} \quad \text{at} \quad z = \pm\eta, \tag{7.23}$$

$$\begin{aligned}
x^* &= \frac{x}{\lambda}, \quad y^* = \frac{y}{\lambda}, \quad z^* = \frac{z}{d}, \quad p^* = \frac{d^2 p}{c\mu_f \lambda}, \quad t^* = \frac{ct}{\lambda}, \quad u^* = \frac{u}{c}, \\
v^* &= \frac{v}{c}, \quad w^* = \frac{w}{c}, \quad \eta^* = \frac{\eta}{d}, \quad \theta = \frac{T - T_0}{T_1 - T_0}, \quad \text{Re} = \frac{\rho_f c d}{\mu_f}, \\
\delta &= \frac{d}{\lambda}, \quad T' = \frac{\text{Re} \Omega d}{c}, \quad M^2 = B_0^2 d^2 \frac{\sigma_f}{\mu_f}, \quad \text{Pr} = \frac{\mu_f C_f}{\kappa_f}, \\
Ec &= \frac{c^2}{C_f (T_1 - T_0)}, \quad Br = \text{Pr} Ec, \quad Rd = \frac{16\sigma^* T_m^3}{3k^* k_f}, \quad E_1 = \frac{-\tau' d^3}{\lambda^3 \mu c}, \\
E_2 &= \frac{m_1 c d^3}{\lambda^3 \mu}, \quad E_3 = \frac{d' d^3}{\lambda^2 \mu}, \quad u = \frac{\partial \psi}{\partial z}, \quad w = -\delta \frac{\partial \psi}{\partial x}. \tag{7.24}
\end{aligned}$$

Using the above mentioned set of non-dimensional variables and parameters one obtains

$$\begin{aligned} \text{Re } \delta A_3 \left[\frac{\partial^2 \psi}{\partial z \partial t} + \frac{\partial \psi}{\partial z} \frac{\partial^2 \psi}{\partial x \partial z} - \frac{\partial \psi}{\partial x} \frac{\partial^2 \psi}{\partial z^2} \right] - 2T' A_3 v &= -\frac{\partial p}{\partial x} + A_2 \left[\delta^2 \frac{\partial^3 \psi}{\partial x^2 \partial z} + \frac{\partial^3 \psi}{\partial z^3} \right] \\ &\quad - A_1 M^2 \frac{\partial \psi}{\partial z}, \end{aligned} \quad (7.25)$$

$$\begin{aligned} \text{Re } \delta A_3 \left[\frac{\partial v}{\partial t} + \frac{\partial \psi}{\partial z} \frac{\partial v}{\partial x} - \frac{\partial \psi}{\partial x} \frac{\partial v}{\partial z} \right] + 2T' A_3 \frac{\partial \psi}{\partial z} &= -\frac{\partial p}{\partial y} + A_2 \left[\delta^2 \frac{\partial^2 v}{\partial x^2} + \frac{\partial^2 v}{\partial z^2} \right] \\ &\quad - A_1 M^2 v, \end{aligned} \quad (7.26)$$

$$-\text{Re } \delta^2 A_3 \left[\frac{\partial^2 \psi}{\partial z \partial t} + \frac{\partial \psi}{\partial z} \frac{\partial^2 \psi}{\partial x^2} - \frac{\partial \psi}{\partial x} \frac{\partial^2 \psi}{\partial z^2} \right] = -\frac{\partial p}{\partial z} + A_2 \left(\delta^3 \frac{\partial^3 \psi}{\partial x^3} - \delta \frac{\partial^3 \psi}{\partial x \partial z^2} \right), \quad (7.27)$$

$$\begin{aligned} \delta \text{Pr Re } A_3 \left[\frac{\partial \theta}{\partial t} + \frac{\partial \psi}{\partial z} \frac{\partial \theta}{\partial x} + v \frac{\partial \theta}{\partial y} - \frac{\partial \psi}{\partial x} \frac{\partial \theta}{\partial z} \right] &= A_4 \left[\delta^2 \frac{\partial^2 \theta}{\partial x^2} + \frac{\partial^2 \theta}{\partial z^2} \right] + Rd \frac{\partial^2 \theta}{\partial z^2} + Br A_2 \\ &\quad \times \left(4\delta^2 \left(\frac{\partial^2 \psi}{\partial x \partial z} \right)^2 + 2 \left(\frac{\partial^2 \psi}{\partial z^2} - \delta^2 \frac{\partial^2 \psi}{\partial x^2} \right)^2 \right). \end{aligned} \quad (7.28)$$

Here Re , δ , T' , M , Pr , Rd , Br and ψ are the Reynolds number, the dimensionless wave number, the Taylors number, the Hartman number, the Prandtl number, the radiation parameter, the Brinkman number and the stream function, respectively. The A_i s ($i = 1 - 4$) are defined below:

$$\begin{aligned} A_1 &= \left(1 + \frac{3 \left(\frac{\sigma_p}{\sigma_f} - 1 \right) \phi}{\left(\frac{\sigma_p}{\sigma_f} + 2 \right) - \left(\frac{\sigma_p}{\sigma_f} - 1 \right) \phi} \right), \\ A_2 &= \frac{1}{(1 - \phi)^{2.5}}, \\ A_3 &= \left[(1 - \phi) + \phi \frac{\rho_p}{\rho_f} \right], \\ A_4 &= \frac{K_p + 2K_f - 2\phi(K_f - K_p)}{K_p + 2K_f + \phi(K_f - K_p)}, \\ A_5 &= A_4 + R, \end{aligned} \quad (7.29)$$

Invoking long wavelength and low Reynolds number analysis, Eqs. (7.25 – 7.28) give

$$-2T' A_3 v = -\frac{\partial p}{\partial x} + A_2 \left[\delta^2 \frac{\partial^3 \psi}{\partial x^2 \partial z} + \frac{\partial^3 \psi}{\partial z^3} \right] - A_1 M^2 \frac{\partial \psi}{\partial z}, \quad (7.30)$$

$$2T' A_3 \frac{\partial \psi}{\partial z} = -\frac{\partial p}{\partial y} + A_2 \left[\delta^2 \frac{\partial^2 v}{\partial x^2} + \frac{\partial^2 v}{\partial z^2} \right] - A_1 M^2 v, \quad (7.31)$$

$$\frac{\partial p}{\partial z} = 0, \quad (7.32)$$

$$(A_4 + Rd) \frac{\partial^2 \theta}{\partial z^2} + 2BrA_2 \left(\frac{\partial^2 \psi}{\partial z^2} \right)^2 = 0. \quad (7.33)$$

It is evident from Eq. (7.32) that pressure does not depend on z . Moreover, the pressure term in Eq. (7.31) can be neglected due to the fact that pressure gradient is not generating the secondary flow. Eliminating pressure from Eqs. (7.30) and (7.31), we obtain

$$A_2 \frac{\partial^4 \psi}{\partial z^4} - A_1 M^2 \frac{\partial^2 \psi}{\partial z^2} + 2T' A_3 \frac{\partial v}{\partial z} = 0. \quad (7.34)$$

Dimensionless form of boundary conditions are

$$\frac{\partial \psi}{\partial z} = 0, \quad v = 0 \quad \text{at} \quad z = \pm \eta, \quad (7.35)$$

$$\left[E_1 \frac{\partial^3}{\partial x^3} + E_2 \frac{\partial^3}{\partial x \partial t^2} + E_3 \frac{\partial^2}{\partial x \partial t} \right] \eta = A_2 \frac{\partial^3 \psi}{\partial z^3} - A_1 M^2 \frac{\partial \psi}{\partial z} + 2T' A_3 v \quad \text{at} \quad z = \pm \eta, \quad (7.36)$$

$$\begin{aligned} \theta &= 1 & \text{at} & \quad z = +\eta, \\ \theta &= 0 & \text{at} & \quad z = -\eta. \end{aligned} \quad (7.37)$$

7.2.1 Entropy generation and viscous dissipation

The volumetric entropy generation of nanofluid in dimensional form is given as [176 – 178] :

$$S''_{gen} = \frac{K_{eff}}{\theta_0^2} \left[\left\{ \left(\frac{\partial T}{\partial x} \right)^2 + \left(\frac{\partial T}{\partial z} \right)^2 \right\} + \frac{16\sigma^* T_m^3}{3k^*} \left(\frac{\partial T}{\partial z} \right)^2 \right] + \frac{\Delta}{\theta_0}, \quad (7.38)$$

The viscous dissipation term Δ in above Eq. is

$$\Delta = \frac{\mu_f}{(1 - \phi)^{2.5}} \left[2 \left\{ \left(\frac{\partial u}{\partial x} \right)^2 + \left(\frac{\partial w}{\partial z} \right)^2 \right\} + \left(\frac{\partial u}{\partial z} + \frac{\partial w}{\partial x} \right)^2 \right]. \quad (7.39)$$

Dimensionless form of entropy generation becomes:

$$N_S = \frac{S''_{gen}}{S''_G} = A_4 (1 + Rd) \left(\frac{\partial \theta}{\partial z} \right)^2 + 2Br\Lambda A_2 \left(\frac{\partial^2 \psi}{\partial z^2} \right)^2. \quad (7.40)$$

In above expression S_G'' and Λ show the entropy generation characteristic and temperature difference parameter defined by

$$S_G'' = \frac{K_f(T_1 - T_0)^2}{\theta_0^2 d^2}, \quad \Lambda = \frac{\theta_0}{(T_1 - T_0)}.$$

Entropy generation defined above comprises of two effects: (a) conduction effect (also known as heat transfer irreversibility) (HTI) and (b) fluid friction irreversibility (FFI). Now we define Bejan number by [175] :

$$Be = \frac{HTI}{HTI + FFI}. \quad (7.41)$$

It is worth mentioning here that the range of Bejan number varies from 0 to 1. For $Be = 0$ the irreversibility is dominated by fluid friction effects whereas $Be = 1$ defines the limit where irreversibility dominates due to heat transfer. The contribution of both heat transfer and fluid friction to entropy generation are equal when $Be = 1/2$.

7.2.2 Solutions

The expressions for stream function, velocity and temperature are obtained in the forms:

$$\psi = B_0 z + B_1 \sinh\left[\sqrt{\frac{\alpha}{A_2}} z\right] + B_2 \sinh\left[\sqrt{\frac{\beta}{A_2}} z\right], \quad (7.42)$$

$$v = F_0 + F_1 \cosh\left[\sqrt{\frac{\alpha}{A_2}} z\right] + F_2 \cosh\left[\sqrt{\frac{\beta}{A_2}} z\right], \quad (7.43)$$

$$\begin{aligned} \theta = & B_3 z + B_4 z^2 + B_5 \cosh\left[2\sqrt{\frac{\alpha}{A_2}} z\right] + B_6 \cosh\left[\frac{(\sqrt{\alpha} - \sqrt{\beta})}{\sqrt{A_2}} z\right] \\ & + B_7 \cosh\left[\frac{(\sqrt{\alpha} + \sqrt{\beta})}{\sqrt{A_2}} z\right] + B_8 \cosh\left[2\sqrt{\frac{\beta}{A_2}} z\right] + B_9, \end{aligned} \quad (7.44)$$

in which

$$\begin{aligned} \alpha' &= A_1 M^2 - 2i A_3 T', \quad \beta' = A_1 M^2 + 2i A_3 T', \\ \zeta &= -i A M^2 + 2 A_3 T', \quad \gamma' = i A M^2 + 2 A_3 T', \end{aligned}$$

$$\begin{aligned}
B_0 &= -\frac{A_1 L_0 M^2}{\alpha \beta}, \quad B_1 = \frac{\sqrt{A_2} L_0 \sec h \left[\sqrt{\frac{\alpha'}{A_2}} \eta \right]}{2\alpha^{3/2}}, \quad B_2 = \frac{\sqrt{A_2} L_0 \sec h \left[\sqrt{\frac{\beta'}{A_2}} \eta \right]}{2\beta'^{3/2}}, \\
B_3 &= \frac{1}{2\eta}, \quad B_4 = \frac{Br(B_1^2 \alpha^2 + B_2^2 \beta^2)}{2A_2 A_5}, \quad B_5 = -\frac{Br B_1^2 \alpha}{4A_5}, \\
B_6 &= \frac{2B_1 B_2 Br \alpha (\sqrt{\alpha} + \sqrt{\beta})^2 \beta}{A_5 (\alpha - \beta)^2}, \quad B_7 = -\frac{2B_1 B_2 Br \alpha (\sqrt{\alpha} - \sqrt{\beta})^2 \beta}{A_5 (\alpha - \beta)^2}, \quad B_8 = -\frac{B_2^2 Br \beta}{4A_5}, \\
B_9 &= \frac{1}{4A_5} \left(2A_5 - \frac{(2Br(B_1^2 \alpha^2 + B_2^2 \beta^2) \eta^2)}{A_2} + B_1^2 Br \alpha \cosh \left[\frac{2\sqrt{\alpha}}{\sqrt{A_2}} \eta \right] \right. \\
&\quad - \frac{32B_1 B_2 Br \alpha^{3/2} \beta^{3/2} \cosh \left[\frac{\sqrt{\alpha}}{\sqrt{A_2}} \eta \right] \cosh \left[\frac{\sqrt{\beta}}{\sqrt{A_2}} \eta \right]}{(\alpha - \beta)^2} + B_2^2 Br \beta \cosh \left[\frac{2\sqrt{\beta}}{\sqrt{A_2}} \eta \right] \\
&\quad \left. + \frac{16B_1 B_2 Br \alpha \beta (\alpha + \beta) \sinh \left[\frac{\sqrt{\alpha}}{\sqrt{A_2}} \eta \right] \sinh \left[\frac{\sqrt{\beta}}{\sqrt{A_2}} \eta \right]}{(\alpha - \beta)^2} \right), \\
F_0 &= \frac{2A_3 L_0 T}{\alpha \beta}, \quad F_1 = -\frac{L_0 \zeta \sec h \left[\frac{\sqrt{\alpha}}{\sqrt{A_2}} \eta \right]}{2\alpha \beta}, \quad F_2 = -\frac{L_0 \gamma' \sec h \left[\frac{\sqrt{\alpha}}{\sqrt{A_2}} \eta \right]}{2\alpha \beta}.
\end{aligned}$$

The numerical values of effective heat transfer $\left(-\frac{K_{eff}}{K_f} \frac{\partial \theta}{\partial z} \right)$ at the walls can be evaluated by using built in NDSolve command of MATHEMATICA. Also the constants $B_i s (i = 1 - 9)$ and $F_i s (i = 1 - 2)$ can also be calculated through MATHEMATICA.

7.3 Discussion

The behaviors of obtained solutions for various values of wall parameters (E_1, E_2, E_3) , Taylors number (T') , Hartman number (M) , volume fraction (ϕ) , radiation parameter (Rd) , Eckert number (Ec) and Brinkman group parameter $(Br\Lambda)$ are discussed through Figs (7.1 – 7.28).

7.3.1 Axial velocity

Here we studied effects of pertinent parameters on axial velocity by plotting Figs. (7.1 – 7.4). The influence of Hartman number M on u is illustrated through Fig. (7.1). It is noticed that velocity decreases as we make increment for M . This is due to the increased strength of magnetic field that shows damping in velocity as magnetic field is resistive in nature. Fig. (7.2) shows the effect of Taylors number T' on u . It is clearly noticed that velocity in axial direction decreases as we increase the rotation. Here rotation causes fluid to flow in secondary direction.

It is revealed by Fig. (7.3) that increasing volume fraction ϕ causes decrease in axial velocity u . Larger nanoparticles volume fraction results an increase in effective viscosity of nanofluid which consequently reduces the ability of fluid to move freely and hence the velocity decays. Large values of wall elastance parameters (E_1 and E_2) enhance the velocity whereas wall damping parameter E_3 reduces the velocity (see Fig. 7.4). The fact behind this behavior is that the elastance of wall creates less obstruction for fluid flow causing an increase in velocity. On the contrary, damping, resistive nature force, causes hindrance for fluid to flow and so the velocity decays. It is observed that magnitude of velocity for Al_2O_3 nanoparticles is greater than that of CuO .

7.3.2 Secondary velocity

The angular velocity Ω induces a velocity component in y -direction i.e. termed as secondary velocity (v). The present subsection deals with the effect of different parameters on v . Fig. (7.5) implies that an increase in the strength of magnetic field makes fluid to move slowly and so decrease in velocity is noticed. Fig. (7.6) depicts that an increase in rotation of the channel draws more fluid in y -direction which in turn increases the velocity. Moreover it can be noticed from the Fig. that there is no secondary velocity in the absence of rotation ($T' = 0$). Fig. (7.7) is prepared to study the behavior of nanoparticle volume ϕ fraction on v . Decrease in v is noticed due to increased resistivity offered by nanoparticles. When analyzing the effect of wall parameters we observed opposite behavior of v to that of u (axial velocity). Increasing wall elastance (E_1, E_2) decreases the secondary velocity whereas damping parameter E_3 enhances the velocity (see Fig. 7.8). The graphical results show that magnitude of secondary velocity is higher for CuO nanoparticles when compared with Al_2O_3 nanoparticles.

7.3.3 Heat transfer analysis

This subsection aims to study the behavior of sundry parameters while dealing with temperature profile θ . Figs. (7.9 – 7.14) have been displayed for such purpose. Impact of Hartman number M on θ is studied through Fig. (7.9). The Fig. elucidates that temperature decreases as the magnetic field strength enhances. This behavior can be linked to the velocity. Since temperature θ is defined as the average kinetic energy of molecules and velocity is decreasing

function for M . Therefore, temperature also reduces. Fig. (7.10) reveals the behavior of Taylors number T' on θ . It can be seen through Fig. that temperature decreases as the value of T' is increased. Fast rotation causes the fluid to move with greater speed. The nanofluid transfers heat more rapidly. Therefore temperature reduces for greater T' . Fig. (7.11) depicts the effect of nanoparticle volume fraction ϕ on θ . It is noticed from the Fig. that temperature decreases as we enhance nanoparticle volume fraction. The nanoparticles (Al_2O_3, CuO) addition enhance the effective thermal conductivity of nanofluid. This results in rapid heat transfer from fluid to ambient and hence temperature decays. It can be visualized from Fig. (7.12) that when the value of wall rigidity parameter (E_1) is increased θ decreases. Similar behavior is shown by wall tension parameter (E_2). It is then further noticed that an enhancement of mass characterizing parameter (E_3) decreases the temperature of fluid. It can be examined through Fig. (7.13) that temperature decays when radiation parameter R attains higher values. Decrease in temperature is by rotation. The viscosity of fluid is responsible for the conversion of kinetic energy to heat energy. This heat generation due to viscous dissipation effect enhances temperature. Eckert number Ec is responsible for this behavior (see Fig. (7.14)). It is observed from these Figs. that temperature is greater in magnitude for Al_2O_3 nanoparticles in comparison to CuO .

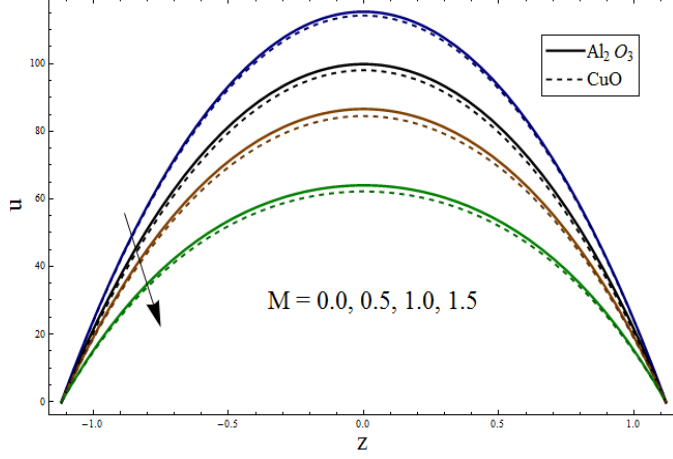
The effective thermal conductivity of nanofluid at the walls $\left(-\frac{K_{eff}}{K_f}\theta'[\eta]\right)$ is studied through Figs. (7.15 – 7.18). Fig. (7.15) is plotted to study the influence of Hartman number M on heat transfer rate. The influence of nanoparticle volume fraction ϕ on heat transfer rate is elucidated in Fig. (7.16). It is clear from this Fig. that the rate increases when nanoparticle volume fraction is increased for both particles. Moreover, it is observed from the results that heat transfer rate of nanofluid is higher than that of water (*i.e. when $\phi = 0$*). Impact of Taylor number T' on heat transfer rate is sketched in Fig. (7.17). Greater rotation enhances the velocity which in turn increases heat transfer rate for both nanoparticles. Fig. (7.18) is prepared to study the impact of radiation parameter R on rate of heat transfer. It is interpreted from the Fig. that heat transfer increases as we make increment in the value of R . It is noticed from the Figs. that heat transfer rate increases for both nanoparticles *i.e. Al_2O_3 and CuO* but it is greater for CuO (represented by back row). It is inferred from the results that ability to transfer heat rapidly makes the CuO more effective in practical applications.

7.3.4 Entropy generation analysis

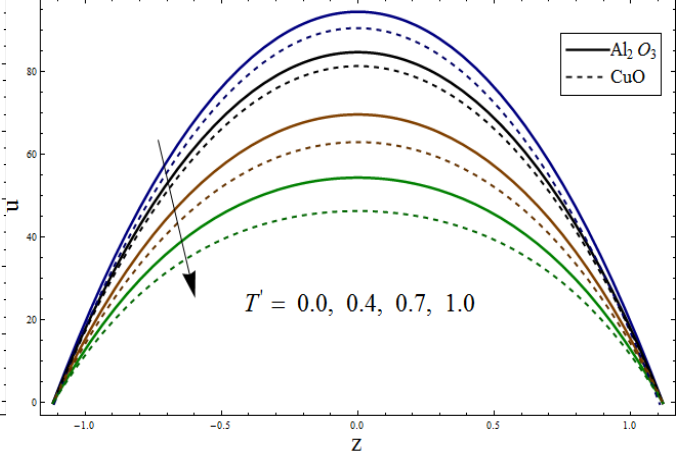
Entropy (N_S) in the fluid is induced due to thermal diffusion and viscosity. Therefore it is essential to study irreversibility or entropy generation in the system to determine its efficiency. To study the behavior of different parameters on N_S Figs. (7.19 – 7.24) are plotted. Increase in the strength of magnetic field obstructs the fluid velocity which in turn reduces the shear in flow resulting in decreased temperature (see Fig. 7.19). Since entropy is directly related with temperature, therefore, it also decreases. Fig. (7.20) portrays the effect of Taylors number on N_S . When the channel is rotated at higher speed, velocity of fluid also increases. This results in rapid heat transfer as expected. Thus heat produced due to shearing forces transfer at increased rate. It causes entropy to decrease. It is evident from Fig. (7.21) that an increase in nanoparticle volume fraction ϕ reduces entropy generation. Blending of nanoparticles in base fluid enhances efficient heat transfer which particularly produces the smoother temperature distribution. Hence it leads to decrease in entropy generation. Fig. (7.22) depicts effect of wall parameters on N_S . It is revealed from the Fig. that with the increase of E_1 and E_2 the entropy generation N_S increases but it shows decrease for higher values of E_3 . Fig. (7.23) shows the variation in entropy generation due to radiation parameter R . It is observed from the Fig. that N_S increases when we enhance the value of R . The Brinkman parameter $Br\Lambda$ studies the viscous effects and it is also related to nanofluid viscosity term mentioned in Eq. (40). The Brinkman parameter $Br\Lambda$ directly effects the square of velocity. Therefore an increase in $Br\Lambda$ enhances the flow which results in increased entropy (Fig. 7.24). The value of entropy generation is higher for Al_2O_3 than CuO .

Figs. (7.25 – 7.29) demonstrate the influence of various thermophysical parameters on Bejan number Be . We have observed that heat transfer irreversibility dominates the flow in central region of the channel with Be very close to 1 whereas fluid friction irreversibility near the channel walls is small. Fig. (7.25) reveals that an increase in nanofluid volume fraction ϕ increases Bejan number Be . It is depicted through Fig. (7.26) that the value of Bejan number enhances as rotation parameter T' increases. It is noticed from the Figs. (7.27) and (7.28) that Bejan number shows similar behavior for both radiation parameter R and Hartman number M . To study the influence of Brinkman group $Br\Lambda$ parameter, Fig. (7.29) is drawn. This Fig. depicts that increasing group parameter decreases Be and it enhances the influence of

fluid friction irreversibility. It is worth mentioning here that an increase in the value of Be for increasing values of involved parameters enhances the heat transfer irreversibility in comparison to total irreversibility due to heat transfer and fluid friction.



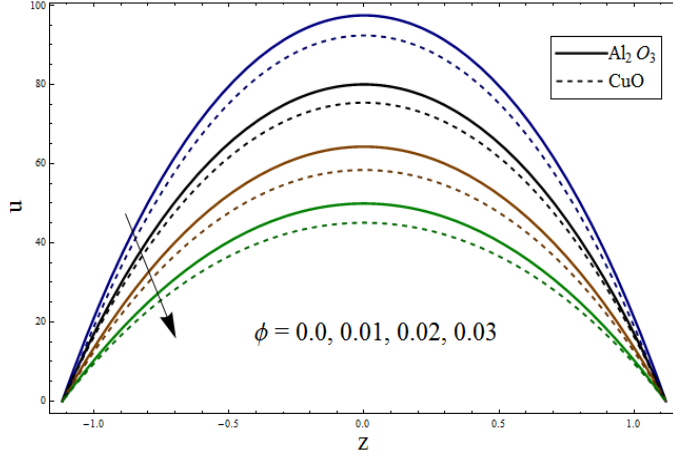
7.1



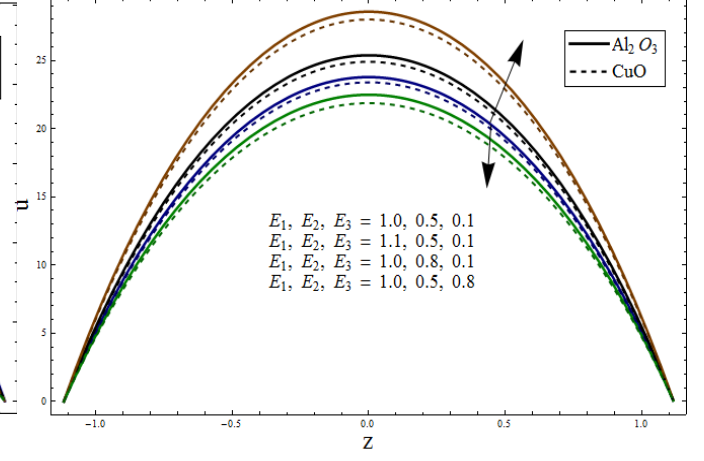
7.2

Fig. 7.1 : Variation of M on u when $E_1 = E_2 = 3.0$, $E_3 = 0.1$, $T' = 0.5$, $\phi = 0.01$, $x = \epsilon = 0.2$, $t = 0.1$.

Fig. 7.2 : Variation of T' on u when $E_1 = E_2 = 3.0$, $E_3 = 0.1$, $M = 0.8$, $\phi = 0.01$, $x = \epsilon = 0.2$, $t = 0.1$.



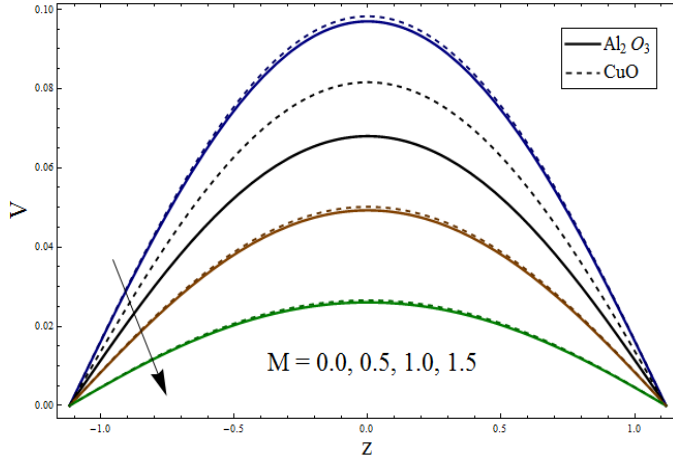
7.3



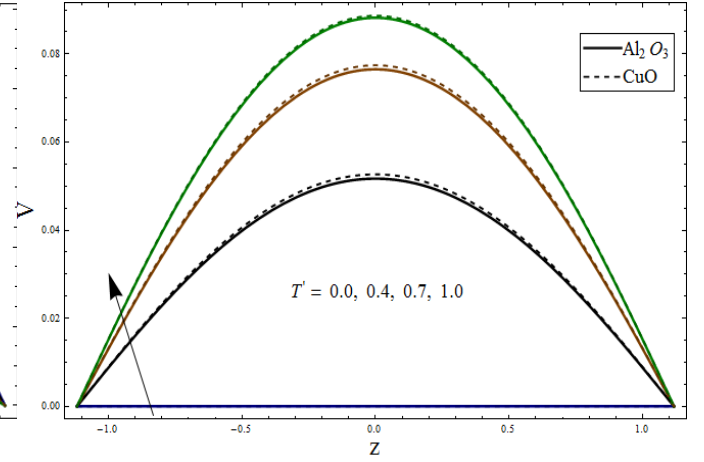
7.4

Fig. 7.3 : Variation of ϕ on u when $E_1 = E_2 = 3.0$, $E_3 = 0.1$, $M = 0.8$, $T' = 0.5$, $x = \epsilon = 0.2$, $t = 0.1$.

Fig. 7.4 : Variation of wall properties on u when $T' = 0.5$, $M = 0.8$, $\phi = 0.01$, $x = \epsilon = 0.2$, $t = 0.1$.



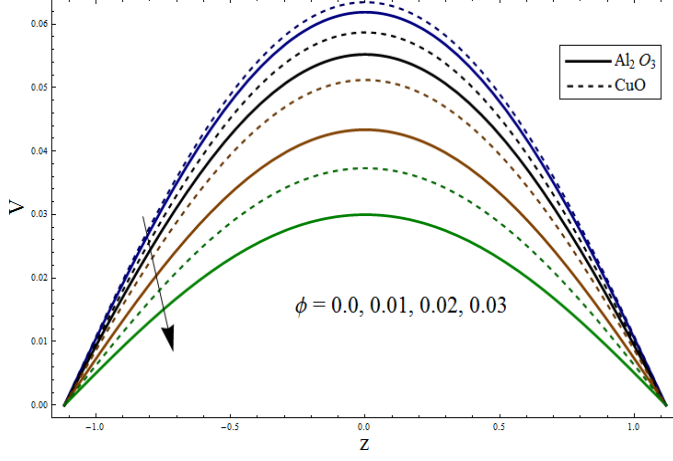
7.5



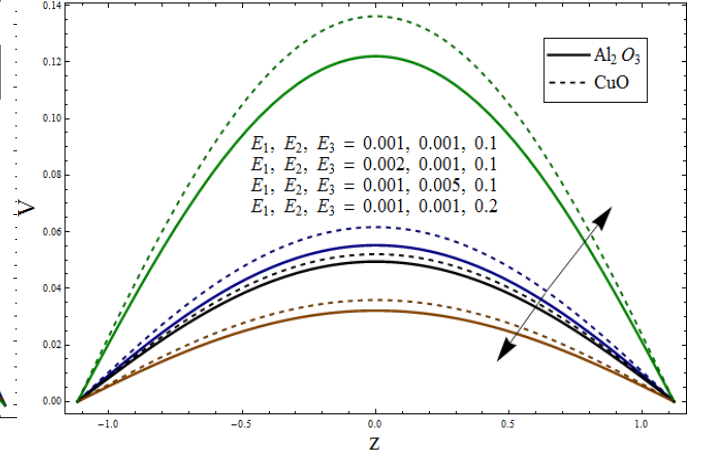
7.6

Fig. 7.5 : Variation of M on v when $E_1 = E_2 = 0.001$, $E_3 = 0.1$, $T' = 0.5$, $\phi = 0.01$, $x = \epsilon = 0.2$, $t = 0.1$.

Fig. 7.6 : Variation of T' on v when $E_1 = E_2 = 0.001$, $E_3 = 0.1$, $M = 0.8$, $\phi = 0.01$, $x = \epsilon = 0.2$, $t = 0.1$.



7.7



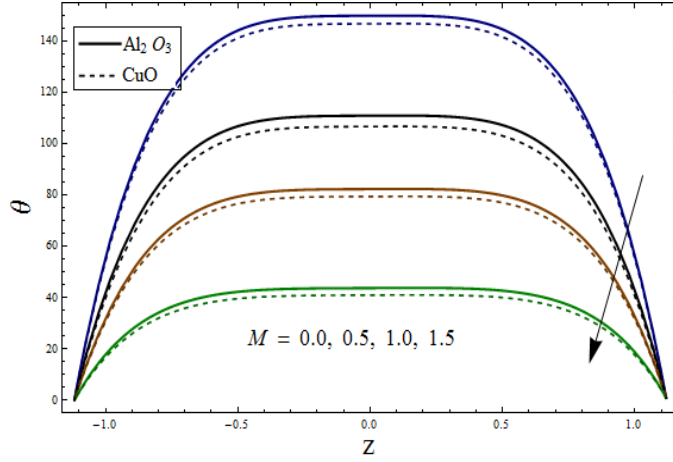
7.8

Fig. 7.7 : Variation of ϕ on v when $E_1 = E_2 = 0.001$, $E_3 = 0.1$, $M = 0.8$, $T' = 0.5$,

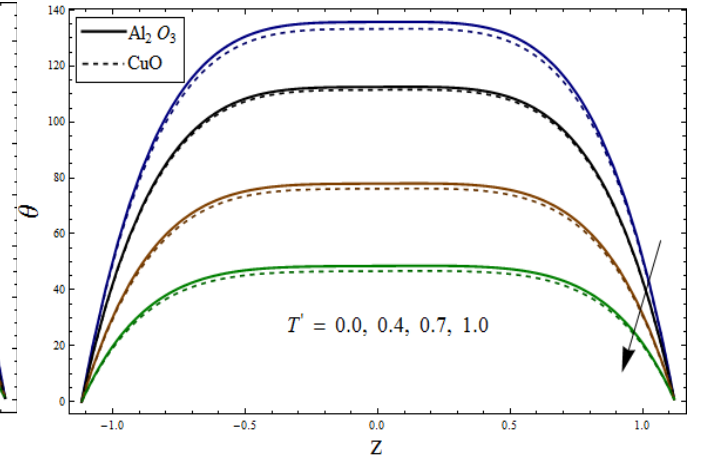
$$x = \epsilon = 0.2, t = 0.1.$$

Fig. 7.8 : Variation of wall properties on v when $T' = 0.5$, $M = 0.8$, $\phi = 0.01$, $x = \epsilon = 0.2$ and

$$t = 0.1.$$



7.9



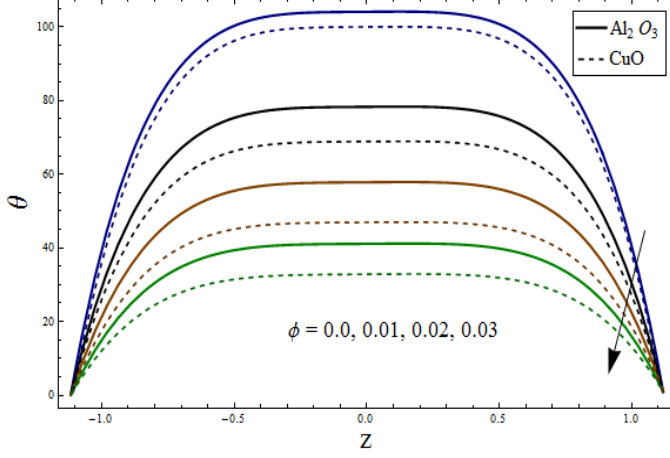
7.10

Fig. 7.9 : Variation of M on θ when $E_1 = E_2 = 3.0$, $E_3 = 0.1$, $Ec = T' = 0.5$,

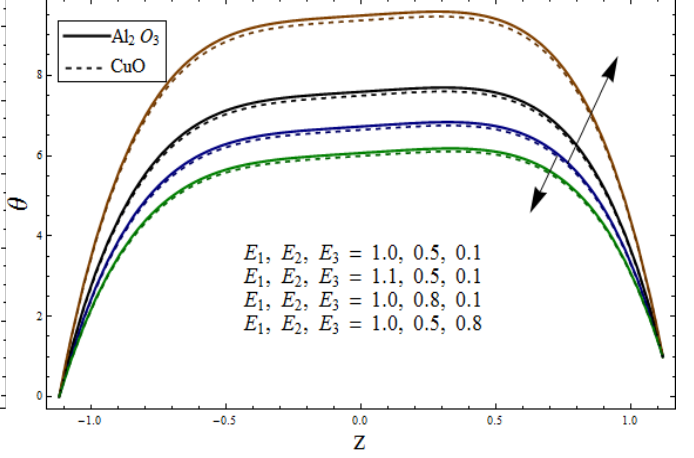
$$R = 0.8, \phi = 0.01, x = \epsilon = 0.2, t = 0.1.$$

Fig. 7.10 : Variation of T' on θ when $E_1 = E_2 = 3.0$, $E_3 = 0.1$, $Ec = 0.5$,

$$M = R = 0.8, \phi = 0.01, x = \epsilon = 0.2, t = 0.1.$$



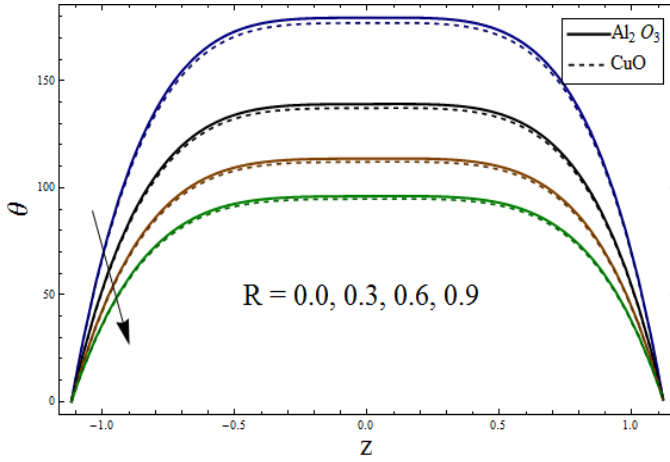
7.11



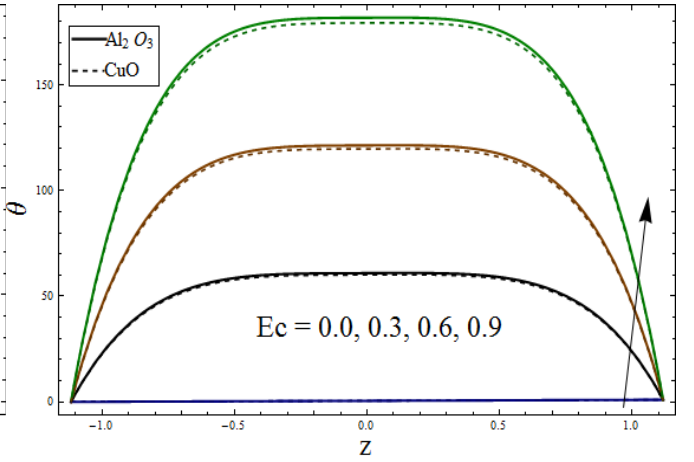
7.12

Fig. 7.11 : Variation of ϕ on θ when $E_1 = E_2 = 3.0$, $E_3 = 0.1$, $Ec = T' = 0.5$, $M = R = 0.8$,
 $x = \epsilon = 0.2$, $t = 0.1$.

Fig. 7.12 : Variation of wall properties on θ when $Ec = T' = 0.5$, $M = R = 0.8$, $\phi = 0.01$,
 $x = \epsilon = 0.2$, $t = 0.1$.



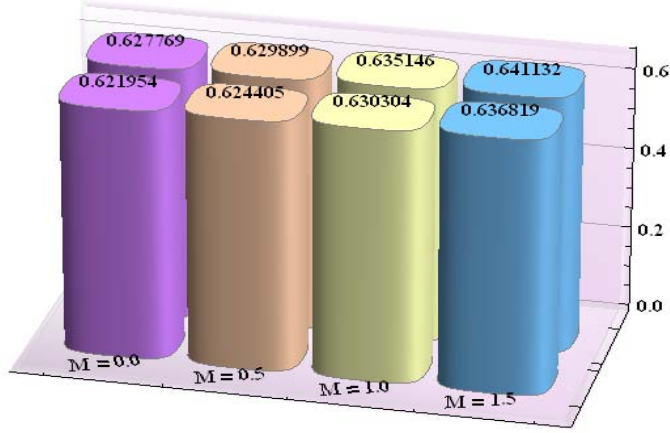
7.13



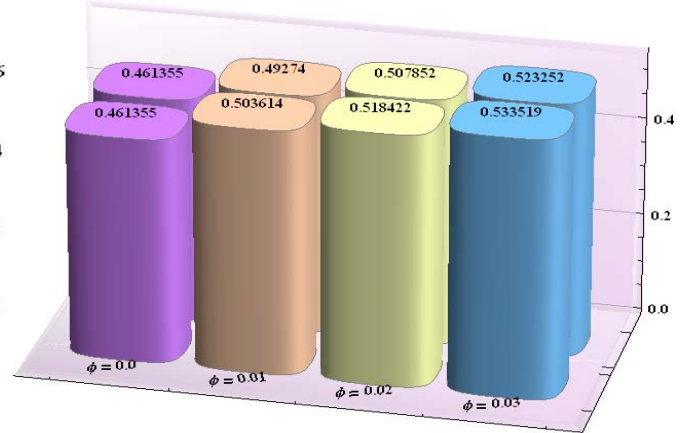
7.14

Fig. 7.13 : Variation of R on θ when $E_1 = E_2 = 3.0$, $E_3 = 0.1$, $Ec = T' = 0.5$,
 $M = 0.8$, $\phi = 0.01$, $x = \epsilon = 0.2$, $t = 0.1$.

Fig. 7.14 : Variation of Ec on θ when $E_1 = E_2 = 3.0$, $E_3 = 0.1$, $T' = 0.5$,
 $M = R = 0.8$, $\phi = 0.01$, $x = \epsilon = 0.2$, $t = 0.1$.



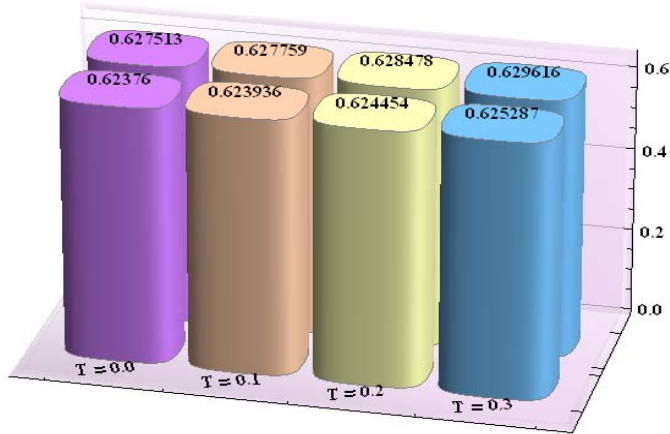
7.15



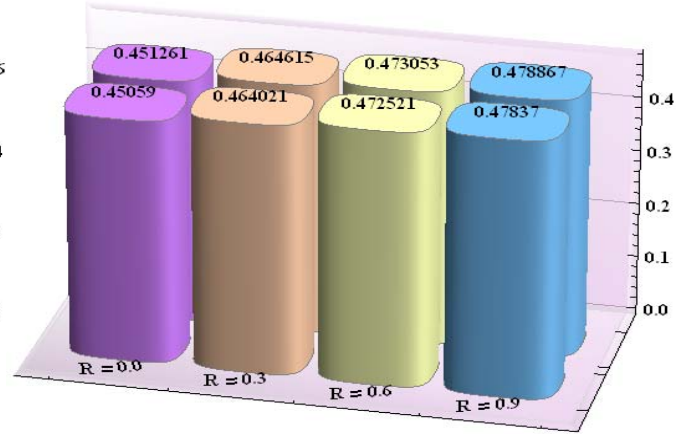
7.16

Fig. 7.15 : Impact of M on heat transfer rate at the wall $(-\frac{K_{eff}}{K_f})\theta'(\eta)$ when $E_1 = E_2 = 0.03$, $E_3 = 0.1$, $Ec = 0.5$, $R = 0.8$, $T' = 0.5$, $\phi = 0.01$, $\epsilon = 0.2$, $t = 0.1$.

Fig. 7.16 : Impact of ϕ on heat transfer rate at the wall $(-\frac{K_{eff}}{K_f})\theta'(\eta)$ when $E_1 = E_2 = 0.03$, $E_3 = 0.1$, $Ec = 0.5$, $M = R = 0.8$, $T' = 0.5$, $\epsilon = 0.2$, $t = 0.1$.



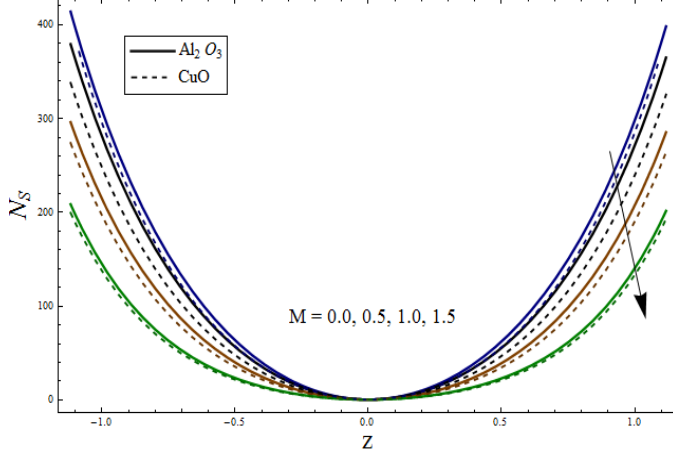
7.17



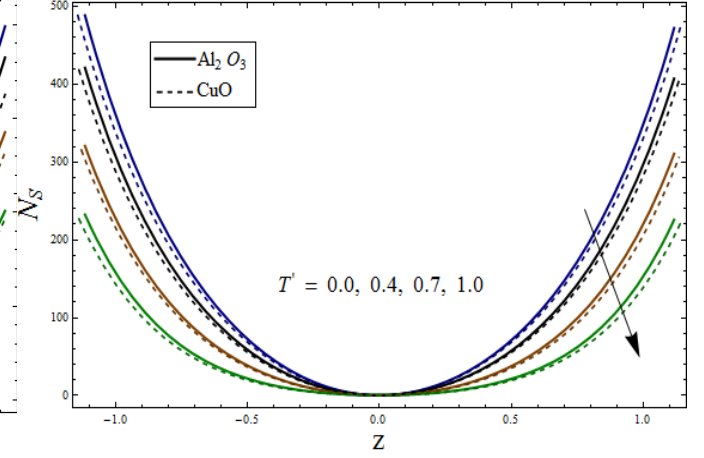
7.18

Fig. 7.17 : Impact of T' on heat transfer rate at the wall $(-\frac{K_{eff}}{K_f})\theta'(\eta)$ when $E_1 = E_2 = 0.03$, $E_3 = 0.1$, $Ec = 0.5$, $M = R = 0.8$, $\phi = 0.01$, $\epsilon = 0.2$, $t = 0.1$.

Fig. 7.18 : Impact of R on heat transfer rate at the wall $(-\frac{K_{eff}}{K_f})\theta'(\eta)$ when $E_1 = E_2 = 0.03$, $E_3 = 0.1$, $T' = Ec = 0.5$, $M = 0.8$, $\phi = 0.01$, $\epsilon = 0.2$, $t = 0.1$.



7.19



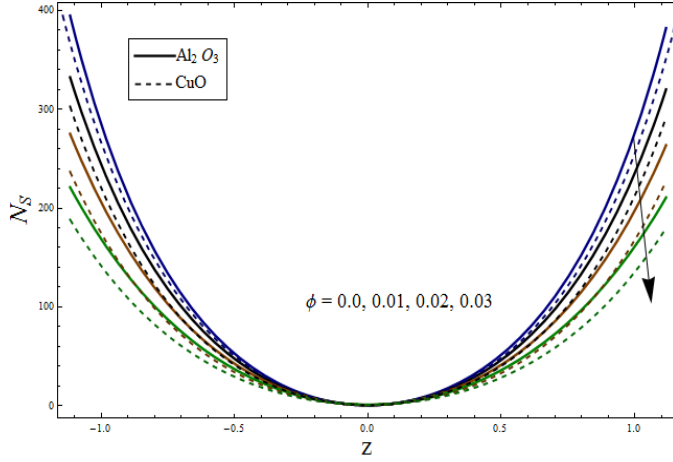
7.20

Fig. 7.19 : Variation of M on N_S when $E_1 = E_2 = 0.3$, $E_3 = 0.1$, $Ec = T' = 0.5$,

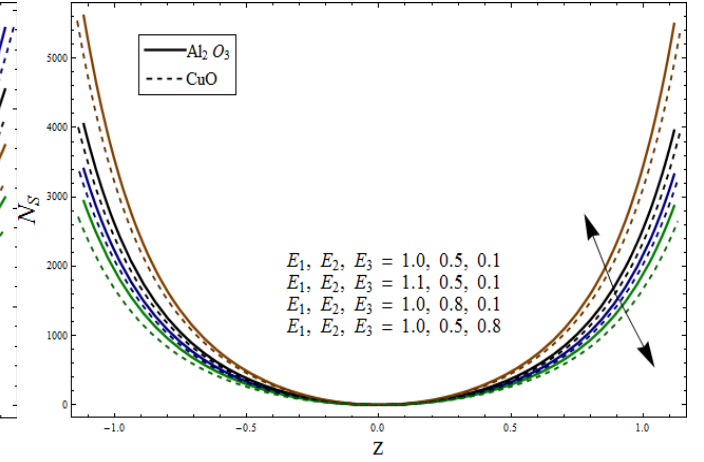
$R = 0.8$, $\phi = 0.01$, $Br\Lambda = 1.0$, $x = \epsilon = 0.2$ and $t = 0.1$.

Fig. 7.20 : Variation of T' on N_S when $E_1 = E_2 = 3.0$, $E_3 = 0.1$, $Ec = 0.5$,

$M = R = 0.8$, $\phi = 0.01$, $Br\Lambda = 1.0$, $x = \epsilon = 0.2$ and $t = 0.1$.



7.21



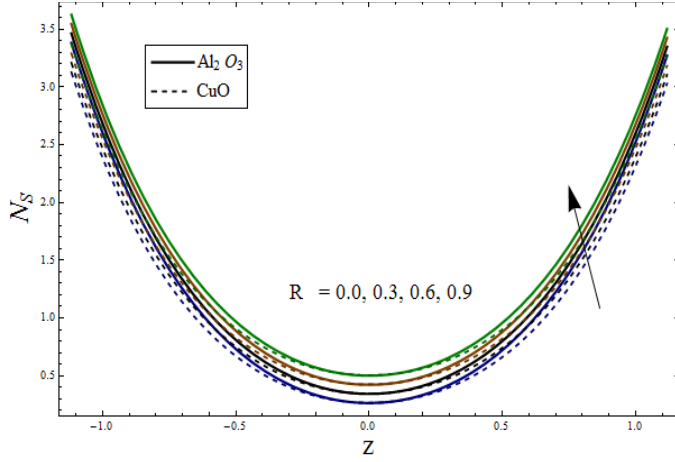
7.22

Fig. 7.21 : Variation of ϕ on N_S when $E_1 = E_2 = 3.0$, $E_3 = 0.1$, $Ec = T' = 0.5$, $M = R = 0.8$,

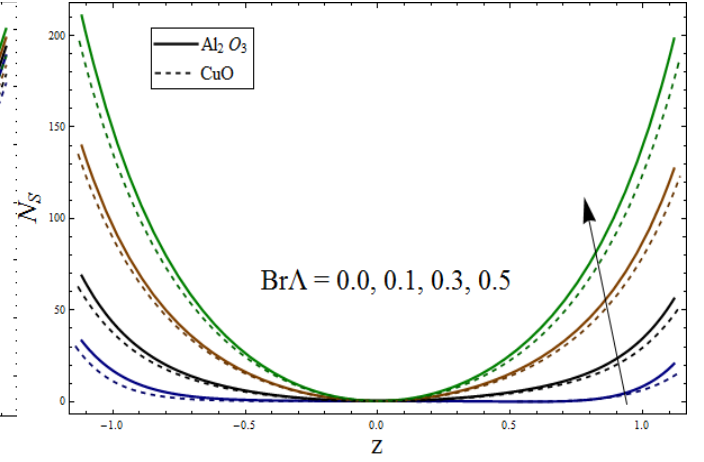
$Br\Lambda = 1.0$, $x = \epsilon = 0.2$, $t = 0.1$.

Fig. 7.22 : Variation of wall properties on N_S when $Ec = T' = 0.5$, $M = R = 0.8$, $\phi = 0.01$,

$Br\Lambda = 1.0$, $x = \epsilon = 0.2$, $t = 0.1$.



7.23



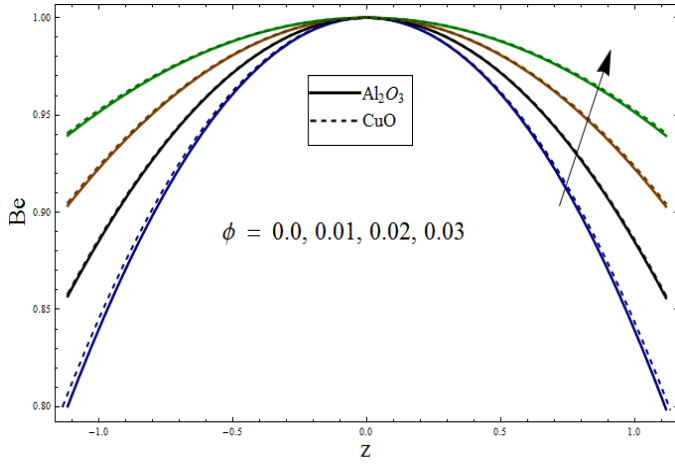
7.24

Fig. 7.23 : Variation of R on N_S when $E_1 = E_2 = 3.0$, $E_3 = 0.1$, $Ec = T' = 0.5$,

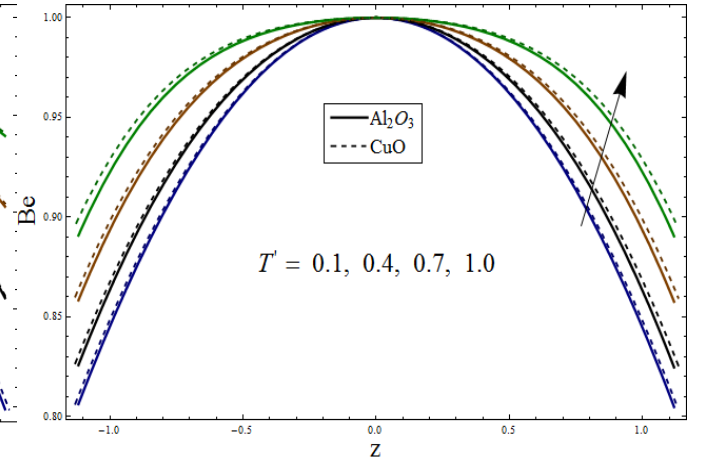
$M = 0.8$, $\phi = 0.01$, $Br\Lambda = 1.0$, $x = \epsilon = 0.2$, $t = 0.1$.

Fig. 7.24 : Variation of $Br\Lambda$ on N_S when $E_1 = E_2 = 3.0$, $E_3 = 0.1$, $Ec = T' = 0.5$,

$M = Rd = 0.8$, $\phi = 0.01$, $x = \epsilon = 0.2$, $t = 0.1$.



7.25



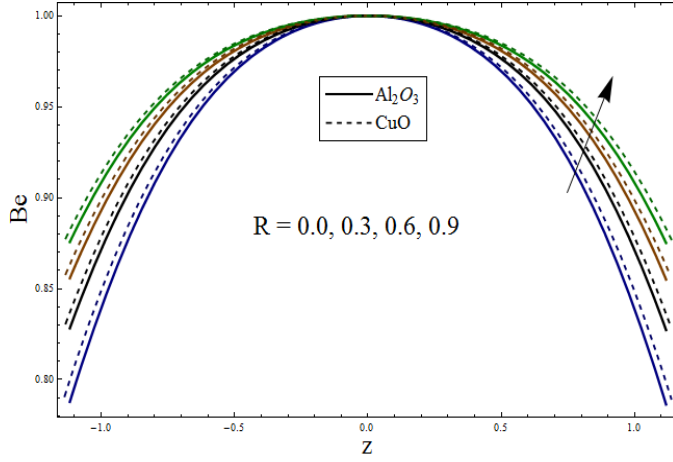
7.26

Fig. 7.25 : Variation of ϕ on Be when $E_1 = E_2 = 0.01$, $E_3 = 0.1$, $Ec = 0.5$,

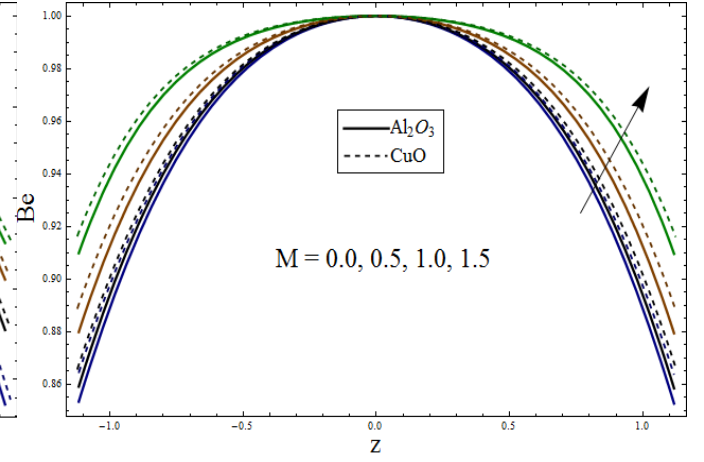
$T' = M = R = 0.8$, $Br\Lambda = 1.0$, $x = \epsilon = 0.2$, $t = 0.1$.

Fig. 7.26 : Variation of T' on Be when $E_1 = E_2 = 0.01$, $E_3 = 0.1$, $Ec = 0.5$, $M = R = 0.8$,

$\phi = 0.01$, $Br\Lambda = 1.0$, $x = \epsilon = 0.2$, $t = 0.1$.



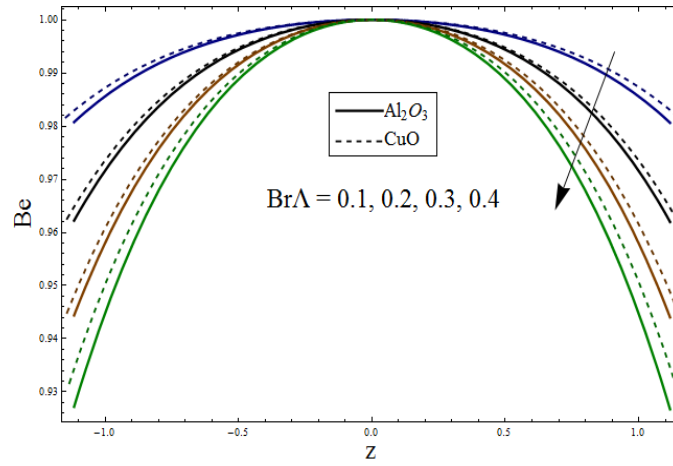
7.27



7.28

Fig. 7.27 : Variation of R on Be when $E_1 = E_2 = 0.01$, $E_3 = 0.1$, $Ec = 0.5$, $M = T' = 0.8$, $\phi = 0.01$, $Br\Lambda = 1.0$, $x = \epsilon = 0.2$, $t = 0.1$.

Fig. 7.28 : Variation of M on Be when $E_1 = E_2 = 0.01$, $E_3 = 0.1$, $Ec = 0.5$, $T' = R = 0.8$, $\phi = 0.01$, $Br\Lambda = 1.0$, $x = \epsilon = 0.2$, $t = 0.1$.



7.29

Fig. 7.29 : Variation of $Br\Lambda$ on Be when $E_1 = E_2 = 0.01$, $E_3 = 0.1$, $Ec = 0.5$, $T' = R = M = 0.8$, $\phi = 0.01$, $x = \epsilon = 0.2$, $t = 0.1$.

7.4 Conclusions

MHD peristaltic flow via nanoparticles Al_2O_3 and CuO is studied in a rotating frame. The channel is considered compliant in nature. Thermal analysis is done in the presence of radiation. Moreover entropy generation is also studied for the present situation. Main outcomes of the study are mentioned below:

- Axial and secondary velocities show similar behavior for M and ϕ i.e. these decrease with the enhancement in M and ϕ .
- Secondary velocity v vanishes in the absence of rotation ($T' = 0$).
- Temperature due to shearing effects for nanofluid is greater when compared with that of water.
- Rate of heat transfer for both nanoparticles enhances by increasing rotation but it is higher for CuO .
- The value of axial velocity u , temperature θ , heat transfer $\left(-\frac{K_{eff}}{K_f}\theta' [\eta]\right)$ and entropy generation N_S for Al_2O_3 is greater than CuO . However, this is not the case of secondary velocity v .
- Bejan number is higher for heat transfer irreversibility when compared with total irreversibility.

Chapter 8

Heat transfer in peristaltic flow of Ree-Eyring fluid with Hall and slip effects in a rotating frame

8.1 Introduction

The present chapter addresses the peristaltic motion of Ree-Eyring fluid in a channel with flexible walls. The whole system is rotating with constant angular velocity. Problem is formulated under the consideration of both Hall current and slip conditions. Thermal radiation effects are also taken. The resulting nonlinear system is simplified by adopting the lubrication approach. Solution expressions for stream function, axial and secondary velocities, temperature and heat transfer coefficient are developed. Influence of pertinent parameters on flow quantities are studied via plotting graphs.

8.2 Flow description

Consider the flow of an incompressible non-Newtonian fluid in a channel with flexible walls. The whole system is undergoing rigid body rotation. An unvarying magnetic field of strength B_0 is applied in transverse direction to the flow. The fluid is conducting and magnetic Reynolds number being small. This assumption helps in neglecting induced magnetic field in comparison

to applied magnetic field. Coordinate system is chosen in such a way that $x - axis$ lies along the channel and $z - axis$ is normal to it. Temperatures of top and bottom walls are defined by T_1 and T_0 . An infinite wave train is propagating along the channel walls with velocity c . Mathematically

$$\begin{aligned} z &= \eta(x, t) = \left[d + a \sin \frac{2\pi}{\lambda} (x - ct) \right] && \text{at top wall,} \\ z &= -\eta(x, t) = - \left[d + a \sin \frac{2\pi}{\lambda} (x - ct) \right], && \text{at bottom wall,} \end{aligned} \quad (8.1)$$

where a , λ and t define the wave amplitude, wavelength and time respectively.

8.3 Mathematical modeling

The balance laws of mass, momentum and energy equations in a rotating frame are

$$\text{div } \mathbf{V} = \mathbf{0}, \quad (8.2)$$

$$\rho \frac{d\mathbf{V}}{dt} + \rho [\mathbf{\Omega} \times (\mathbf{\Omega} \times \mathbf{r}) + 2\mathbf{\Omega} \times \mathbf{V}] = \text{div } \boldsymbol{\tau} + \mathbf{J} \times \mathbf{B}, \quad (8.3)$$

$$\rho C_p \frac{dT}{dt} = \kappa \nabla^2 T + \boldsymbol{\tau} \cdot \mathbf{L} - \nabla \mathbf{q}_r, \quad (8.4)$$

where \mathbf{V} is the velocity field defined by

$$\mathbf{V} = [u(x, z, t), v(x, z, t), w(x, z, t)]. \quad (8.5)$$

In above Eqs. ρ is the density, $\mathbf{\Omega} = \Omega \hat{k}$ the angular velocity, \hat{k} the unit vector, $\boldsymbol{\tau}$ the Cauchy stress tensor, \mathbf{J} the current density, \mathbf{B} the applied magnetic field, C_p the specific heat, T the temperature of the fluid, κ the thermal conductivity and $\mathbf{L} = \text{grad } \mathbf{V}$. The radiative heat flux \mathbf{q}_r :

$$\mathbf{q}_r = - \frac{4\sigma^*}{3k^*} \frac{\partial T^4}{\partial z}. \quad (8.6)$$

Here σ^* and k^* in the above relation are the Stefan-Boltzman and Rosseland mean absorption coefficients respectively. Generalized Ohms law in the presence of Hall current takes the form:

$$\mathbf{J} = \sigma \left[\mathbf{E} + \mathbf{V} \times \mathbf{B} - \frac{1}{en_e} [\mathbf{J} \times \mathbf{B}] \right]. \quad (8.7)$$

In the above Eq. σ is the electrical conductivity, E the electric field, e and n_e the electron charge and number density of free electrons respectively.

Lorentz force in the absence of electric field becomes

$$\mathbf{J} \times \mathbf{B} = \left[\frac{\sigma B_0^2}{1+m^2} (-u+mv), \frac{-\sigma B_0^2}{1+m^2} (v+mu), 0 \right], \quad (8.8)$$

where $m (= \sigma B_0 / en_e)$ is the Hall parameter. The constitutive relation for Ree-Eyring liquid is defined as

$$\boldsymbol{\tau} = -p\mathbf{I} + \mathbf{S},$$

where component form of extra stress tensor \mathbf{S} is written as [173] :

$$\mathbf{S}_{ij} = \mu \frac{\partial V_i}{\partial x_j} + \frac{1}{B} \sinh^{-1} \left(\frac{1}{C} \frac{\partial V_i}{\partial x_j} \right). \quad (8.9)$$

Since $\sinh^{-1} x \approx |x|$ with $x \leq 1$, then

$$\mathbf{S}_{ij} = \mu \frac{\partial V_i}{\partial x_j} + \frac{1}{B} \left(\frac{1}{C} \frac{\partial V_i}{\partial x_j} \right), \quad (8.10)$$

where μ defines the dynamic viscosity, B and C are the fluid parameters respectively.

Eqs. (8.2 – 8.4) after using Eqs. (8.5 – 8.10) take the form:

$$\frac{\partial u}{\partial x} + \frac{\partial w}{\partial z} = 0, \quad (8.11)$$

$$\rho \left[\frac{du}{dt} - 2\Omega v \right] = -\frac{\partial \hat{p}}{\partial x} + \frac{\partial S_{xx}}{\partial x} + \frac{\partial S_{xy}}{\partial y} + \frac{\partial S_{xz}}{\partial z} - \frac{\sigma B_0^2}{1+m^2} (u-mv), \quad (8.12)$$

$$\rho \left[\frac{dv}{dt} + 2\Omega u \right] = -\frac{\partial \hat{p}}{\partial y} + \frac{\partial S_{yx}}{\partial x} + \frac{\partial S_{yy}}{\partial y} + \frac{\partial S_{yz}}{\partial z} - \frac{\sigma B_0^2}{1+m^2} (v+mu), \quad (8.13)$$

$$\rho \frac{dw}{dt} = -\frac{\partial \hat{p}}{\partial z} + \frac{\partial S_{zx}}{\partial x} + \frac{\partial S_{zy}}{\partial y} + \frac{\partial S_{zz}}{\partial z}, \quad (8.14)$$

where modified pressure is defined as:

$$\hat{p} = p - \frac{1}{2}\rho\Omega^2(x^2 + y^2).$$

The thermal expression is

$$\rho C_p \frac{dT}{dt} = \kappa \left(\frac{\partial^2 T}{\partial x^2} + \frac{\partial^2 T}{\partial z^2} \right) + S_{xx} \frac{\partial u}{\partial x} + S_{xz} \left(\frac{\partial u}{\partial z} + \frac{\partial w}{\partial x} \right) + S_{zz} \frac{\partial w}{\partial z} + \frac{16\sigma^* T_m^3}{3k^*} \frac{\partial^2 T}{\partial z^2}, \quad (8.15)$$

where T_m is the mean temperature of fluid.

The movement of flexible wall is defined as

$$L = p - p_0,$$

where p_0 is the pressure on the outer surface of wall. The motion of stretched membrane in the presence of viscous damping forces is expressed by an operator L defined as

$$L = -\tau' \frac{\partial^2}{\partial x^2} + m_1 \frac{\partial^2}{\partial t^2} + d' \frac{\partial}{\partial t}. \quad (8.16)$$

In above Eq. τ' , m_1 and d' show elastic tension, mass/area and viscous damping coefficient respectively. For making problem simple we take p_0 equal to zero.

The continuity of stress at $z = \pm\eta$ ensures that pressure exerted by walls on the fluid is equal and opposite to the pressure exerted by fluid on the walls. Moreover transverse displacements shown by the walls are same as z-displacements exhibited by the fluid at the interfacial positions. Combining the continuity of stress and deformation condition we have

$$\begin{aligned} \frac{\partial}{\partial x} L(\eta) = \frac{\partial p}{\partial x} = \frac{\partial S_{xx}}{\partial x} + \frac{\partial S_{xy}}{\partial y} + \frac{\partial S_{xz}}{\partial z} - \frac{\sigma B_0^2}{1+m^2} (u - mv) \\ - \rho \left[\frac{du}{dt} - 2\Omega v \right] \quad \text{at } z = \pm\eta. \end{aligned} \quad (8.17)$$

The slip conditions at the walls are represented as:

$$u \pm \beta_1 \tau_{xz} = 0 \quad \text{at } z = \pm\eta, \quad (8.18)$$

$$v \pm \beta_2 \tau_{yz} = 0 \quad \text{at} \quad z = \pm \eta, \quad (8.19)$$

$$T \pm \beta_3 \frac{\partial T}{\partial z} = \begin{Bmatrix} T_1 \\ T_0 \end{Bmatrix} \quad \text{at} \quad z = \pm \eta. \quad (8.20)$$

We define the non-dimensional parameters as:

$$\begin{aligned} x^* &= \frac{x}{\lambda}, \quad y^* = \frac{y}{\lambda}, \quad z^* = \frac{z}{d}, \quad p^* = \frac{d^2 p}{c \mu_f \lambda}, \quad t^* = \frac{ct}{\lambda}, \quad u^* = \frac{u}{c}, \\ v^* &= \frac{v}{c}, \quad w^* = \frac{w}{c}, \quad \eta^* = \frac{\eta}{d}, \quad \theta = \frac{T - T_0}{T_1 - T_0}, \quad \text{Re} = \frac{\rho c d}{\mu}, \\ \delta &= \frac{d}{\lambda}, \quad T' = \frac{\text{Re} \Omega d}{c}, \quad M^2 = B_0^2 d^2 \frac{\sigma}{\mu}, \quad \text{Pr} = \frac{\mu C_p}{\kappa}, \quad \bar{\alpha} = \frac{1}{\mu B C}, \\ Ec &= \frac{c^2}{C_p (T_1 - T_0)}, \quad Br = \text{Pr} Ec, \quad E_1 = \frac{-\tau d^3}{\lambda^3 \mu c}, \quad E_2 = \frac{m_1 c d^3}{\lambda^3 \mu}, \\ E_3 &= \frac{d' d^3}{\lambda^2 \mu}, \quad \beta_{i's}^* = \frac{\beta_i}{d}, \quad u = \frac{\partial \psi}{\partial z}, \quad w = -\delta \frac{\partial \psi}{\partial x}. \end{aligned} \quad (8.21)$$

Omitting the asteriks and adopting lubrication approach one can write

$$-2T'v = -\frac{\partial p}{\partial x} + \frac{\partial S_{xz}}{\partial z} - \frac{M^2}{1+m^2} \left(\frac{\partial \psi}{\partial z} - mv \right), \quad (8.22)$$

$$2T' \frac{\partial \psi}{\partial z} = -\frac{\partial p}{\partial y} + \frac{\partial S_{yz}}{\partial z} - \frac{M^2}{1+m^2} \left(v + m \frac{\partial \psi}{\partial z} \right), \quad (8.23)$$

$$\frac{\partial p}{\partial z} = 0, \quad (8.24)$$

$$(1+R) \frac{\partial^2 \theta}{\partial z^2} + 2Br \left(\frac{\partial^2 \psi}{\partial z^2} \right) S_{xz} = 0, \quad (8.25)$$

where

$$S_{xz} = (1 + \bar{\alpha}) \frac{\partial^2 \psi}{\partial z^2}, \quad (8.26)$$

$$S_{yz} = (1 + \bar{\alpha}) \frac{\partial v}{\partial z}, \quad (8.27)$$

$$S_{zz} = 0. \quad (8.28)$$

It is noticed from Eq. (8.24) that pressure does not depend on z . Also the pressure term in Eq. (8.23) can be ignored as secondary flow is not caused by the pressure gradient but due to

rotation. Solving Eqs. (8.22) and (8.24) along with Eqs. (8.26 – 8.28) we get

$$(1 + \bar{\alpha}) \frac{\partial^4 \psi}{\partial z^4} - \frac{M^2}{1 + m^2} \left(\frac{\partial^2 \psi}{\partial z^2} - m \frac{\partial v}{\partial z} \right) + 2T' \frac{\partial v}{\partial z} = 0, \quad (8.29)$$

whereas Eqs. (8.23) and (8.25) take the form as under:

$$(1 + \bar{\alpha}) \frac{\partial^2 v}{\partial z^2} - \frac{M^2}{1 + m^2} \left(v + m \frac{\partial \psi}{\partial z} \right) - 2T' \frac{\partial \psi}{\partial z} = 0, \quad (8.30)$$

$$(1 + R) \frac{\partial^2 \theta}{\partial z^2} + 2Br(1 + \bar{\alpha}) \left(\frac{\partial^2 \psi}{\partial z^2} \right)^2 = 0. \quad (8.31)$$

Boundary conditions for the flow analysis now become

$$\frac{\partial \psi}{\partial z} \pm (1 + \bar{\alpha}) \beta_1 \frac{\partial^2 \psi}{\partial z^2} = 0 \quad \text{at} \quad z = \pm \eta, \quad (8.32)$$

$$v \pm (1 + \bar{\alpha}) \beta_2 \frac{\partial v}{\partial z} = 0 \quad \text{at} \quad z = \pm \eta, \quad (8.33)$$

$$\left[E_1 \frac{\partial^3}{\partial x^3} + E_2 \frac{\partial^3}{\partial x \partial t^2} + E_3 \frac{\partial^2}{\partial x \partial t} \right] \eta = (1 + \bar{\alpha}) \frac{\partial^3 \psi}{\partial z^3} - \frac{M^2}{1 + m^2} \left(\frac{\partial \psi}{\partial z} - mv \right) + 2T' v \quad \text{at} \quad z = \pm \eta, \quad (8.34)$$

$$\theta \pm \beta_3 \frac{\partial \theta}{\partial z} = \begin{cases} 1 \\ 0 \end{cases} \quad \text{at} \quad z = \pm \eta, \quad (8.35)$$

where T' is the Taylors number, M^2 the Hartman number, Br the Brinkman number, E_1 , E_2 and E_3 define the wall elastance parameters, $\bar{\alpha}$ the non-Newtonian fluid parameter whereas $\beta_{i's}$ are the slip parameters at upper and lower walls respectively.

8.4 Exact solutions

The exact solutions for the Eqs. (8.29 – 8.31) subject to the boundary conditions (8.32 – 8.35) are expressed as

$$\psi = F_1 z + F_2 \sinh[d_1 z] + F_3 \sinh[d_2 z], \quad (8.36)$$

$$v = F_4 + F_5 \cosh[d_1 z] + F_6 \cosh[d_2 z], \quad (8.37)$$

$$\begin{aligned} \theta = & B_1 + B_2 z + B_3 z^2 + B_4 (\cosh[(d_1 - d_2) z] + \cosh[(d_1 + d_2) z]) + B_6 \cosh[2d_1 z] \\ & + B_7 \cosh[2d_2 z], \end{aligned} \quad (8.38)$$

where

$$\begin{aligned} d_1 &= \sqrt{a_2 - i\sqrt{a_1 a_3}}, \quad d_2 = \sqrt{a_2 + i\sqrt{a_1 a_3}}, \quad a_1 = \frac{1}{(1 + \bar{\alpha})} \left(2T' + \frac{mM^2}{1 + m^2} \right), \\ a_2 &= \frac{1}{(1 + \bar{\alpha})} \frac{M^2}{(1 + m^2)}, \quad a_3 = \frac{1}{(1 + \bar{\alpha})} \left(2T' - \frac{mM^2}{1 + m^2} \right), \quad a_4 = \frac{(1 + \bar{\alpha})}{(1 + R)}. \end{aligned}$$

Heat transfer coefficient defined at the walls is

$$Z(x) = \eta_x \theta_z(\eta). \quad (8.39)$$

The constant $F_{i's}$ ($i = 1 - 6$) and $B_{i's}$ ($i = 1 - 7$) are defined as follows:

$$\begin{aligned} F_1 &= \frac{a_2(-a_1 C_1 + a_2 C_4 - C_6)}{(a_2^2 + a_1 a_3)}, \quad F_2 = \frac{(-i\sqrt{a_1}(a_2 C_1 + a_3 C_4) + \sqrt{a_3} C_6)}{2(a_2 - i\sqrt{a_1 a_3})^{3/2} \sqrt{a_3}}, \\ F_3 &= \frac{(ia_2 + \sqrt{a_1 a_3})(\sqrt{a_1}(a_2 C_1 + a_3 C_4) - i\sqrt{a_3} C_6)}{2(a_2 - i\sqrt{a_1 a_3})(a_2 + i\sqrt{a_1 a_3})^{3/2} \sqrt{a_3}}, \\ F_4 &= \frac{a_3(a_1 C_1 - a_2 C_4 + C_6)}{a_2^2 + a_1 a_3}, \quad F_5 = \frac{(a_2 + i\sqrt{a_1 a_3})(\sqrt{a_1}(a_2 C_1 + a_3 C_4) + i\sqrt{a_3} C_6)}{2\sqrt{a_1}(a_2^2 + a_1 a_3)}, \\ F_6 &= \frac{(a_2 - i\sqrt{a_1 a_3})(\sqrt{a_1}(a_2 C_1 + a_3 C_4) - i\sqrt{a_3} C_6)}{2\sqrt{a_1}(a_2^2 + a_1 a_3)}, \end{aligned}$$

$$\begin{aligned}
B_1 &= \frac{1}{2} - B_3\eta(2\beta_3 + \eta) - B_6 \cosh[2d_1\eta] - B_4 \cosh[(d_1 - d_2)\eta] - B_7 \cosh[2d_2\eta] \\
&\quad - B_5 \cosh[(d_1 + d_2)\eta] - \beta_3(B_4(d_1 - d_2) \sinh[(d_1 - d_2)\eta] + 2(B_6d_1 \sinh[2d_1\eta] \\
&\quad + B_7d_2 \sinh[2d_2\eta]) + B_5(d_1 + d_2) \sinh[(d_1 + d_2)\eta]), \\
B_2 &= \frac{1}{2(\beta_3 + \eta)}, \quad B_3 = \frac{a_4 Br(a_2 a_3 C_6^2 - a_1(a_2 C_1 + a_3 C_4)(a_2^2 C_1 + a_2 a_3 C_4 - 2a_3 C_6))}{4a_3(a_2^2 + a_1 a_3)}, \\
B_4 &= \frac{d_1 d_2 a_4 Br(a_1(a_2 C_1 + a_3 C_4)^2 + a_3 C_6^2)}{2(d_1 - d_2)^2 a_3(a_2^2 + a_1 a_3)}, \quad B_5 = -B_4, \\
B_6 &= -\frac{a_4 Br(\sqrt{a_1}(a_2 C_1 + a_3 C_4) + i\sqrt{a_3} C_6)^2}{16(ia_2 + \sqrt{a_1 a_3})^2 a_3}, \quad B_7 = -B_6.
\end{aligned}$$

8.5 Discussion

This section studies the effect of sundry variables on axial (u) and secondary (v) velocities, temperature (θ) and heat transfer coefficient (Z) via graphs (see Figs. 8.1 – 8.23).

8.5.1 Axial velocity

Figs. (8.1 – 8.5) show the impact of different physical parameters against the axial velocity (u). In particular the effect of wall parameters (E_1 , E_2 , E_3), Taylors number (T'), Hall, slip and fluid parameters (m , β_1 , $\bar{\alpha}$) on axial velocity is studied. Velocity is found increasing function for wall rigidity (E_1) and tension (E_2) parameters respectively. Since these parameters represent the elastic nature of walls therefore increasing wall elastance lowers the resistance to the flow and velocity enhances. Viscous damping (E_3) is the oscillatory resistance which is inversely related to velocity. Therefore decrease in velocity is noticed for higher values of E_3 (see *Fig. 8.1*). Influence of rotation on axial velocity is depicted through *Fig. 8.2*. The Fig. shows that velocity decreases as we keep on increasing the rotation. Furthermore it is noticed that velocity is higher in the absence of rotation ($T' = 0$). *Fig. 8.3* illustrates the effect of Hall parameter m on u . Less values of m decrease magnetic damping which causes velocity to increase. Thin inhomogeneous layer of film along the walls assists the motion of fluid. The slip effect enhances when this film becomes less viscous and there is fluid velocity enhancement (see *Fig. 8.4*). The impact of fluid parameter ($\bar{\alpha}$) on velocity can be seen through *Fig. 8.5*. As the value of fluid parameter increases the viscosity decreases which enhances the velocity of fluid.

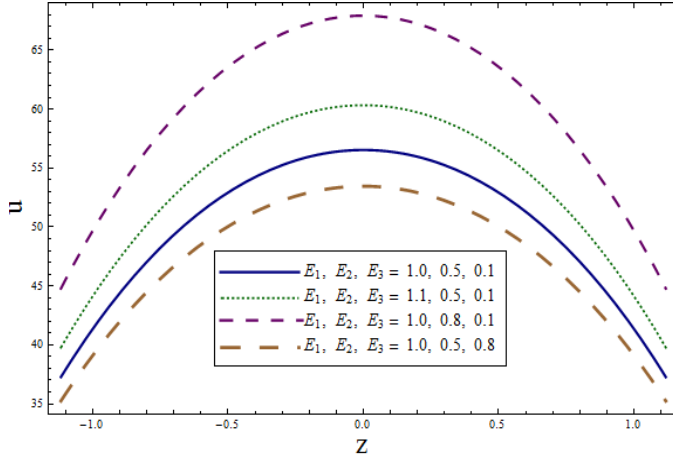
8.5.2 Secondary Flow

Channel rotation generates a velocity in y-direction which is termed as secondary velocity. This subsection studies the influence of pertinent parameters $(E_1, E_2, E_3, T', m, \beta_1)$ on secondary velocity v by plotting *Figs. 8.6 – 8.10*. Increasing behavior of secondary velocity v is noticed for higher values of damping parameter (E_3) . On contrary velocity increases for the elastance parameters (E_1, E_2) (see *Fig. 8.6*). It is revealed by *Fig. 8.7* that secondary velocity increases as we rotate the channel rapidly. It is also noteworthy to mention that there is no secondary velocity when the channel is non-rotating $(T' = 0)$. *Fig. 8.8* displays the influence of Hall parameter m on v . This *Fig.* illustrates that the secondary velocity accelerates as the Hall effects get stronger. To study the effect of slip parameter β_2 on v *Fig. 8.9* is plotted. It is revealed from the *Fig.* that velocity enhances as we increase the slip effects. The results obtained for fluid parameter $\bar{\alpha}$ shows that secondary velocity increases for higher values of $\bar{\alpha}$ (see *Fig. 8.10*). The reason behind this fact is the low viscosity of fluid.

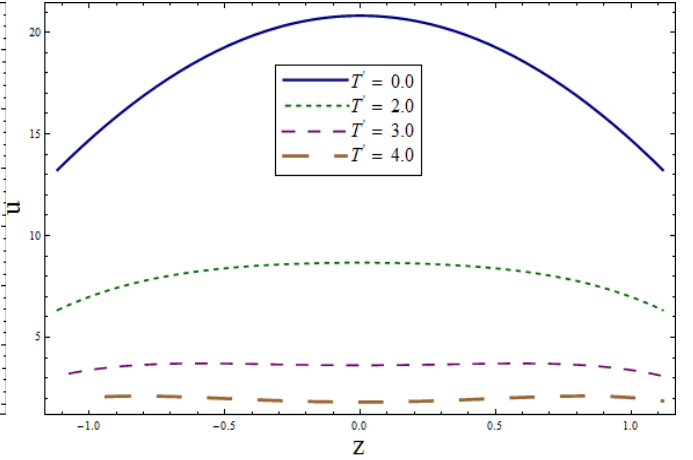
8.5.3 Heat transfer analysis

This subsection is organized to show variation of different emerging parameters on temperature θ and heat transfer mechanism Z . *Fig. 8.11* displays the significance of wall parameters on θ . It is revealed from the *Fig.* that increasing values of elastance parameters (E_1, E_2) enhances the temperature whereas it decreases as viscous damping (E_3) is increased. As velocity of fluid increases for higher values of rotation which results in decrease of temperature. This result is clearly visible from *Fig. 8.12*. Influence of Hall parameter m on θ is revealed through *Fig. 8.13*. It is observed that temperature rises for higher values of m . It is the result of strong magnetic field. *Fig. 8.14* elucidates the influence of thermal slip parameter β_3 on θ . It is seen from the *Fig.* that temperature attains a higher value as we increase the thermal slip parameter. To discuss the effect of fluid parameter α on θ *Fig. 8.15* is sketched. Less resistance is offered to the flow due to decreased viscosity larger $\bar{\alpha}$. Hence causing increased velocity enhances the temperature. It is also noticed from the *Fig.* that temperature is higher for non-Newtonian case. For larger radiation parameter R temperature of the fluid decreases (*Fig. 8.16*). The internal friction generated in the fluid by shearing forces produces energy in the form of heat which further enhances the temperature θ of the fluid. Brinkman number Br in the problem

is responsible for this effect. Hence increasing shear will give higher value of Br which in turn rises the temperature θ (see Fig. 8.17). The plots for heat transfer coefficient $Z(x)$ are shown through Figs. (8.18 – 8.23). Basically $Z(x)$ defines the heat flux or heat transfer at the walls and mathematically expressed as $Z(x) = \eta_x \theta_z(\eta)$. The sinusoidal waves propagating beside the walls causes heat transfer coefficient to exhibit oscillatory behavior. Fig. 8.18 reveals that the rate of heat transfer $Z(x)$ increases as we rotate the channel with greater velocity. To explore the impact of radiation parameter R on heat transfer coefficient Fig. 8.19 is plotted. It can be noticed from the Fig. that heat transfer rate decreases for larger radiation parameter. Influence of Hall parameter m on $Z(x)$ can be studied through Fig. 8.20. We observed enhancement in the rate of heat transfer through larger Hall parameter m . To analyze the impact of thermal slip β_3 and fluid parameter $\bar{\alpha}$ the Figs. 8.21 and 8.22 are plotted. It is clearly visible from the Figs. that heat transfer rate increases by making increment in the values of these parameters. The graphical results show that the rate of heat transfer is higher when shearing forces between fluid layers are enhanced (see Fig. 8.23).



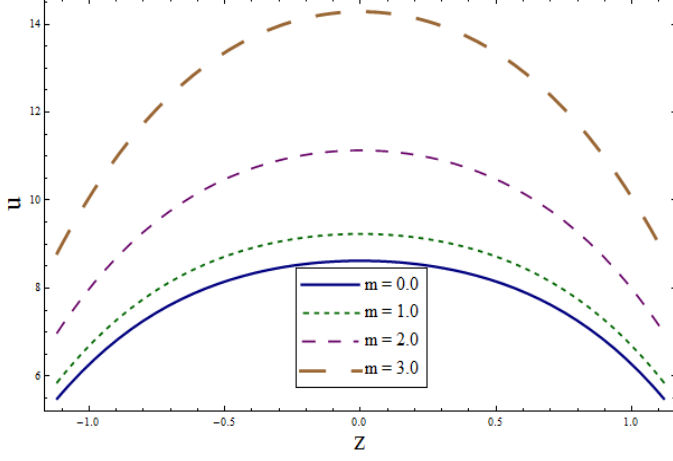
8.1



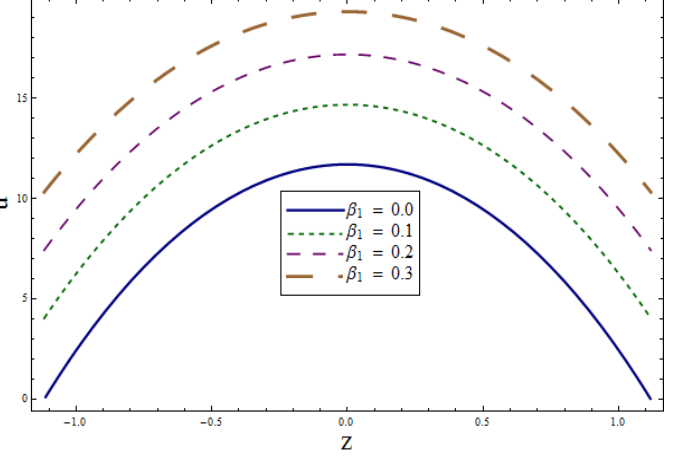
8.2

Fig. 8.1 : Variation of wall properties on u when $\bar{\alpha} = T' = 1.0$, $m = M = 2.0$, $\beta_1 = \beta_2 = 0.5$,
 $x = \epsilon = 0.2$, $t = 0.1$.

Fig. 8.2 : Variation of T' on u when $E_1 = E_2 = 0.3$, $E_3 = 0.01$, $m = M = 2.0$, $\beta_1 = \beta_2 = 0.5$,
 $\bar{\alpha} = 1.0$, $x = \epsilon = 0.2$, $t = 0.1$.



8.3



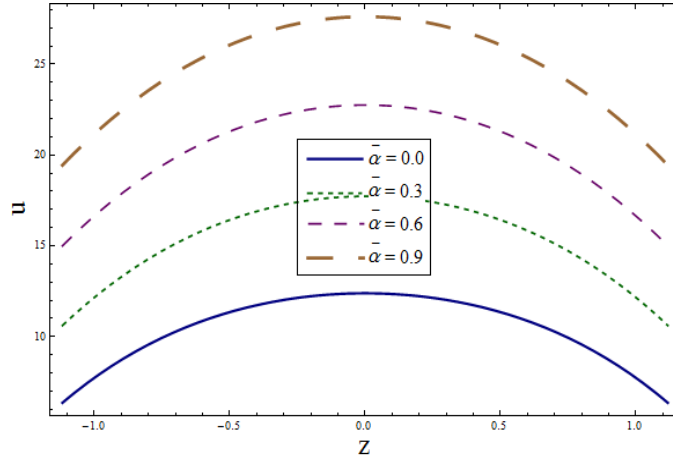
8.4

Fig. 8.3 : Variation of m on u when $E_1 = E_2 = 0.3$, $E_3 = 0.01$, $M = 2.0$, $\beta_1 = \beta_2 = 0.5$,

$$\bar{\alpha} = T' = 1.0, x = \epsilon = 0.2, t = 0.1.$$

Fig. 8.4 : Variation of β_1 on u when $E_1 = E_2 = 0.3$, $E_3 = 0.01$, $m = M = 2.0$, $\beta_2 = 0.5$,

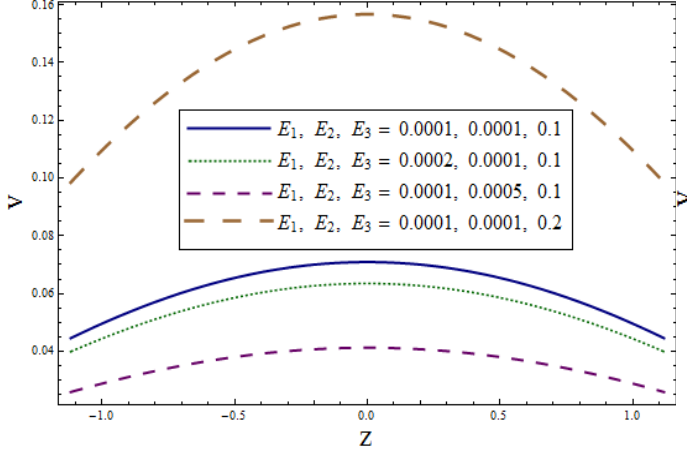
$$\bar{\alpha} = T' = 1.0, x = \epsilon = 0.2, t = 0.1.$$



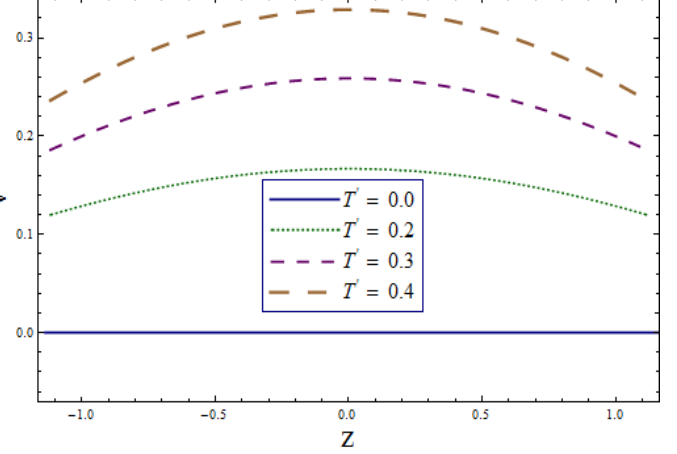
8.5

Fig. 8.5 : Variation of $\bar{\alpha}$ on u when $E_1 = E_2 = 0.3$, $E_3 = 0.01$, $T' = 1.0$, $m = M = 2.0$,

$$\beta_1 = \beta_2 = 0.5, x = \epsilon = 0.2, t = 0.1.$$



8.6



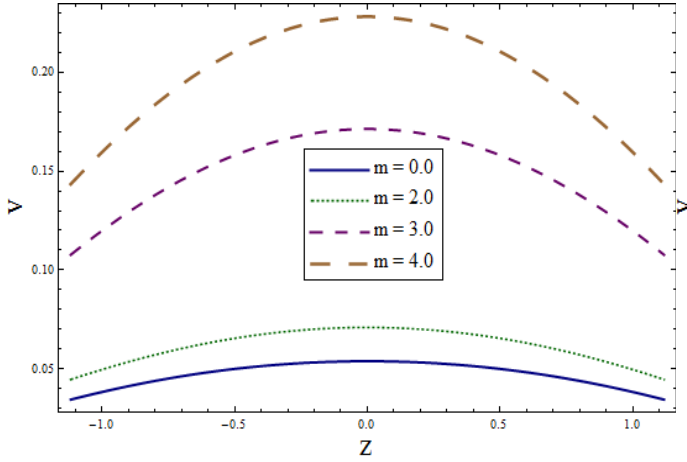
8.7

Fig. 8.6 : Variation of wall properties on v when $\bar{\alpha} = T' = 1.0$, $m = M = 2.0$,

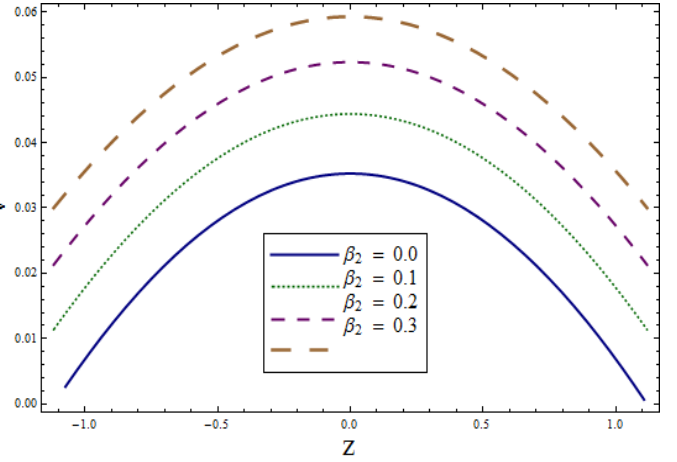
$$\beta_1 = \beta_2 = 0.5, x = \epsilon = 0.2, t = 0.1.$$

Fig. 8.7 : Variation of T' on v when $E_1 = E_2 = 0.001$, $E_3 = 0.1$, $m = M = 2.0$, $\bar{\alpha} = 1.0$,

$$\beta_1 = \beta_2 = 0.5, x = \epsilon = 0.2, t = 0.1.$$



8.8



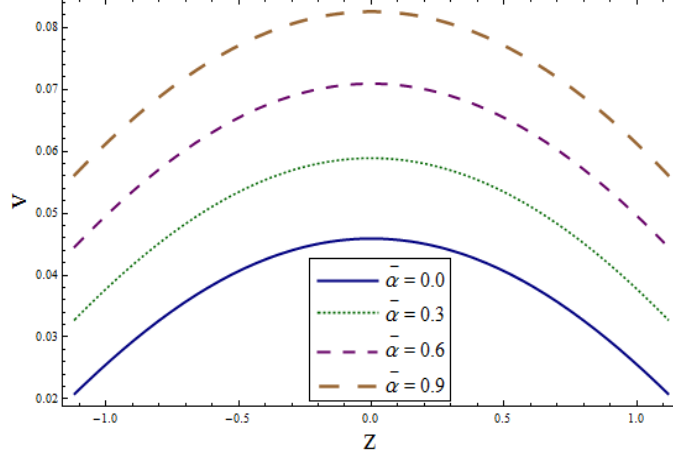
8.9

Fig. 8.8 : Variation of m on v when $E_1 = E_2 = 0.001$, $E_3 = 0.1$, $M = 2.0$, $\bar{\alpha} = T' = 1.0$,

$$\beta_1 = \beta_2 = 0.5, x = \epsilon = 0.2, t = 0.1.$$

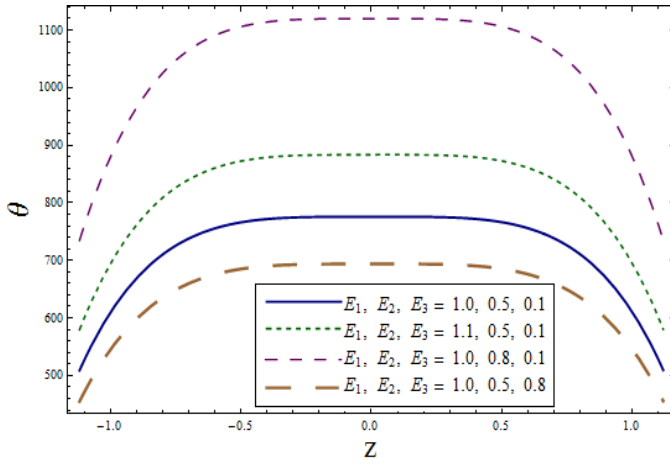
Fig. 8.9 : Variation of β_2 on v when $E_1 = E_2 = 0.001$, $E_3 = 0.1$, $m = M = 2.0$, $\bar{\alpha} = T' = 1.0$,

$$\beta_1 = 0.5, x = \epsilon = 0.2, t = 0.1.$$

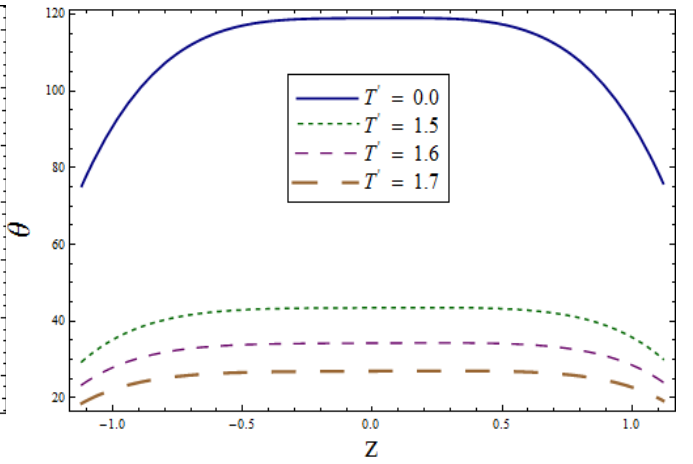


8.10

Fig. 8.10 : Variation of $\bar{\alpha}$ on v when $E_1 = E_2 = 0.001$, $E_3 = 0.1$, $m = M = 2.0$, $T' = 1.0$,
 $\beta_1 = \beta_2 = 0.5$, $x = \epsilon = 0.2$, $t = 0.1$.



8.11



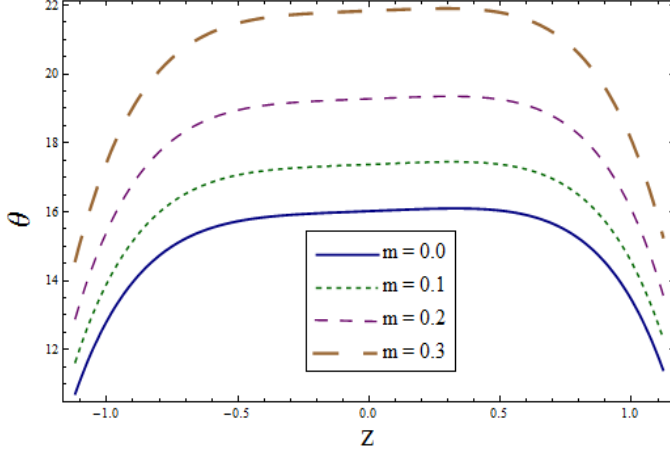
8.12

Fig. 8.11 : Variation of *wall properties* on θ when $m = M = 2.0$, $R = 0.8$,

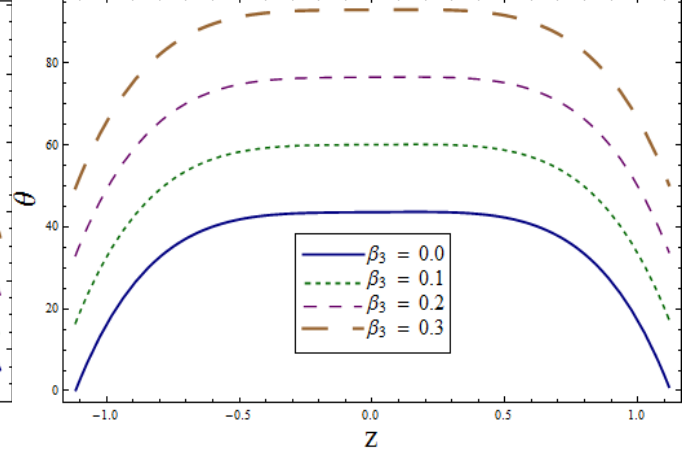
$$\beta_1 = \beta_2 = \beta_3 = 0.5, \bar{\alpha} = T' = Br = 1.0, x = \epsilon = 0.2, t = 0.1.$$

Fig. 8.12 : Variation of T' on θ when $E_1 = E_2 = 0.3$, $E_3 = 0.01$, $m = M = 2.0$, $R = 0.8$,

$$\beta_1 = \beta_2 = \beta_3 = 0.5, \bar{\alpha} = Br = 1.0, x = \epsilon = 0.2, t = 0.1.$$



8.13



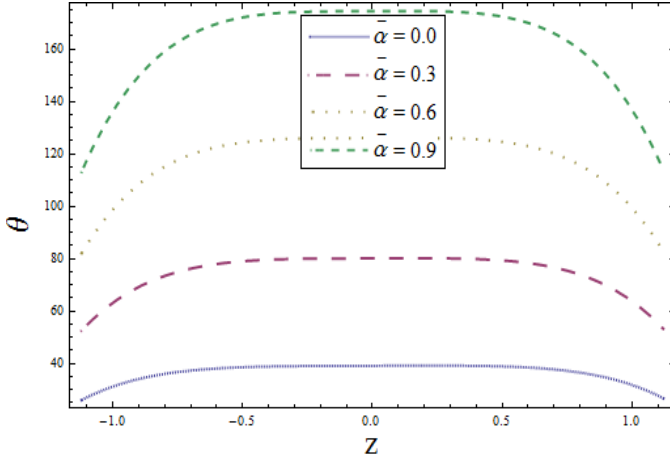
8.14

Fig. 8.13 : Variation of m on θ when $E_1 = E_2 = 0.3$, $E_3 = 0.01$, $M = 2.0$, $R = 0.8$,

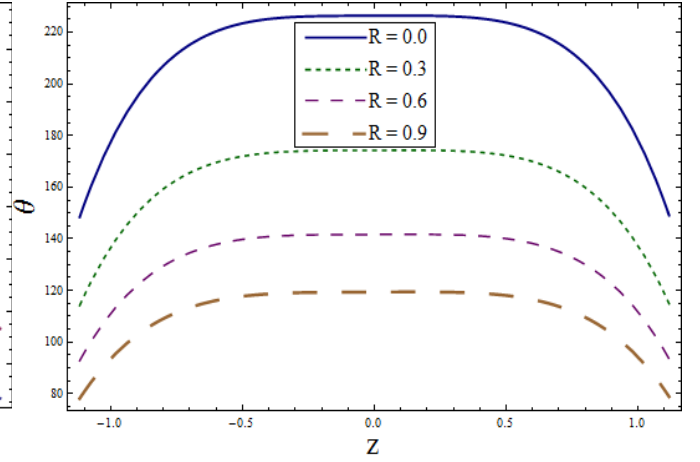
$$\beta_1 = \beta_2 = \beta_3 = 0.5, \bar{\alpha} = T' = Br = 1.0, x = \epsilon = 0.2, t = 0.1.$$

Fig. 8.14 : Variation of β_3 on θ when $E_1 = E_2 = 0.3$, $E_3 = 0.01$, $m = M = 2.0$, $R = 0.8$,

$$\beta_1 = \beta_2 = 0.5, \bar{\alpha} = T' = Br = 1.0, x = \epsilon = 0.2, t = 0.1.$$



8.15



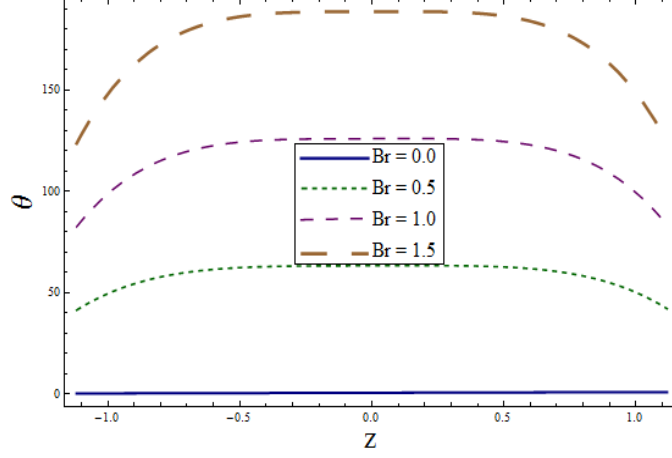
8.16

Fig. 8.15 : Variation of $\bar{\alpha}$ on θ when $E_1 = E_2 = 0.3$, $E_3 = 0.01$, $m = M = 2.0$, $R = 0.8$,

$$\beta_1 = \beta_2 = \beta_3 = 0.5, T' = Br = 1.0, x = \epsilon = 0.2, t = 0.1.$$

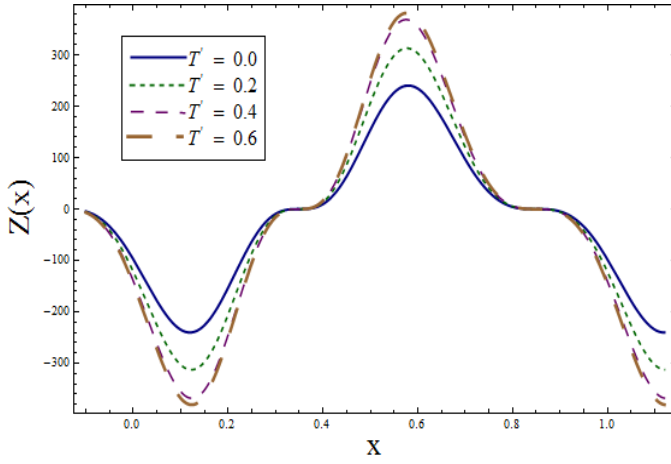
Fig. 8.16 : Variation of R on θ when $E_1 = E_2 = 0.3$, $E_3 = 0.01$, $m = M = 2.0$,

$$\beta_1 = \beta_2 = \beta_3 = 0.5, \bar{\alpha} = T' = Br = 1.0, x = \epsilon = 0.2, t = 0.1.$$

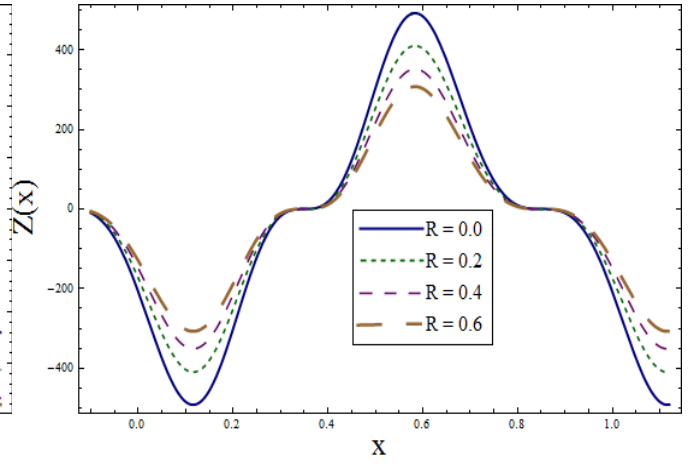


8.17

Fig. 8.17 : Variation of Br on θ when $E_1 = E_2 = 0.3$, $E_3 = 0.01$, $m = M = 2.0$, $R = 0.8$,
 $\beta_1 = \beta_2 = \beta_3 = 0.5$, $\bar{\alpha} = T' = 1.0$, $x = \epsilon = 0.2$, $t = 0.1$.



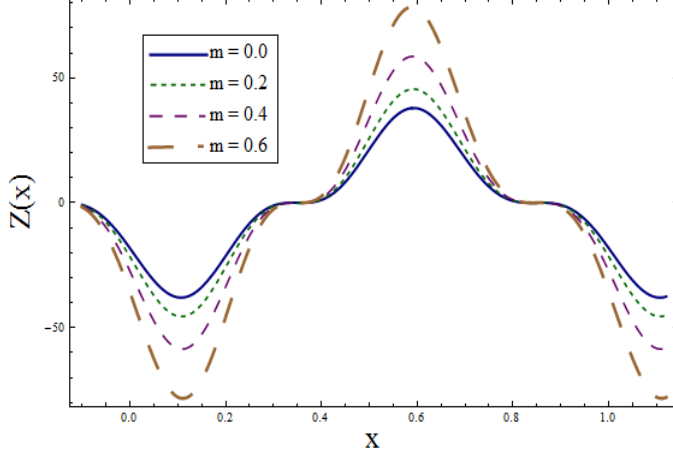
8.18



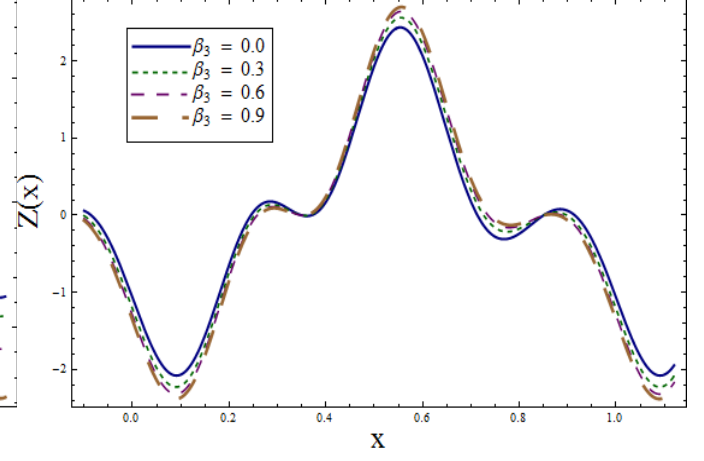
8.19

Fig. 8.18 : Variation of T' on Z when $E_1 = E_2 = 0.3$, $E_3 = 0.01$, $m = M = 2.0$, $R = 0.8$,
 $\beta_1 = \beta_2 = \beta_3 = 0.5$, $\bar{\alpha} = Br = 1.0$, $\epsilon = 0.2$, $t = 0.1$.

Fig. 8.19 : Variation of R on Z when $E_1 = E_2 = 0.3$, $E_3 = 0.01$, $m = M = 2.0$,
 $\beta_1 = \beta_2 = \beta_3 = 0.5$, $\bar{\alpha} = T' = Br = 1.0$, $\epsilon = 0.2$ and $t = 0.1$.



8.20



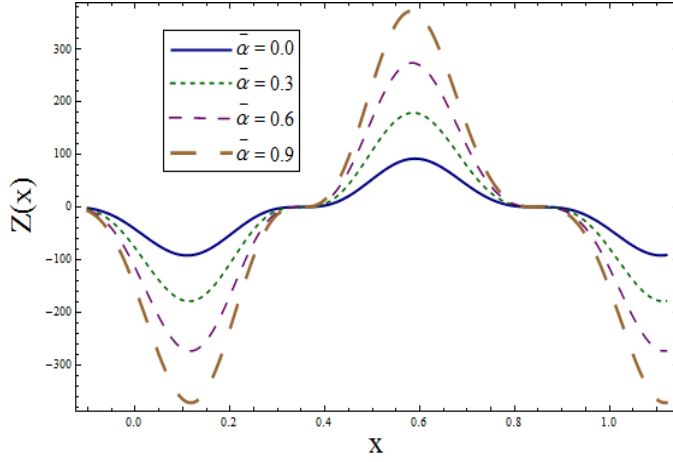
8.21

Fig. 8.20 : Variation of m on θ when $E_1 = E_2 = 0.3$, $E_3 = 0.01$, $M = 2.0$, $R = 0.8$,

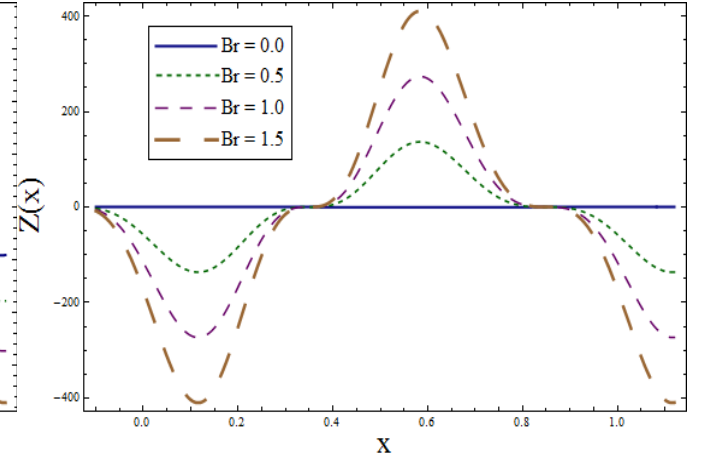
$$\beta_1 = \beta_2 = \beta_3 = 0.5, \bar{\alpha} = T' = Br = 1.0, \epsilon = 0.2, t = 0.1.$$

Fig. 8.21 : Variation of β_3 on Z when $E_1 = E_2 = 0.3$, $E_3 = 0.01$, $m = M = 2.0$, $R = 0.8$,

$$\beta_1 = \beta_2 = 0.5, \bar{\alpha} = T' = Br = 1.0, \epsilon = 0.2, t = 0.1.$$



8.22



8.23

Fig. 8.22 : Variation of $\bar{\alpha}$ on Z when $E_1 = E_2 = 0.3$, $E_3 = 0.01$, $m = M = 2.0$, $R = 0.8$,

$$\beta_1 = \beta_2 = \beta_3 = 0.5, T' = Br = 1.0, \epsilon = 0.2, t = 0.1.$$

Fig. 8.23 : Variation of Br on Z when $E_1 = E_2 = 0.3$, $E_3 = 0.01$, $m = M = 2.0$, $R = 0.8$,

$$\beta_1 = \beta_2 = \beta_3 = 0.5, \bar{\alpha} = T' = 1.0, \epsilon = 0.2, t = 0.1.$$

8.6 Conclusions

The main features for peristaltic transport of Ree-Eyring liquid in a rotating frame with Hall effects are discussed. Impact of slip conditions and thermal radiation are also considered. The main observation are mentioned below.

- Axial velocity decreases via channel rotation.
- Velocities (u, v) are increasing functions of fluid parameter $\bar{\alpha}$.
- In non-rotating case $(T' = 0)$ the secondary velocity vanishes.
- Velocities (u, v) and temperature θ are enhanced for an increase in the slip parameters β_1, β_2 and β_3 .
- Rotation parameter T' has opposite effects on temperature when compared with secondary velocity v .
- Fluid and radiation parameters $(\bar{\alpha}$ and $R)$ exhibit opposite behavior for temperature θ .
- Rate of heat transfer Z enhances for β_3 (thermal slip parameter), α (fluid parameter) and Br (Brinkman number).

Chapter 9

Summary

The research carried out in the present thesis is summed up through chapters two to eight. The main objective of all these chapters is to study the impact of magnetohydrodynamics on peristaltic flow of viscous and non-Newtonian fluids in a compliant wall channel when the whole system is in rigid body rotation. Effect of secondary velocity, which is generated due to the rotation is given major attention. Mathematical modelling is simplified by adopting the lubrication approach. Results for stream function, axial and secondary velocities, temperature and concentration are obtained. Exact as well as numerical solutions using NDSolve command of MATHEMATICA, are calculated and analyzed. Variation of pertinent parameters on velocities, temperature, concentration and heat transfer coefficient is shown graphically and discussed physically. Moreover the streamlines are also drawn and discussed. Main outcomes of the conducted research are summerized as follows:

- Axial velocity shows decrease through increase in rotation parameter and Hartman number.
- Wall elastance parameters E_1 and E_2 show similar behavior whereas E_3 , E_4 and E_5 show opposite behavior to E_1 and E_2 .
- Axial velocity enhances as the permeability of porous medium (K_1), nanoparticle volume fraction (ϕ), Hall parameter (m), fluid parameter ($\bar{\alpha}$) and velocity slip increases.
- It is worthmentioning that axial velocity is graeter for aluminium nanoparticles than that

of copper.

- Secondary velocity shows opposite behavior for λ_1 , T' and wall properties except for M .
- Secondary velocity exhibits similar results for involved parameter when compared with axial velocity.
- Temperature is found decreasing function of rotation parameter, thermal radiation, wall characterising parameters (E_3 , E_4 and E_5), nanoparticle volume fraction (ϕ) and λ_1 .
- Temperature exhibits increasing behavior when we make increment in the values of fluid parameter ($\bar{\alpha}$), Hartman, Eckert, Prandtl, Brinkman and Soret and Dufour numbers. Moreover increasing permeability and Hall and slip effects also enhance the temperature. In addition it is noticed that temperature is higher for heat generation ($S > 0$) coefficient when compared with heat absorption coefficient ($S < 0$).
- It is noteworthy that large non-uniform temperature field inside the fluid has decreasing effect on temperature which is represented through Biot number Bi .
- Irreversibility or entropy generation (N_S) is helpful in determining the efficiency of system. Therefore entropy generation analysis is performed for pertinent parameters. Hartman number, rotation parameter and nanoparticle volume fraction show decreasing effect for N_S . It is also noticed that magnitude of entropy generation is higher for aluminium when compared to copper nanoparticles.
- Brinkman parameter $Br\Lambda$ studying viscous effects shows an enhancement in entropy generation.
- Bejan number close to 1 shows the dominance of heat transfer irreversibility at central part of channel.
- Concentration of fluid increases with the enhancement in the values of rotation, thermal radiation, thermophoresis, constructive chemical reaction and wall elastance parameters (E_3 , E_4 and E_5).
- An increase in the values of Soret, Dufour, Hartman and Schmidt numbers shows decreasing behavior for concentration field.

- Magnitude of heat transfer increases for Eckert, Prandtl, Soret, Dufour and Schmidt numbers. Similar behavior is noticed for Hall, thermal slip and fluid parameters. It decreases for Hartman and Biot numbers, radiation and rotation parameters.
- Effective thermal conductivity of nanofluid enhances for increasing Biot, Brinkman and Hartman numbers. Thermal slip parameter and nanoparticle volume fraction also exhibit similar impact on thermal conductivity.
- Size of trapped bolus decreases for wall parameters (E_1 , E_2 and E_5), Taylors and Hartman number whereas its size increases for (E_3 and E_4).

It is a known fact that fluid enters a peristaltic pump through a rotating axis and thus theoretical investigations regarding peristaltic flows in a rotating frame is an interesting area which has been addressed in the present thesis. Moreover the rotational flows and magnetic field generate heat due to an increase in frictional forces. Therefore studying heat transfer in rotating system is of great importance.

All chapters discussed in this thesis analyze the flow problems of viscous and non-Newtonian fluids under the influence of magnetic field when the whole system is in rigid body rotation. These investigations can be extended to discuss more complicated situations in connection with rotation and peristalsis. Following are some possible extensions that can be studied regarding to the peristalsis:

- Soret and Dufour effects on peristaltic flow with different non-Newtonian fluids in rotating geometry.
- Impact of rotation on peristalsis in curved channel etc.
- Convective heat and mass transfer on peristaltic flow in non-uniform channel for rotating frame.
- Rotating peristaltic flow of nanofluids in an inclined channel.

Bibliography

- [1] Merriam-Webster's. (1995). Medical Dictionary, Merriam-Webster's, Inc.
- [2] W. M. Bayliss and E. H. Starling, The movements and innervation of the small intestine, J. Physiol., 24 (1899) 99-143.
- [3] T. W. Engelmann, Zur Physiologie des Ureter, Pflug. Arch. Ges. Physiol., 2 (1869) 243-293.
- [4] J. Lapedes, The physiology of the intact human ureter., J. Urol., 59 (1948) 501-537.
- [5] F. Kiil, Function of the ureter and renal pelvis, Annals. Sur., 148 (1958) 280-291.
- [6] S. Boyarsky, Surgical physiology of the renal pelvis and ureter, Monogr. Sur. Sci., 1 (1964) 173-213.
- [7] R. C. Graves and L. M. Davidoff, Studies on the ureter and bladder with especial reference to regurgitation of vesical contents, J. Urol., 12 (1924) 93-103.
- [8] A. J. Hutch, Vesicoureteral reflux, Bergman, Ed. The ureter, Harper and Row, (1967) 465-479.
- [9] A. H. Shapiro, Pumping and retrograde diffusion in peristaltic waves, In "Proceedings of the Workshop on ureteral reflux in children". Nat. Acad. Sci., Washington, D. C., (1967) 109-126.
- [10] T. W. Latham, Fluid motion in a peristaltic pump, M.I.T Cambridge MA, (1966).
- [11] E. C. Eckstein, Experimental and theoretical pressure studies of peristaltic pumping, M. S. Thesis, Dep. Mech. Eng., M.I.T., Cambridge, MA (1970).

- [12] S. L. Weinberg, A theoretical and experimental treatment of peristaltic pumping and its relation to ureteral function, PhD Thesis, Dep. Mech. Eng., M.I.T., Cambridge, MA (1970).
- [13] S. L. Weinberg, M. Y. Jaffrin and A. H. Shapiro, A hydrodynamical model of ureteral function. In "Proceedings Workshop Hydrodynam. Upper urinary tract", Nat. Acad. Sci., Washington, D. C. (1971).
- [14] P. S. Lykoudis, Peristaltic pumping: a bioengineering model. In "Proceedings Workshop Hydrodynam. Upper urinary tract", Nat. Acad. Sci., Washington, D. C. (1971).
- [15] Y. C. Fung, Peristaltic pumping, a bioengineering model, In: S. Boyarsky (Ed.) *Urodynam.: Hydrodynam. Ureter renal pelvis*, Acad. Press, New York, (1971a).
- [16] Y. C. Fung, Muscle controlled flow, Proc. 12th Midwestern Mech. Conf. Univ. Notre Dame, South Bend, Indiana, (1971b).
- [17] J. C. Burns and T. Parkes, Peristaltic motion, *J. Fluid Mech.*, 29 (1967) 731-743.
- [18] C. Barton and S. Raynor, Peristaltic flow in tubes, *Bull. Math. Bio.*, 30 (1968) 663-680.
- [19] M. Hanin, The flow through a channel due to transversely oscillating walls, *Israel J. Technol.*, 6 (1968) 67-71.
- [20] Y. C. Fung and C. S. Yih, Peristaltic transport, *J. Appl. Mech.*, 33 (1968) 669-675.
- [21] A. H. Shapiro, M. Y. Jaffrin and S. L. Weinberg, Peristaltic pumping with long wavelengths at low Reynolds number, *J. Fluid Mech.*, 37 (1969) 799-825.
- [22] C. C. Yin and Y. C. Fung, Peristaltic wave in circular cylindrical tubes, *J. Appl. Mech.*, 36 (1969) 579-587.
- [23] T. F. Zien and S. Ostrach, A long wave approximation to peristaltic motion, *J. Biomech.*, 3 (1970) 63-75.
- [24] C. H. Li, Peristaltic transport in circular cylindrical tubes, *J. Biomech.*, 3 (1970) 513-523.
- [25] S. T. Chow, Peristaltic transport in a circular cylindrical pipe, *J. Appl. Mech.*, 37 (1970) 901-906.

- [26] J. R. Meginniss, An analytical investigation of flow and hemolysis in peristaltic type blood pumps, M.S. Thesis, Dep. Mech. Eng., M.I.T., Cambridge, MA (1970).
- [27] P. S. Lykoudis and R. Roos, The fluid mechanics of the ureter from a lubrication theory point of view, *J. Fluid Mech.*, 43 (1970) 661-674.
- [28] M. Y. Jaffrin and A. H. Shapiro, Peristaltic pumping, *Ann. Rev. Fluid Mech.*, 3 (1971) 13-36.
- [29] H. S. Lew, Y. C. Fung and C. B. Lowenstein, Peristaltic carrying and mixing of chyme in the small intestine (An analysis of a mathematical model of peristalsis of the small intestine), *J. Biomech.*, 4 (1971) 297-315.
- [30] H. S. Lew and Y. C. Fung, A study on the low Reynolds number in a valved vessel, *J. Biomech.*, 4 (1971) 85-94.
- [31] S. L. Weinberg, E. C. Eckstein and A. H. Shapiro, An experimental study of peristaltic pumping, *J. Fluid Mech.*, 49 (1971) 461-479.
- [32] P. Tong and D. Vawter, An analysis of peristaltic pumping, *J. Appl. Mech.*, 39 (1972) 857-862.
- [33] M. Y. Jaffrin, Inertia and streamline curvature effects on peristaltic pumping, *Int. J. Eng. Sci.*, 11 (1973) 681-699.
- [34] R. E. Semleser, W. J. Shack and T. J. Lardner, The swimming of spermatozoa in an active channel, *J. Biomech.*, 7 (1974) 349-355.
- [35] T. K. Mitra and S. N. Prasad. Interaction of peristaltic motion with Poiseuille flow, *Bull. Math. Biol.*, 36 (1974) 127-141.
- [36] M. P. Negrin, W. J. Shack and T. J. Lardner, A note on peristaltic pumping, *J. Appl. Mech.*, 96 (1974) 520-521.
- [37] M. J. Manton, Long-wavelength peristaltic pumping at low Reynolds number, *J. Fluid Mech.*, 68 (1975) 467-476.

- [38] T. K. Hung and T. D. Brown, Solid-particle motion in two-dimensional peristaltic flows, *J. Fluid Mech.*, 73 (1976) 77-96.
- [39] N. Liron, On peristaltic flow and its efficiency, *Bull. Math. Biol.*, 38 (1976) 573-596.
- [40] T. D. Brown and T. K. Hung, Computational and experimental investigations of two-dimensional nonlinear peristaltic flows, *J. Fluid Mech.*, 83 (1977) 249-272.
- [41] L. M. Srivastava and V. P. Srivastava, Peristaltic transport of a two-layered model of physiological fluid, *J. Biomech.*, 15 (1982) 257-265.
- [42] L. M. Srivastava and V. P. Srivastava, Interaction of peristaltic flow with pulsatile flow in a circular cylindrical tube, *J. Biomech.*, 18 (1985) 247-253.
- [43] S. Takabatake, K. Ayukawa and A. Mori, Peristaltic pumping in circular cylindrical tubes: a numerical study of fluid transport and its efficiency, *J. Fluid Mech.*, 193 (1988) 267-283.
- [44] M. Li and J. G. Brasseur, Non-steady peristaltic transport in finite-length tubes, *J. Fluid Mech.*, 248 (1993) 129-151.
- [45] O. Eytan and D. Elad, Analysis of intrauterine fluid motion induced by uterine contractions, *Bull. Math. Bio.*, 61 (1999) 221-238.
- [46] A. R. Rao and M. Mishra, Nonlinear and curvature effects on peristaltic flow of a viscous fluid in an asymmetric channel, *Acta. Mech.*, 168 (2004) 35-59.
- [47] Kh. S. Mekheimer, Peristaltic transport of a Newtonian fluid through a uniform and non-uniform annulus, *Arab. J. Sci. Eng.*, 30 (2005) 69-83.
- [48] N. Casson, A flow equation for pigment oil-suspensions of the printing ink type In: C. C. Mill, editor, *Rheology of disperse system*, London: Pergamon Press, (1959) 84-105.
- [49] A. C. Eringen, Nonlinear theory of simple micro-elastic solids-I, *Int. J. Eng. Sci.*, 2 (1964) 189-203.
- [50] A. C. Eringen, Theory of micropolar fluids, *J. Math. Mech.*, 16 (1966) 1-16.

- [51] K. K. Raju and R. Devanathan, Peristaltic motion of a non-Newtonian fluid, *Rheol. Acta.*, 11 (1972) 170-178.
- [52] R. G. Devi and R. Devanathan, Peristaltic transport of micropolar fluid, *Proc. Indian Acad. Sci.*, 81(A) (1975) 149-163.
- [53] M. W. Johnson and D. Segalman, A model for viscoelastic fluid behavior which allows non-affine deformation, *J. Non-Newtonian Fluid Mech.*, 2 (1977) 255-270.
- [54] G. Radhakrishnamacharya, Long wavelength approximation to peristaltic motion of power law fluid, *Rheol. Acta.*, 21 (1982) 30-35.
- [55] G. Bohme and R. Friedrich, Peristaltic flow of viscoelastic liquids, *J. Fluid Mech.*, 128 (1983) 109-122.
- [56] L. M. Srivastava and V. P. Srivastava, Peristaltic transport of blood: Casson fluid II, *J. Biomech.*, 17 (1984) 821-829.
- [57] P. Chaturani and R. P. Samy, A study of non-Newtonian aspects of blood flow through stenosed arteries and its application in arterial diseases, *J. Biorheol.*, 22 (1985) 521-531.
- [58] A. M. Siddiqui and W. H. Schwarz, Peristaltic motion of a third order fluid in a planar channel, *Rheol. Acta.*, 32 (1993) 47-56.
- [59] A. M. Siddiqui and W. H. Schwarz, Peristaltic flow of a second order fluid in tubes, *J. Non-Newtonian Fluid Mech.*, 53 (1994) 257-284.
- [60] V. P. Srivastava and M. Saxena, A two-fluid model of non-Newtonian blood flow induced by peristaltic waves, *Rheol. Acta.*, 34 (1995) 406-414.
- [61] S. Usha and A. R. Rao, Peristaltic transport of a two-layered power-law fluids, *J. Biomech. Eng.*, 119 (1997) 483-488.
- [62] E. F. Elshehawey, A. M. El Misery and A. E. H. Abd El Naby, Peristaltic motion of generalized Newtonian fluid in a non-uniform channel, *J. Phys. Soc. Jpn.*, 67 (1998) 434-440.

- [63] O. Eytan and D. Elad, Analysis of intrauterine fluid motion induced by uterine contractions, *Bull. Math. Biol.*, 61 (1999) 221-238.
- [64] J. C. Misra and S. K. Pandey, A mathematical model for oesophageal swallowing of a food-bolus, *Math. Comput. Model.*, 33 (2001) 997-1009.
- [65] A. V. Mernone, J. N. Mazumdar and S. K. Lucas, A mathematical study of peristaltic transport of Casson fluid, *Math. Comput. Model.*, 35 (2002) 894-912.
- [66] T. Hayat, Y. Wang, K. Hutter, S. Asghar and A. M. Siddiqui, Peristaltic transport of an Oldroyd-B fluid in a planar channel, *Math. Prob. Eng.*, 2004 (2004) 347-376.
- [67] K. Vajravelu, S. Sreenadh and V. R. Babu, Peristaltic transport of a Herschel-Bulkley fluid in contact with a Newtonian fluid, *Quarterly J. Appl. Mech.*, 64 (2006) 593-604.
- [68] P. Hariharana, V. Seshadrib and R. K. Banerjee, Peristaltic transport of non-Newtonian fluid in a diverging tube with different wave forms, *Math. Comput. Model.*, 48 (2008) 998-1017.
- [69] S. Nadeem and S. Akram, Peristaltic transport of a hyperbolic tangent fluid model in an asymmetric channel, *Z. Naturforsch.*, 64a (2009) 559-567.
- [70] M. D. Shera, A. S. Gladman, S. R. Davidson, J. Trachtenberg and M. R. Gertner, Helical antenna arrays for interstitial microwave thermal therapy for prostate cancer: tissue phantom testing and simulations for treatment, 46 (2001) 1905-1918.
- [71] D. C. Sanyal and N. K. Maji, Thermoregulation through skin under variable atmospheric and physiological conditions, *J. Theor. Biol.*, 208 (2001) 451-456.
- [72] R. J. Goldstein, W. E. Ibele, S. V. Patankar, T. W. Simon, T. H. Kuehn, P. J. Strykowski, K. K. Tamma, J. V. R. Heberlein, J. H. Davidson, J. Bischof, F. A. Kulacki, U. Kortshagen, S. Garrick and V. Srinivasan, Heat transfer-A review of 2003 literature, *Int. J. Heat Mass Transfer*, 49 (2006) 451-534.
- [73] A. Costa and G. Macedonio, Viscous heating in fluids with temperature-dependent viscosity: implications for magma flows, *Nonlin. Proc. Geophys.*, 10 (2003) 545-555.

- [74] G. Tunc and Y. Bayazitoglu, Heat transfer in microtubes with viscous dissipation, *Int. J. Heat Mass Transfer*, 44 (2001) 2395-2403.
- [75] C. Alexiou, W. Arnold, R. J. Klein, F. G. Parak, P. Hulin, C. Bergemann, W. Erhardt, S. Wagenpfeil, A. S. Lübke, Locoregional cancer treatment with magnetic drug targeting, *Cancer Res.*, 60 (2000) 6641-6648.
- [76] J. M. R. Carlton, C. A. Yowell, K. A. Sturrock and J. B. Dame, Biomagnetic separation of contaminating host leukocytes from plasmodium infected erythrocytes, *Exp. Parasitol.*, 97 (2001) 111-115.
- [77] J. R. Oleson, Hyperthermia by magnetic induction: I. Physical characteristics of the technique, *Int. J. Radiation Oncology (Biology and Physics)*, 8 (2001) 1747-1756.
- [78] P. A. Voltairas, D. I. Fotiadis and M. K. Michalis, Hydrodynamics of magnetic drug targeting, *J. Biomech.*, 35 (2002) 813-820.
- [79] A. Ogulu, Hydromagnetic heat transfer to blood flow in the microcirculation, *J. Fizik Malaysia*, 17 (1996) 135-140.
- [80] G. C. Sharma and J. Kapoor, Finite element computations of two-dimensional arterial flow in the presence of a transverse magnetic field, *Int. J. Numer. Methods Fluids*, 20 (1995) 1153-1161.
- [81] K. Cramer and S. I. Pai, *Magnetofluid dynamics for engineers and applied physicist*, MCGra-Hill Book. Co. (1973).
- [82] V. K. Sud, G. S. Sekhon and R. K. Mishra, Pumping action on blood by a magnetic field, *Bull. Math. Biol.*, 39 (1977) 385-390.
- [83] H. L. Agarwal and B. Anwaruddin, Peristaltic flow of blood in a branch, *Ranchi Univ. Math. J.*, 15 (1984) 111-121.
- [84] G. Radhakrishnamacharya and V. R. Murty, Heat transfer to peristaltic transport in a non-uniform channel, *Defence Sci. J.* 43 (1993) 275-280.

- [85] Kh.S. Mekheimer, Peristaltic flow of blood under effect of a magnetic field in a non-uniform channels, *Appl. Math. Comput.*, 153 (2004) 763-777.
- [86] E. E. Tzirtzilakis, A mathematical model for blood flow in magnetic field, *Phys. Fluids*, 17 (2005) 077103-077117.
- [87] M. Elshahed And M. H. Haroun, Peristaltic transport of Johnson-Segalman fluid under effect of a magnetic field, *Math. Probl. Eng.*, 2005 (2005) 663-677.
- [88] T. Hayat, M. Khan, A. M. Siddiqui, K. Hutter and S. Asghar, Non-linear peristaltic flow of a non-Newtonian fluid under effect of a magnetic field in a planner channel, *Commun. Nonlinear Sci. Numer. Simul.*, 12 (2007) 910-919.
- [89] Y. Wang, T. Hayat, N. Ali and M. Oberlack, Magnetohydrodynamic peristaltic motion of a Sisko fluid in a symmetric or asymmetric channel, *Physica A*, 387 (2008) 347-362.
- [90] Kh. S. Mekheimer and Y. Abd elmaboud, The influence of heat transfer and magnetic field on peristaltic transport of a Newtonian fluid in a vertical annulus: Application of an endoscope, *Phys. Lett. A*, 372 (2008) 1657-1665.
- [91] S. Srinivas and M. Kothandapani, Peristaltic transport in an asymmetric channel with heat transfer-A note, *Int. Commun. Heat Mass Transfer*, 34 (2008) 514-522.
- [92] S. Nadeem and N. S. Akbar, Effects of heat transfer on the peristaltic transport of MHD Newtonian fluid with variable viscosity: Application of Adomian Decomposition Method, *Comm. Nonlinear Sci. Numer. Simul.*, 14 (2009) 3844-3855.
- [93] S. Nadeem and N. S. Akbar, Influence of heat transfer on peristaltic flow of Jhonson-Segalman fluid in a non-uniform tube, *Int. J. Heat Mass Transfer*, 36 (2009) 1050-1059.
- [94] A. M. Sobh, S. S. Al Azab and H. H. Madi, Heat transfer in peristaltic flow of viscoelastic fluid in an asymmetric channel, *Appl. Math. Sci.*, 4 (2010) 1583-1606.
- [95] T. Hayat and S. Noreen, Peristaltic transport of fourth grade fluid with heat transfer and induced magnetic field, *C. R. Mecanique*, 338 (2010) 518-528.

- [96] N. Ali, M. Sajid, T. Javed and Z. Abbas, Heat transfer analysis of peristaltic flow in a curved channel, *Int. J. Heat Mass Transfer*, 53 (2010) 3319-3325.
- [97] S. Nadeem and S. Akram, Magnetohydrodynamic peristaltic flow of a hyperbolic tangent fluid in a vertical asymmetric channel with heat transfer, *Acta Mech. Sin.*, 27 (2011) 237-250.
- [98] T. Hayat, F. M. Abbasi and A. A. Hendi, Heat transfer analysis for peristaltic mechanism in variable viscosity fluid, *Chin. Phys. Lett.*, 28 (2011) 044701.
- [99] D. Tripathi, A mathematical model for swallowing of food bolus through the oesophagus under the influence of heat transfer, *Int. J. Therm. Sci.*, 51 (2012) 91-101.
- [100] A. C. T. Aarts and G. Ooms, Net flow of compressible viscous liquids induced by travelling waves in porous media, *J. Eng. Math.*, 34 (1998) 435-450.
- [101] N. A. S. Afifi and S. Gad, Interaction of peristaltic flow with pulsatile magneto-fluid through a porous medium, *Acta Mech.*, 149 (2001) 229-237.
- [102] Kh. S. Mekheimer, Nonlinear peristaltic transport through a porous medium in an inclined planar channel, *J. Porous Med.*, 6 (2003) 189-202.
- [103] A. R. Rao and M. Mishra, Peristaltic transport of a power-law fluid in a porous tube, *J. Non-Newtonian Fluid Mech.*, 121 (2004) 163-174.
- [104] M. Mishra and A. R. Rao, Peristaltic transport in a channel with a porous peripheral layer: model of a flow in gastrointestinal tract, *J. Biomech.*, 38 (2005) 779-789.
- [105] E. F. Elshehawey, N. T. Eldabe, E. M. Elghazy and A. Ebaid, Peristaltic transport in an asymmetric channel through a porous medium, *Appl. Math. Comput.*, 182 (2006) 140-150.
- [106] T. Hayat, N. Ali and S. Asghar, Hall effects on peristaltic flow of a Maxwell fluid in a porous medium, *Phys. Lett. A*, 363 (2007) 397-403.

- [107] M. Kothandapani and S. Srinivas, Non-linear peristaltic transport of a Newtonian fluid in an inclined asymmetric channel through a porous medium, *Phys. Lett. A*, 372 (2008) 1265-1276.
- [108] S. Srinivas and R. Gayathri, Peristaltic transport of a Newtonian fluid in a vertical asymmetric channel with heat transfer and porous medium, *Appl. Math. Comput.*, 215 (2009) 185-196.
- [109] Kh. S. Mekheimer, S. Z. A. Husseny and Y. Abd Elmaboud, Effects of heat transfer and space porosity on peristaltic flow in a vertical asymmetric channel, *Numer. Meth. Part. D. E.*, 26 (2010) 747-770.
- [110] S. K. Pandey and M. K. Chaube, Peristaltic flow of a micropolar fluid through a porous medium in the presence of an external magnetic field, *Commun. Nonlinear Sci. Numer. Simul.*, 16 (2011) 3591-3601.
- [111] P. S. Gupta and A. S. Gupta, Heat and mass transfer on stretching sheet with suction or blowing, *Cand. J. Chem. Eng.*, 55 (1977) 744-746.
- [112] A. Ogulu, Effect of heat generation on low Reynolds number fluid and mass transport in a single lymphatic blood vessel with uniform magnetic field, *Int. Commun. Heat Mass Transfer*, 33 (2006) 790-799.
- [113] N. T. M. Eldabe, M. F. El-Sayed, A. Y. Ghaly and H. M. Sayed, Mixed convective heat and mass transfer in a non-Newtonian fluid at a peristaltic surface with temperature-dependent viscosity, *Arch. Appl. Mech.*, 78 (2008) 599-624.
- [114] S. Nadeem and N. S. Akbar, Influence of heat and mass transfer on a peristaltic motion of a Jeffrey-six constant fluid in an annulus, *Heat Mass Transfer*, 46 (2010) 485-493.
- [115] S. Srinivas, R. Gayathri and M. Kothandapani, Mixed convective heat and mass transfer in an asymmetric channel with peristalsis, *Commun. Nonlinear Sci. Numer. Simulat.*, 16 (2011) 1845-1862.

- [116] S. Akram, A. Ghafoor and S. Nadeem, Mixed convective heat and mass transfer on peristaltic flow of a non-Newtonian fluid in a vertical asymmetric channel, *Heat Transfer-Asian Res.*, 41 (2012) 613-633.
- [117] T. Hayat, S. Noreen, M. S. Alhothuali, S. Asghar and A. Alhomaideen, Peristaltic flow under the effects of an induced magnetic field and heat and mass transfer, *Int. J. Heat Mass Transfer*, 55 (2012) 443-452.
- [118] N. T. Eldabe, K. A. Kamel, G. M. Abd-Allah and S. F. Ramadan, Heat absorption and chemical reaction effects on peristaltic motion of micropolar fluid through a porous medium in the presence of magnetic field, *Afr. J. Math. Comput. Sci. Res.*, 6 (2013) 94-101.
- [119] A. A. Shaaban and M. Y. Abou-zeid, Effects of heat and mass transfer on MHD peristaltic flow of a non-Newtonian fluid through a porous medium between two coaxial cylinders, *Math. Prob. Eng.*, 2013 (2013) 11 pages.
- [120] A. Aziz, A similarity solution for laminar thermal boundary layer over a flat plate with a convective surface boundary condition, *Commun. Nonlin. Sci. Numer. Simulat.*, 14 (2009) 1064-1068.
- [121] O. D. Makinde, Thermal stability of a reactive viscous flow through a porous saturated channel with convective boundary conditions, *Appl. therm. Eng.*, 29 (2009) 1773-1777.
- [122] T. Hayat, H. Yasmin and M. Al-Yami, Soret and Dufour effects in peristaltic transport of physiological fluids with chemical reaction: A mathematical analysis, *Comput. Fluids*, 89 (2014) 242-253.
- [123] T. Hayat, A. Tanveer, H. Yasmin and A. Alsaedi, Effects of convective conditions and chemical reaction on peristaltic flow of Eyring-Powell fluid, *Appl. Bionics Biomech.*, 11 (2014) 221-233.
- [124] F. M. Abbasi, T. Hayat and B. Ahmad, Peristaltic flow in an asymmetric channel with convective boundary conditions and Joule heating, *J. Cent. South Univ.*, 21 (2014) 1411-1416.

- [125] N. S. Akbar, Natural convective MHD peristaltic flow of a nanofluid with convective surface boundary conditions, *J. Comput. Theor. Nanosci.*, 12 (2015) 257-262.
- [126] T. Hayat, M. Iqbal, H. Yasmin, F. E. Alsaadi and H. Gao, Simultaneous effects of Hall and convective conditions on peristaltic flow of couple-stress fluid in an inclined asymmetric channel, *Pranama J. Phys.*, 85 (2015) 125-148.
- [127] C. L. M. H. Navier Mem, *Acad. Sci. Inst. France*, 1 (1923) 414-416.
- [128] W. K. Chu and J. Fang, On the peristaltic transport in small knudsen number flow, *Mecc.*, 35 (2000) 69-74.
- [129] X. Mandiwala and R. Archer, The influence of slip boundary condition on the peristaltic pumping in a rectangular channel, *J. Fluid Eng.*, 130 (2008) 124501-124505.
- [130] T. Hayat, Q. Hussain and N. Ali, Influence of partial slip on the peristaltic flow in a porous medium, *Physica A*, 387 (2008) 3399-3409.
- [131] N. Ali, Y. Wang, T. Hayat and M. Oberlack, Slip effects on the peristaltic flow of a third grade fluid in a circular cylindrical tube, *J. Appl. Mech.*, 76 (2009) 011006-011016.
- [132] S. Nadeem and S. Akram, Slip effects on the peristaltic flow of a Jeffrey fluid in an asymmetric channel under the effect of induced magnetic field, *Int. J. Numer. Meth. Fluids*, 63 (2010) 374-394.
- [133] T. Hayat, S. Hina and N. Ali, Simultaneous effects of slip and heat transfer on the peristaltic flow, *Commun. Nonlin. Sci. Numer. Simul.*, 15 (2010) 1526-1537.
- [134] A. Yildirim and S. A. Sezer, Effects of partial slip on the peristaltic flow of a MHD Newtonian fluid in an asymmetric channel, *Math. Comput. Model.*, 52 (2010) 618-625.
- [135] Y. V. K. Ravi Kumar¹, S. V. H. N. K. Kumari, M. V. Ramana Murthy and S. Sreenadh, Peristaltic transport of a power-law fluid in an asymmetric channel bounded by permeable walls, *Adv. Appl. Sci. Res.*, 2 (2011) 396-406.
- [136] K. Das, Slip effects on heat transfer and peristaltic pumping of a Johnson–Segalman fluid in an inclined asymmetric channel, *Arab. J. Math.*, 1 (2012) 159-174.

- [137] R. Saravana, R. H. Reddy, S. Sreenadh, S. Vekataramana and A. Kavitha, Influence of slip, heat and mass transfer on the peristaltic transport of a third order fluid in an inclined asymmetric channel, *Int. J. Appl. Math. Mech.*, 9 (2013) 51-86.
- [138] B. Jyothi and P. K. Rao, Slip effects on MHD peristaltic transport of a Williamson fluid through a porous medium in a symmetric channel, *J. Math. Comput.*, 3 (2013) 1306-1324.
- [139] F. M. Abbasi, T. Hayat, B. Ahmad and G. Q. Chen, Slip effects on mixed convective peristaltic transport of Copper-water nanofluid in an inclined channel, *PLoS ONE*, 9 (2014) e105440.
- [140] T. K. Mitra and S. N. Prasad, On the influence of wall properties and Poiseuille flow in peristalsis, *J. Biomech.*, 6 (1973) 681-693.
- [141] G. Camenschi, The motion of a Newtonian viscous fluid through thin pipe with thin linear elastic wall, *Lett. Appl. Eng. Sc.*, 5 (1977) 447-455.
- [142] G. Camenschi and N. Sandru, A model of a viscous fluid motion through an axisymmetrical deformable pipe with thin linear elastic wall, *Roum. Math. Pures Et Appl.*, 24 (1979) 719-724.
- [143] E. O. Carew and T. J. Pedley, An active membrane model for peristaltic pumping: part 1-Periodic activation waves in an infinite tube, *Trans. ASME J. Biomech. Eng.*, 119 (1997) 66-76.
- [144] C. Davies and P. W. Carpenter, Instabilities in a plane channel flow between compliant walls, *J. Fluid Mech.*, 352 (1997) 205-243.
- [145] P. Muthu, B. V. R. Kumar and P. Chandra, Peristaltic motion in circular cylindrical tubes: Effect of wall properties, *Indian J. Pure Appl. Math.*, 32 (2001) 1317-1328.
- [146] M. H. Haroun, Effect of wall compliance on peristaltic transport of a Newtonian fluid in an asymmetric channel, *Math. Prob. Eng.*, 2006 (2006) 61475-61493.
- [147] G. Radhakrishnamacharya and Ch. Srinivasulu, Influence of wall properties on peristaltic transport with heat transfer, *C. R. Mecanique*, 335 (2007) 369-373.

- [148] P. Muthu, B. V. R. Kumar and P. Chandra, Peristaltic motion of micropolar fluid in circular cylindrical tubes: Effect of wall properties, *Appl. Math. Model.*, 32 (2008) 2019-2033.
- [149] M. Kothandapani and S. Srinivas, On the influence of wall properties in the MHD peristaltic transport with heat transfer and porous medium, *Phys. Lett. A*, 372 (2008) 4586-4591.
- [150] M. A. Abd Elnaby and M. H. Haroun, A new model for study the effect of wall properties on peristaltic transport of a viscous fluid, *Comm. Nonlinear Sci. Numer. Simul.*, 13 (2008) 752-762.
- [151] T. Hayat, M. Javed and S. Asghar, MHD peristaltic motion of Jhonson-Segalman fluid in a channel with compliant walls, *Phys. Lett. A*, 372 (2008) 5026-5036.
- [152] N. Ali, T. Hayat and S. Asghar, Peristaltic flow of a Maxwell fluid in a channel with compliant walls, *Chaos Solitons Fractals*, 39 (2009) 407-416.
- [153] S. Srinivas, R. Gayathri and M. Kothandapani, The influence of slip conditions, wall properties and heat transfer on MHD peristaltic transport, *Comput. Phys. Commun.*, 180 (2009) 2115-2122.
- [154] S. Srinivas and M. Kothandapani, The influence of heat and mass transfer on MHD peristaltic flow through a porous space with compliant walls, *Appl. Math. Comput.*, 213 (2009) 197-208.
- [155] M. Mustafa, S. Hina, T. Hayat and A. Alsaedi, Influence of wall properties on the peristaltic flow of a nanofluid: Analytical and numerical solutions, *Int. J. Heat and Mass Transfer*, 55 (2012) 4871-4877.
- [156] M. Mustafa, S. Hina, T. Hayat and A. Alsaedi, Slip effects on the peristaltic motion of nanofluid in a channel with wall properties, *ASME J. Heat Trans.*, 135 (2013) ID 041701 (7 pages).
- [157] N. T. M. Eldabe, A. S. Zaghrou, H. M. Shawky and A. S. Awad, Effects of chemical reaction with heat and mass transfer on peristaltic motion of power-law fluid in an

- asymmetric channel with wall's properties, *Int. J. Research and Reviews in Appl. Sci.*, 15 (2013) 280-292.
- [158] D. G. Salih and A. M. Abdulhadi, Effects of MHD and wall properties on the peristaltic transport of a Carreau fluid through porous medium, *J. Adv. Phys.*, 6 (2014) 1106-1121.
- [159] T. Hayat, M. Rafiq, A. Alsaedi and B. Ahmad, Radiative and Joule heating effects on peristaltic transport of dusty fluid in a channel with wall properties, *Eur. Phys. J. Plus*, 129 (2014) 225-242.
- [160] M. Kothandapani and J. Prakash, Effects of thermal radiation parameter and magnetic field on the peristaltic motion of Williamson nanofluids in a tapered asymmetric channel, *Int. J. Heat Mass Transfer*, 81 (2015) 234-245.
- [161] L. M. Srivastava and V. P. Srivastava, Peristaltic transport of a non-Newtonian fluid: Applications to the vas deferens and small intestine, *Ann. Biomed. Eng.*, 13 (1985) 137-153.
- [162] H. Strohmer, A. Obruca, K. M. Rander and W. Feichtinger, Relationship of the individual uterine size and the endometrial thickness in stimulated cycles, *Fertil. Steril.*, 61 (1994) 972-975.
- [163] S. A. Shehzad, A. Alsaedi, T. Hayat and M. S. Alhuthali, Thermophoresis particle deposition in mixed convection three-dimensional radiative flow of an Oldroyd-B fluid, *J. Taiwan Inst. Chem. Eng.*, 45 (2014) 787-794.
- [164] M. Sheikholeslami, D. D. Ganji, M. Y. Javed and R. Ellahi, Effect of thermal radiation on magnetohydrodynamics nanofluid flow and heat transfer by means of two phase model, *J. Magn. Magn. Mater.*, 374 (2015) 36-43.
- [165] F. M. Abbasi, T. Hayat and B. Ahmad, Peristalsis of silver-water nanofluid in the presence of Hall and Ohmic heating effects: Applications in drug delivery, *J. Mol. Liq.*, 207 (2015) 248-255.
- [166] J. C. Maxwell, *A Treatise on Electricity and Magnetism*, 2nd Edition Oxford University Press, Cambridge, (1904) 435-441.

- [167] T. Hayat, S. Qayyum, M. Imtiaz, F. Alzahrani and A. Alsaedi, Partial slip effect in flow of magnetite- Fe_3O_4 nanoparticles between rotating stretchable disks, *J. Magn. Magn. Mater.*, 413 (2016) 39-48.
- [168] M. G. Reddy and K. V. Reddy, Influence of Joule heating on MHD peristaltic flow of a nanofluid with compliant walls, *Procedia Eng.*, 127 (2015) 1002-1009.
- [169] M. Sheikholeslami and D. D. Ganji, Magnetohydrodynamic flow in a permeable channel filled with nanofluid, *Sci. Iran B*, 21 (2014) 203-212.
- [170] F. M. Abbasi, T. Hayat and B. Ahmad, Peristaltic transport of copper-water nanofluid saturating porous medium, *Physica E*, 67 (2015) 47-53.
- [171] H. F. Oztop and E. Abu-Nada, Numerical study of natural convection in partially heated rectangular enclosures filled with nanofluids, *Int. J. Heat Fluid Flow*, 29 (2009) 1326-1336.
- [172] P. A. Thompson and S. M. Troian, A general boundary condition for liquid flow at solid surfaces, *Lett. Nature*, 389 (1997) 360-362.
- [173] H. M. Shawky, Pulsatile flow with heat transfer of dusty magnetohydrodynamic Ree-Eyring fluid through a channel, *Heat Mass Transfer*, 45 (2009) 1261-1269.
- [174] W. C. Tan and T. Masuoka, Stokes' first problem for an Oldroyd-B fluid in a porous half space, *Phys. Fluid*, 17 (2005) 023101-023107.
- [175] A. Bejan, A study of entropy generation in fundamental convective heat transfer, *J. Heat Transfer*, 101 (1979) 718-725.
- [176] M. K. Drost and M. D. White, Numerical prediction of local entropy generation in an impinging jet, *J. Heat Transfer*, 113 (1991) 823-829.
- [177] H. F. Oztop, A. Z. Sahin and I. Dagtekin, Entropy generation through hexagonal cross-sectional duct for constant wall temperature in laminar flow, *Int. J. Energy Res.*, 28 (2004) 725-737.
- [178] N. S. Akbar, Entropy generation and energy conversion rate for the peristaltic flow in a tube with magnetic field, *Energy*, 82 (2015) 23-30.

- [179] R. E. Rosensweig, Ferrohydrodynamics, Cambridge University press, Cambridge, London (1985) .
- [180] S. S. Papell, Low viscosity magnetic field obtained by the colloidal suspension of magnetic particles, United States Patent Office Filed, 215 (1963) 096.

Plagiarism Undertaking

I solemnly declare that research work presented in the thesis titled "**Peristaltic activity in frames of hydromagnetics and rotation**" is solely my research work with no significant contribution from any other person. Small contribution/help wherever taken has been duly acknowledged and that complete thesis has been written by me.

I understand the zero tolerance policy of the HEC and **Quaid-i-Azam University** towards plagiarism. Therefore, I as an Author of the above titled thesis declare that no portion of my thesis has been plagiarized and any material used as reference is properly referred/cited.

I undertake that if I am found guilty of any formal plagiarism in the above titled thesis even afterward of PhD degree, the University reserves the rights to withdraw/revoke my PhD degree and that HEC and the University has the right to publish my name on the HEC/University Website on which names of students are placed who submitted plagiarized thesis.

Student/Author Signature: _____

Maimona Rafiq

Name: _____

Maimona Rafiq